William & Mary
CHARTERED 1693

W&M ScholarWorks

Dissertations, Theses, and Masters Projects

Theses, Dissertations, & Master Projects

2005

Planar oxides as a novel approach to metal ion sorption studies: from the lab to the field

Christine F. Conrad
College of William and Mary - Virginia Institute of Marine Science

Follow this and additional works at: https://scholarworks.wm.edu/etd

 Part of the Environmental Sciences Commons, and the Geochemistry Commons

Recommended Citation

Conrad, Christine F., "Planar oxides as a novel approach to metal ion sorption studies: from the lab to the field" (2005). *Dissertations, Theses, and Masters Projects.* Paper 1539616617.
https://dx.doi.org/doi:10.25773/v5-chz6-md62

This Dissertation is brought to you for free and open access by the Theses, Dissertations, & Master Projects at W&M ScholarWorks. It has been accepted for inclusion in Dissertations, Theses, and Masters Projects by an authorized administrator of W&M ScholarWorks. For more information, please contact scholarworks@wm.edu.

PLANAR OXIDES AS A NOVEL APPROACH TO METAL ION SORPTION STUDIES: FROM THE LAB TO THE FIELD

A Dissertation

Presented to

The Faculty of the School of Marine Science

The College of William and Mary in Virginia

In Partial Fulfillment

Of the Requirements for the Degree of

Doctor of Philosophy

---

by

Christine F. Conrad

2004

Reproduced with permission of the copyright owner. Further reproduction prohibited without permission.

APPROVAL SHEET

This dissertation is submitted in partial fulfillments of

The requirements for the degree of

Doctor of Philosophy

Christine F. Conrad

Approved, December 2004

Elizabeth A. Canuel, Ph.D.
Committee Chairman/Advisor

Michael J. Kelley, Ph.D.
Co-Advisor

Catherine J. Chisholm-Brause, Ph.D.

Rebecca M. Dickhut, Ph.D.

Michael C. Newman, Ph.D.

Paul M. Bertsch, Ph.D.
University of Georgia
Savannah River Ecological Laboratory
Aiken, South Carolina

Reproduced with permission of the copyright owner. Further reproduction prohibited without permission.

DEDICATION

To my parents, for all of your sacrifices

Reproduced with permission of the copyright owner. Further reproduction prohibited without permission.

"If we knew what it was we were doing, it would not be called research, would it?"
- *Albert Einstein*

Reproduced with permission of the copyright owner. Further reproduction prohibited without permission.

TABLE OF CONTENTS

Page

ACKNOWLEDGEMENTS.....vi

LIST OF TABLES.....vii

LIST OF FIGURES.....ix

LIST OF EQUATIONS.....xiii

ABSTRACT.....xiv

CHAPTER 1: INTRODUCTION.....2

CHAPTER 2: PLANAR γ-Al_2O_3 CHARACTERIZATION.....19

CHAPTER 3: PLANAR VS BULK γ-Al_2O_3: PB(II) SORPTION.....37

CHAPTER 4: Pb(II) SORPTION: XAS ANALYSIS 54

CHAPTER 5: MIXED PLANAR OXIDES.....82

CHAPTER 6: EMPLACEMENT IN NATURAL SEDIMENTS.....125

CHAPTER7: CONCLUSIONS.....159

APPENDIX 1: SPECTROSCOPIC METHODS.....166

APPENDIX 2: BET SURFACE AREA MEASUREMENTS.....174

APPENDIX 3: XAFS DATA COLLECTION AND ANALYSIS.....182

APPENDIX 4: FE COATING PB/AL RATIOS.....190

APPENDIX 5: PLANAR EMPLACEMENT DATA.....194

LITERATURE CITED.....199

VITA.....210

Reproduced with permission of the copyright owner. Further reproduction prohibited without permission.

ACKNOWLEDGEMENTS

At the end of this experience, I have looked back and thought about all of the people who have helped me along the way and know that I would not have made it without them. I am deeply thankful to my advisors over the course of this project, Michael Kelley, Elizabeth Canuel and Catherine Chisholm-Brause. They have all given generously of their time and been sources of intellectual, professional and personal support. I also wish to thank my committee members, Rebecca Dickhut, Michael Newman and Paul Bertsch, for their expertise and insightful comments that have greatly strengthened this dissertation.

Funding for this work was provided by a variety of external sources as well as various VIMS departments. I wish to thank the National Science Foundation, The Clay Minerals Society, The Virginia Water Resources Research Center and Sigma Xi for grants and fellowships that allowed me to complete this work. The VIMS community has also been a steady source of support. The Office of the Dean of Graduate Studies and the Department of Physical Sciences provided much needed support at critical times. A very special thanks is due to Dennis Manos and Bernadette Kulas. Although I was not a student in the department of Applied Sciences, they eagerly provided support for research trips and conferences when I had no resources of my own. I am extremely grateful and honored to have worked with them both.

A large portion of this work was carried out at the College of William & Mary facilities at the Thomas Jefferson National Accelerator Facility Applied Research Center. There are a number of people there that were essential to helping my collect data, primarily Amy Wilkerson. Not only can Amy make any instrument do what she wants, she is a wonderful, compassionate person who has taught me that a little kindness can go a long way. I also owe a great thanks to Natalie Pearcy. For whatever reason, equipment always seemed to malfunction while I was using it. Unfortunately, Natalie was the one who usually ended up fixing it.

There are also a multitude of people who have helped with experimental setup and data collection for this project. Sam Webb, a postdoc at Stanford, was most generous not only in helping me analyze the XAS data for this work, but also in showing me some of the best wineries in Southern California. Patrice Mason, Alanna McIntyre and Mary Ann Vogelbein all provided technical assistance with various aspects of this work. I also wish to thank the staff of beamline X-10C at Brookhaven National Lab for their help in setting up and executing the XAS experiments.

Most importantly, I wish to thank my family and friends. They have been a constant source of support and have helped me keep things in perspective. To my parents, I thank you for all of the sacrifices you made over the years to make this happen. I am forever grateful. And to my husband, Chip, I thank you for all that you have brought into my life. I can't imagine having gone through this experience with anyone else by my side.

Reproduced with permission of the copyright owner. Further reproduction prohibited without permission.

LIST OF TABLES

Table Page

1. Structure and reactivity of γ-Al_2O_3 surface hydroxyl sites.....21

2. Scan parameters used for XRD analyses of planar γ-Al_2O_3.....25

3. XRD peak positions by rank on planar and bulk γ-Al_2O_3.....31

4. SSA summary of planar and bulk γ-Al_2O_3.....31

5. Spectroscopic sample preparation conditions for pH 6 sorption experiments.....42

6. ToF-SIMS and XPS Pb(II) sorption samples analytical peaks.....44

7. XAFS sorption sample parameters.....58

8. Dilution of XAFS powder samples.....59

9. XAFS quantitative fit parameters.....73

10. Fe(III) coating experimental parameters.....86

11. Fe(III) coating quantification: effect of concentration and time.....89

12. Fe(III) coating quantification: effect of sequential coatings.....89

13. SSA of common Fe oxides.....106

14. SSA of Fe(III) coated planar γ-Al_2O_3: effect of concentration and time.....108

15. SSA of Fe(III) coated planar γ-Al_2O_3: effect of sequential coatings.....108

16. ToF-SIMS Pb/Al of pre-emplaced planar γ-Al_2O_3.....129

Reproduced with permission of the copyright owner. Further reproduction prohibited without permission.

17. ToF-SIMS analytical peaks for emplaced planar γ-Al_2O_3.....131

18. Nested random model results for emplaced planar γ-Al_2O_3.....134

19. Pb(II) correlations for emplaced planar γ-Al_2O_3.....139

20. Summary of surface analytical techniques.....166

21. EXAFS data collection scan parameters.....185

22. EXAFS data reduction parameters.....185

Reproduced with permission of the copyright owner. Further reproduction prohibited without permission.

LIST OF FIGURES

Figure Page

1. Surface Complex Formation....4
2. Schematic representation of surface complex structures....5
3. Planar and bulk γ-Al_2O_3 SEM....27
4. Planar γ-Al_2O_3 SEM....29
5. Planar γ-Al_2O_3 SEM....30
6. X-ray diffraction patterns of planar and bulk γ-Al_2O_3....32
7. Adsorption isotherm, linear BET region and t-plot for planar γ-Al_2O_3....35
8. Adsorption isotherm, liner BET region and t-plot for bulk γ-Al_2O_3....36
9. % Pb(II) uptake isotherms....46
10. ToF-SIMS and XPS Pb/Al ratios vs. coverage....47
11. ToF-SIMS and XPS Pb/Al ratios planar vs. bulk γ-Al_2O_3....49
12. Oligomeric Pb(II) species as detected by ToF-SIMS....50
13. Normalized XANES of Pb(II)/bulk γ-Al_2O_3 sorption samples....62
14. Normalized XANES of Pb(II)/bulk γ-Al_2O_3 sorption samples....63
15. First derivative XANES spectra of Pb(II)/bulk γ-Al_2O_3 sorption samples....64
16. First derivative XANES spectra of Pb(II)/planar γ-Al_2O_3 sorption samples....65

Reproduced with permission of the copyright owner. Further reproduction prohibited without permission.

17. χ functions of Pb(II)/bulk γ-Al_2O_3 sorption samples.....69

18. χ functions of Pb(II)/planar γ-Al_2O_3 sorption samples.....70

19. Fourier transforms of Pb(II)/bulk γ-Al_2O_3 EXAFS spectra.....71

20. Fourier transforms of Pb(II)/planar γ-Al_2O_3 EXAFS spectra.....72

21. Characteristic Pb-Al distances of Pb(II) sorption complexes.....78

22. Fe(III) quantitative analysis: concentration and time.....90

23. Fe(III) quantitative analysis: sequential coatings.....91

24. ToF-SIMS elemental Fe(III) maps: 4 day samples.....94

25. ToF-SIMS elemental Fe(III) maps: 14 day samples.....96

26. ToF-SIMS elemental Fe(III) maps: sequential coatings.....96

27. SEM Fe(III) coated planar γ-Al_2O_3: 4 day samples.....99

28. SEM Fe(III) coated planar γ-Al_2O_3: 14 day samples.....100

29. SEM Fe(III) coated planar γ-Al_2O_3: sequential coatings.....101

30. XRD spectra of Fe(III) coated planar γ-Al_2O_3: 4 day samples.....103

31. XRD spectra of Fe(III) coated planar γ-Al_2O_3: 14 day samples.....104

32. XRD spectra of Fe(III) coated planar γ-Al_2O_3: sequential coatings.....105

33. SSA plots for Fe(III) coated planar γ-Al_2O_3: 0.125 mM Fe(III), 4 day.....109

34. SSA plots for Fe(III) coated planar γ-Al_2O_3: 1.25 mM Fe(III), 4 day.....110

35. SSA plots for Fe(III) coated planar γ-Al_2O_3: 12.5 mM Fe(III), 4 day.....111

36. SSA plots for Fe(III) coated planar γ-Al_2O_3: 0.125 mM Fe(III), 14 day.....112

37. SSA plots for Fe(III) coated planar γ-Al_2O_3: 1.25 mM Fe(III), 14 day.....113

38. SSA plots for Fe(III) coated planar γ-Al_2O_3: 12.5 mM Fe(III), 14 day.....114

Reproduced with permission of the copyright owner. Further reproduction prohibited without permission.

39. SSA plots for Fe(III) coated planar γ-Al_2O_3: 2 coatings.....115

40. SSA plots for Fe(III) coated planar γ-Al_2O_3: 5 coatings.....116

41. SSA plots for Fe(III) coated planar γ-Al_2O_3: 10 coatings.....117

42. Planar γ-Al_2O_3 emplacement sample diagram.....130

43. Emplacement experimental design.....131

44. Pb/Al ratios of emplaced planar γ-Al_2O_3.....134

45. Pb(II) sorption kinetics on emplaced unreacted planar γ-Al_2O_3.....136

46. SEM of planar γ-Al_2O_3 prior to emplacement.....140

47. SEM of emplaced ureacted planar γ-Al_2O_3 over time: oxic.....141

48. SEM of emplaced ureacted planar γ-Al_2O_3 over time: boundary.....142

49. SEM of emplaced ureacted planar γ-Al_2O_3 over time: anoxic.....143

50. SEM of emplaced low Pb(II) loaded planar γ-Al_2O_3 over time: oxic.....144

51. SEM of emplaced low Pb(II) loaded planar γ-Al_2O_3 over time: boundary.....145

52. SEM of emplaced low Pb(II) loaded planar γ-Al_2O_3 over time: anoxic.....146

53. SEM of emplaced high Pb(II) loaded planar γ-Al_2O_3 over time: oxic.....149

54. SEM of emplaced high Pb(II) loaded planar γ-Al_2O_3 over time: boundary.....150

55. SEM of emplaced high Pb(II) loaded planar γ-Al_2O_3 over time: anoxic.....151

56. XPS photoelectron ejection.....167

57. ToF-SIMS collision cascade.....169

58. Regions of an x-ray absorption spectrum.....171

59. Wavefunction of a photoelectron from x-ray absorbing atom.....172

60. Single and multiple photoelectron scattering paths.....172

Reproduced with permission of the copyright owner. Further reproduction prohibited without permission.

61. Steps for analysis of EXAFS data.....183

62. Feff input model complex.....186

Reproduced with permission of the copyright owner. Further reproduction prohibited without permission.

LIST OF EQUATIONS

Equation Page

1. Metal-surface hydrolysis reaction....3
2. BET equation....25
3. t-plot standardization....26
4. EXAFS oscillations model....60
5. XPS coated substrate model....92
6. XPS coating thickness....92
7. Single Site Saturation Ligand Binding Model....135
8. Kinetic energy of a photoelectron....167
9. BET linear transform equation....174
10. Calculation of SSA from N_2 adsorption isotherm....174
11. Calculation of C parameter from N_2 adsorption isotherm....174
12. EXAFS equation....182

Reproduced with permission of the copyright owner. Further reproduction prohibited without permission.

ABSTRACT

While much research has been conducted to understand how the mineralogy, chemical composition and surface properties of the solid phase affect metal sorption under controlled laboratory conditions, there has been limited success in translating these results to larger, field scale processes. The purpose of this work is to investigate the use of planar oxides as tools for metal ion sorption studies that can be used in both laboratory and field settings. To do this, a three-step approach was used.

In the first step, Pb(II) sorption to planar γ-Al_2O_3 surfaces relative to pure phase γ-Al_2O_3 was investigated using a suite of spectroscopic techniques (ToF-SIMS, XAS and XPS). The relative quantitative sorption of Pb(II) to the planar γ-Al_2O_3 was found to be comparable to that on the bulk. XAS analysis showed that the coordination geometry and local binding environment of the Pb(II) complexes were similar on the two surfaces over a range of Pb(II) loadings, a mixture of corner-sharing monodentate and edge-sharing bidentate complexes with Pb(II) coordination geometries ranging from distorted trigonal pyramidal to distorted pentagonal.

Second, the complexity of the planar surface was increased by creating mixed Fe-Al oxides of varying elemental composition, morphology and crystallinity. This was accomplished by coating the planar γ-Al_2O_3 using different initial Fe(III) concentrations, reaction times and number of coating sequences. The chemical and physical forms of the resultant coatings were characterized using ToF-SIMS, XPS, XRD, SEM and N_2 BET surface area measurements. Significant changes in the elemental composition and distribution of Fe(III) were seen with changes in the reaction parameters. The crystalline form of the Fe phase present in the coating could not be identified. This, coupled with unexpectedly low SSAs suggests the presence of a mixed Fe-Al oxide rather than a layer of Fe(III) on top of the planar surface. The relative differences in composition and form of these coatings should lead to variations in both the chemical and biological reactivities of these surfaces.

The third step involved placing the planar γ-Al_2O_3 with varying Pb(II) loadings directly into natural sediments. Changes in Pb(II) concentrations as a result of initial Pb(II) loading, emplacement time and redox conditions were examined using ToF-SIMS, and changes in the surface morphology were examined by SEM. Pb/Al ratios, as well as interaction between the emplaced planars and the surrounding sediments, varied as a function of time and initial Pb(II) loading as evidenced by the changes in the surface morphologies, Pb(II) surface concentrations and changes in correlations with Fe and S present in the surrounding sediments. Results from these experiments provide new information about the sorption behavior of Pb(II) under various experimental conditions and indicate that planar oxides can be used in a variety of ways to better understand factors controlling metal sorption processes in natural environments.

Reproduced with permission of the copyright owner. Further reproduction prohibited without permission.

PLANAR OXIDES AS A NOVEL APPROACH TO METAL ION SORPTION STUDIES: FROM THE LAB TO THE FIELD

Reproduced with permission of the copyright owner. Further reproduction prohibited without permission.

INTRODUCTION

Trace metals are often essential to life in aquatic systems acting as nutrients at low concentrations. However, at elevated levels, many metals can have profoundly adverse effects on aquatic plant and animal communities. Understanding the behavior of trace metals in aquatic systems is paramount to being able to effectively predict these toxic effects. Of particular importance are the fate, transport, and bioavailability of toxic metals in aquatic sediments. In the natural environment, a combination of biotic and abiotic processes affect the speciation and distribution of heavy metal contaminants, including incorporation into precipitates and coprecipitates (Bourg, 1983; Katz and Hayes, 1995; Yong et al., 1998; Brown et al., 1999; Trainor et al., 2000), release through dissolution of minerals (Brown et al., 1999), interaction with plants and microbes which may produce unstable oxidation states not predicted by physical chemistry alone (Aston, 1978; Müller and Sigg, 1990; Brown et al., 1999), and complexation by organic compounds of marine and continental origin (Aston, 1978). In addition, sorption reactions at solid-water interfaces decrease solute mobility and often control the transport, fate and bioavailability of toxic heavy metals bound to sediments (Tewari and Lee, 1975; Bourg, 1983; Dzombak and Morel, 1987; Davis and Hem, 1989; Scheidigger et al., 1997; Bertsch and Seaman, 1999; Brown et al., 1999; Sposito et al., 1999).

Clay minerals play an important role in sorption processes in sediments due to their colloidal size, permanent structural charge and surface reactivity (Davis and Hem,

Reproduced with permission of the copyright owner. Further reproduction prohibited without permission.

1989; Bertsch and Seaman, 1999; Sposito et al., 1999). However, the overall surface chemistry of reactive phases in soils and sediments is often controlled by surface modifiers (organics and metal oxide coatings) rather than bulk mineralogical composition (Bertsch and Seaman, 1999). Most sorption reactions at the solid-water interface are initially fast followed by a decrease in the sorption rate. Possible mechanisms that may explain this change in rate are diffusion into micropores of solids, with subsequent sorption onto interior sites; sorption to sites of lower activity; or surface precipitation reactions (Strawn et al., 1998).

Factors that influence the effectiveness of sorption reactions in binding an ion are the pH of the system, the charge on the mineral surface as a function of pH, competition among different ions for the same type of reactive sites, the presence of organic/inorganic ligands that can inhibit or enhance sorption of a metal, and the presence of surface coatings such as biofilms that may block reactive sites and/or create new sorption sites (Tewari and Lee, 1975; Bourg, 1983; Dzombak and Morel, 1987; Chisholm-Brause et al., 1990; Robertson and Leckie, 1997; Brown et al., 1999). The type of sorption complex formed also influences the strength with which the metal is sorbed to the mineral surface (Fig. 1). Specific adsorption (or inner-sphere adsorption) is relatively independent of ionic strength and has a pH dependency more closely related to the hydrolysis of the adsorbate than to the properties of the solid (Chisholm-Brause et al., 1990; Sposito et al., 1999). The equilibria of inner-sphere reactions can therefore often be described through a hydrolysis reaction including the surface species as a reactant,

$$SOH_{sfc} + Me^{2+}(aq) + H_2O = SO^{-}_{sfc}Me(OH)^{+} + 2H^{+} \quad (1)$$

Reproduced with permission of the copyright owner. Further reproduction prohibited without permission.

Ions forming inner-sphere complexes are relatively difficult to desorb, with the exception of large changes in pH. The strength of binding and stability of an inner-sphere complex will depend in part on how many bonds the cation forms with the surface functional groups (Brown et al., 1999). For example, a bidentate or tridentate surface complex involving bonds to two or three surface functional groups will be more difficult to desorb than a monodentate complex attached by a single bond. In the case of non-specific, or outer-sphere, adsorption, metal ions form a weak complex with the surface whereby the ion is surrounded by at least its primary waters of hydration. No direct chemical bonds to the surface reactive groups are formed, and the metal can be easily desorbed with changes in pH or ionic strength (Stumm and Morgan, 1996; Brown et al., 1999).

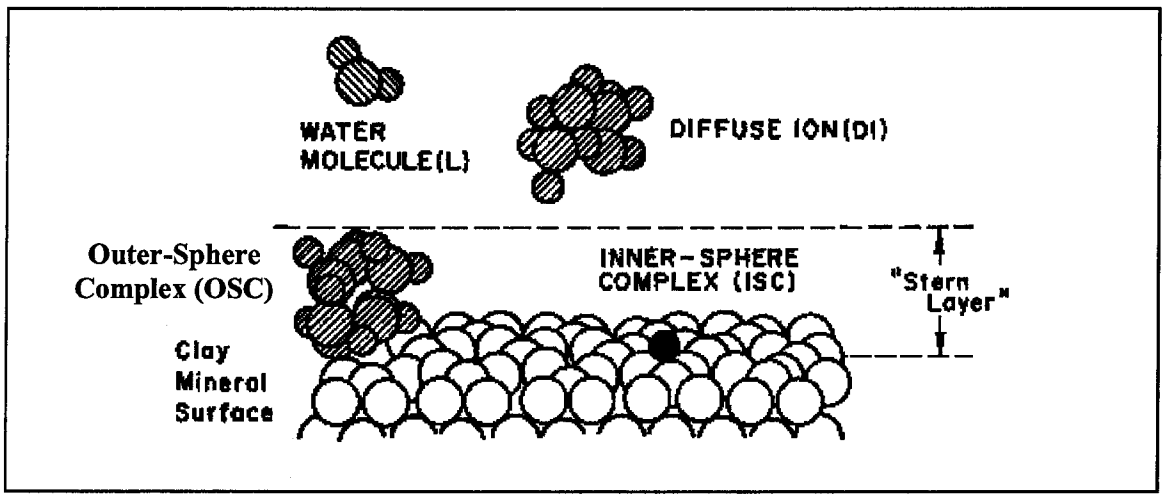

Figure 1. Surface complex formation of an ion on a hydrous oxide surface. The ion may form an inner-sphere complex (ISC) in which it is chemically bound directly to reactive surface sites, an outer-sphere complex (OSC) where the ion is loosely held to the surface through electrostatic forces, or be in the diffuse swarm of the electric double layer. (From Sposito, 1984)

Reproduced with permission of the copyright owner. Further reproduction prohibited without permission.

The strength of an outer-sphere complex can be measured by observing the degree of reduction in metal ion uptake as a function of electrolyte intensity. When an increase in ionic strength reduces metal ion uptake, the ion is less strongly bound to the surface than when the adsorbate shows no dependence on ionic strength (Chisholm-Brause et al., 1990; Brown et al., 1999; Sposito et al., 1999). The pH dependency of uptake for outer-sphere complexes is determined largely by the properties of the solid rather than the adsorbate itself (Chisholm-Brause et al., 1990; Brown et al., 1999). In addition, surface coverage can influence the type of surface complex formed. At low surface coverages, monomeric surface species may form, while at higher surface coverages, polymeric species or surface precipitates may form (Fig. 2) (James and Healy, 1972).

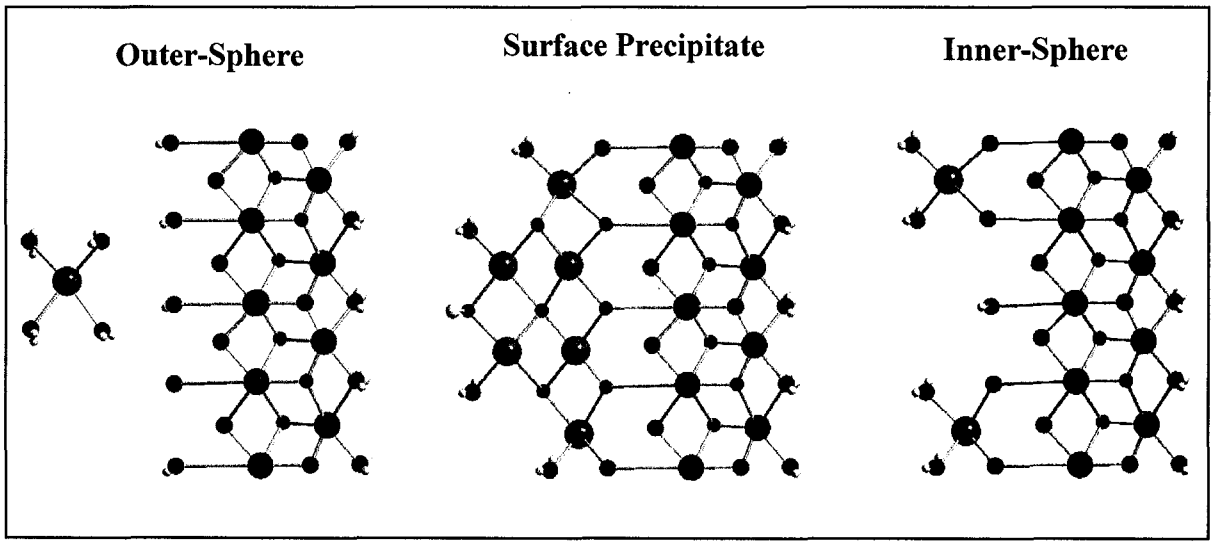

Figure 2. Schematic representation of various surface complex structures.

Until recently, most of the research on metal sorption to mineral surfaces has been conducted utilizing a macroscopic approach. Through these studies, a large body of empirical and theoretical knowledge has been developed and factors that influence

Reproduced with permission of the copyright owner. Further reproduction prohibited without permission.

Until recently, most of the research on metal sorption to mineral surfaces has been conducted utilizing a macroscopic approach. Through these studies, a large body of empirical and theoretical knowledge has been developed and factors that influence adsorption at the oxide-water interface are understood reasonably well (Dzombak and Morel, 1987; Davis and Kent, 1990; Dzombak and Morel, 1990; Coston et al., 1995). However, macroscopic adsorption phenomenon have generally been described using thermodynamics, often neglecting the structure of the surface complexes and the types of reactive surface sites present (Heimstra and Van Riemsdijk, 1999). Because associated results can be ambiguous, spectroscopic verification of the mode of sorption is needed (Katz and Hayes, 1995; Bargar et al., 1997; Brown et al., 1999).

While it is well understood that a molecular-level understanding is needed to explain the underlying mechanisms controlling the fate and transport of contaminants, there has been limited success in translating molecular-level information to observations made at the larger scales (Dzombak and Morel, 1987; Tessier, 1992; Bertsch and Seaman, 1999; Brown et al., 1999). The presence of both multiple reactive phases and the distinct characteristics of these phases compared with the laboratory solids, as well as the inherent complexity of natural systems, have hindered a broad-based application of pure phase data to describe metal ion sorption in the natural environment.

Several approaches have been used to compensate for the complex nature of aquatic systems and to allow for the application of laboratory data to describe metal sorption to natural sediments. A major advance in predicting and modeling metal-ion sorption behavior was the introduction of surface complexation models. The goal of most SCMs is to describe hydrolysis and adsorption at metal oxide surfaces (Westall and

Reproduced with permission of the copyright owner. Further reproduction prohibited without permission.

Hohl, 1980; Dzombak and Morel, 1987). Early SCMs have been successful in describing metal ion sorption processes at the monolayer level. However, at higher coverages, these models fail to accurately predict the metal ion behavior on the sorbate surface. To correct for this, models were formulated to allow for a continuum between adsorption at low coverages and surface precipitation (Farley et al., 1985; Dzombak and Morel, 1987; Katz and Hayes, 1995). Surface precipitation on the solid was described as the formation of a surface phase whose composition varied continuously between that of the original solid and a pure precipitate of the sorbing cation (Katz and Hayes, 1995). Though SCMs can successfully fit adsorption data and predict adsorption outside the range of calibrating data, they have not been used in practice because of the lack of consensus as to the best model and the lack of a coherent body of adsorption constants (Dzombak and Morel, 1987; Davis and Kent, 1990). Also, in contrast to experimental microscopic techniques, SCMs do not account for the surface-complex structure of the adsorbed ion, the various corresponding electrostatic contributions, and the number and type of surface sites involved with the corresponding affinities (Robertson and Leckie, 1997; Heimstra and Van Riemsdijk, 1999). The major drawback to the widespread use of SCMs is that the values for surface complexation obtained from a specific data set are model dependent and therefore cannot be compared to existing adsorption data that have been interpreted from a variety of other methods.

Other approaches involved laboratory sorption studies which investigated metal-ion binding to clay and oxide surfaces through the use of pure phase oxides. Metal-ion sorption to a sediment was modeled as a combination of sorption to a few individual reactive phases; specifically, in surface complexation models, the sediments are treated as

Reproduced with permission of the copyright owner. Further reproduction prohibited without permission.

a combination of several generalized surface sites whose character is representative of those of the individual pure laboratory analogs (Westhall and Hohl, 1980; Dzombak and Morel, 1987; Fu and Allen, 1992; Davis et al., 1998; Wen and Tang, 1998). This 'assemblage model' approach is based on the assumption of additive sorption behavior, i.e., that the net sorption behavior of a multi-component system could be described by the weighted sums of the constituent adsorbents (Oakley et al., 1981, Honeyman, 1984; Davies-Colley et al., 1984). However, it has been demonstrated that oxide systems do not behave additively, and some studies of natural systems suggest little or no additive behavior (Honeyman, 1984; Tipping et al., 1983; Bassett and Melchior, 1990; Meng and Letterman, 1993; Zachara et al., 1994). In some cases, the addition of a second adsorbent can decrease the overall adsorption (Anderson and Benjamin, 1990). Thus, while the chemical reactivities of model oxides have been well studied and characterized, there has been limited success in translating results from these studies to observations made at the larger scales (Dzombak and Morel, 1987; Tessier, 1992; Bertsch and Seaman, 1999; Brown et al., 1999).

Researchers have also attempted to describe and model the array of surface phases on natural sediments to more accurately model trace metal sorption to complex assemblages. This method is both time consuming and difficult because the reactive phases of each sediment must be quantified (Bertsch and Seaman, 1999). More importantly, natural sediment phases typically have a reactivity distinct from the laboratory phases, which inhibits the direct application of laboratory phase surface complexation parameters to natural sediments (Tessier, 1992; Leppard and Droppo,

Reproduced with permission of the copyright owner. Further reproduction prohibited without permission.

2003). Thus, the challenge of "bridging the gap" between metal ion behavior in laboratory studies and that in natural systems remains.

This study utilizes a novel approach for connecting results from laboratory studies to the sorption behavior of metals in the field. Previous studies have focused on either using pure phase analogs to describe metal ion behavior in the natural environment, or conducting studies on natural sediment phases under controlled laboratory conditions, i.e. bringing the field into the lab. This study takes the converse approach—taking the lab into the field through a novel approach using planar oxides. Planar oxides are thin oxide coatings (~ 20 nm in thickness) prepared on a metal substrate support. As such, they are more similar than pure, bulk oxides to natural reactive oxides which typically have variable composition and are present as coatings on a mineral substrate. Because of their planar orientation, the structure and reactivity of the planar oxide surface can be thoroughly characterized using a suite of analytical and spectroscopic methods (Cocke et al., 1984). Moreover, since the oxide is bound to a substrate, the possibility of emplacing them into natural sediments in the environment exists, thus allowing them to react *in situ*, and be subsequently removed and studied. By placing planar oxides directly in a natural environment where biological, chemical, and physical forcings influence sorption processes, the complexes formed can be compared directly to complexes formed under controlled laboratory conditions.

To test the usefulness of planar oxides in metal-ion sorption studies, a hierarchical approach was used. The reactivity of planar γ-Al_2O_3 was compared to that of bulk γ-Al_2O_3 under controlled laboratory conditions through Pb(II) sorption studies. This system was chosen for two reasons. First, the adsorption of Pb(II) onto natural alumina

Reproduced with permission of the copyright owner. Further reproduction prohibited without permission.

oxide and hydroxide surfaces plays an important role in the fate and transport of Pb(II) in contaminated environments. Secondly, this system has been studied extensively using pure phase γ-Al_2O_3 providing a solid basis for comparison between the planar oxide and bulk oxide behaviors. Thus, results from this work can be directly connected to the wealth of information already known about this system from pure phase studies providing further insight into the reactivity of the planar γ-Al_2O_3 surfaces as well as Pb(II) sorption behavior. This simple system was then scaled up to include more complex surfaces through the creation of mixed Fe/Al planar oxides. Theses materials can be characterized and used in future Pb(II) sorption studies to investigate the additive effects of a mixed oxide phase relative to the simple Pb(II)/γ-Al_2O_3 system. The complexity of the reaction environment was also increased by emplacing planar γ-Al_2O_3 into natural sediments and waters maintained in mesocosms. The planars were allowed to react in situ to evaluate the ability to use planar oxides to quantitatively characterize sorption behavior under conditions approaching that of the natural environment. The combination of these three experiments investigates the range of conditions under which planar oxides may be useful. Additionally, results from these studies will provide insight into the reactivity of Pb(II) under such conditions, creating a direct link between Pb(II) sorption behavior in simple systems and that under more complex conditions.

Background Experimental Information

Pb in the Environment

Lead occurs in the environment naturally and its distribution is altered by human activities. Lead primarily occurs in the 2+ oxidation state in inorganic compounds, the

Reproduced with permission of the copyright owner. Further reproduction prohibited without permission.

state with the most complex hydrolysis behavior (Baes and Mesmer, 1976; Brown et al., 1999). Lead is not sensitive to oxidation or reduction over the normal range of Eh and pH values encountered in surface environments. The most common forms of Pb pollution, both atmospheric and aquatic, arise from its use in the petroleum industry as an antiknock agent. Other sources of Pb contaminants to the environment are batteries, paints, alloys and solder, ammunition, and byproducts from mining and smelting activities (Elbaz-Poulichet et al., 1984; Müller and Sigg, 1990; Tingle et al., 1993; Brown et al., 1999). The bioavailability and mobility of Pb within the environment varies dramatically with its speciation (Ostergren et al., 2000). The solubility of Pb and its dispersal in soils, aquifers, and sediments is significantly impacted by its adsorption onto particulate surfaces (Davis and Leckie, 1978; Bargar et al., 1998; Brown et al., 1999).

The adsorption of Pb onto natural oxide surfaces plays an important role in controlling the residence time and dispersal of Pb in contaminated environments (Hem, 1976; Rubin, 1976; Kinniburgh and Jackson, 1981; Coston et al., 1995). Because Pb exists as a cation over a wide pH range, its affinity for a given mineral generally increases with increasing pH (Brown et al., 1999). Lead forms inner-sphere complexes on many mineral and metal oxide surfaces, the strength and stability of which depends on how many bonds it forms with surface functional groups (Chisholm-Brause et al., 1990; Brown et al., 1999; Ostergren et al., 2000). When present as a sorbed species on mineral surfaces, Pb is more bioavailable than when it is present in crystalline solids as Pb may be easily removed from the mineral surface with a reduction in pH (e.g., when a Pb contaminated sediment is ingested by an animal) (Brown et al., 1999; Ostergren et al., 2000).

Reproduced with permission of the copyright owner. Further reproduction prohibited without permission.

Trying to predict the speciation of Pb in estuarine waters is a difficult but important task to assess the toxicity of this metal. One reason for this is that biological cycling of trace metals in an estuary may produce unstable oxidation states of the elements not predicted by physical chemistry alone (Müller and Sigg, 1990; Brown et al., 1999). Secondly, estuaries contain organic matter from a variety of marine and continental sources. As such, Pb complexation in estuaries by organic compounds whose nature is variable and sometimes not well defined is often difficult to predict (Aston, 1978). While the equilibrium speciation for Pb in a model estuary has been shown to be predominantly adsorbed Pb up to a salinity of approximately 20 and then $PbCl^+$ at higher salinities, Pb is not necessarily at equilibrium within a given natural system (Aston, 1978; Bourg, 1983). Furthermore, discrepancies between various thermodynamic models and SCMs have hampered the ability to predict the speciation of Pb and other trace metals in estuarine waters. Nonetheless, Pb has been shown to be toxic to a variety of marine organisms as well as humans making it an environmentally important metal to understand.

The Pb(II)/γ-Al_2O_3 System

Recent studies on the surface complexation of Pb(II) have produced a well-established database on the characteristics of the resultant surface species. In addition, the Pb/γ-Al_2O_3 system has been extensively studied by solution chemists (Hohl and Stumm, 1976; Davis and Leckie, 1978; Chisholm-Brause et al., 1990; Bargar et al., 1997). Pb(II) uptake on γ-Al_2O_3 increases dramatically over a narrow pH range (1-2 pH units). This behavior is related to the pH of the first hydrolysis constant of the metal in

Reproduced with permission of the copyright owner. Further reproduction prohibited without permission.

solution. The 'adsorption edge' for Pb(II) is generally between pH 4.5 and 6.5 (Stumm, 1992) with maximum absorption typically occurring at or above pH 6.0. The pH at which γ-Al_2O_3 has a zero net surface charge (point of zero charge, or PZC) is ~ pH 8.3. Thus it appears that Pb(II) is attracted to a net positively charged oxide surface. This attraction, coupled with the lack of an effect of ionic strength of the solution on uptake suggests that Pb(II) forms a strong inner-sphere complex with γ-Al_2O_2 (Hohl and Stumm, 1976; Chisholm-Brause et al., 1990; Bargar et al., 1996; Bargar et al., 1997). Additionally, Pb(II) has been found to form two types of adsorption complexes on the γ-Al_2O_3 surface depending on the sorption density of the surface. Monomeric surface species have been observed at low surface coverages, while polymeric surface complexes or precipitates have been observed at high surface coverages (Chisholm-Brause et al., 1990; Bargar et al., 1997). Bonding geometry of the Pb(II) surface complex is primarily a distorted trigonal pyramid bound to edges of AlO_6 octahedra mixed with smaller amounts of monodentate complexes (Bargar et al., 1997; Strawn et al., 1998). The formation of mixed precipitates has not been observed as a sorption mechanism for Pb(II) sorption to aluminum (hydr)oxides over relatively short periods of time (Strawn et al., 1998), and the formation of a solid solution phase is unlikely as the radius of Pb is too large to substitute for Al in a mineral structure (Towle et al., 1997).

Spectroscopic Characterization Techniques

Many spectroscopic techniques have been used with success in characterizing metal ion complexes formed on oxide surfaces (Kim, et al., 1973; Chisholm-Brause et al., 1990; Bargar et al., 1996; Scheidigger et al., 1996; Scheidigger et al., 1997; Bargar et al.,

Reproduced with permission of the copyright owner. Further reproduction prohibited without permission.

1998; Trainor et al., 2000). Each of these spectroscopic methods provides insight into the interaction of the adsorbing metal with the surface. Extended X-ray Absorption Fine Structure Spectroscopy (EXAFS) is an element specific probe of the metal's local atomic environment and provides quantitative molecular information including metal-oxygen bond lengths, coordination numbers, and the chemical identities of ions in the immediate vicinity of the absorbed metal ions (Chisholm-Brause et al., 1990; Bargar et al., 1997; Trainor et al., 2000). As such, EXAFS can be used to define the average stoichiometry of the sorption complexes formed. Time of Flight Secondary Ion Mass Spectroscopy (ToF/SIMS) offers ultimate surface sensitivity, viewing only the first monolayers, and provides detection limits for metals on light element oxides better than 1 ppm of the surface (Benninghoven, 1994). Additionally, peaks in the ToF/SIMS spectra may be able to be used as a measure of coverage based on their relative intensities. X-ray Photoelectron Spectroscopy (XPS) provides compositional information, oxidation states, and binding energies of atoms located at or near the surface and has been used extensively to investigate metal-ion complexation on metal oxide surfaces (Tewari and Lee, 1974; Schenk et al., 1983; Chisholm-Brause et al., 1990). A more complete discussion of these methods can be found in Appendix 1.

Objectives and Hypotheses

The overall objective of this study is to develop the use of planar oxides as a tool for understanding metal-ion sorption behavior under a range of environmental conditions. When moving from laboratory to field studies, there are two main factors that contribute

Reproduced with permission of the copyright owner. Further reproduction prohibited without permission.

to the increase in complexity. The first is the complexity of natural reactive phases. Predicting the reactivity of mixed organic and oxide phases is much more difficult than predicting metal sorption to model phases due to additive effects of multiple phases. Secondly, laboratory experiments are often performed in simple salt solutions with only the adsorbing cation present. Organic species and competing ions in natural waters make predicting metal sorption behavior much more difficult in natural aquatic systems. The first portion of this work explores the use of planar oxides in laboratory studies. Initially, Pb(II) sorption to pure phase planar γ-Al_2O_3 under controlled laboratory conditions was studied by traditional wet-chemical techniques coupled with a unique suite of spectroscopic probes (ToF/SIMS, XAS, XPS) to compare the reactivity of the planar γ-Al_2O_3 surface to its bulk analogue. These results form the foundation for increasing the complexity of both the planar surface and the reactive environment. Methods to manipulate the planar surface to create more complex mixed oxide phases were also developed. Various techniques to create planar oxides of varying Fe/Al concentrations and morphologies were investigated, and the resultant oxide coatings were chemically and physically characterized. Finally, the use of planar oxides as a field deployable tool was explored. Planar γ-Al_2O_3 were emplaced in mesocosms containing natural sediments and waters and allowed to react *in situ* to demonstrate the range of scales over which planar oxides can be used. Results from this research will provide insight regarding the conditions under which planar oxides may be useful for investigating metal-ion sorption processes, as well as provide insight into the sorption behavior of Pb(II) under such conditions.

Reproduced with permission of the copyright owner. Further reproduction prohibited without permission.

The first goal of this work is to compare the reactivity of the planar γ-Al_2O_3 to the bulk phase analogues through Pb(II) sorption studies. This will allow for a connection to be made to previous studies of the Pb(II)/ γ-Al_2O_3 system. The surface reactivity of any solid is ultimately dependent on its chemical composition, atomic structure and fine-scale morphology (Hochella et al., 1990). While the chemical composition and structure of the planar oxides are comparable to bulk γ-Al_2O_3, the morphology of the two phases are different. Because the planar oxides are formed as a coating on a metal support, they may be more similar to natural oxides which are often found as coatings on mineral surfaces. It has been shown that coatings often have reactivities that are distinctly different from their bulk phase counterparts. This work will test the following hypothesis relating to the character of the planar and bulk oxides.

> H_1: The reactivity of planar γ-Al_2O_3 is similar to that of the pure phase γ-Al_2O_3 as measured through Pb(II) sorption behavior.
>
> 1. The quantitative uptake of Pb(II) on planar γ-Al_2O_3 will be the same as that on the bulk.
> 2. The structure of the Pb(II) sorption complexes formed over a range of surface coverages will be the same as those formed on the bulk under comparable experimental conditions.

The second objective of this research is to develop a method for creating well-characterized mixed Fe/Al planar oxides using the planar γ-Al_2O_3 as a template. In addition to the well-established effects of solution chemistry (e.g. pH, ionic strength, metal speciation), trace metal adsorption is governed by the composition of the solid phase, specifically the content of metal oxides and organic materials (Dong et al., 2000). Interactions between the constituents of these coatings can alter the metal adsorption properties of the individual components. This work will use the well-characterized planar γ-Al_2O_3 surface as a template for creating mixed Fe/Al planar oxides. Various

Reproduced with permission of the copyright owner. Further reproduction prohibited without permission.

coating techniques will be used to closely control the distribution and morphology of the resulting oxide phase. Specifically, this work will test the following hypothesis:

> H_2: Mixed planar Fe(III)/Al coatings of varying physical and chemical properties can be created using planar γ-Al_2O_3 as a substrate.
>
> 1. Increasing the initial Fe(III) concentration, reaction time and number of coating sequences will produce mixed Fe/Al planar oxides with higher Fe content.
> 2. Variations in the initial Fe(III) concentration and reaction times will lead to Fe phases of varying mineralogical composition. Lower Fe(III) concentrations and shorter reaction times will favor the formation of goethite, while higher Fe(III) concentrations and longer reaction times will favor the formation of hematite.

One of the main advantages of using planar oxides is that because the oxide phase is anchored to a metal support, they can be emplaced in natural sediments and subsequently retrieved. The complexes formed under natural conditions can then be analyzed and compared to those formed on identical materials under controlled laboratory conditions. Thus, planar oxides can provide a direct link between laboratory and field experiments. The specific objective of this work is to investigate the ability to use planar oxides as a field deployable tool, providing boundary limits for the environments in which planar oxides can be useful. The Pb(II)/γ-Al_2O_3 system will be used to allow for a connection to be made to the first phase of this research. By using the same materials under a wide range of conditions, information may be gained on differences between observed laboratory and field sorption behavior. By understanding what factors cause metal-ion sorption in natural systems to differ from laboratory studies of pure phases, we may make better use of the abundant laboratory data to model and predict the consequences of contaminated sites. The specific hypothesis for this work is as follows:

Reproduced with permission of the copyright owner. Further reproduction prohibited without permission.

H_3: Planar γ-Al_2O_3 can be emplaced in natural sediments in mesocosm systems to quantitatively evaluate changes in Pb(II) concentrations on the planar γ-Al_2O_3 surface as a function of initial Pb(II) loading, emplacement time and redox conditions. Additionally, associations with other environmentally important complexants (e.g. Fe, S) can be identified.

1. Planar γ-Al_2O_3 with higher initial Pb(II) loadings will have the smallest change in Pb(II) concentrations after emplacement.
2. Longer emplacement times will result in decreased Pb(II) concentrations.
3. Because neither Pb(II) nor Al are redox reactive metals, Pb(II) concentrations will be unaffected by the local redox conditions of the sediments.
4. Associations with Fe are expected in the oxic zone, as well as in the boundary layer between oxic and anoxic sediments. Sulfur is expected to exhibit the strongest associations with Pb(II) in the anoxic sediments.

This work provides the framework for a novel technique that can be used in a variety of environments to understand sorption processes occurring at the oxide-water interface while also providing valuable insight into the sorption behavior of Pb(II) over a range of experimental conditions. While the experiments contained in this work are designed to display the range of opportunities afforded by using planar oxides, they are not intended to be all inclusive as there are numerous scenarios in which planar oxides can be utilized to provide new insight into sorption behavior of contaminant ions.

Reproduced with permission of the copyright owner. Further reproduction prohibited without permission.

CHAPTER 2

Characterization of Planar γ-Al_2O_3

Introduction

Aluminum (hydr)oxide surfaces have been widely used in industry, and as such, there are extensive data on the morphological and chemical properties of these materials (Peri and Hannan, 1960; Hart and Maurin, 1965; Huang and Stumm, 1972; Knözinger and Ratnasamy, 1978; Scokart and Rouhxet, 1982; Van Veen, 1988; Davis and Hem, 1989; Benfer et al., 1997; Baumgarten and Dick, 1999; Harju et al., 2004; Stefanov et al., 2004). Much of the character of the aluminum oxides is derived from their depositional regimes. For instance, Al_2O_3 coatings with high specific surface areas are used as supports in catalytic converters for various catalytic systems (Stefanov et al., 2004). These materials are usually made by depositing the coatings on thin foils of stainless steel by a dipping process followed by drying and calcination. These materials have different properties than those formed using low temperature deposition procedures such as electrochemical deposition. Using this technique, creation of thin films of Al_2O_3 on stainless steel has been carried out resulting in coatings of high purity and controlled thickness of the film. Plasma sprayed oxides are also often used in applications where high wear resistance or chemical of thermal stability are required. These materials are formed by melting the oxide powder raw material in a high-temperature plasma and

Reproduced with permission of the copyright owner. Further reproduction prohibited without permission.

propelling the melted material to the substrate (Harju et al., 2004). When the melted oxide particles hit the substrate, they solidify rapidly forming a solid oxide. However, information about the surface properties of plasma sprayed oxides is very limited in comparison to the traditionally manufactured oxides, mainly powders.

Aluminas also play an important role in the environment. The composition of soil solutions and the flux of solutes through soils are often controlled by reactions at the mineral-water interface. Aluminum oxides and hydroxides are abundant in nature, and their surfaces are particularly reactive in comparison to other minerals in the environment making them of great interest in fields such as geochemistry, oceanography, and pollution control (Davis and Hem, 1989; Baumgarten and Kirchhausen-Düsing, 1997; Baumgarten and Dick, 1999). While gibbsite is probably the most important aluminum-bearing oxide mineral in soils and sediments, γ-Al_2O_3 serves as a useful analog of naturally occurring aluminum oxides and hydroxides containing reactive amphoteric (i.e., can act as an acid or a base) surface sites (Chisholm-Brause et al., 1990; Bargar et al., 1996). Also, more is known about the surface chemistry of γ-Al_2O_3 because of its extensive use in the catalyst industry as well as in sorption studies (Cocke et al., 1984; Davis and Hem, 1989). The γ-Al_2O_3 surface may contain up to at least five distinct surface sites distributed unequally among the various crystallographic faces (Knözinger and Ratnasamy, 1978; Cocke et al, 1984; Davis and Hem, 1989; Baumgarten and Dick, 1999) (Table 1). The reactivity of each type of surface site largely depends on the number of bonds to surface hydroxyl groups, and the number and type of each site is determined by which crystal planes are exposed preferentially and how aluminum ions are distributed on the surface (Knözinger and Ratnasamy, 1978 ; Davis and Hem, 1989). Thus, the different types of

Reproduced with permission of the copyright owner. Further reproduction prohibited without permission.

hydroxyl groups may well play different roles in reactions on alumina (Peri and Hannan, 1960). For example, surface hydroxyls coordinated to a single aluminum are more basic and more likely to participate in ligand exchange reactions than surface hydroxyls which are coordinated by more than one aluminum (Davis and Hem, 1989).

Table 1. Structure and reactivity of γ-Al_2O_3 surface hydroxyl sites

Net OH^- Charge[†]	Type	Configuration[‡]	Comments
-0.50	Ib	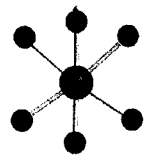	Only present at defect sites
-0.25	Ia	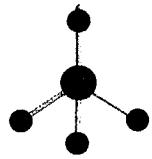	
0.00	IIb	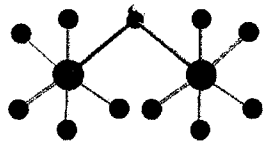	Three times more common than type III
0.25	IIa	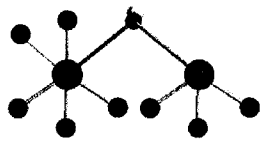	Three times more common than type Ia
0.50	III	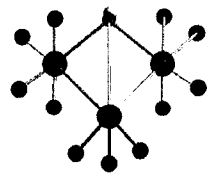	

[†]Net charges are based on Paulings Rule.
[‡]Atoms are: Al = grey, O = red, H = white. The OH group is the surface site while all other oxygens are part of the Al_2O_3 structure. The Al is either octahedrally coordinated or tetrahedrally coordinated by O.

Reproduced with permission of the copyright owner. Further reproduction prohibited without permission.

γ-Al_2O_3 is the high pressure and high temperature polymorph of alumina. However, the surface of γ-Al_2O_3 becomes completely hydrated when exposed to moisture, creating a layer of chemisorbed water along the basal plane of the mineral analogous to the behavior of low temperature aluminas (Knözinger and Ratnasamy, 1978; Goldberg and Glaubig, 1988; Bargar et al., 1997). Additionally, the surface sites of γ-Al_2O_3 is thought to contain only octahedrally coordinated aluminum upon hydration of the surface (Bargar et al., 1997), which is also true for naturally occurring aluminum oxides and hydroxides making it a useful proxy for (hydr)oxide coatings found on mineral surfaces in the natural environment.

This work introduces a novel approach to understanding sorption behavior by combining the broad environmental applications of the γ-Al_2O_3 surface with technology and knowledge derived from industrial applications. γ-Al_2O_3 coatings have been produced on metal foil supports that can be used as an analogue to the bulk phase γ-Al_2O_3 powders often used in laboratory studies. Because they are formed on a metal support, planar γ-Al_2O_3 coatings can be used in a variety of environments that the bulk phase powders cannot. However, to make a connection between these "planar γ-Al_2O_3" and the extensive basis of knowledge on the characteristics of the bulk phase powders, the physical and chemical characteristics of the γ-Al_2O_3 coating must be compared to those of the bulk phase analogues. The objective of this chapter is to describe the morphology and crystallinity of the planar γ-Al_2O_3 relative to the well-characterized bulk γ-Al_2O_3.

Reproduced with permission of the copyright owner. Further reproduction prohibited without permission.

Materials and Methods

γ-Al_2O_3

Aluminum Oxide C (γ-Al_2O_3) was obtained from DeGussa Corp. According to the manufacturer, this material is produced analogous to the AEROSIL® process developed by Degussa. It is a very fine pyrogenic metal oxide with a reported specific surface area of 100 ± 15 m^2 g^{-1}. The powders are $\geq 99.6\%$ γ-Al_2O_3 with an average particle diameter of 13 nm.

The basic nucleation processes for oxides on metal surfaces involve a period of induction during which no visible changes occur at the metal surface. The duration of this phase has been found to depend on such variables as temperature, pressure, surface condition and metal orientation. This phase is followed by nucleation and growth of oxide islands leading to coalescence and a continuous film formation (Hart and Maurin, 1970). The planar materials used in this study were prepared at DuPont using a procedure modified from the work of Hart and Maurin (1965). Loosely coiled aluminum foil was placed in an autoclave with a small amount of water, sealed and purged with N_2. The temperature was raised to 540 °C over a time span of approximately 2 hours. The pressure inside the reaction vessel was maintained at 45 psi by a back-pressure controller. After the two hour period, the autoclave was cooled to room temperature under the steam and N_2 atmosphere. For reactions under these conditions, only γ-Al_2O_3 has been found to form, although different crystallite morphologies can be caused by variations in pressure (Hart and Maurin, 1965). It is important to note that the reaction vessel and specimen must be brought up to reaction conditions as quickly as possible as the speed of the start

Reproduced with permission of the copyright owner. Further reproduction prohibited without permission.

up process can produce vastly different corrosion behaviors. For example, mainly at low temperatures, when the start up procedure is not fast enough, specimens were often found to partially or wholly disintegrate into white crystalline oxides (Hart and Maurin, 1965).

Scanning Electron Microscopy

Scanning electron microscopy (SEM) was used to investigate the morphology and homogeneity of the planar surfaces used. Photomicrogaphs of the bulk γ-Al_2O_3 were also collected. Micrographs were collected using a LEO 435VP Zeiss (LEO) / Cambridge microscope with a beam current of 12 pA and a beam energy of 10 KV. A minimum of five fields were examined for each sample, and representative images were chosen for inclusion here.

X-Ray Diffraction

The properties of the planar γ-Al_2O_3 used in this study were characterized relative to the bulk oxides using microscopic and spectroscopic techniques. The composition of the oxide surfaces of the planar and bulk γ-Al_2O_3 was characterized using x-ray diffraction (XRD). Samples were analyzed using a Scintag ADS diffractometer with a copper anode (λ = 1.540598 Å) and a solid state Peltier detector. Scans were typically run over a region of 2 to 120° 2θ range in steps of 0.02° with count times varying from 4.0 to 8.0 seconds depending on the region (Table 2).

Reproduced with permission of the copyright owner. Further reproduction prohibited without permission.

Table 2. Scan parameters used for XRD analyses of planar γ-Al_2O_3		
Region (° 2θ)	**Count Time (s)**	**Step Size (° 2θ)**
2-26	8.0	0.02
26-80	6.0	0.02
80-120	4.0	0.02

Specific Surface Area and Porosity

The specific surface areas (SSA) of the planar and bulk γ-Al_2O_3 were measured using the Brunauer, Emmet, Teller (BET) N_2-adsorption method (Webb and Orr, 1997). This technique measures the amount of N_2 gas adsorbed (V_{Ads}) onto a solid at a given relative pressure (P_{Rel}). Over the range of P_{Rel} = 0.05 to 0.30, the uptake of N_2 is generally linear with increasing pressure. This region is referred to as the multilayer region, where successive monolayers of gas are assumed to be forming (Gregg and Sing, 1982). Using the following equation over this linear region provides a measure of SSA:

$$\frac{1}{V_{Ads}} \bullet \frac{x}{(1-x)} = \frac{(C-1)}{CV_m} x + \frac{1}{V_m} \qquad (2)$$

where x is the relative pressure (P/P_0 or P_{Rel}), V_m is the volume of gas in a monolayer, V_{Ads} is the volume of gas adsorbed at x, and C is a dimensionless parameter related to the heat of adsorption that can be used to assess porosity (Hiemenz and Rajagopalan, 1997). To calculate SSA, the left-hand side of the equation is plotted against x and a linear regression is performed over the multilayer region. Further details of the BET method and its calculations can be found in Appendix 2.

While the BET equation provides a measure of surface area, it does not provide information on the porosity of the material. Comparison plots such as t-plots can be used for this purpose. Adsorption isotherms were standardized to create t-plots using the

Reproduced with permission of the copyright owner. Further reproduction prohibited without permission.

method of Lippins et al (1964). Briefly, the vertical axis was normalized to the average thickness of the absorbed N_2 layer, V_m. The thickness, t, of the adsorbed layer is determined at any point on the isotherm by multiplying the fraction of monolayer capacity V_{Ads}/V_m at that point by the thickness of the monolayer. If the thickness of a nitrogen monolayer t_m is taken to be 3.54Å, the thickness of any adsorbed layer is

$$t = 3.54\left(\frac{V_a}{V_m}\right) \text{ Å} \qquad (3)$$

Prior to the experiment, samples of bulk and planar γ-Al_2O_3 of known weights were degassed overnight at 250°C with a N_2 flow rate fixed at 18.0 mL/min. Nitrogen gas adsorption isotherms were measured using a Micromeritics Gemini 2365 Surface Area Analyzer over a range of 0.5% to 98% saturation.

Results

Scanning Electron Microscopy

Photomicrographs of the planar and bulk γ-Al_2O_3 materials at 500 X are shown in Figure 3. The difference in morphology of the two surfaces is clear. The bulk γ-Al_2O_3 is comprised of roughly spherical particles that are relatively homogeneous in size. Some deviation in particle size appears due to the fact that the powders were compressed onto the SEM mount. In contrast, the planar γ-Al_2O_3 is a relatively flat surface. The alumina phase present on the planar oxides forms in a manner in which the aluminum foil is evenly coated with the γ-Al_2O_3 phase. Some irregularities, termed oxide islands, in the coating can be seen in the right-hand portion of the photomicrograph (Fig. 3b). A closer view of the planar surface is shown in Figure 4. Inspection of different batches of planar

Reproduced with permission of the copyright owner. Further reproduction prohibited without permission.

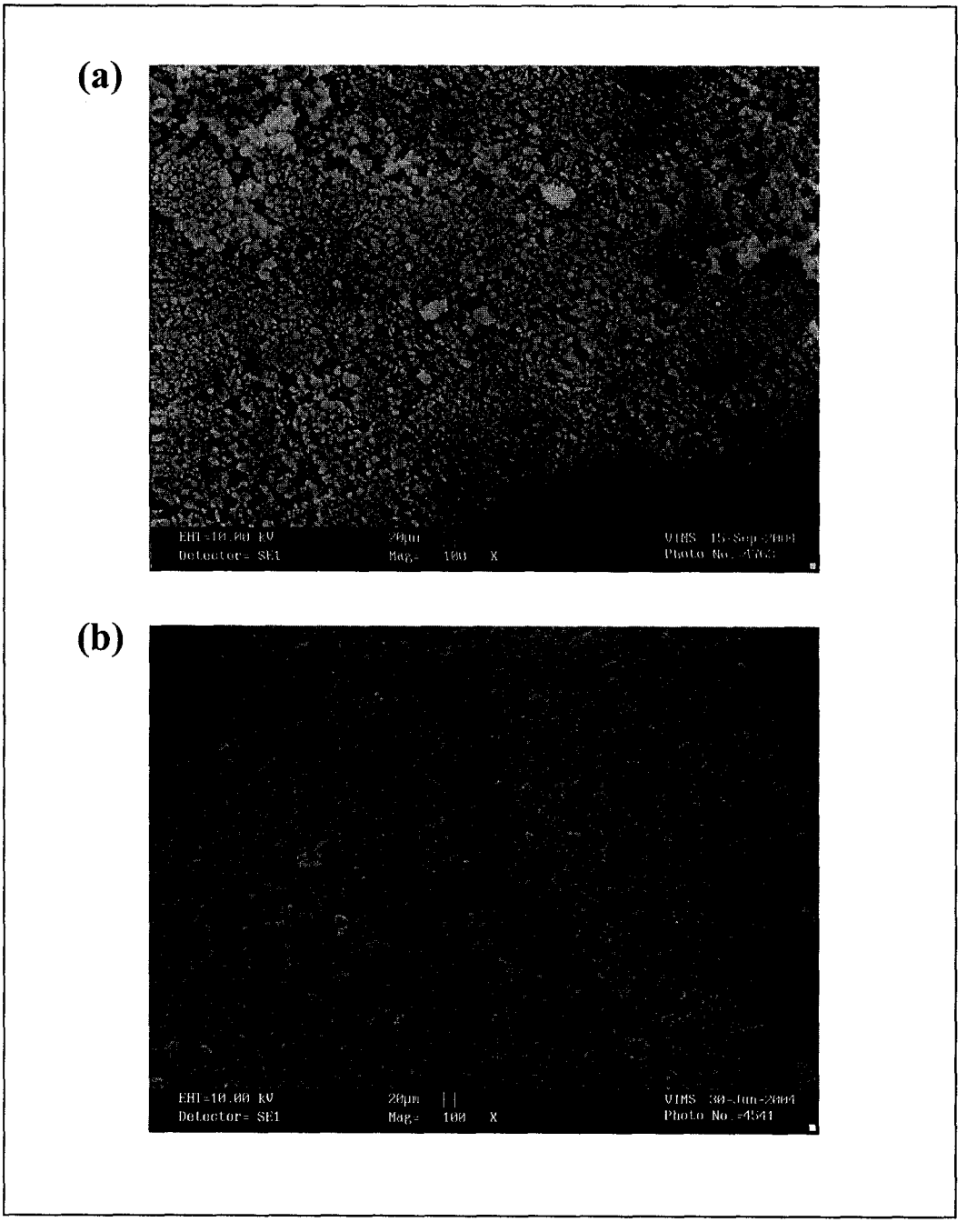

Figure 3. Photomicrographs of (a) bulk and (b) planar γ-Al_2O_3 at 100 X. Although the morphologies of the two oxides are obviously different, XRD and BET analyses confirm the chemical and physical similarity of the planar alumina phase relative to the bulk phase.

Reproduced with permission of the copyright owner. Further reproduction prohibited without permission.

γ-Al_2O_3 showed differences in the morphologies of the oxide islands on the planar surfaces. Two main types were observed: needle-like, crystalline islands (Fig. 5a) and islands of a more amorphous form (Fig. 5b).

X-ray Diffraction

A total of twelve peaks were identified for the planar γ-Al_2O_3 and eight were identified for the bulk γ-Al_2O_3. The peak positions are listed in order of relative intensities on each material in Table 3. The most intense peak for both the planar and bulk γ-Al_2O_3 is the peak at 44.2°. The next most intense peaks are 64.5° and 77.7°. Beyond these three peaks, the diffraction patterns begin to diverge. For the planar materials, the next largest peak is found at 37.8°, followed by the peak at 42.1°. The remaining peaks are small and are at 40.0°, 36.0°, 48.4°, 64.0°, 81.6°,61.5° and 52.6° in decreasing intensity, respectively. For the bulk materials, the peaks at 37.8° and 40.0° are the same intensity. Again, the remaining peaks are relatively small and are found at 42.1°, 52.6° and 81.6° in order of decreasing intensity.

BET Specific Surface Area

Both the planar and bulk isotherms have a region of slow uptake at low P_{Rel} (0.0 – 0.50 % saturation) followed by a region of rapid increase in the amount of N_2 adsorbed (0.50 – 100%) (Figs 7 and 8). For N_2 adsorption on the planar γ-Al_2O_3, the linear region of the BET equation ranged from a P_{Rel} of 0.05 to 0.20 (Fig. 7b), whereas for the bulk γ-Al_2O_3, the range was from a P_{Rel} of 0.05 to 0.16 (Fig. 8b). The calculated BET surface area of the bulk alumina was 95.6 $m^2\ g^{-1}$ which is within the range reported by DeGussa,

Reproduced with permission of the copyright owner. Further reproduction prohibited without permission.

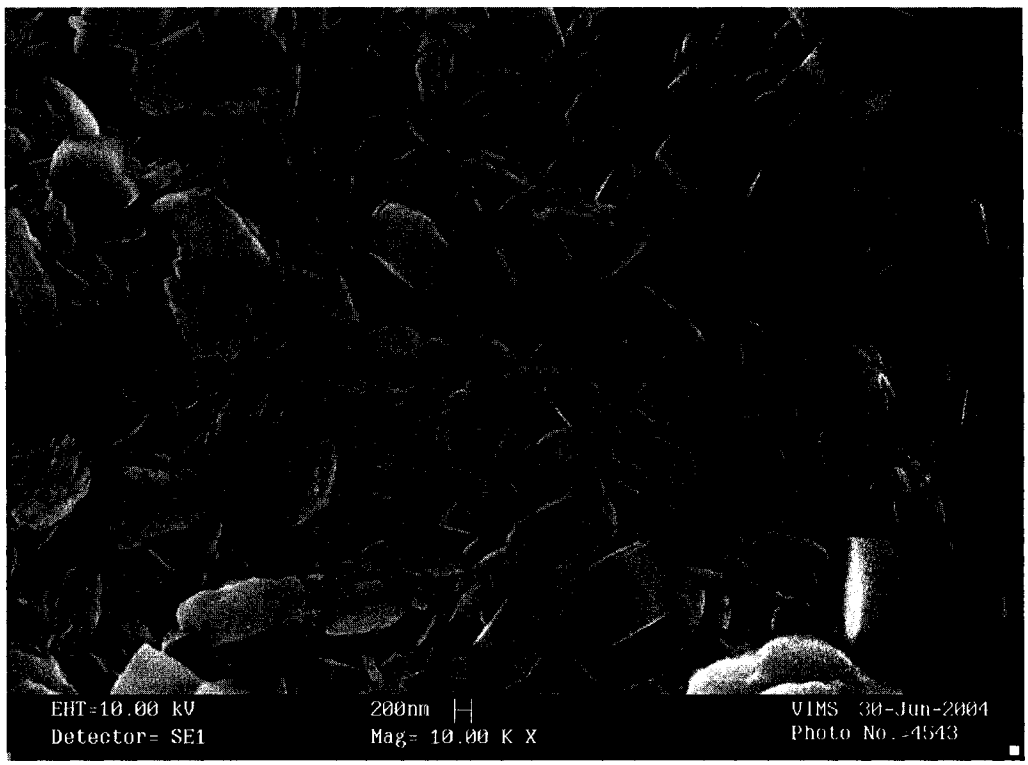

Figure 4. Photomicrograph of unreacted planar γ-Al_2O_3 at 10K X. Cube shaped crystallites and hexagonally shaped crystallites are prevalent on this surface. The distribution of different crystalline shapes depends largely on the pressure at which the oxide layer was formed.

Reproduced with permission of the copyright owner. Further reproduction prohibited without permission.

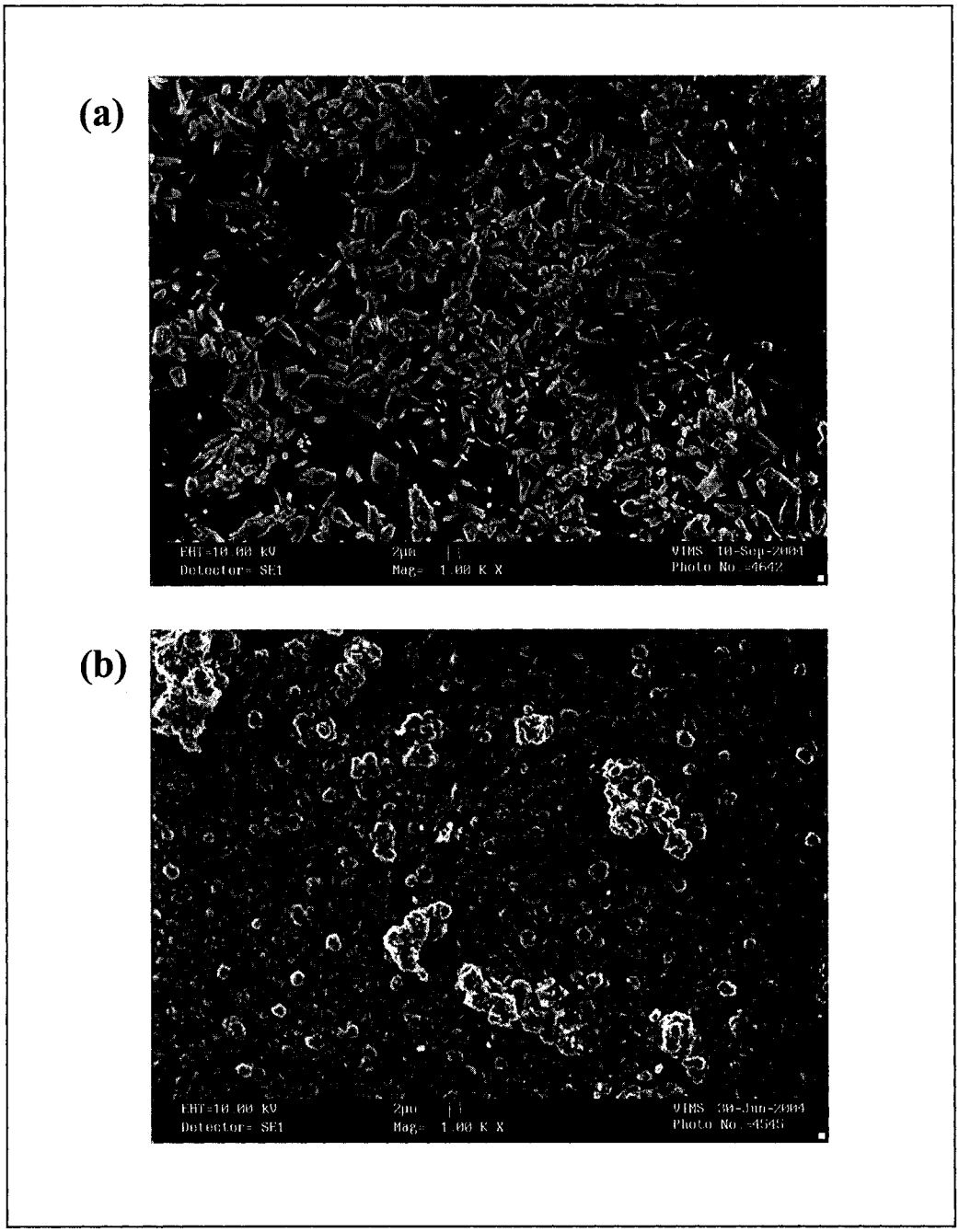

Figure 5. Photomicrographs of the two main types of oxide islands seen on unreacted planar γ-Al_2O_3 from two different production batches. The top micrograph (a) illustrates the needle-shaped crystalline islands, while the more amorphous type islands are shown in the bottom photomicrograph (b). Although the morphologies are different, both phases have been confirmed to be γ-Al_2O_3 by XRD.

Reproduced with permission of the copyright owner. Further reproduction prohibited without permission.

and the BET SSA for the planar alumina was 11.5 $m^2 g^{-1}$ (Table 4). The t-plots for both the planar and bulk γ-Al_2O_3 samples (Figs. 7c and 8c, respectively) were linear with y-intercepts of the linear fit near zero indicating little to no internal porosity for either material.

Table 3. XRD peak positions and assignments for planar and bulk γ-Al_2O_3

Peak Label #	Bulk γ-Al_2O_3			Planar γ-Al_2O_3		
	2θ	d	Al/Spinel (*hkl*)	2θ	d	Al/Spinel (*hkl*)
1	19.28	4.60	110	19.28	4.60	110 (d) †
2	37.80	2.38	Al	34.92	2.57	220 (w)
3	42.10	2.15	Al	37.80	2.38	Al
4	42.94	2.28	222	38.70	2.32	311 (w)
5	44.20	2.05	Al	40.70	2.22	222
6	47.48	1.99	400	42.10	2.15	Al
7	47.60	1.96	400	44.20	2.05	Al
8	64.50	1.44	Al	46.50	1.95	400 (vw)
9	71.42	1.32	440	58.44	1.58	333/511
10	71.46	1.31	440	61.16	1.51	440
11	77.7	1.23	Al	61.32	1.51	440
12				64.50	1.44	Al
13				77.70	1.23	Al

†Weak peaks are denoted by (w), very weak peaks by (vw) and doublets by (d).

Table 4. Summary of BET analysis

Sample	SSA ($m^2 g^{-1}$)	C	y-intercept	Slope
Bulk	95.6 ± 0.20	142.5	0.007 ± 0.0003	0.99 ± 0.002
Planar	11.5 ± 0.01	116.1	0.070 ± 0.0010	8.2 ± 0.007

Reproduced with permission of the copyright owner. Further reproduction prohibited without permission.

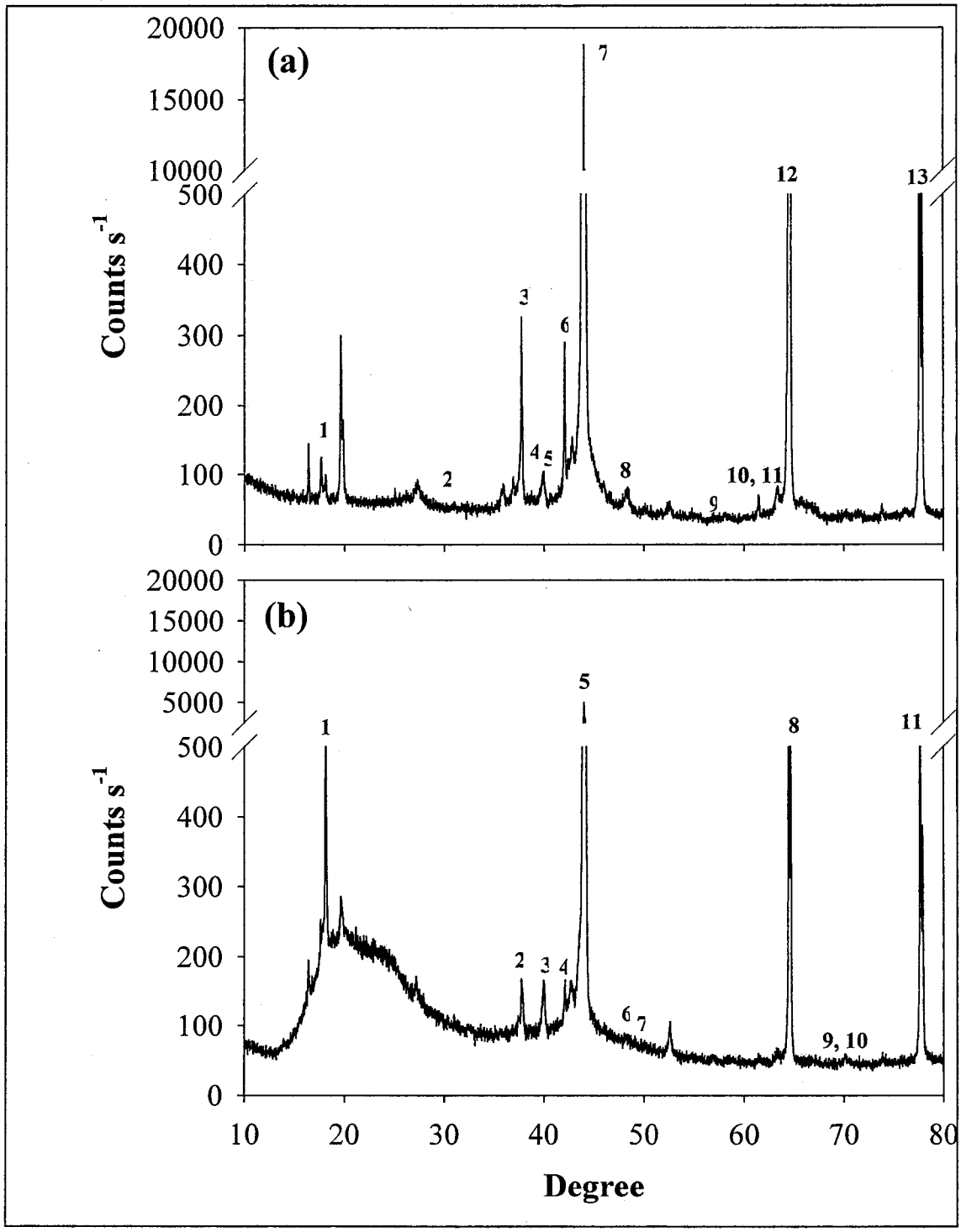

Figure 6. X-ray diffraction patterns of (a) planar and (b) bulk γ-Al_2O_3. Although there are differences in the relative intensities of the major peaks, the overall composition of the diffractograms of the two materials are similar. Peak numbers correspond to Table 3. Diffraction patterns were aligned using the Al metal peak at 44.2 °2θ.

Reproduced with permission of the copyright owner. Further reproduction prohibited without permission.

Discussion

The oxides grown on aluminum foils used in this study appear to be similar to those produced by others (Hart and Maurin, 1965; Hart and Maurin, 1970). At low magnification (100 X), the oxide film appears to be nearly flat with only small variations being visible. These variations can be seen more clearly at higher magnification (1000 X) revealing both well-defined and less-distinct oxide islands. These oxide islands are similar to those observed by Hart and Maurin (1970). While the distribution of alumina phases between α-Al_2O_3 and γ-Al_2O_3 were related to the temperature of the reaction, Hart and Maurin (1965) noted that the presence of more than one oxide form was related to the pressure of the reaction. At temperatures above 500 °C, only γ-Al_2O_3 was found to be present. Growth of the oxide phase at these temperatures consisted of the rapid formation of a thin, highly resistant film ~ 300 Å in thickness. The presence of this film drastically slowed down the reaction process. Outcroppings from this film were then seen ranging in size from 0.1 to 1.0 μm. The morphology of the outcroppings were closely related to pressure, with the prevalence of hexagonally shaped crystallites being observed only at pressures > 42 kg cm^{-3} and increasing rapidly with increasing pressure. Thus, the differences in the crystallite forms of γ-Al_2O_3 seen in the different batches are likely due to variations in the pressures at
which the aluminum foils were reacted.

It was seen that the morphologies of the planar γ-Al_2O_3 materials are significantly different than their bulk phase counterparts (Fig. 3). However, results from the XRD and SSA analyses indicate that the structural form of the planar and bulk aluminas are very similar. Comparison of the XRD diffraction pattern of the planar γ-Al_2O_3 to the bulk

Reproduced with permission of the copyright owner. Further reproduction prohibited without permission.

XRD pattern confirms that the oxide present on the planar alumina is the gamma phase. The three major peaks in the bulk phase diffraction pattern are all found in the planar pattern at the same positions and relative intensities (Fig. 6). Deviations are seen in the occurrences and intensities of some of the minor peaks. This suggests that the overall crystallinities of the two oxides are the same, although the planar oxides may have a preferred orientation compared to the random-mount bulk phase.

Further evidence of the similarity of the planar aluminas to the bulk aluminas is given by the SSA measurements (Figs. 7 and 8). Both oxides showed typical BET behavior with increasing relative pressure (i.e. a linear region followed by a sharp increase in adsorption). In addition, the shapes of the adsorption isotherms are most similar to a Type II isotherm, or a non-porous material (Hiemenz and Rajagopalan, 1997; Webb and Orr, 1997). The lack of porosity of both oxides is further supported by the C parameter values of 142.5 and 116.1 for the bulk and planar oxides, respectively (Table 4). These values are typical for oxides which generally have c parameters ranging from 50-100. Solids with extensive microporosity have c values in the range of 700 (Davis and Kent, 1990). In addition, the y-intercept of the t-plots for each material is zero, indicating no measurable porosity in either material as operationally defined by N_2 adsorption.

Reproduced with permission of the copyright owner. Further reproduction prohibited without permission.

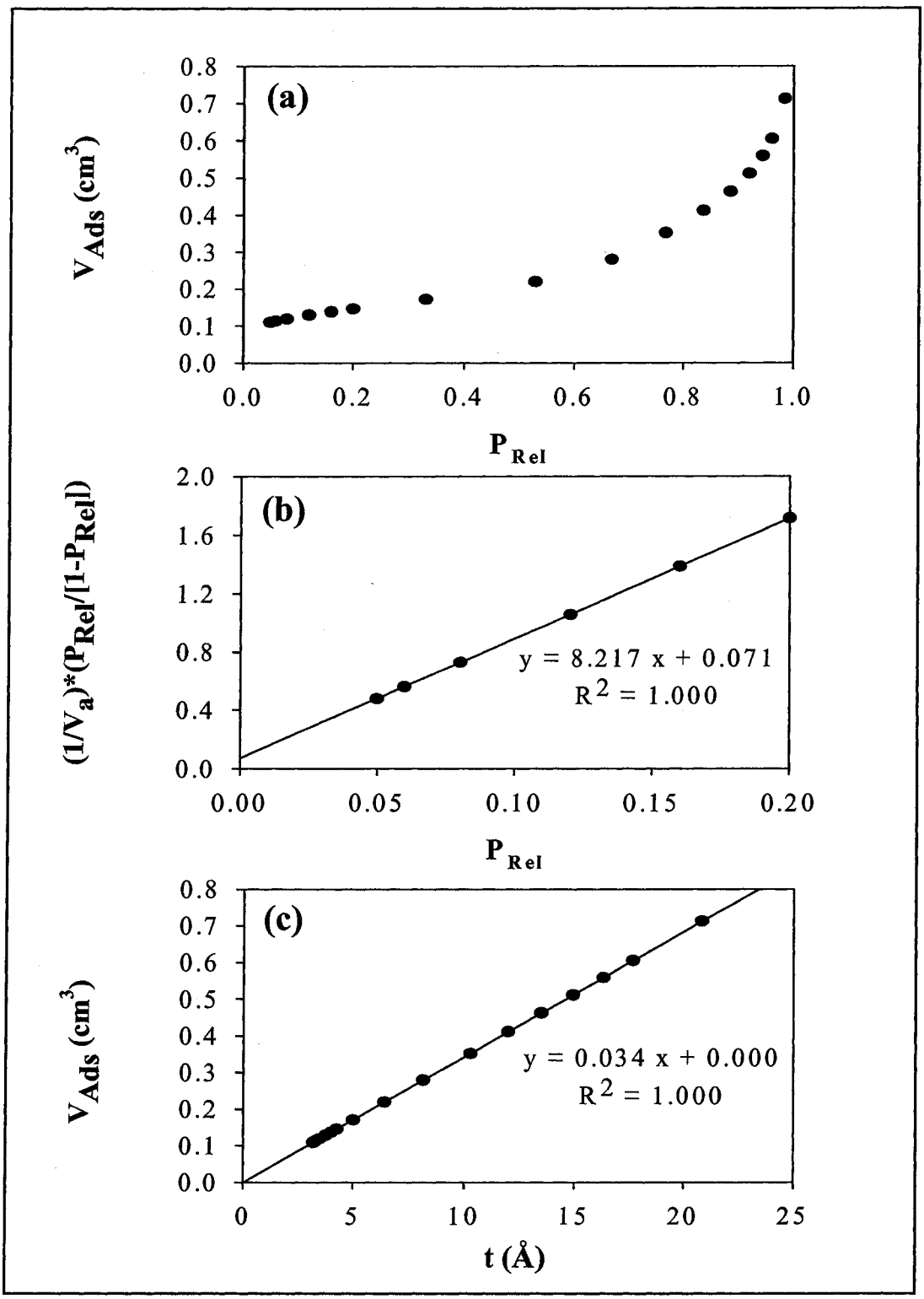

Figure 7. Plots illustrating the (a) adsorption isotherm, (b) linear region of the BET and (c) t-plot for N_2 adsorption on planar γ-Al_2O_3.

Reproduced with permission of the copyright owner. Further reproduction prohibited without permission.

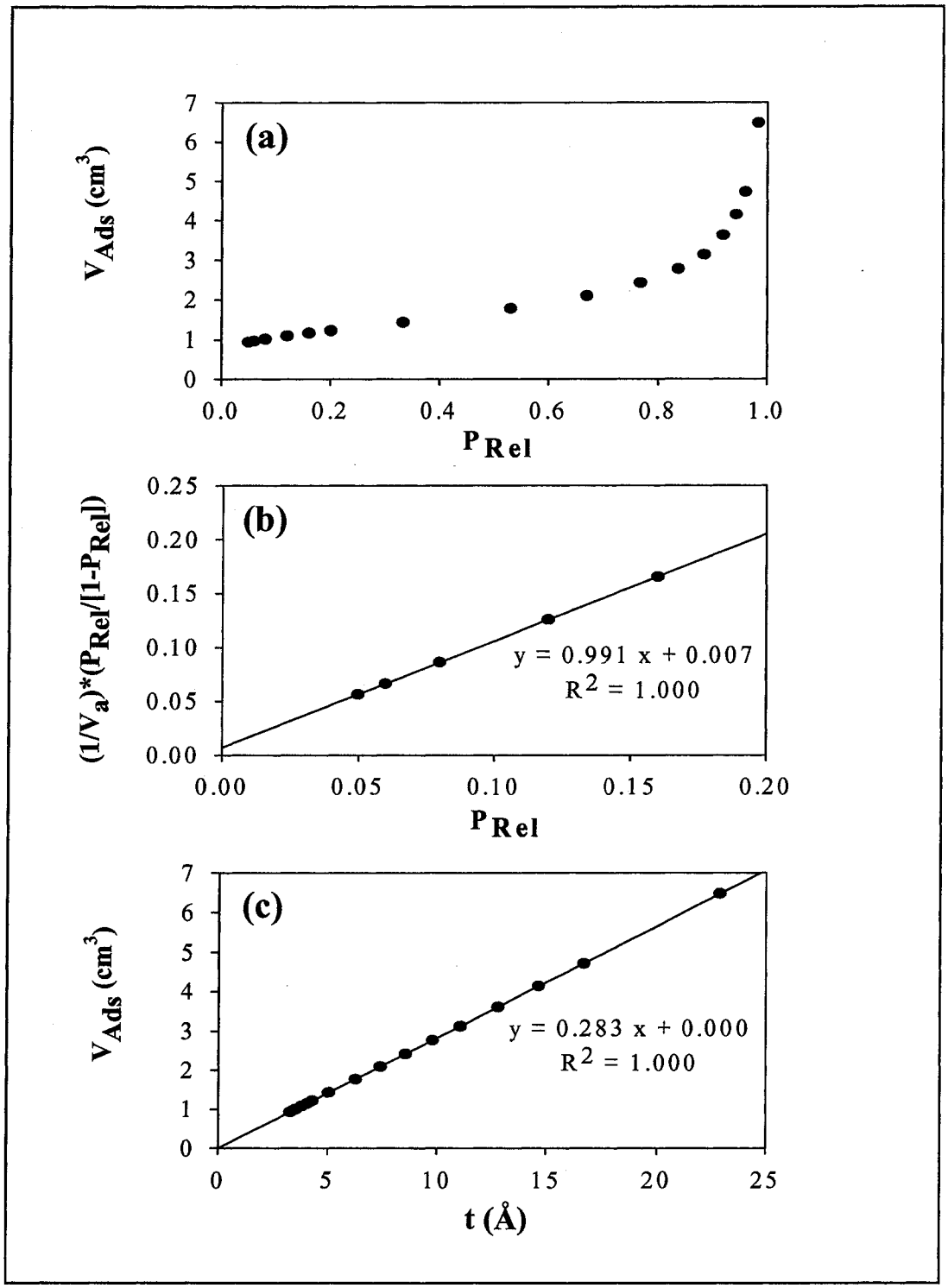

Figure 8. Plots illustrating the (a) adsorption isotherm, (b) linear region of the BET and (c) t-plot for N_2 adsorption on bulk γ-Al_2O_3.

Reproduced with permission of the copyright owner. Further reproduction prohibited without permission.

CHAPTER 3

Pb(II) Sorption to Planar and Bulk γ-Al_2O_3

Introduction

Reactions at the solid-water interface play a major role in controlling the fate and transport of heavy metals in natural aquatic environments. Understanding the binding mechanism of these metals to sediment surfaces is paramount to being able to accurately assess the hazard and risk of contaminated sediments in aquatic systems (Müller and Sigg, 1990; Scheidegger et al., 1997). In the past, studies using pure phase bulk oxides have investigated metal binding through both wet-chemical and spectroscopic techniques (Tewari and Lee, 1975; Chisholm-Brause et al., 1990; Davis and Kent, 1990; Dzombak and Morrel, 1990; Bargar et al., 1996; Scheidegger et al., 1996; Bargar et al., 1997; Baumgarten and Kirchhausen-Düsing, 1997; Bargar et al., 1998; Chisholm-Brause et al., 2000; Trainor et al., 2000). These studies have produced a large body of data describing metal ion sorption onto individual pure phases providing a solid theoretical basis for understanding metal ion sorption mechanisms. However, the ability to apply these data directly to the natural environment has been limited by the complex character of natural sediment phases as well as the inherent complexity of natural systems due to the variety of physical, chemical, and biological forcings influencing metal ion sorption. Thus, a disconnect between laboratory studies of metal ion sorption and natural metal ion

Reproduced with permission of the copyright owner. Further reproduction prohibited without permission.

behavior remains. The objective of this work is to connect the pure phase bulk oxide studies to metal ion sorption on natural sediment particles in the aqueous environment through the use of a novel technique that affords markedly expanded opportunity for direct surface characterization.

An analog phase, specifically planar oxides, has been constructed in order to satisfy the requirements of being more similar to natural phases and of being useful in a variety of experimental environments, including natural systems. Planar oxides are thin oxide coatings of ~ 20 nm in thickness prepared on an underlying metal substrate. The protocols for their preparation are well established as they have been used previously in catalyst research (Hart and Maurin, 1970; Cocke et al., 1984). Because planar oxides are formed as thin layers on a metal support, they are more similar than bulk oxides to natural reactive phases which are present as coatings on mineral particles. A particularly useful experimental convenience in using planar oxides is that they are easily recovered from field emplacements. That is, since the oxide is bound to a substrate (e.g. a metal foil), the assemblage may be placed directly into the sediments of a natural system, allowed to react *in situ*, and subsequently removed and studied by a variety of spectroscopic techniques (EXAFS, ToF/SIMS, XPS, etc.). Placing the planar oxides in a natural environment where they are subject to all of the natural forcings influencing sorption processes results in formation of complexes that can be compared directly to sorption complexes formed under controlled laboratory conditions also on the planar oxides. Thus, a continuum can be made from the metal ion complexes formed in pure phase laboratory studies to those formed in the field.

Reproduced with permission of the copyright owner. Further reproduction prohibited without permission.

In order to assess the validity of this new method, Pb(II) sorption onto γ-Al_2O_3 was studied. The adsorption of Pb(II) onto natural alumina oxide and hydroxide surfaces plays an important role in controlling the residence time and dispersal of Pb(II) in contaminated environments (Hem, 1976; Rubin, 1976; Kinniburgh and Jackson, 1981; Coston et al., 1995). Oxides and hydroxides of aluminum are ubiquitous in nature as coatings, e.g. on aluminosilicate clay minerals in temperate zones (Cheah et al., 1998). γ-Al_2O_3 is the high pressure and temperature polymorph of alumina. The surface of γ-Al_2O_3 completely hydrates when exposed to moisture, creating a layer of chemisorbed water along its basal plane which dissociates to form surface hydroxyl sites (Knözinger and Ratnasamy, 1978; Goldberg and Glaubig, 1988; Bargar et al., 1996). Additionally, the surface sites of γ-Al_2O_3 contain octahedrally coordinated Al making it a useful analog for aluminum oxide and hydroxide minerals commonly found in soils (Bargar et al., 1997; Strawn et al., 1998). The Pb/γ-Al_2O_3 system has been studied extensively using pure phase γ-Al_2O_3 (Davis and Leckie, 1978; Chisholm-Brause et al., 1990; Strawn et al., 1998) providing a solid basis for comparison between the planar oxide and bulk oxide behaviors. Pb(II) complexes formed on alumina surfaces have been well characterized through the use of many spectroscopic techniques, most notably EXAFS and XPS. Direct structural and compositional information about the average Pb(II) complexes formed, as well as metal-oxygen bond lengths, coordination numbers, and chemical identities of neighboring ions in the immediate vicinity of the sorbed ion has been obtained through these techniques (Chisholm-Brause et al., 1990; Bargar et al., 1997; Strawn et al., 1998) Combined EXAFS and wet-chemical studies have shown that Pb(II) forms inner sphere complexes on γ-Al_2O_3 that are relatively independent of ionic

Reproduced with permission of the copyright owner. Further reproduction prohibited without permission.

strength and that Pb(II) sorption has a pH dependence closely related to Pb hydrolysis (Hohl and Stumm, 1976; Chisholm-Brause et al., 1990;). Additionally, Pb(II) has been found to form two general types of adsorption complexes, mononuclear and multinuclear, on the γ-Al_2O_3 surface depending on the sorption density of the surface complex (Chisholm-Brause et al., 1990; Bargar et al., 1997). The formation of mixed precipitates has not been observed as a sorption mechanism for Pb(II) sorption to aluminum (hydr)oxides over relatively short periods of time (Strawn et al., 1998), and the formation of a solid solution phase is unlikely as the radius of Pb is too large to substitute for Al in a mineral structure (Towle et al., 1997).

In order to successfully use planar oxides to bridge laboratory and field studies, the reactivity of the planar γ-Al_2O_3 relative to the pure phase analogues must first be determined. Sorption studies were carried out to measure whether or not the planar oxides behave in a similar manner to the bulk oxides using Pb(II) as a probe, i.e. Pb(II) will form inner-sphere mono and multinuclear sorption complexes on the planar γ-Al_2O_3 as has been observed on the bulk materials. By demonstrating that the planar oxides are a practical surrogate for the bulk oxide surfaces, a connection to the fundamental database of metal ion sorption to pure phases can be made.

Materials and Methods

Oxides:

The bulk γ-Al_2O_3 from Degussa Corp (Degussa Alumina C) was used as received in this experiment as it is obtained in a relatively pure state (confirmed by powder X-ray diffraction using a Scintag ADS diffractometer with a solid state Peltier detector). The

Reproduced with permission of the copyright owner. Further reproduction prohibited without permission.

N_2-BET specific surface area is 95.6 ± 0.20 m^2 g^{-1}. Nitrogen adsorption/desorption data obtained using a Micromeretics Gemini 2375 surface area analyzer indicate that the material is neither micro- nor mesoporous.

The planar γ-Al_2O_3 was prepared following the procedure of Hart and Maurin (1965). High purity aluminum foil was exposed to steam rapidly heated to 550°C and pressurized to 45 psi resulting in a γ-Al_2O_3 surface coating approximately 20 nm thick supported by the metal substrate. The relative intensities of the powder XRD peaks are different for the planar and bulk oxides used in this study indicating that the γ-Al_2O_3 crystallites of the planar oxide have a preferred orientation as bound to the metal substrate. Additionally, the peaks of the bulk oxide are significantly broader, reflective of the much smaller crystallite size of this material. The N_2-BET surface area of the planar oxide used in this work is 11.51 ± .01 m^2 g^{-1}.

Batch Studies:

Pb(II) sorption to bulk γ-Al_2O_3 in the presence of planar oxides was determined for a range of Pb/γ-Al_2O_3 ratios (Table 1). Previous wet-chemical and spectroscopic studies of Pb(II) sorption to bulk γ-Al_2O_3 under similar conditions serve as a basis for these experiments (Hohl and Stumm, 1976; Chisholm-Brause et al., 1990; Bargar et al., 1997). Pb(II) sorption on bulk and planar γ-Al_2O_3 at pH 6.0 was studied as well as the pH dependence of Pb(II) uptake on bulk γ-Al_2O_3 in the presence of planar oxides for select coverages over the range of 4.0 to 7.0. All experiments were conducted in a N_2 glove box using N_2-sparged solutions to exclude CO_2 from the atmosphere in order to prevent the formation of Pb(II) carbonate complexes and precipitates. All solutions were

Reproduced with permission of the copyright owner. Further reproduction prohibited without permission.

prepared with ACS reagent grade chemicals and doubly deionized water (18 mΩ). Planar and bulk oxides were reacted together in the same vessels in order to ensure identical experimental conditions.

After equilibrating in the glove box for 20-24 hours, the dry solids were mixed with a 0.01M $NaNO_3$ (pH 3.5) solution equal to one-half of the total reaction volume (V_T typically 32 mL) and mixed for 24 hours to fully hydroxylate the solid in equilibrium with the salt solution. At the beginning of the adsorption experiment, one-half of the reaction volume of $Pb(NO_3)_2$ was added and the samples were mixed. After approximately 1 hour, the pH was checked and adjusted to that desired by the addition of carbonate-free 1M NaOH and was maintained by the addition of small aliquots of this base. The initial Pb(II) concentration was 130 or 25 μM (± 5% standard error), with different maximum coverages (Γ_{max} = 0.01 to 4.0 μmol m^{-2}) obtained by varying the solid/solution ratio (Table 5). In each system, the bulk oxides dominated the total available surface area by 4 to 6 orders of magnitude; the surface area of the planar oxide phase was ≈ 0.0012 m^2 in each system while the surface area of the bulk oxides ranged from 31.5 m^2 to 2625 m^2 depending on the amount of solid used.

Table 5. Spectroscopic sample preparation conditions for pH 6 sorption experiments

	Γ_{max}[1] =	Γ_{max}=	Γ_{max}=	Γ_{max}=	Γ_{max}=	Γ_{max}=
Sample	**0.01**	**0.05**	**0.26**	**1.00**	**2.00**	**4.00**
g γ-Al_2O_3/L	25.0	25.0	5.00	1.23	0.619	0.307
$[Pb]_F$	3.63	20.71	16.53	35.44	40.94	42.39
Final pH	6.09	6.10	6.12	5.91	5.90	5.95
Actual Γ[2]	0.01	0.044	0.23	0.73	1.4	2.7
% Uptake	85.48	84.10	87.28	72.74	68.51	67.39

[1]Γ in units of μmol Pb m^{-2} γ-Al_2O_3. Values are based on m^2 bulk γ-Al_2O_3 present.
[2]Calculated as total [Pb] removed from system divided by m^2 bulk γ-Al_2O_3 present.

Reproduced with permission of the copyright owner. Further reproduction prohibited without permission.

After mixing for 24 hours, the solids and supernatants were separated by centrifugation. Samples were centrifuged at 10,000 rpm for a minimum of 20 minutes, until the particles formed a coherent pellet and the supernatant was visibly clear. The samples were placed back into the glove box where the pH of the supernatant was measured with an Orion 520A pH meter with a Ross semi-micro glass electrode. The solutions were acidified with 1M HNO_3 (10% by volume) and stored for Pb(II) analysis. Total aqueous Pb(II) concentrations were determined spectrophotometrically using a Thermo Jarrell Ash TraceScan Inductively Coupled Plasma Atomic Emission Spectrophotometer (ICP-AES). The amount of Pb(II) sorbed was calculated as the difference between the initial and final Pb concentrations. Solids were freeze-dried prior to spectroscopic analysis involving vacuum or dry conditions. Time of Flight Secondary Ion Mass Spectroscopy (ToF/SIMS) and X-Ray Photoelectron Spectroscopy (XPS) (see below) were used to compare the Pb(II) complexes formed on both the bulk and planar oxides over the range of coverages at pH 6.0. For both spectroscopic analyses, the powdered samples were pressed into wafers and the planar oxides were run as is.

Surface Analysis

Surface compositions were determined by Time of Flight Secondary Ion Mass Spectroscopy (ToF/SIMS) and by X-ray Photoelectron Spectroscopy (XPS, also known as ESCA). ToF/SIMS offers ultimate surface sensitivity, viewing only the first monolayers, and provides detection limits for metals on light element oxides better than 1 ppm of the surface (Benninghoven, 1994; Douglas and Chen, 1998). Combining such

Reproduced with permission of the copyright owner. Further reproduction prohibited without permission.

surface sensitivity with the multi-monolayer sampling depth of XPS allows for the detection of three-dimensional metal entities such as precipitates.

Samples of the planar γ-Al_2O_3 materials were examined as-is. The powder materials were mounted onto aluminum foil by pressing a sandwich (foil-powder-foil) and then removing the top foil layer. Both planar and powder samples were mounted on the instrument sample holders without further preparation. The ToF/SIMS instrument is a Physical Electronics TFS-2100 TRIFT II and was operated with a 15 KeV Ga^+ beam and rastered over an area of 100 μm. Complete mass spectra were collected at each location in the raster. The XPS data were collected using a SPECSlab "Phoibos" multi-technique surface science instrument operated with 200 W input power to the Mg anode; emitted photoelectrons were collected from an approximately 5 mm diameter circle.

Element peaks were separated from the background and their intensity quantified using the software provided by the instrument manufacturer (Table 6). As expected, the Al and O signals from the alumina substrate dominate all the spectra, so the results are best viewed as the ratio of the target element (Pb, C, Cl, etc.) to Al. Sensitivity factors provided by the instrument manufacturer were used to convert the XPS peak intensity ratios to true atom ratios.

Table 6. Analytical peaks used for XPS and ToF/SIMS analysis of Pb(II) sorption to bulk and planar γ-Al_2O_3.

Element	ToF/SIMS (Mass)	XPS
Al	27	2p
C	12	1s
Cl	35	2p
O	16	1s
Pb	Pb_{Total}= 208+225+449	$4f_{5/2} + 4f_{7/2}$

Reproduced with permission of the copyright owner. Further reproduction prohibited without permission.

Results

pH Dependence of Pb(II) Sorption

Uptake of Pb by bulk γ-Al_2O_3 in the presence of the planar oxides as a function of pH is shown in Figure 9. Overall, Pb(II) sorption increases markedly between a pH of 4.0 and 5.5. At the lower coverage, Γ_{max}=0.26 μmol/m^2, the adsorption edge (the pH at which 50% of the total adsorbate present is sorbed) occurs around pH 4.2. At the higher coverage, Γ_{max}=1.3 μmol/m^2, the pH edge is shifted to a higher pH of 5.3. The shift of the adsorption edge to a higher pH with higher Γ_{max} is consistent with previous studies performed on bulk γ-Al_2O_3 (Hohl and Stumm, 1976; Davis and Leckie, 1978), indicating that the presence of the planar oxides does not discernibly alter the behavior of Pb(II) sorption to the bulk γ-Al_2O_3 surface.

Pb(II) Sorption at pH 6.0

Pb/Al ratios as a function of coverage illustrate the quantitative abilities of ToF/SIMS and XPS for analyzing Pb sorption to both phases. The coverages indicated in Figure 10 are calculated based on the concentrations of bulk alumina present in each system as this is the controlling surface phase on a surface area basis (bulk surface area is 10^3-10^4 times greater than that of the planar oxide). Using ToF/SIMS allowed for the detection of Pb(II) at the lowest surface concentrations studied ($\Gamma \approx 0.01$ μmol/m^2 corresponding to < 1% monolayer coverage). Pb/Al ratios from XPS are highly correlated to surface coverage for both the planar oxides (r^2=0.939; Fig. 10a) and the bulk oxides (r^2=0.983; Fig. 10b). The ratios obtained from ToF/SIMS analysis also show a

Reproduced with permission of the copyright owner. Further reproduction prohibited without permission.

good correlation to surface coverage, although the relationship is not as strong for the planar oxides (r^2=0.854; Fig. 10c) as for the bulk oxides (r^2=0.996; Fig. 10d).

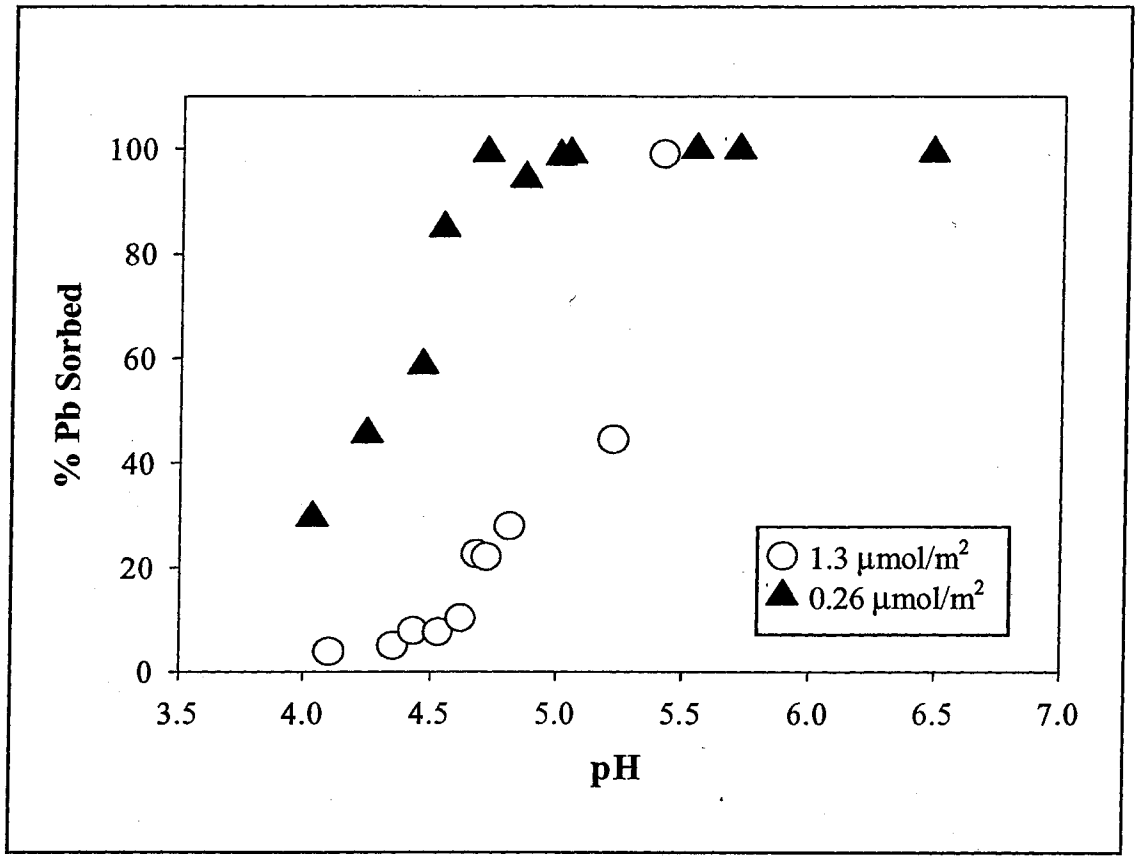

Figure 9. pH Pb(II) adsorption curve as a function of pH for co-equilibrated bulk and planar γ-Al_2O_3 at different Pb(II)/ γ-Al_2O_3 ratios. The classic behavior of shifting the adsorption edge, or region of rapid increase in Pb(II) uptake, to a higher pH with increasing coverage is seen indicating that Pb(II) sorption behavior in the presence of the planar oxides is similar to the expected sorption behavior to bulk γ-Al_2O_3.

Pb/Al ratios determined by XPS and ToF/SIMS for the planar vs. bulk γ-Al_2O_3 were compared to assess the sorption behavior on each material over the range of coverages studied. There is a relatively high degree of linearity between the XPS Pb/Al ratios as well as the ToF/SIMS ratios (r^2=0.881 and 0.863, respectively) demonstrating that with increasing total Pb(II)/solid ratios, the surface coverage on the planar oxides

Reproduced with permission of the copyright owner. Further reproduction prohibited without permission.

Reproduced with permission of the copyright owner. Further reproduction prohibited without permission.

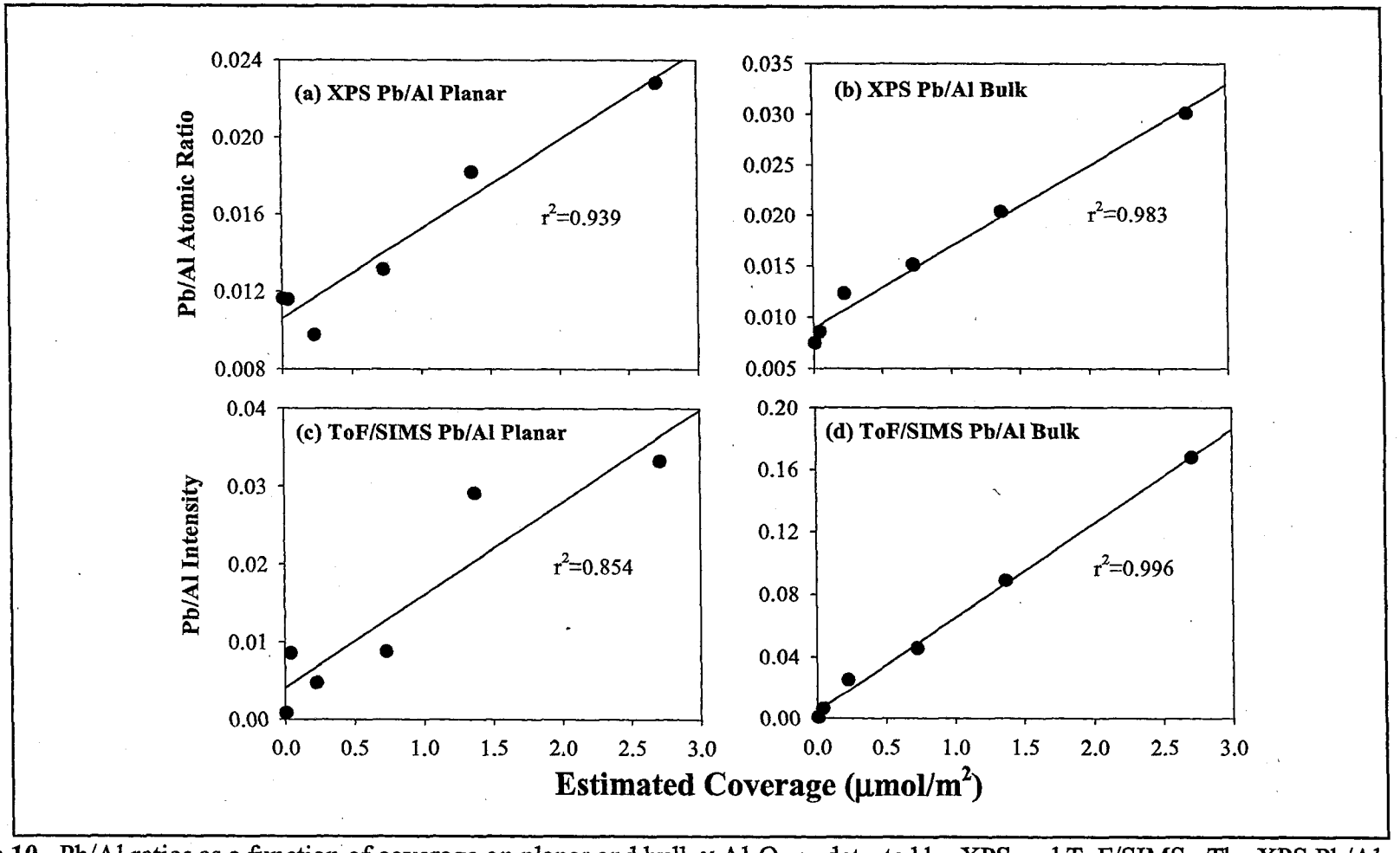

Figure 10. Pb/Al ratios as a function of coverage on planar and bulk γ-Al_2O_3 as detected by XPS and ToF/SIMS. The XPS Pb/Al ratios for both the planar (a) and the bulk (b) are highly correlated to surface coverage. ToF/SIMS ratios also show strong correlations to surface coverage although the relationship for the planar oxides (c) is not as strong as for the bulk oxides (d). The agreement between the ToF/SIMS and XPS data suggests the formation of Pb monolayers on both oxide phases and also illustrates the quantitative abilities of ToF/SIMS analysis.

accurately tracks that on the bulk oxides (Fig. 11). However, note that Pb preferentially binds to the bulk oxide surface as indicated by the higher Pb/Al intensities on the bulk γ-Al_2O_3 surface compared to those seen on the planar oxide surface.

ToF/SIMS was used to probe the possible presence of oligomeric species on both the planar and bulk γ-Al_2O_3 surfaces. Figure 12 shows the intensity of Pb_2^+ and Pb_4^+ emission from each material as a function of coverage. At low coverages (Γ_{max}=0.01-1.0 $\mu mol/m^2$) neither dimeric nor tetrameric species were detected. Both dimers and tetramers were seen at coverages greater than Γ_{max}=1.0 $\mu mol/m^2$ for the bulk oxides but not for the planar oxide surfaces.

Discussion

The objective of this study was to demonstrate that Pb(II) sorption onto the planar oxide aluminum surface was similar to that of the bulk oxides. This was a necessary step in order to be able to connect studies using planar γ-Al_2O_3 to the existing knowledge based on Pb(II) sorption to bulk γ-Al_2O_3. The adsorption of Pb(II) as a function of pH (Fig. 9) showed the classic relationship of increasing metal adsorption with increasing hydroxyl activity; i.e., the presence of an adsorption edge corresponding to a sharp increase in adsorption due to decreasing competition with hydronium ions. Also, the adsorption edge was displaced to a higher pH with an increased adsorbate-adsorbent ratio in the presence of the planar oxides. This indicates that the complexation behavior of Pb(II) on bulk γ-Al_2O_3 is not perturbed by the presence of planar oxides.

Reproduced with permission of the copyright owner. Further reproduction prohibited without permission.

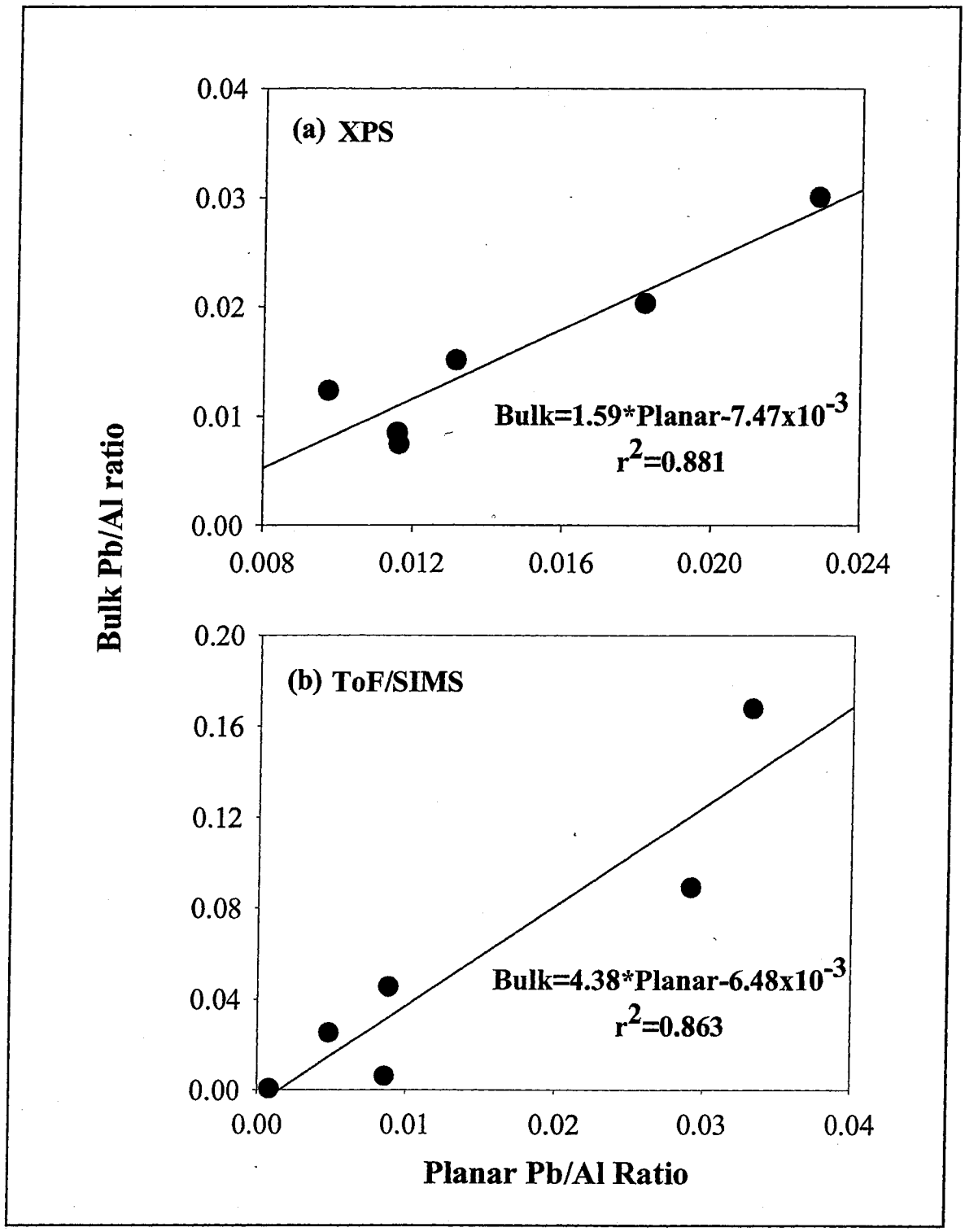

Figure 11. (a) XPS and (b) ToF/SIMS Pb(II) intensities normalized to Al for the planar oxides vs. the bulk oxides over a range of coverages. The high degree of linearity in both cases suggests that increases in Pb(II) sorption coverage on the planar oxides with increasing Pb(II) solution concentrations are proportional to that on the bulk. However, the slopes of the regression lines combined with the higher Pb/Al intensities found on the bulk γ-Al_2O_3 indicate that Pb preferentially binds to the bulk oxide surface.

Reproduced with permission of the copyright owner. Further reproduction prohibited without permission.

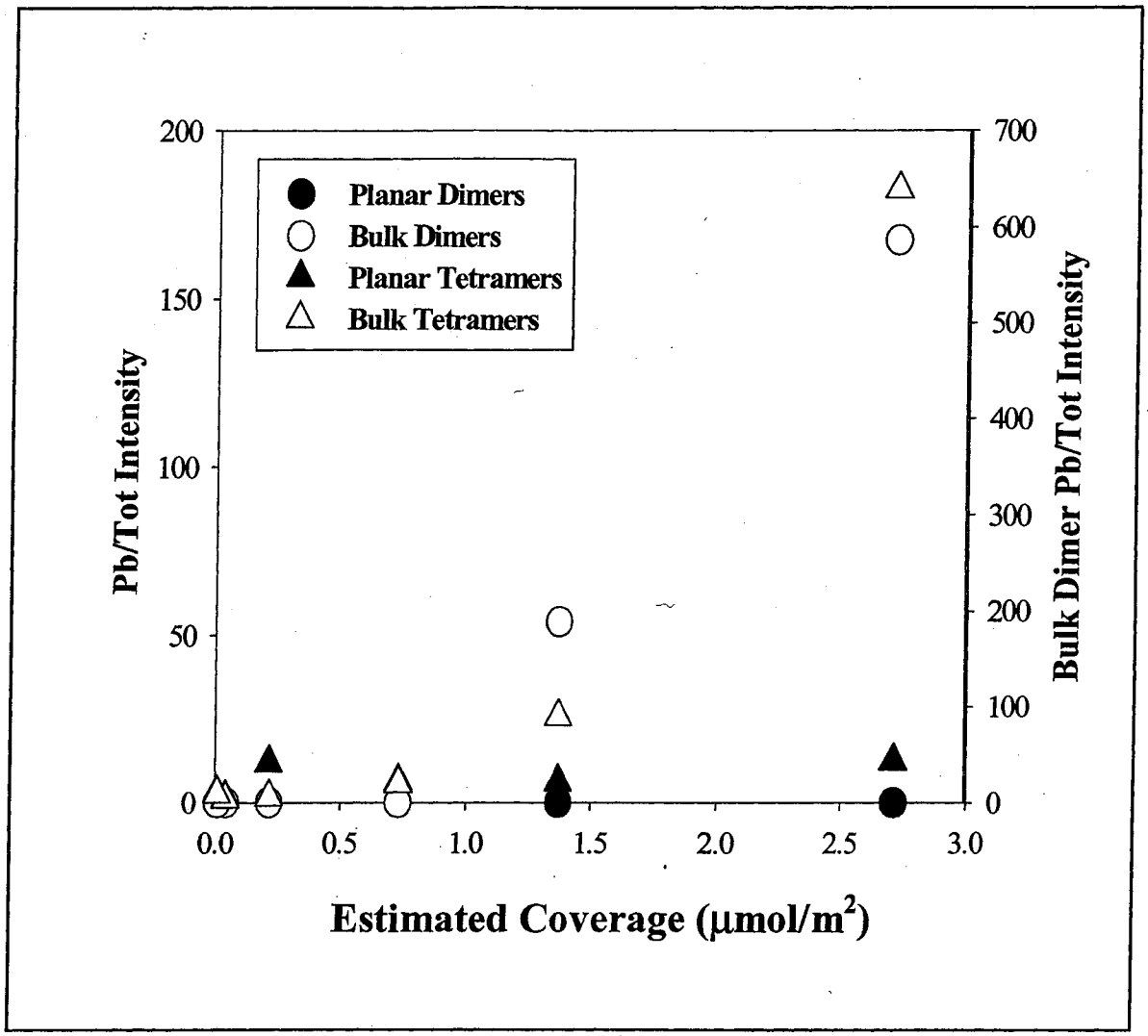

Figure 12. Presence of oligomeric Pb species over a range of surface coverages as detected by ToF/SIMS Pb intensities normalized to total counts. The y-axis on the right side of the figure indicates the Pb/Tot intensities for the dimeric species found on the bulk γ-Al_2O_3. At coverages < 1.0 $\mu mol/m^2$, there are no detectable dimers or tetramers on either the planar or bulk oxide surface. At coverages > 1.0 $\mu mol/m^2$, Pb dimers and tetramers are found on the bulk γ-Al_2O_3 only also supporting the conclusion that Pb preferentially binds to this phase.

Reproduced with permission of the copyright owner. Further reproduction prohibited without permission.

The direct relationship between sorbed Pb(II) concentrations on the bulk and planar γ-Al_2O_3 strongly suggests that the Pb(II) surface complexes formed on each oxide are similar. Specifically, ToF/SIMS results show that the increases in coverage with increasing Pb(II) solution concentrations on bulk γ-Al_2O_3 are accompanied by a proportional increase with coverage on the planar oxide surface (Fig. 11). Additionally, in both the ToF/SIMS and XPS spectra, the Pb/Al ratios for the planar and for the bulk oxides exhibit a strong relationship with Pb coverage (Fig. 10). The concurrence of these two analytical tools suggests that the character of the Pb sorption complexes formed on both solids under comparable conditions ($[Pb]_{TOT}$ and pH) is similar for a large range of surface coverages (Γ=0.008-2.7 $\mu mol/m^2$). Specifically, based on the solution composition, it is not expected that Pb precipitates will form at the lowest coverages. The XPS and ToF/SIMS data are linear with loading indicating a common sorption regime suggesting the formation of monolayers on both the planar and bulk oxides over the range of coverages studied. If multilayers of sorbed Pb were forming on the surface, XPS Pb/Al ratios would not show the same agreement with coverage as ToF/SIMS because of the different penetrations depths associated with each method (ToF/SIMS≈single monolayer vs. XPS≈several monolayers); the ToF/SIMS ratios would indicate a lower concentration of sorbed Pb than was actually present.

While the overall character of the sorption complexes was similar on each surface, the data suggest that Pb preferentially binds to bulk γ-Al_2O_3. In particular, both the higher ToF/SIMS and XPS ratios for co-equilibrated samples and the slopes > 1 of the regression lines for Pb/Al intensities on the planar vs. bulk oxides illustrate this (Fig. 11). Also, while spectroscopic relationships for the bulk and planar oxides were similar,

Reproduced with permission of the copyright owner. Further reproduction prohibited without permission.

the relationship between Pb/Al ratios and coverage was slightly weaker for the planar γ-Al_2O_3 (Fig. 10). These results may be due to differences in the distribution of reactive sites on the two surface phases. Five distinct reactive sites exist on bulk γ-Al_2O_3, the number and type of which depending on the crystallographic planes exposed (Cocke et al., 1984; Knözinger and Ratnasamy, 1978; Davis and Hem, 1989); in contrast, the planar oxide surfaces may be preferentially oriented and thus may contain only a subset or a different distribution of the reactive surface sites seen in the bulk phase. Thus, the relative abundance of high-affinity binding sites may differ between the two forms of γ-Al_2O_3. Two potential sources of artifacts may also be causing the apparent preferential binding and cannot be ruled out at this point. One is the familiar "cherry pit" effect, which would enhance the Pb XPS signal from the bulk γ-Al_2O_3. Similarly, because the ToF/SIMS ion penetration depth is much greater than the bulk γ-Al_2O_3 particle diameter, enhancement of the Pb signal may also occur. While this may lead to a seemingly higher amount of Pb on the bulk oxides, the sorption mechanism for high affinity sites seems to be equivalent on the planar and bulk oxides.

The formation of oligomeric species as detected by ToF/SIMS also suggests that Pb(II) preferentially binds to the bulk oxide surface (Fig. 12). The formation of dimers and tetramers is consistent with aqueous Pb(II) speciation behavior (both dimers and tetramers from at higher Pb concentrations and pH) as well as other studies of Pb(II) sorption (Baes and Mesmer, 1976; Chisholm-Brause et al., 1990; Bargar et al., 1997). While it is not certain whether these species were present on the surface or formed in the plume as a result of excitation of surface atoms, their appearance from only the bulk oxides at equivalent Pb loadings points toward a surface origin. Further investigation of

Reproduced with permission of the copyright owner. Further reproduction prohibited without permission.

these samples using complimentary spectroscopic methods such as EXAFS will greatly clarify the presence and sizes of Pb oligomeric species, as well as confirm that they exist on the surface itself and are not an artifact of instrumental operation.

Reproduced with permission of the copyright owner. Further reproduction prohibited without permission.

CHAPTER 4

XAS Investigation of Pb(II) Sorption to Planar and Bulk γ-Al_2O_3

Introduction

Lead contamination of surface waters, aquifers, soils and sediments result from its use in the petroleum industry as an antiknock agent as well as from other sources such as batteries, paints, alloys and solder, ammunition, and byproducts from mining and smelting activities (Elbaz-Poulichet et al., 1984; Müller and Sigg, 1990; Brown et al., 1999). The fate of lead, which is found primarily in the divalent form (Pb(II)), in natural aquatic systems is highly coupled to sorption and desorption reactions on particle surfaces. Among the phases controlling Pb dispersal in aquatic systems are natural Al-oxides and Al-hydroxides. These phases are abundant in soils and sediments as high-surface area colloids, minerals and mineral coatings (Hem, 1976; Rubin, 1976; Kinniburgh and Jackson, 1981; Coston et al., 1995). To accurately model and predict the transport of Pb(II) through natural systems, knowledge of the molecular scale interactions of Pb(II) with aluminum oxides is necessary. Recently, many studies have relied on x-ray absorption fine structure (XAFS) spectroscopy to obtain this type of information for Pb(II) sorbed to bulk phase or single crystal aluminum oxides (Chisholm-Brause et al., 1990; Bargar et al., 1997; Strawn et al., 1998).

XAFS spectroscopy is well suited to studying metal sorption on oxide surfaces as it provides quantitative molecular information including metal-oxygen bond lengths,

Reproduced with permission of the copyright owner. Further reproduction prohibited without permission.

coordination numbers, and the chemical identities of atoms in the immediate vicinity of the adsorbed metal ions (Norman and King, 1990; Brown, 1988). As such, XAS can be used to distinguish between different types of sorption complexes based on differences in the second coordination shell of the sorbing atom. For example, in an inner-sphere complex (Fig. 2, Chapter 1), the second neighbor metal atoms for a monomeric complex would be those in the solid substrate, whereas for a precipitate (Fig. 2, Chapter 1) they would be other sorbate metal ions (Roe et al., 1991). Additionally, the metal-sorbate bond distances for an inner-sphere complex would be much shorter than the metal-sorbate bond distances for an outer-sphere complex (Fig. 2, Chapter 1) where the sorbing ion retains its inner hydration sphere.

Lead sorption to oxide surfaces, mainly Al and Fe oxides, has been extensively studied using XAFS under a wide range of conditions (Chisholm-Brause et al., 1990; Yu et al., 1990; Roe et al., 1991; Bargar et al., 1996; Bargar et al., 1997; Bargar et al., 1998; Cheah et al., 1998; Strawn et al., 1998; Bargar et al., 1999; Morin et al., 1999; Ostergren et al., 1999; Strawn and Sparks, 1999; Strawn and Sparks, 2000; Elzinga et al., 2001; Trivedi et al., 2003). In most cases, Pb(II) has been found to form inner sphere complexes on both iron and aluminum oxides. At low surface coverages, Pb(II) is predominantly found as a monomeric inner-sphere complex. However, at higher surface coverages (generally >1.5 $\mu mol/m^2$) polymeric species have been observed on various oxide surfaces (Chisholm-Brause et al., 1990; Roe et al., 1991; Bargar et al., 1997). The formation of Pb(II) surface complexes has also been studied in the presence of complexing ligands such as chlorides, sulfates and EDTA. In these cases, Pb(II) was generally found to form outer-sphere complexes on iron and alumina oxide surfaces

Reproduced with permission of the copyright owner. Further reproduction prohibited without permission.

(Bargar et al., 1999; Strawn and Sparks, 1999; Elzinga et al., 2001). Pb(II) sorption can also be affected by the crystallographic faces present. Bargar et al. (1996) demonstrated that Pb(II) formed well-defined outer-sphere surface complexes at specific surface sites on the α-Al_2O_3 (0001) single crystal surface, while more strongly bound inner-sphere complexes were found on α-Al_2O_3 (1102) surfaces.

Previously, we have investigated and compared Pb(II) sorption to planar and bulk γ-Al_2O_3 to asses the reactivity of the planar oxides relative to their pure phase counterparts (Conrad et al., 2002). It was found that while the overall uptake behavior on the planar oxides was comparable to that seen on the bulk, there were minor differences in the quantitiy of Pb(II) sorbed as well as the type of complex present. Lead was found to preferentially sorb to the bulk γ-Al_2O_3 relative to the planar materials as evidenced by higher Pb/Al ratios measured by ToF-SIMS and XPS. Also, ToF-SIMS detected the presence of polymeric species on the bulk oxides at coverages greater than 1.0 $\mu mol/m^2$ while these speices were not seen on the planar γ-Al_2O_3. However, it could not be determined by the methods used whether or not these polymeric species were actually present on the γ-Al_2O_3 surface or simply an instrumental artifact.

The purpose of this study is to characterize and compare the structure of Pb(II) sorption complexes formed on planar and bulk γ-Al_2O_3 over a range of surface coverages using XAFS spectroscopy. The number, identities and distances of atoms surrounding the sorbed Pb(II) will be identified to allow for a molecular-level comparison of the sorption complexes formed that will be complementary to the quantitative analysis performed in Chapter 2.

Reproduced with permission of the copyright owner. Further reproduction prohibited without permission.

Materials and Methods

Aluminas

γ-Alumina powders were obtained from DeGussa Corp (DeGussa Alumina C) and was used as received. Planar γ-Al_2O_3 were prepared according to Hart and Maurin (1965) and were obtained from DuPont. More information on the chemical and physical properties of these materials can be found in chapter 2.

Sorption Samples

Pb(II) sorption on bulk γ-Al_2O_3 in the presence of planar oxides was determined for a range of Pb/γ-Al_2O_3 ratios (Table 7). All samples were prepared in a glove box under N_2 using N_2-sparged solutions to exclude CO_2 from the atmosphere. All solutions were prepared with ACS reagent grade chemicals and doubly deionized water (DDI). Planar and bulk oxides were reacted together in the same vessels in order to ensure identical experimental conditions. After equilibrating in the glove box for 20-24 hours, the dry solids were mixed with a slightly acidic 0.01M $NaNO_3$ solution for 24 hours prior to the addition of $Pb(NO_3)_2$. The pH was adjusted to 6.0 ± 0.1 by the addition of carbonate-free 1M NaOH. The initial Pb(II) concentration was 130 μM (± 5%), with different maximum coverages (Γ_{max} = 0.27 to 2.3 μmol/m^2) obtained by varying the ratio of bulk γ-Al_2O_3/solution (Table 7). A total of 25 planar aluminas measuring 3cm x 1cm were used for each coverage. After mixing for 24 hours, the solids and supernatants were separated by centrifugation. The pH of the supernatant was measured, and the solutions were acidified with 1M HNO_3 (10% by volume) for Pb(II) analysis. Total aqueous Pb(II) concentrations were determined spectrophotometrically using a Perkin Elmer AAnalyst

Reproduced with permission of the copyright owner. Further reproduction prohibited without permission.

Atomic Absorption Spectrophotometer (AA). The amount of Pb sorbed was calculated as the difference between the initial and final Pb concentrations.

Table 7. XAFS Pb(II) sorption sample preparation conditions*

Sample	1	2	3	4
Sol/Liq (g/L)	2.48	0.62	0.31	0.21
V_T (L)	0.038	0.038	0.038	0.038
$[Pb]_T$ (mM)	0.143	0.149	0.149	0.149
$[Pb]_{eq}$ (mM)	0.071	0.113	0.109	0.098
Γ ($\mu mol/m^2$)	0.27 ± 0.02	0.45 ± 0.01	1.2 ± 0.2	2.3 ± 0.6

*All samples were prepared in 0.01M $NaNO_3$ and adjusted to pH 6.0. $[Pb]_T$ is the total amount of lead (molarity) in the system and $[Pb]_{eq}$ is the final concentration of dissolved Pb(II). Γ is the Pb coverage on the oxide based on the g bulk γ-Al_2O_3 present in the system.

XAFS Data Collection

For XAFS data collection, the bulk γ-Al_2O_3 were packed in 25mm x 4mm x 2mm wells cut into a solid aluminum block measuring 37mm x 12mm x 12mm and sealed with Kapton tape. When needed, samples were diluted with H_3BO_3 to prevent self-adsorption effects (Table 8). The aluminum blocks were then mounted on a copper cold finger with a 3cm x 1cm opening. The planar oxides (25 strips, each measuring 3cm x 1cm) were stacked one on top of the other and mounted to the copper cold finger. All samples were cooled to 77 K prior to analysis by placing them in liquid nitrogen.

Fluorescence-yield Pb L_{III}-edge XAFS data were collected using a 30 element solid state detector at the National Synchrotron Light Source (NSLS) on beamline X-10C in April 2004. A Si 220 crystal monochromator was used to tune the incident x-rays to the Pb-L_{III} absorption edge (13055 eV). Tantalum coated bent cylindrical mirrors were used to reject high-energy harmonics. Slits were used to define a 0.3mm vertical beam as

Reproduced with permission of the copyright owner. Further reproduction prohibited without permission.

x-rays entered the hutch. The sample was positioned at 45° to the incident x-rays, and the detector was positioned at 90° to the incoming x-ray path. An arsenic filter was used to reject elastically scattered primary x-rays. For the bulk sorption samples, four to ten scans were typically collected. For the planar sorption samples, 25 scans were collected. Scan parameters can be found in Appendix 3.

Table 8. Dilution factors of XAFS powder samples

Sample Γ ($\mu mol\ m^{-2}$)	mg Bulk γ-Al_2O_3 Sorption Sample	mg H_3BO_3	% Pb by wt.
0.27	200	0	6.2
0.45	200	0	10.4
1.2	100	100	1.2
2.3	30	170	0.7
PbO (tetrahedral)	20	200	0.5

XAFS Data Analysis

The XANES region extends from about a few eV below to about 50 eV above the absorption edge (13055 eV) and results from multiple-scattering resonances of the photoelectrons ejected at low energies. While quantitative analysis of the XANES region is difficult and will not be dealt with here, there is still useful qualitative information in this portion of the spectra. In this study, the XANES region will be used to qualitatively assess similarities and differences in the local geometry surrounding the sorbing Pb(II) atom.

The EXAFS region extends from approximately 50 eV to approximately 1000 eV above the absorption edge. In this region, the dominant process is single-scattering of electrons off neighboring atoms. EXAFS spectra of sorption samples and model

Reproduced with permission of the copyright owner. Further reproduction prohibited without permission.

compounds were quantitatively analyzed using IFEFFIT (Newvill, 2001) and SixPACK version 0.52 analysis software (Webb, 2002). Spectra were background subtracted by a linear extrapolation of the pre-edge absorbance through the energy region above the edge. Fitting a quadratic spline through the background-subtracted data isolated EXAFS oscillations. The EXAFS was then analyzed in k-space, where k is the momentum of the photoelectron (in $Å^{-1}$). A k-weighting of 3 was used to fit the oscillations, which are described by the equation:

$$\chi(k) = S_0^2 \sum_{i=1}^{n} \frac{N_i F_i(k,R_i)}{kR_i^2} \exp\left(\frac{-2R_i}{\lambda(k,R_i)}\right) \times \exp(-2\sigma_i^2 k_i^2) \sin[2kR_i + \varphi_i(k,R_i) + \varphi_c(k)] \quad (4)$$

In this equation, S_0 is an amplitude reduction factor, N_i is the number of atom type i coordinated to the central atom, F_i is the effective EXAFS scattering amplitude function, R_i is the absorber-backscatterer distance for atom i, λ is the photoelectron mean-free path, σ_i is the harmonic Debye-Waller factor which describes the reduction in the backscattered amplitude due to thermal and static disorder, φ_i is the backscatterer EXAFS phase function, and φ_c is the central atom phase function.

Data were fit using a non-linear least squares procedure. Unsmoothed EXAFS data were fit using all components (i.e. all shells of backscattering neighbors) simultaneously to account for overlap of Fourier transform frequencies. The soundness of the fit was determined through visual inspection as well as through examination of the residual (F factor) and error terms of the fit. Backscattering functions required for spectra fitting were obtained from FEFF 7.0 calculations. The FEFF input parameters can be found in Appendix 3. Parameters derived from FEFF calculations were tested by fitting well-characterized crystalline model compounds. Spectra for tetrahedral Pb (PbO

Reproduced with permission of the copyright owner. Further reproduction prohibited without permission.

yellow) were collected using the methods described previously. $Pb(NO_3)_2$ (aq) spectra were collected from a 50 mM $Pb(NO_3)_2$ solution at room temperature as outlined in Roe et al. (1991). The β-$Pb_6O(OH)_6(ClO_4)_4 \bullet H_2O$ data were collected at room temperature and were provided by J. R. Bargar through a personal communication. From other studies of similar materials, it has been found that the distances of Pb-O bonds, $R_{Pb\text{-}O}$, and Pb-Pb bonds, $R_{Pb\text{-}Pb}$, are accurate to approximately ± 0.03 Å and ± 0.03 Å, respectively, and S_0^2 was set to 0.834. These parameters have been shown to predict the coordination numbers to ± 20% for first shell ions (Bargar et al., 1997). While it is not possible to directly evaluate the accuracy of bond distances of 2nd shell Al-backscatterers, it can be inferred from studies of other metal ions that the accuracy of the bond lengths for second shell Al backscatterers is approximately the same as for Pb backscatterers (O'Day et al., 1994; Cheah et al., 1996; Thompson et al., 1997). The error in the coordination numbers is likely quite large (20-30%) and therefore should be used for relative comparison of similarities and differences among sorption samples. During initial fitting of sorption samples, σ^2 values for oxygen, aluminum and lead backscatterers were allowed to vary and found to be ≤ 0.005 for oxygen and ≤ 0.004 for Al and Pb. To reduce the number of degrees of freedom, σ^2 values were fixed to these levels during further refinement.

Results

Interpretation of XANES Spectra

The Pb L_{III}-XANES spectra for the Pb(II) sorption samples to bulk γ-Al_2O_3 are shown in Figs. 13 and 15, and in Figs. 14 and 16 for the planar γ-Al_2O_3 samples. Spectral features in the XANES region are particularly sensitive to changes in the 1st-shell

Reproduced with permission of the copyright owner. Further reproduction prohibited without permission.

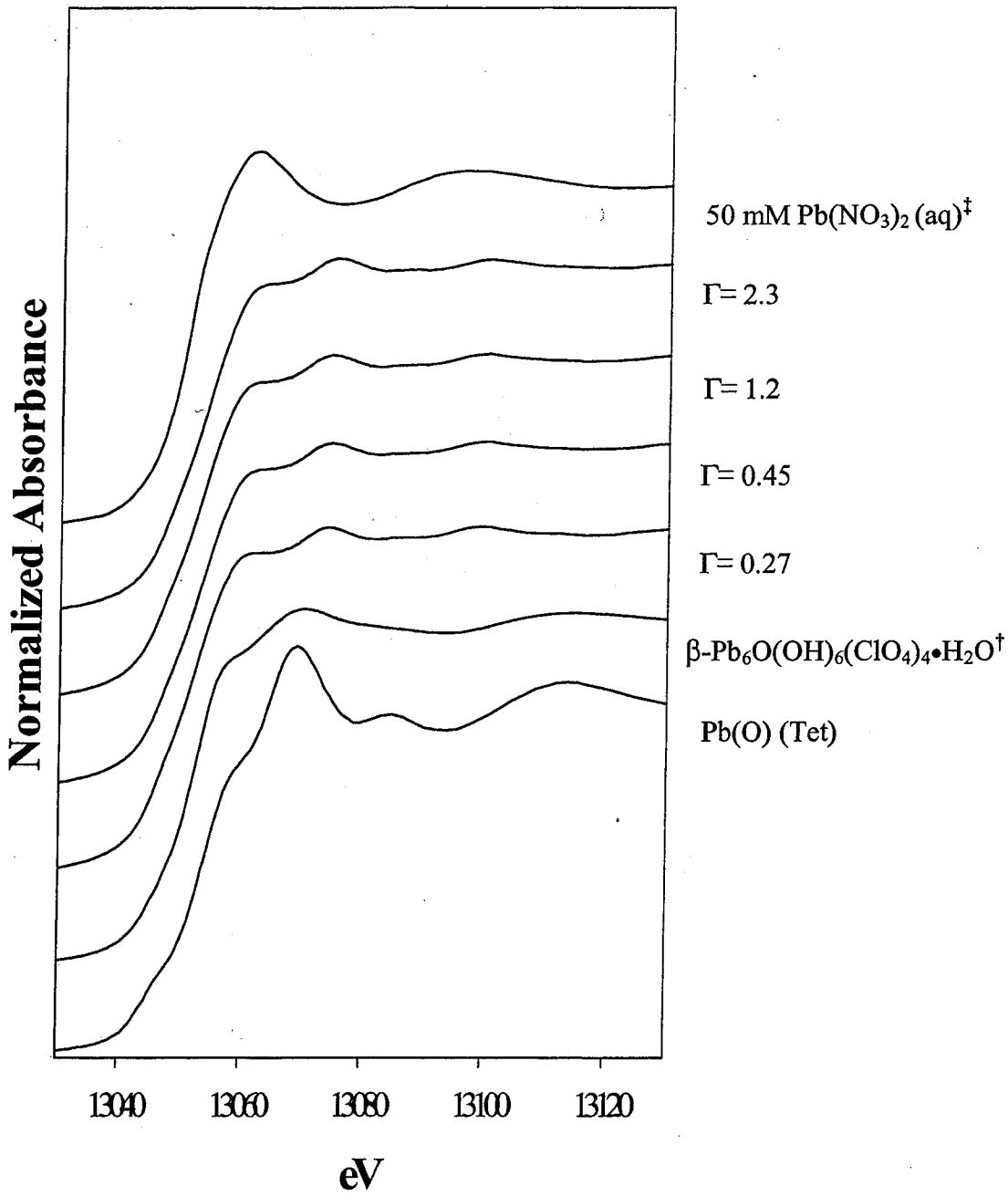

Figure 13. Normalized XANES spectra of Pb(II)/powder γ-Al_2O_3 sorption samples compared to XANES spectra of select model compounds. All sorption sample spectra were collected at 10K. †This compound contains $Pb_6(OH)_8$ units that serve as analogs to aqueous $Pb_6(OH)_8^{4+}$ complexes. ‡This solution contains >99% fully hydrated Pb(II) ions.

Reproduced with permission of the copyright owner. Further reproduction prohibited without permission.

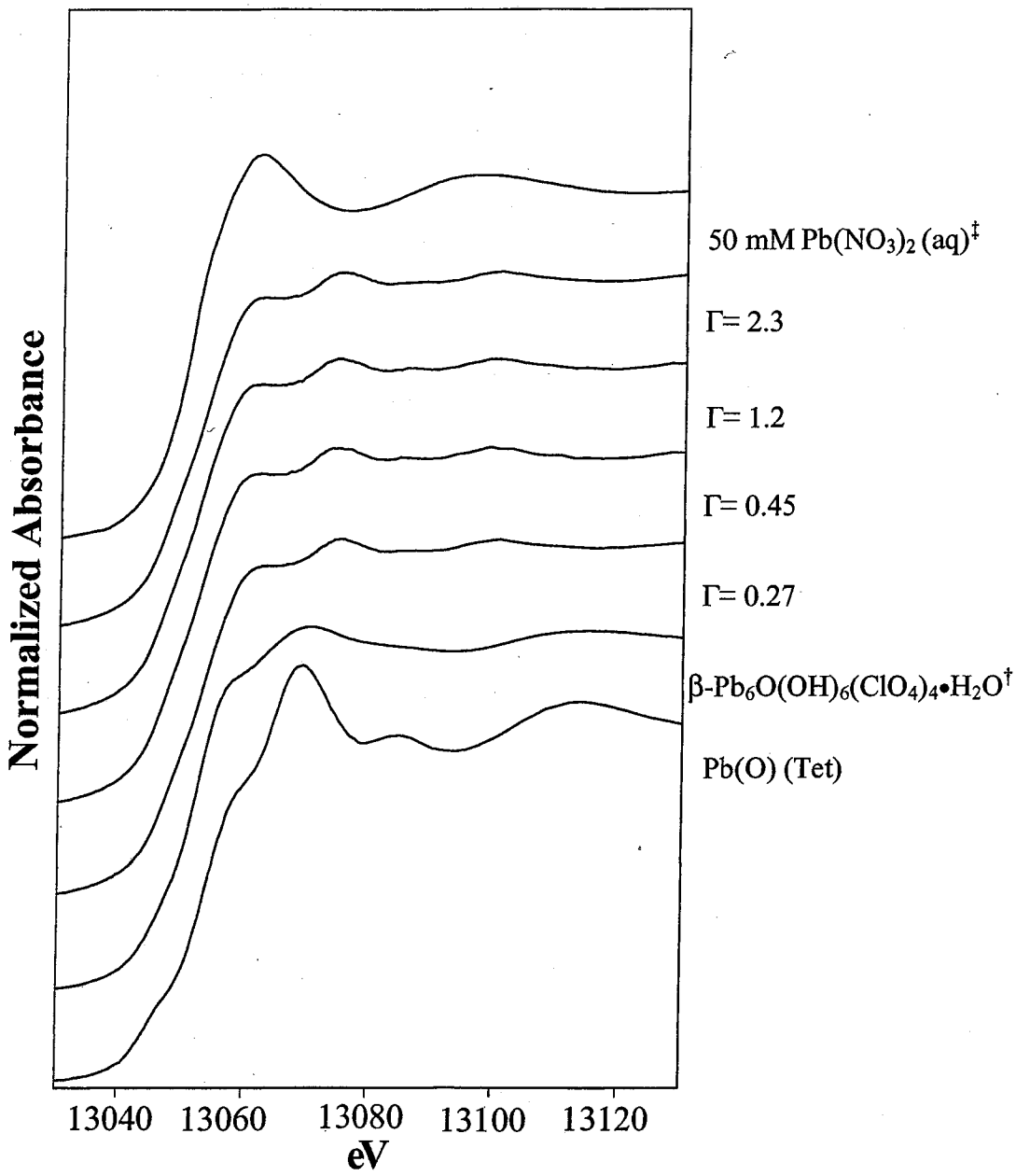

Figure 14. Normalized XANES spectra of Pb(II)/planar γ-Al_2O_3 sorption samples compared to XANES spectra of select model compounds. All sorption sample spectra were collected at 10K. †This compound contains $Pb_6(OH)_8$ units that serve as analogs to aqueous $Pb_6(OH)_8^{4+}$ complexes. ‡ This solution contains >99% fully hydrated Pb(II) ions.

Reproduced with permission of the copyright owner. Further reproduction prohibited without permission.

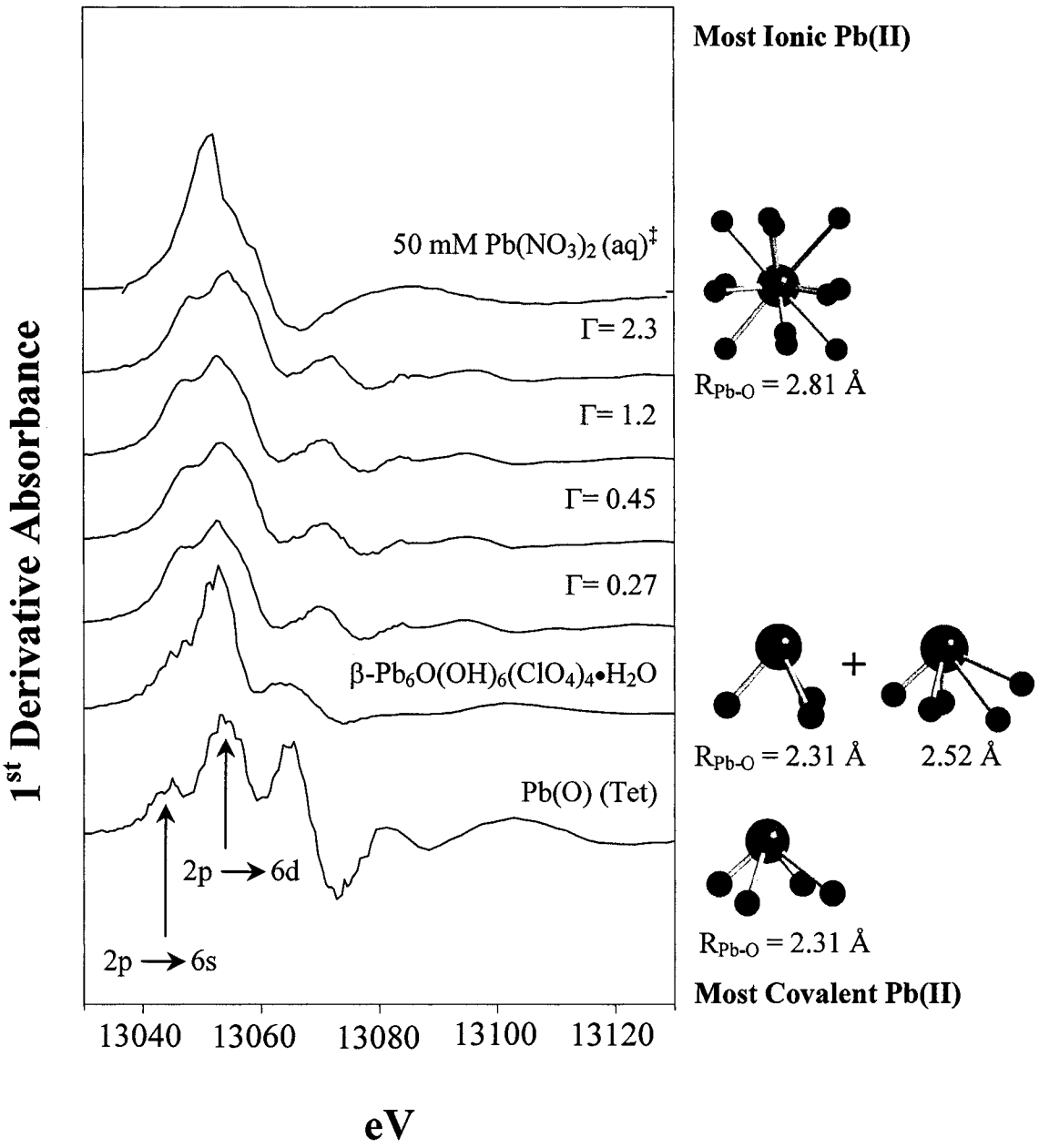

Figure 15. Normalized first derivatives of XANES spectra of Pb(II)/powder γ-Al_2O_3 sorption samples and model compounds shown in figure 14. Pb(II) coordination environments in the model compounds are illustrated to the right. Lead atoms are shown in green and oxygen atoms are shown in red.

Reproduced with permission of the copyright owner. Further reproduction prohibited without permission.

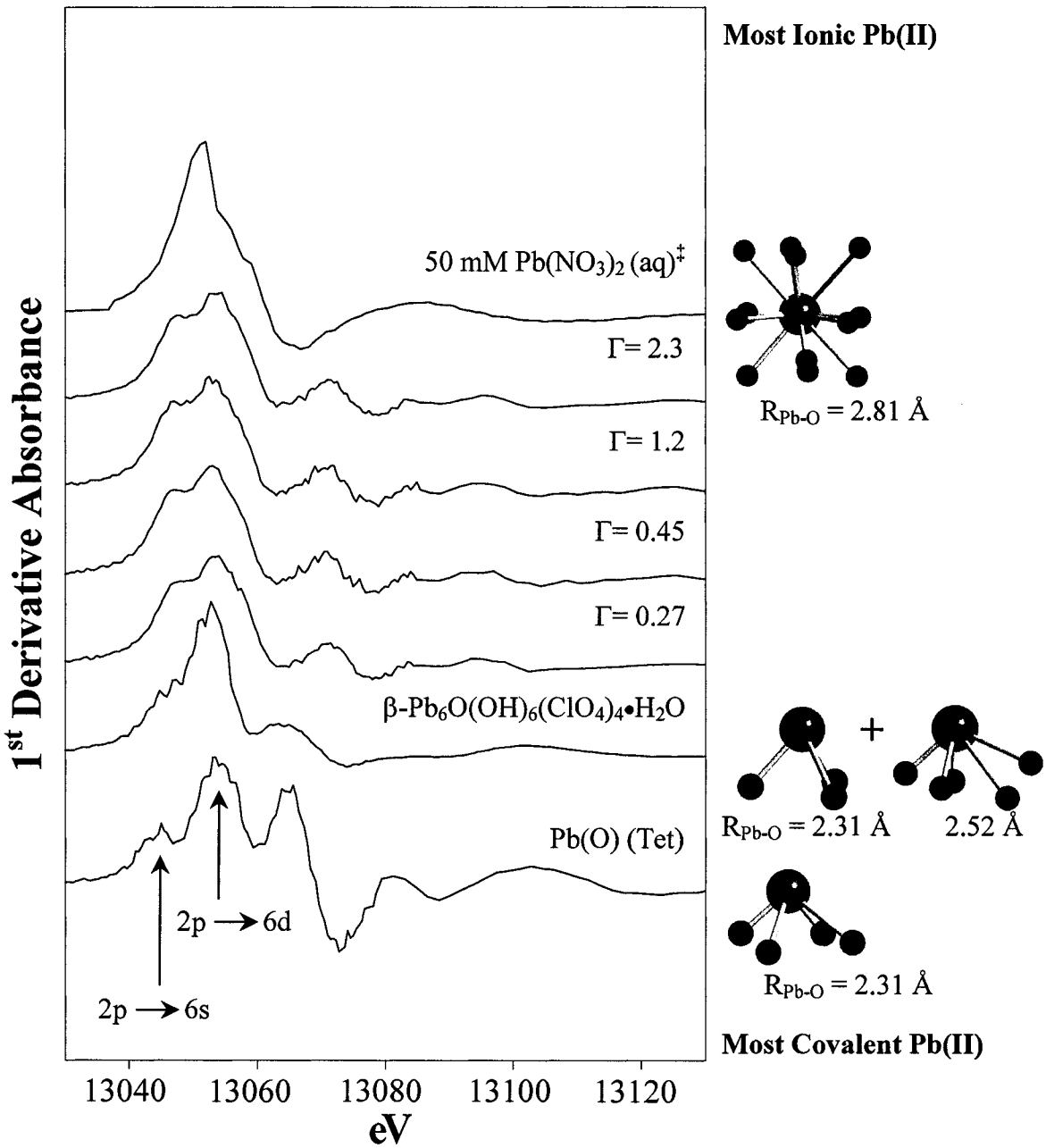

Figure 16. Normalized first derivatives of XANES spectra of Pb(II)/planar γ-Al_2O_3 sorption samples and model compounds shown in figure 15. Pb(II) coordination environments in the model compounds are illustrated to the right. Lead atoms are shown in green and oxygen atoms are shown in red.

Reproduced with permission of the copyright owner. Further reproduction prohibited without permission.

coordination environment of Pb(II), and as such can be used to assess differences and similarities in the Pb(II) sorption complexes formed on the alumina surfaces. Investigation of the model compound XANES spectra can illustrate how small changes in the 1st-neighbor oxygens around the absorbing Pb(II) atom can lead to significant differences in the structure of the XANES spectra. Consider PbO (s) with Pb tetrahedrally coordinated and β-$Pb_6O(OH)_6(ClO4)_4 \bullet H_2O$ (s) where Pb is both in a distorted trigonal pyramidal (Tyliszczak et al., 1990) and pentagonal pyramidal coordination (Spiro et al., 1969; Olin and Söderquist, 1972). The first compound has a small shoulder in its Pb L_{III} absorption edge followed by a very pronounced peak at 13075 eV. A smaller peak is seen at 13090 eV followed by a much broader peak at 13120 eV. In the XANES of the second compound, the shoulder is much more visible and the peak at 13075 eV is broader. There is no peak visible at 13090 eV and the peak at 13120 eV is barely visible as it is extremely broad.

The XANES spectra of the Pb(II) sorption samples to the bulk vs. the planar γ-Al_2O_3 oxides were very similar and did not change with increasing coverage, indicating a similar Pb-O environment on the planar vs. the bulk at all coverages studied. Both the bulk and planar Pb(II)/γ-Al_2O_3 sorption sample XANES spectra are characterized by a slight shoulder at 13063 eV followed by a low, broad peak at 13076 eV (Figs. 13 and 14). A small, broad peak can also be seen at 13101 eV. They are not entirely similar to any one model compound. The β-$Pb_6O(OH)_6(ClO4)_4 \bullet H_2O$ (s) has the same shoulder seen in the sorption samples, but the main peak is at 13070 eV with a smaller, broader peak at 13117 eV. The sorption samples are also dissimilar from the spectra for aqueous Pb(II). In this model compound, there is a very sharp peak at 13065 eV while no such peak is

Reproduced with permission of the copyright owner. Further reproduction prohibited without permission.

seen in the sorption sample XANES. The sorption samples do, however, contain the same weak, broad peak at 13100 eV that is seen in this model compound. This suggests that the molecular structure of Pb(II) adions on bulk γ-Al_2O_3 are different from Pb(II) bonded exclusively to water molecules. The sorption samples were also different from the PbO model compound. In the PbO XANES spectrum, a defined peak is seen at 13069 eV with a second well-defined peak at 13085 eV. No peaks are seen in the sorption spectra in these regions.

Plots of the 1st derivatives on the XANES spectra further illustrate the differences between the model compounds and the sorption samples (Figs. 15 and 16). The main peak in all compounds is found at 13055 eV, confirming the presence of Pb(II). Other peaks in the PbO model compound derivative spectrum are found at 13045 eV, 13065 eV, 13082 eV and 13103 eV. A peak similar to the 13045 eV peak is seen in the sorption samples at 13048 eV, although it is somewhat weaker. The β-$Pb_6O(OH)_6(ClO4)_4 \bullet H_2O$ (s) compound is missing the peaks at 13045 eV and 13082 eV relative to PbO. Only one other peak is seen in the derivative spectra of $Pb(NO_3)_2$ aside from the 13055 eV peak. It is found at 13089 eV. In contrast, the sorption sample derivatives all exhibit peaks at 13048 eV, 13073 eV, 13086 eV and 13097 eV. The sorption sample derivative spectra are most similar to the β-$Pb_6O(OH)_6(ClO4)_4 \bullet H_2O$ (s) spectra. Similar numbers and intensities of peaks are seen, but the peak positions are shifted to a lower eV in the model compound spectrum. These data support the assertion that the coordination environments of Pb(II) on the planar or bulk aluminas are not fully described by any one of the chosen model compounds.

Reproduced with permission of the copyright owner. Further reproduction prohibited without permission.

Interpretation of EXAFS Spectra

The k^3-weighted EXAFS spectra for the bulk and planar γ-Al_2O_3 sorption samples are shown in Figs. 17 and 18, respectively. The Fourier transforms of these spectra are shown in Fig. 19 for the bulk sorption samples and Fig. 20 for the planar sorption samples. The features seen in the EXAFS spectra of the bulk and planar γ-Al_2O_3 sorption samples were similar at low k ($k < 7$) but showed some deviations in peak amplitudes at higher k, likely reflecting differences in the second shell coordination environment of Pb(II) on the two oxides.

1st-Shell Pb(II) Coordination

All spectra have a dominant sinusoidal frequency which arises from 1st-shell oxygen backscattering. The frequency of this component can be seen in the uncorrected Fourier transforms (Figs. 19 and 20) as a large peak between 1.5 and 2.0 Å. Two Pb-O shells were used to fit these peaks with Pb-O distances of 2.21 - 2.32 Å for the first oxygen and 2.46 – 2.60 Å for the second oxygen in both the planar and bulk sorption samples (Table 9). The range of coordination numbers for Pb with oxygen was 3.8 – 4.5 and 3.0 – 4.0 in the bulk and planar sorption samples, respectively. These results are in good agreement with the XANES interpretation which suggested that the Pb-O coordination environment was similar on the bulk and planar γ-Al_2O_3 samples. The coordination numbers are also in agreement with previous studies which have showed typical coordination numbers for aqueous Pb(II) sorption samples being 3-4 (Chisholm-Brause et al., 1990; Bargar et al., 1997).

Reproduced with permission of the copyright owner. Further reproduction prohibited without permission.

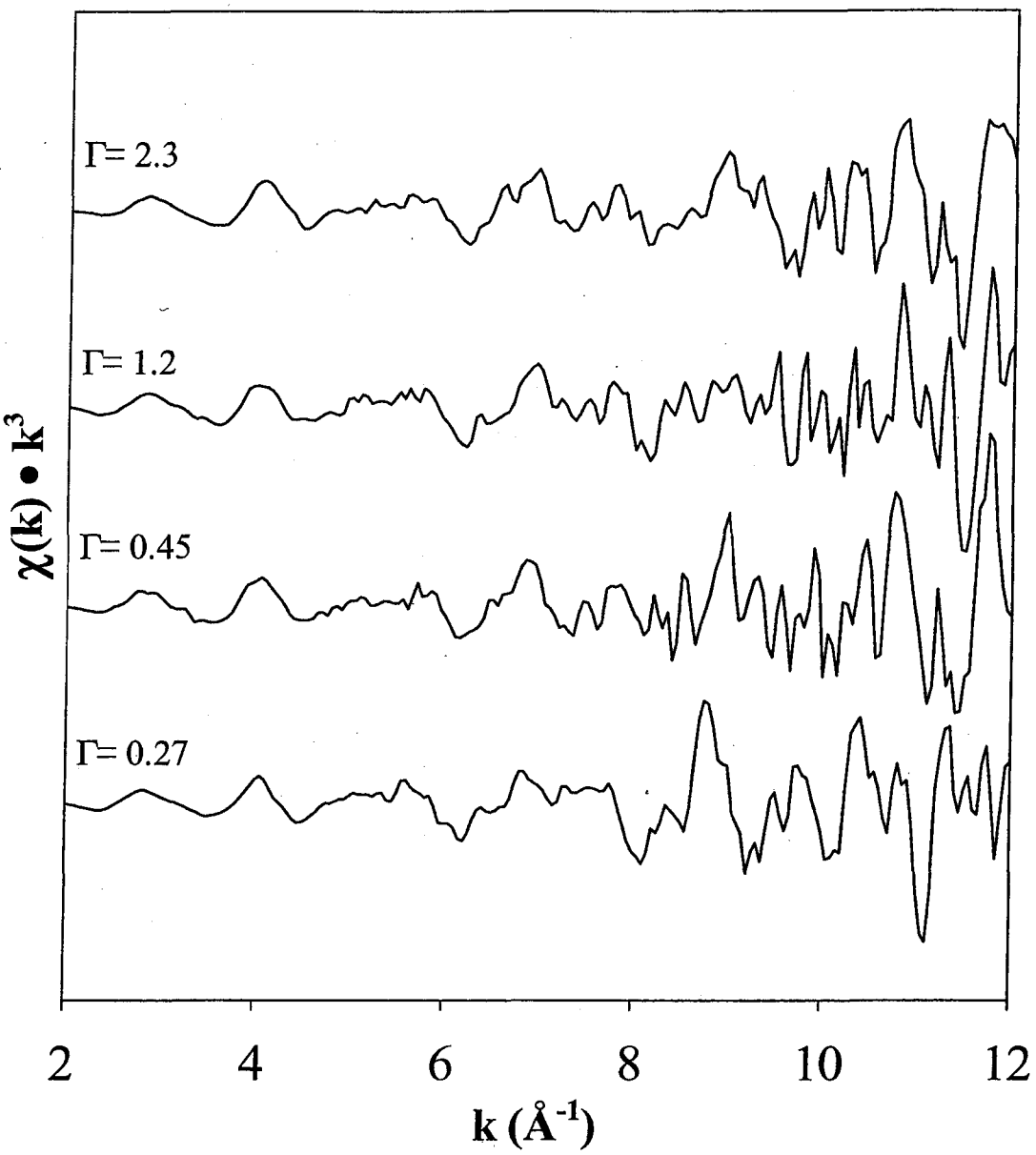

Figure 17. k^3-weighted normalized χ functions of Pb(II)/powder γ-Al_2O_3 sorption samples.

Reproduced with permission of the copyright owner. Further reproduction prohibited without permission.

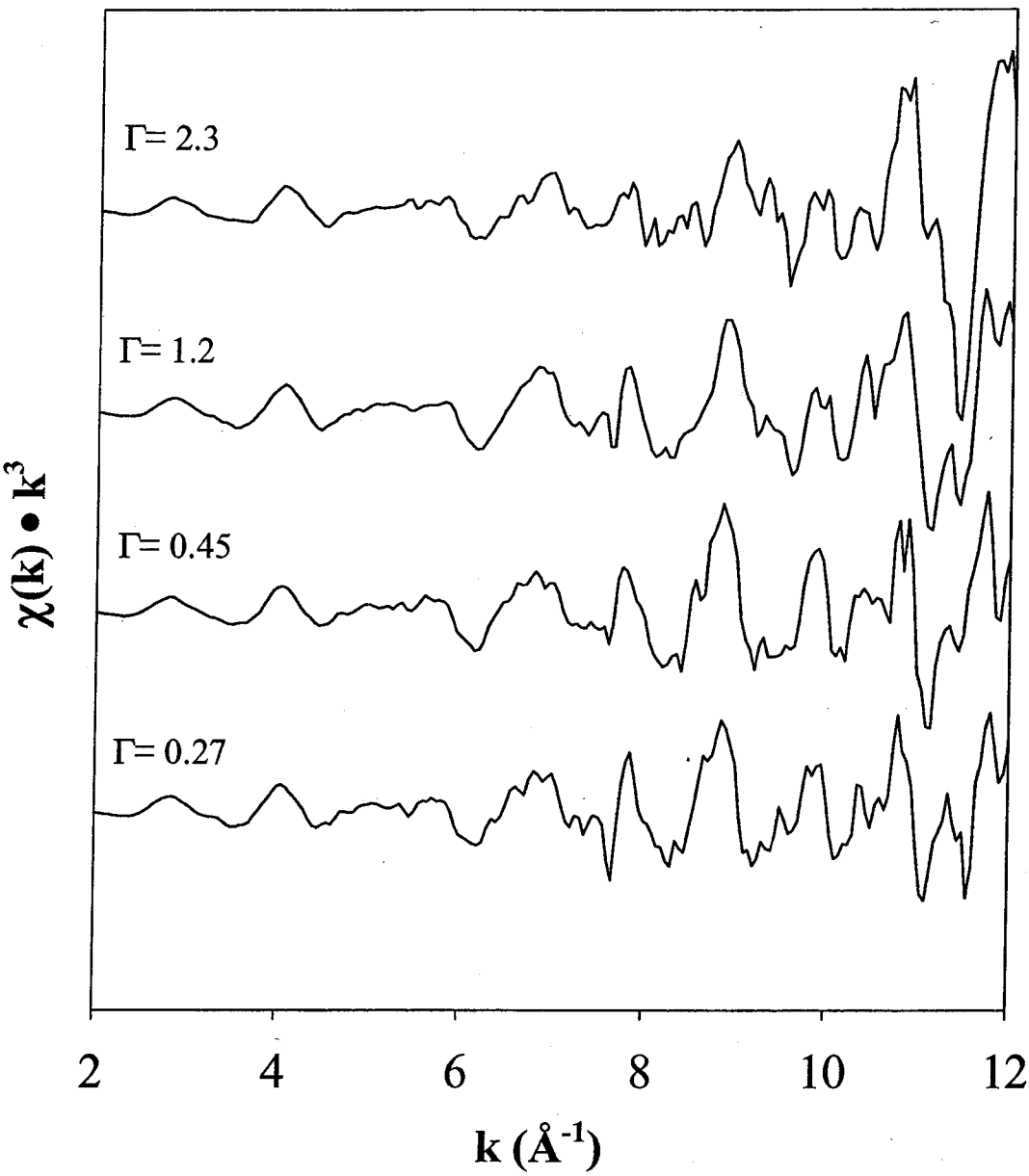

Figure 18. k^3-weighted normalized χ functions of Pb(II)/planar γ-Al_2O_3 sorption samples.

Reproduced with permission of the copyright owner. Further reproduction prohibited without permission.

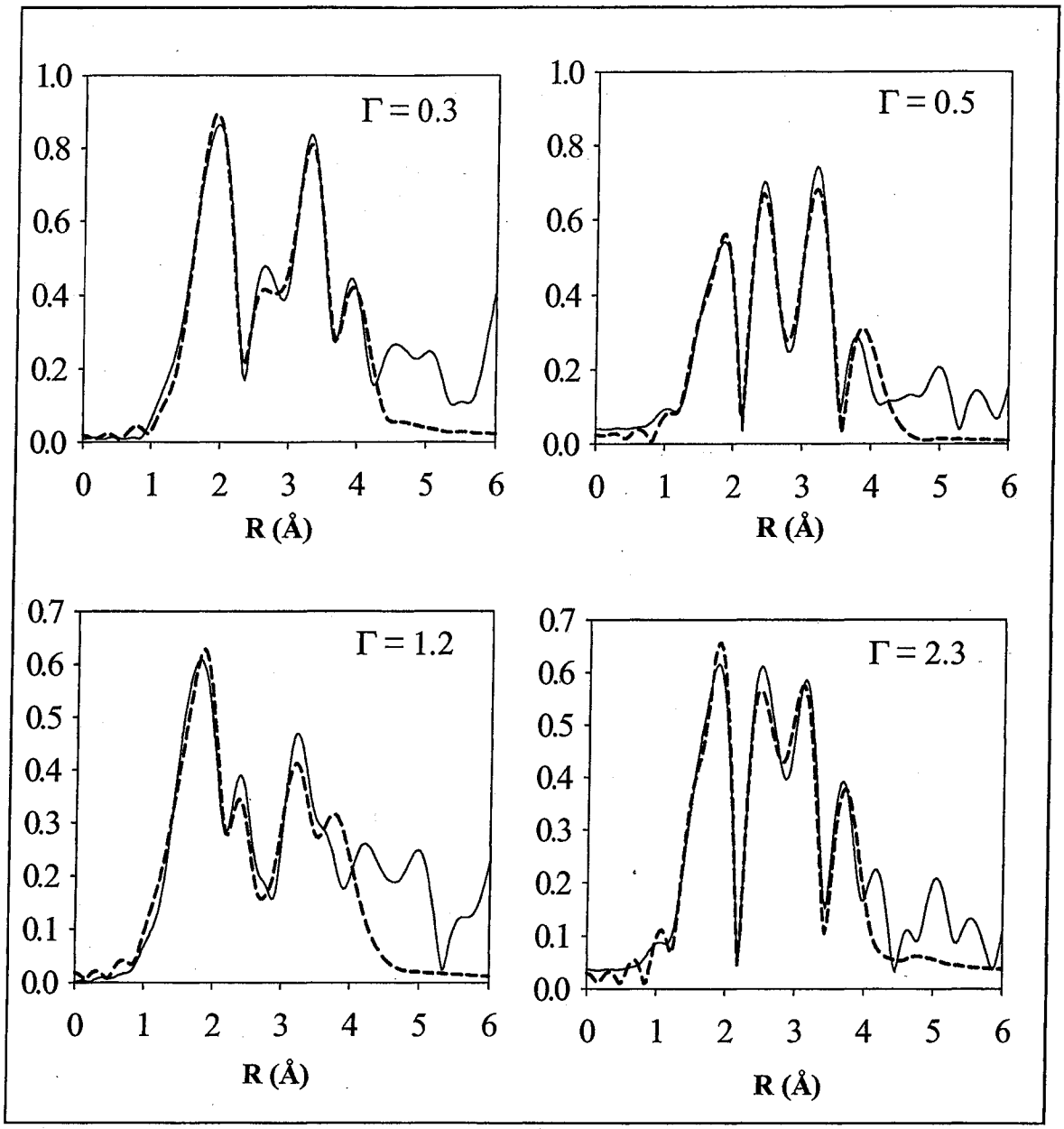

Figure 19. Fourier transforms of EXAFS spectra of Pb(II)/powder γ-Al_2O_3 sorption samples, uncorrected for phase shift. The data are shown with solid lines and the fits are shown with dashed lines.

Reproduced with permission of the copyright owner. Further reproduction prohibited without permission.

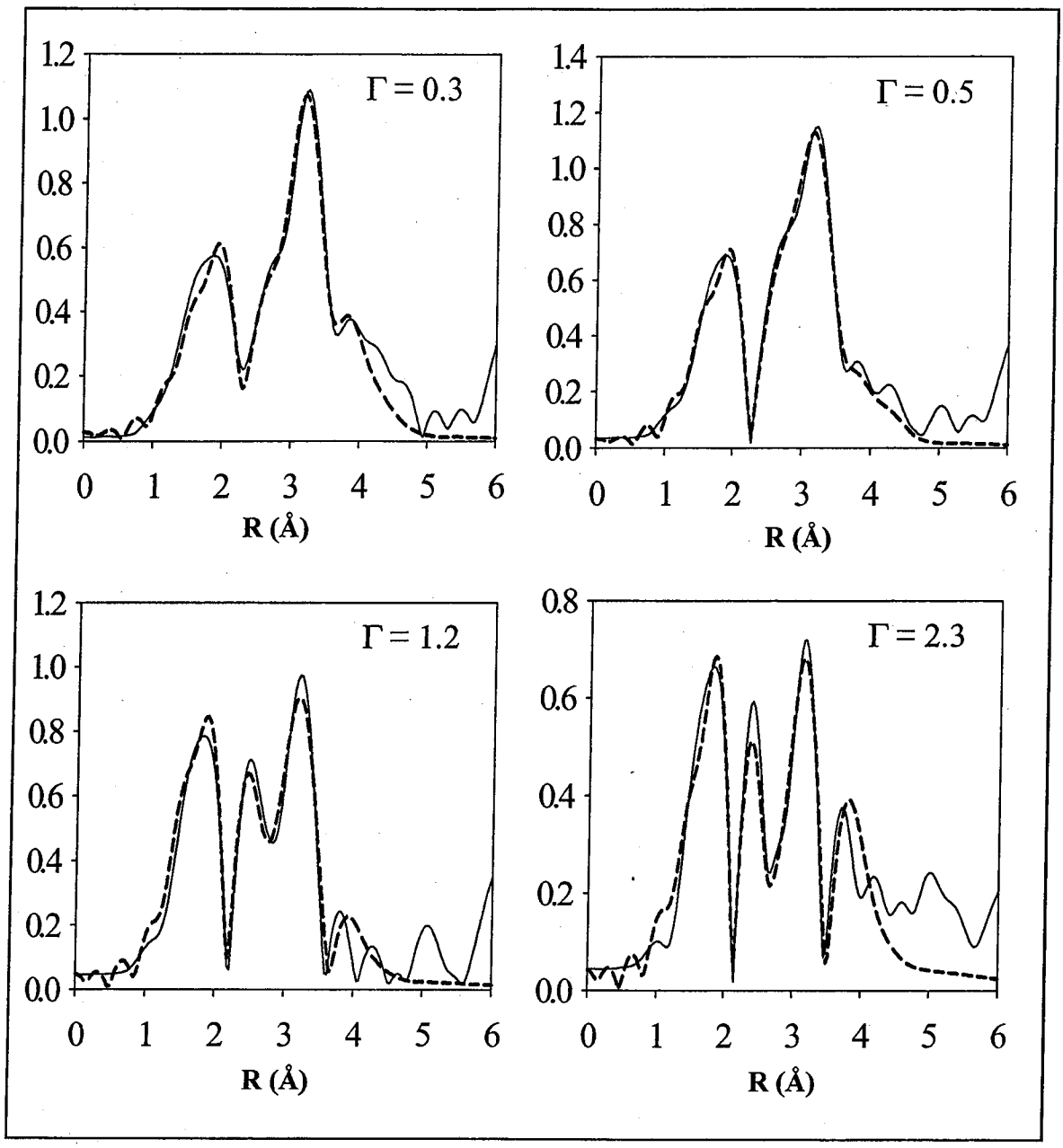

Figure 20. Fourier transforms of EXAFS spectra of Pb(II)/planar γ-Al_2O_3 sorption samples, uncorrected for phase shift. The data are shown with solid lines and the fits are shown with dashed lines.

Reproduced with permission of the copyright owner. Further reproduction prohibited without permission.

Reproduced with permission of the copyright owner. Further reproduction prohibited without permission.

Table 9. EXAFS fitting results for sorption samples and model compounds

	Pb-O 1		Pb-O 2			Pb-Al$_1$		Pb-Al$_2$			Pb-Pb			
Sample	**CN**	**R(Å)**	**CN**	**R(Å)**	‡‡σ^2	**CN**	**R(Å)**	**CN**	**R(Å)**	σ^2	**CN**	**R(Å)**	σ^2	**ΔE_0 (eV)**
Bulk Pb(II)/γ-Al_2O_3														
$\Gamma = 0.3$	1.50	2.31	2.35	2.60	0.006	0.66	3.17	2.18	4.06	0.007	1.62	3.69	0.002	-43.86
$\Gamma = 0.5$	1.56	2.25	2.50	2.50	0.005	1.41	3.28	3.66	4.33	0.006	1.57	3.54	0.005	-62.23
$\Gamma = 1.2$	1.87	2.21	2.22	2.49	0.009	1.09	3.23	3.89	4.22	0.007	1.48	3.54	0.006	-67.54
$\Gamma = 2.3$	2.05	2.25	2.45	2.48	0.006	0.75	3.30	4.56	4.23	0.003	1.20	3.52	0.004	-65.86
Planar Pb(II)/γ-Al_2O_3														
$\Gamma = 0.3$	2.10	2.32	1.99	2.59	0.008	1.42	3.50	2.33	4.14	0.006	1.46	3.62	0.004	-46.47
$\Gamma = 0.5$	1.92	2.31	1.82	2.56	0.006	1.50	3.50	1.68	4.17	0.004	1.03	3.61	0.003	-47.16
$\Gamma = 1.2$	1.92	2.25	1.92	2.49	0.004	0.90	3.32	2.56	4.32	0.003	1.72	3.56	0.004	-63.88
$\Gamma = 2.3$	1.45	2.22	1.52	2.46	0.004	0.81	3.24	3.78	4.23	0.003	1.77	3.53	0.003	-69.20
Model Pb(II)														
‡PbO (tet)	2.23	2.28			0.008						2.05	3.65	0.003	-5.60
β-$Pb_6O(OH)_6(ClO_4)_4$	3.16	2.29			0.008						3.10	3.77	0.030	-3.33
†$Pb(NO_3)_2$ (aq)	2.30	2.81			0.010						2.70	3.77	0.010	

‡Collected at 77 K. Other model compounds collected at room temperature. †Roe et al. (1991). ‡‡Values of σ^2 for Pb-Al 2 were fixed at the same values as σ^2 for Pb-Al 1. CN = coordination number (± 20 % for 1st-shell neighbors; because of the large error associated with the second shell CN, these numbers should be used as relative values and not absolute parameters), R = interatomic distance (± 0.03 Å for closest oxygens and ± 0.04 Å for Pb and Al), and σ^2 = Debye-Waller factor (Å^2).

Coordination environments of the model compounds are shown in figures 15 and 16. These compounds are arranged in order of increasing Pb-O distances, corresponding to a decrease in the covalent character of the bonding environment. As bond distances increase, the overlap of the molecular orbitals decreases creating bonds that are more ionic in character. The bond distances determined for the sorption samples on both the planar and bulk γ-Al_2O_3 samples are more covalent in nature as compared to the model compounds and agree most closely with the Pb-O distances seen in β-$Pb_6O(OH)_6(ClO_4)_4$, supporting the earlier XANES interpretation.

2nd Shell Pb(II) Coordination

Backscattering from 2nd neighbor atoms is also present in the EXAFS spectra of the sorption samples and can be seen in the Fourier transform at distances >2.5 Å. These peaks are due to Al and Pb backscatterers. For both the planar and bulk sorption samples, two Pb-Al shells could be fit to the data. The distances for the first Al backscatterers (Pb-Al_1) ranged from 3.17 – 3.30 Å for the bulk sorption samples and from 3.24 – 3.50 Å for the planar sorption samples. The second Al backscatterers (Pb-Al_2) were at distances of 4.06 - 4.33 Å in the bulk samples and 4.14-4.32 Å in the planar samples. Second shell Pb atoms were fit at distances of 3.52 – 3.69 Å and 3.53 – 3.62 Å for the bulk and planar sorption samples, respectively.

A trend in the second shell Al atoms can be seen in the bulk and planar Pb(II) sorption samples. For the bulk sorption samples with $\Gamma = 0.27$ μmol m^{-2}, the Pb-Al coordination numbers and distances seem to be unique from those at the higher coverages. A similar trend can be seen in the planar sorption samples at coverages ≤ 0.45

Reproduced with permission of the copyright owner. Further reproduction prohibited without permission.

μmol m^{-2} as the coordination numbers and bond distances are distinct from those at higher coverages. This trend is also evident in the fitting results of the second shell Pb atom (Table 9). Additionally, the relative proportions of Pb-Al_1 to Pb-Al_2 change as coverage increases, most notably on the bulk γ-Al_2O_3 samples.

Discussion

Pb-O Geometry

The lack of agreement of the sorption XANES and derivative spectra with the $Pb(NO_3)_2$ model compound indicates that the predominant Pb(II) species do not retain the primary hydration sphere upon sorption. This suggests that Pb(II) forms primarily inner sphere complexes with both the planar and bulk alumina surfaces at the coverages studied. This is in agreement with previous studies of Pb(II) sorption to bulk γ-Al_2O_3 at similar Pb(II) loadings (Chisholm-Brause et al., 1990; Bargar et al., 1997; Conrad et al., 2002). Comparing the planar and bulk γ-Al_2O_3 Pb(II) sorption samples to the model compounds, it is difficult to determine the exact coordination of the oxygen atoms surrounding Pb. XANES spectra of the sorption samples were not similar to any of the chosen model compounds, and differences were seen in the derivative spectra as well. The sorption samples appear to most similar to β-$Pb_6O(OH)_6(ClO4)_4 \bullet H_2O$. Thus, the 1st shell coordination environment of Pb is probably a mixture of distorted trigonal pyramidal and pentagonal pyramidal environments.

Distortion of the 1st shell coordination environment of Pb(II) is quite common due to the stereoactivity of a lone pair of electrons in Pb(II) complexes (i.e. non-bonded electron density localized in space) which repel oxygen atoms (Greenwood and

Reproduced with permission of the copyright owner. Further reproduction prohibited without permission.

Earnshaw, 1985; Huheey et al., 1993). Evidence for a distorted coordination environment in the sorption samples can be found in both the XANES and EXAFS spectra. In the XANES derivative spectra, it can be seen in the peak at 13,048 eV (Figs. 15, 16). From molecular orbital theory and comparison with other model compounds not discussed in this paper, it has been determined that the peak at 13,045 eV in the PbO derivative spectra (Figs. 15, 16) arises from a 2p→6s electronic transition, and that the peak at 13,055 arises from a 2p→6d electronic transition (Rao and Wong, 1984; Chisholm-Brause et al., 1990; Bargar et al., 1997). The energy difference between the Pb 6s and Pb 6d levels should correspond to the energy separation between the two peaks in the first derivative spectrum and is found to be 7 eV. However, this transition is not as defined in the sorption samples as it is in the PbO spectra. The lack of definition can be attributed to a distortion of the Pb(II) binding environment. If the Pb-O bond lengths were all of equal distance, the electronic splitting would be of equal energy. However, distortion of the binding environment would result in unequal Pb-O distances, causing the energies of the Pb 6s—6p to differ resulting in the broadening of the 2p→6s feature (Bargar et al., 1997). Supporting evidence for this distorted environment, or mixture of environments, is also seen in the EXAFS spectra by the need to use two Pb-O distances to fully fit the 1st shell peak of the Fourier transforms of the planar and bulk sorption samples (Figs. 19, 20). Generally, EXAFS is only sensitive to the oxygens closest to the Pb(II) atom in a distorted coordination environment. However, because our data were collected at low temperatures, it is possible to observe backscattering from slightly more distant 1st shell oxygens. The need to use two distinct Pb-O distances supports the

Reproduced with permission of the copyright owner. Further reproduction prohibited without permission.

presence of oxygen atoms positioned over a range of distances away from the Pb(II) atom.

Pb(II) Sorption Geometry

The range of distances for the Al backscatterers, combined with the 1st shell Pb-O distances can be used to constrain the structure of the Pb-Al sorption complex on the planar and bulk γ-Al_2O_3 surface. There are a finite number of ways in which Pb(II) can bind to Al_2O_3 surfaces. Each binding mechanism results in a characteristic Pb-Al distance (Bargar et al., 1997). Based on the Al-O bond lengths for AlO_6 octahedra and the EXAFS determined Pb-O bond lengths, the range of Pb-Al separations that could arise for Pb(II) ions adsorbed to alumina surfaces is $R_{Pb\text{-}Al}$ = 4.10-4.22 Å for a monodentate complex sorbed to the corners of an AlO_6 octahedra, $R_{Pb\text{-}Al}$ = 3.87-3.99 Å for a bridging bidentate complex sorbed to the corners of neighboring AlO_6 octahedra, and $R_{Pb\text{-}Al}$ = 2.91-3.38 Å for sorption to the edges of AlO_6 octahedra (Fig. 21).

The EXAFS-derived Pb-Al distances for the planar and bulk γ-Al_2O_3 Pb(II) sorption samples range fall into the ranges of two of these sorption geometries, corner-sharing monodentate and edge-sharing bidentate (Table 9). This supports the conclusion that Pb(II) is bound in an inner-sphere manner on both the planar and bulk oxide surfaces as predominantly monodentate complexes with smaller amounts of bidentate Pb-Al present. While the overall identity of the surface complexes are the same for the entire sample set, the local structure of these complexes differs at low vs. high coverages. At low coverage (Γ = 0.27 μmol m^{-2}), the Pb-Al distances for both the monodentate and bidentate complexes are shorter than those at higher coverages on the bulk γ-Al_2O_3. At

Reproduced with permission of the copyright owner. Further reproduction prohibited without permission.

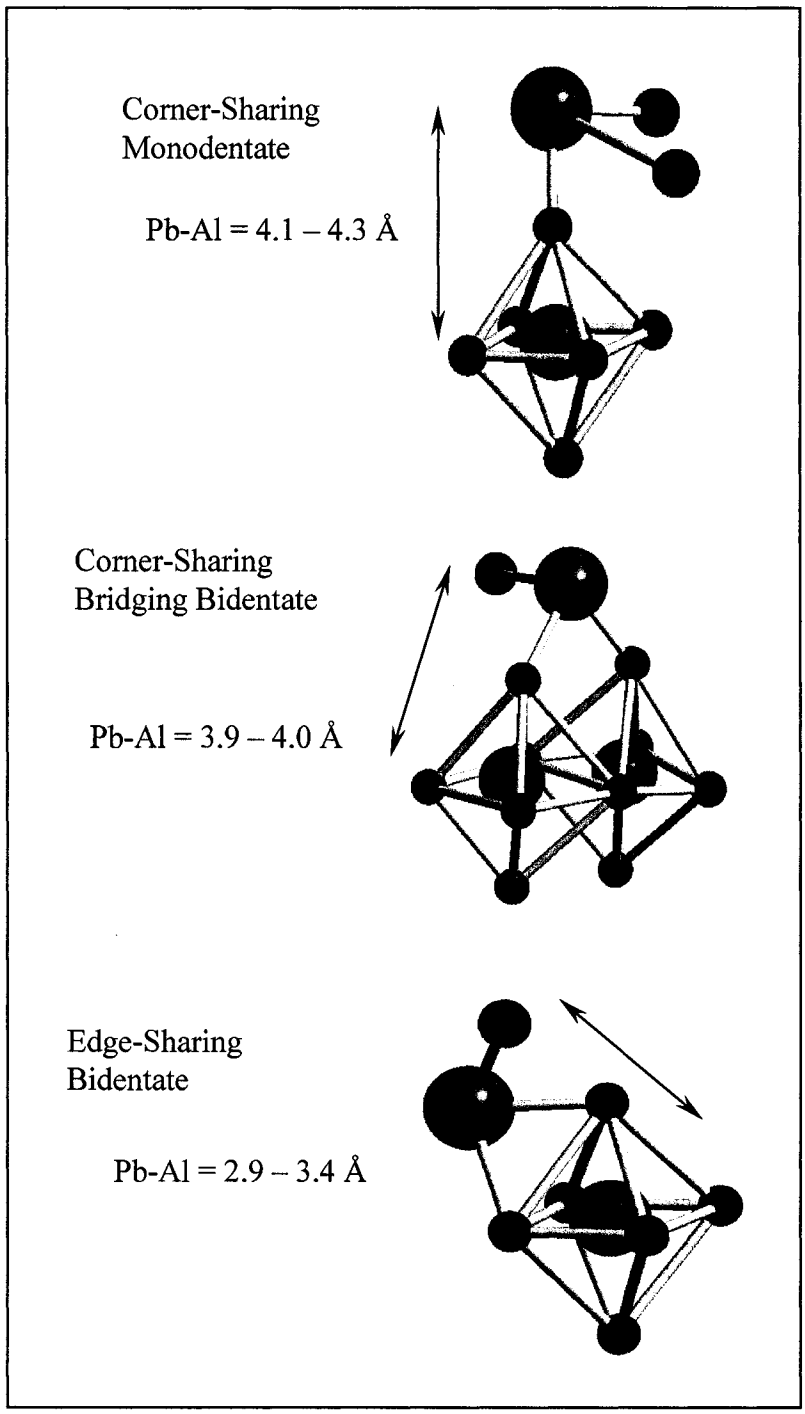

Figure 21. Characteristic Pb-Al separations for Pb(II) adsorbed to AlO_6 octahedra. Ions are depicted as having trigonal pyramidal geometries (from Bargar et al., 1997). Pb atoms are depicted in green, oxygen atoms (possibly present as hydroxyl or water atoms) are depicted in red, and Al atoms, located at the center of the octahedral, are shown in grey. H atoms, which cannot be detected by EXAFS, are not shown.

Reproduced with permission of the copyright owner. Further reproduction prohibited without permission.

lower coverages on the planar γ-Al_2O_3 ($\Gamma \leq 0.45$ μmol m^{-2}), the Pb-Al distances for the bidentate complexes are longer and the distances for the monodentate complexes are shorter compared with those at higher coverages. On both the planar and bulk γ-Al_2O_3, the same sorption complexes seem to be forming at higher coverages as evidenced by the similar Pb-Al distances, but the relative proportion of monodentate vs. bidentate changes with increasing coverage. This is especially evident on the bulk γ-Al_2O_3 where Pb(II) the proportion of monodentate Pb-Al complexes increases with increasing coverage (Table 9). The differences in sorption complexes at low coverages likely reflect the importance of the identity and number of high affinity reactive surface sites on metal sorption behavior. As coverage increases, these sites become occupied and similar Pb-Al sorption complexes are formed on the planar and bulk surfaces.

Polynuclear Pb(II) Complexes

A third frequency is present in the EXAFS which, along with the Al from the mondentate sorption complexes, is the cause of the peak in the Fourier transform centered at about 3.5 Å. This frequency component is due to backscattering from Pb neighbors at distances of 3.52-3.69 Å. In contrast to the findings in Conrad et al. (2002), ToF-SIMS measurements of polynuclear Pb(II) sorption complexes on the bulk and planar γ-Al_2O_3 sorption samples used in this study did not indicate the presence of these complexes on either the planar or bulk γ-Al_2O_3. However, the results from this study indicate the presence of 2nd neighbor Pb backscatterers in all sorption samples and indicate the presence of polynuclear Pb complexes on both the planar and bulk γ-Al_2O_3 at all coverages examined.

Reproduced with permission of the copyright owner. Further reproduction prohibited without permission.

Examination of the XANES and EXAFS can be used to determine that these Pb atoms are not the result of a precipitation of a crystalline or amorphous phase. Neither the XANES nor the EXAFS from any of the sorption samples completely matches the spectra from Pb(II) (hydr)oxide model compound examined. The Pb-Pb distances observed for both sets of sorption samples are within the characteristic range of Pb-Pb separations for edge-sharing compounds between PbO_3 or PbO_4 polyhedra ($R_{Pb\text{-}Pb}$ = 3.54-3.95 Å) (Bargar et al., 1997). In tetragonal PbO, neighboring Pb atoms share polyhedra edges and have Pb-Pb distances of 3.67 Å (Hong and Olin, 1974). In pyramidal PbO_3 and PbO_4 polyhedra that are corner-linked, Pb-Pb distances are ≥ 3.76Å (Spiro et al., 1969).

Previous investigations of polynuclear Pb(II) sorption complexes on alumina surfaces found that these compounds were small (most likely binuclear) and that many or all of the Pb(II) in the complexes are bound directly to the alumina surface (Bargar et al., 1997). This implies that the complexes lie flat on the surface despite the considerable mismatch between the ionic radii and coordination geometries of Pb(II)- and Al(III)-oxygen polyhedra. A large, two-dimensional multinuclear complex would require repeated O-O spacings larger than those in alumina (Hong and Olin, 1974). Pb(II) sorption complexes on both the planar and bulk γ-Al_2O_3 contained some character of the β-$Pb_6O(OH)_6(ClO4)_4 \bullet H_2O$ complex, which contains analogs for small multinuclear complexes. Given this fact, along with the similarities between the results for the sorption samples in this study and the results from previous studies, it is reasonable to assume that this scenario can be used to describe the composition of the multinuclear species present in our samples.

Reproduced with permission of the copyright owner. Further reproduction prohibited without permission.

The finding of this study show that the reactivity of planar γ-Al_2O_3 is comparable to that of pure phase γ-Al_2O_3 over the range of Pb(II) coverages studied. XANES results suggested that the Pb-O coordination environment for all samples is a mixture of distorted trigonal pyramidal and tetragonal pyramidal geometries. Results from the EXAFS fitting indicated that two Pb-Al complexes were present on the surface, predominantly corner-sharing monodentate with smaller amounts of edge-sharing bidentate complexes, although these complexes were found at different relative proportions with increasing coverage. The effects of differences in the number and/or identity of high affinity surface sites were suggested by differences in the local structure of the Pb-Al complexes on the planar vs. bulk γ-Al_2O_3 at low coverages. Additional similarities between the complexes formed on each oxide were found in the presence of Pb-Pb complexes on all sorption samples. The Pb-Pb distances of these complexes correspond to small, flat binuclear complexes similar to those seen in other studies of the Pb(II)/ γ-Al_2O_3 system.

Reproduced with permission of the copyright owner. Further reproduction prohibited without permission.

CHAPTER 5

Characterization of Mixed Fe/Al Planar Oxides

Introduction

A combination of high surface charge and small particle size make the surfaces of colloids and clay minerals particularly reactive. However, it is often the presence of surface coatings, such as organic and metal oxides (e.g., Al, Fe and Mn) that effectively determine the surface characteristics of soils and sediments. For example, the high reactivity of hydrous metal oxides results from the fact that hydroxyl groups of the active sites on these materials form an ideal template for binding heavy metals. The OH-OH bond distances of these materials often match well with the geometry of the coordination polyhedra of many heavy metals (Manceau et al., 1992).

Particle coatings may have several important consequences in determining sediment characteristics, as the properties of these coatings are largely different from the underlying mineral substrate (Scheidegger et al. 1993, Stipp et al., 1997; Zhuang and Yu, 2002). Coatings can effectively shield the mineral surface from the aqueous environment, thereby creating a novel solid-water interface (Stipp et al., 1997). Even small fractions of metal oxides or organic coatings may have the potential to alter the surface electrochemical properties of sediments, and therefore the trace metal sorption behavior (Hendershot and Lavkulich, 1983; Sakurai et al., 1990; Zhuang and Yu, 2002). Coatings can also alter the physical properties of sediments, leading to flocculation and

Reproduced with permission of the copyright owner. Further reproduction prohibited without permission.

particle association thereby changing the hydraulic properties of the sediments (Scheidegger et al., 1993). Particle coatings largely influence the transport and behavior of strongly sorbing pollutants such as metal ions, radionuclides and hydrophobic organics. Coated particles usually have strong adsorption affinities leading to retention of the contaminant. Also, particle coatings can detach from the sediment surface and act as carriers for pollutant transport (Scheidegger et al., 1993).

Minerals such as kaolinite, montmorillonite and illite are usually coated by organic material and small amorphous crystalline inorganic materials, Fe and Al oxides and hydroxides (Fitzpatrick, 1980; Sposito, 1984; Robert and Terce, 1989; Davis and Kent, 1990; Scheidegger et al., 1993; Zhuang and Yu, 2002). Iron and aluminum oxides are produced through weathering reactions making them ubiquitous in soils and sediments (Benjamin and Leckie, 1981; Anderson and Benjamin, 1990; Davis and Kent, 1990; Dzombak and Morel, 1990). Because weathering reactions result in complex mixed oxide and/or mixed silicate phases, Fe and Al oxides are generally found as co-precipitates rather than individual phases (Coston et al., 1995; Cornell and Schwertmann, 1996; Sposito 1996; Violante et al., 2002; Zhuang and Yu, 2002).

While recent studies have taken into account the effects of coatings on the overall reactivity or particles, there is still insufficient understanding of the interactions of mixed reactive phases with the mineral substrate, other reactive phases and the sorbing species. Few studies have attempted to systematically compare the effects of coating composition with the resultant sorption reactions at the surface. Efforts to model multicomponent systems have relied on the simplifying assumption that the heterogeneous solids could be represented either by some average collective property for the group or as a collection of

Reproduced with permission of the copyright owner. Further reproduction prohibited without permission.

discrete pure solid phases, a concept Honeyman called "adsorptive additivity" (Honeyman, 1984; Davis-Colley et al., 1984; Anderson and Benjamin, 1990). Investigations into the behavior of systems containing multiple oxides showed that particle interactions in these systems can lead to significant deviations from the adsorptive additivity concept, and in some cases, the addition of a second oxide to the system actually resulted in decreased uptake of some metals (Tipping et al., 1983; Anderson and Benjamin, 1990; Zachara et al., 1994).

The purpose of this work is to create mixed metal oxide coatings of varying Fe/Al ratios using well-characterized planar γ-Al_2O_3 as a template. Various methods for coating the planar γ-Al_2O_3 with ferric iron will be investigated. The objective is to be able to closely control the extent of coverage, distribution and crystallinity of iron on the planar surface resulting in a set of mixed Fe- Al- oxides that can be systematically varied through experimental conditions. These mixed oxides could be used in future work to understand differences in reactivity of the mixed oxides relative to their pure phase counterparts through metal sorption studies.

Materials and Methods

Materials

All chemicals used in the experiment were ACS grade or better. The planar oxides used as a substrate in the iron coating procedures were prepared according to Hart and Maurin (1965). Briefly, high purity aluminum foil was exposed to steam and rapidly heated to 550°C and pressurized to 45 psi resulting in a γ-Al_2O_3 surface coating

Reproduced with permission of the copyright owner. Further reproduction prohibited without permission.

approximately 20 nm thick supported by the metal substrate. Further details of their characterization can be found in Chapter 1.

Coating Method

The method used for coating the planar γ-Al_2O_3 with iron was adapted from several sources (Schwertmann and Cornell, 2000; Duckenfield, 2004; Edwards et al., 1989; Lai et al., 2002; Schmitt et al., 1996). In general, planar aluminas were suspended in DDI (18 mΩ) water for at least 18 hours to hydrate the oxide surface. Five planar γ-Al_2O_3 strips measuring approximately 3 cm x 1 cm (~ 0.05 g) were then added to 40 mL of $Fe(NO_3)_3$ solution in polyethylene containers. The pH of the solution was adjusted to 9.7 using small quantities (on the order of 10 µL) of 150.5 mM NaOH to minimize any areas of localized Fe hydroxide supersaturation in the solution. The solutions were allowed to equilibrate at this pH for approximately 15 minutes. They were then placed in a 50°C water bath and periodically shaken (several times on the first day, and at least once a day on subsequent days). The planars were removed from the solution, rinsed copiously with DDI water, air-dried and stored in polyethylene containers for further analysis.

Modifications to the general coating procedure were made to examine the effects of varying Fe concentration, reaction time and number of coating sequences on the resultant coatings (Table 10). To assess the effect of varying the starting Fe(III) concentration, solutions with $Fe(NO_3)_3$ concentrations of 0.125 mM, 1.25 mM and 12.5 mM were used. Each treatment was reacted for both 4 and 14 days to examine the effect of reaction time on the resultant coatings. In addition to altering the starting concentration of $Fe(NO_3)_3$ and the total reaction time, a sequential coating technique was

Reproduced with permission of the copyright owner. Further reproduction prohibited without permission.

used. In this method, a starting $Fe(NO_3)_3$ concentration of 1.25 mM was used with a 4 day reaction period. At the end of the 4 day period, the planars were rinsed with DDI and the coating process was repeated with fresh $Fe(NO_3)_3$ solution. Using this method, planars were prepared that had been through 2, 5 and 10 coating sequences.

Table 10. Experimental parameters for coating planar γ-Al_2O_3 with Fe(III).

Sample Information	Initial [Fe(III)] (mM)	Reaction Time	Coating Sequences
Varying Initial [Fe(III)]	0.125	4 days	1
	1.25	4 days	1
	12.5	4 days	1
Varying Reaction Time	0.125	14 days	1
	1.25	14 days	1
	12.5	14 days	1
Sequential Coatings	1.25	4 days	2
	1.25	4 days	5
	1.25	4 days	10

Fe(III) Extraction

The total concentration of Fe(III) deposited on the planar surface in each treatment was determined through acid dissolution of the coatings and determination of the concentration of Fe(III) removed. Specifically, Fe-coated planars were extracted with 2M HCl at a solid:solution ratio of 0.25 g planar:10 mL HCl at 50°C. Samples were centrifuged, and the supernatants were diluted to 20 mL using DDI H_2O. Iron(III) was determined by complexing Fe(III) in the diluted supernatant with 1 mL of 0.5 wt% ferrozine buffered with 1.4 M hydroxylamine hydrochloride and 1.3 M ammonium

Reproduced with permission of the copyright owner. Further reproduction prohibited without permission.

acetate. Fe(III) was measured by reading the absorbance of the sample solutions at 562 nm using a Shimadzu UV-Vis spectrophotometer.

Surface Analysis

The composition and distribution of the surface coatings were measured using Time of Flight Secondary Ion Mass Spectrometry (ToF-SIMS) and X-ray photoelectron spectroscopy (XPS). ToF-SIMS measures only the first few monolayers of the surface and was used to generate elemental maps showing the distribution of Fe on the planar γ-Al_2O_3 surface. XPS probes deeper into the bulk (~ 5-10 monolayers) providing quantitative information about the average chemical composition of the surface coating.

The Fe coated planars were examined as-is. ToF-SIMS spectra were collected using a Physical Electronics TFS-2100 TRIFT II with a 15 KeV Ga^+ beam. A raster area of 200 μm x 200 μm was used for a total ion dose of $3.0x10^{11}$ ions/cm^2. Total Fe was taken to be the sum of the peak intensities between 55 and 57 amu. The Al peak (27 amu) was used to normalize Fe intensities. XPS spectra were obtained using a VG Scientific Ltd. ESCA-LAB MKII spectrometer with an Mg anode and a 200W X-ray current. Energies were corrected for charging effects using the C1s peak (284.5 eV) of adventitious carbon as a reference. Quantitative measurement of Fe and Al was performed using the $2p_{3/2}$ peak (706.8 eV) and 2p peak (74.4 eV), respectively. Iron intensities, normalized to Al, were quantified using the manufacturers software program, Eclipse.

Reproduced with permission of the copyright owner. Further reproduction prohibited without permission.

Scanning Electron Microscopy

Photomicrogaphs of the bulk γ-Al_2O_3 were collected using scanning electron microscopy (SEM). Micrographs were obtained using a LEO 435VP Zeiss (LEO) / Cambridge microscope with a beam current of 12 pA and a beam energy of 10 KeV. Three to five fields were inspected, and the images shown here are representative of the typical morphology seen. Confirmation of the Fe phase was done by energy dispersive x-ray spectroscopy (EDS) on samples on a 10° tilt from normal with a beam current of 300 pA and a beam energy of 20 KeV.

X-ray Diffraction

X-ray diffraction (XRD) data were collected on a Scintag ADS diffractrometer with a copper anode (λ = 1.540598 nm) and a Peltier solid state detector. Scans were typically run over a region of 2 to 120° 2θ range in steps of 0.02° with count times varying from 4.0 to 8.0 seconds depending on the region (see Table 2, Ch. 1).

Surface Area and Porosity

The surface area of the Fe coated planar γ-Al_2O_3 was measured using the BET-N_2 method. Nitrogen gas adsorption isotherms were measured using a Micromeritics Gemini 2365 Surface Area Analyzer over a range of 0.5% to 98% saturation. Porosity of the coated materials was assessed through the use of t-plots.

Reproduced with permission of the copyright owner. Further reproduction prohibited without permission.

Results

Fe(III) Quantitative Analysis

The highest Fe/Al ratio seen for the planars coated with varying initial concentrations of Fe(III) were for the 1.25 mM sample for both the 4 and 14 day reaction times (Table 11; Fig. 22). This sample also corresponded to the highest amount of Fe on a weight % basis for these samples. For the planar aluminas subjected to sequential coatings, there was a steady increase in ToF-SIMS and XPS Fe/Al ratios as well as % Fe (Table 12; Fig. 23). The samples with two coatings had the lowest values and the sample undergoing ten coatings had the highest Fe/Al ratios and % Fe.

Table 11. Quantitative analysis of Fe coatings on planar γ-Al_2O_3 resulting from varying starting Fe(III) concentrations and reaction times.

Reaction Time	Initial [Fe(III)] mM	ToF-SIMS Fe/Al	XPS Fe/Al	% Fe (by wt)	Coating Thickness (nm)
4 Days	0.125	0.091 ± 0.018	ND‡	ND	ND
	1.25†	0.253 ± 0.058	0.026	0.085	0.105
	12.5	0.163 ± 0.068	0.018	ND	0.075
14 Day	0.125	0.209 ± 0.010	ND	0.107	ND
	1.25	0.446 ± 0.093	0.056	0.620	0.225
	12.5	0.107 ± 0.045	0.026	ND	0.106

†Note that this sample also serves as the 1 coating sample in the sequential coating group.
‡ND = no detectable Fe.

Table 12. Quantitative analysis of Fe coatings on planar γ-Al_2O_3 resulting from sequential coatings using 1.25 mM $Fe(NO_3)_3$ and a 4 day reaction.

Coating Sequences	ToF-SIMS Fe/Al	XPS Fe/Al	% Fe (wt)	Coating Thickness (nm)
2	0.353 ± 0.062	0.061	0.237	0.243
5	0.910 ± 0.112	0.197	0.675	0.715
10	1.734 ± 0.001	0.268	1.441	0.934

Reproduced with permission of the copyright owner. Further reproduction prohibited without permission.

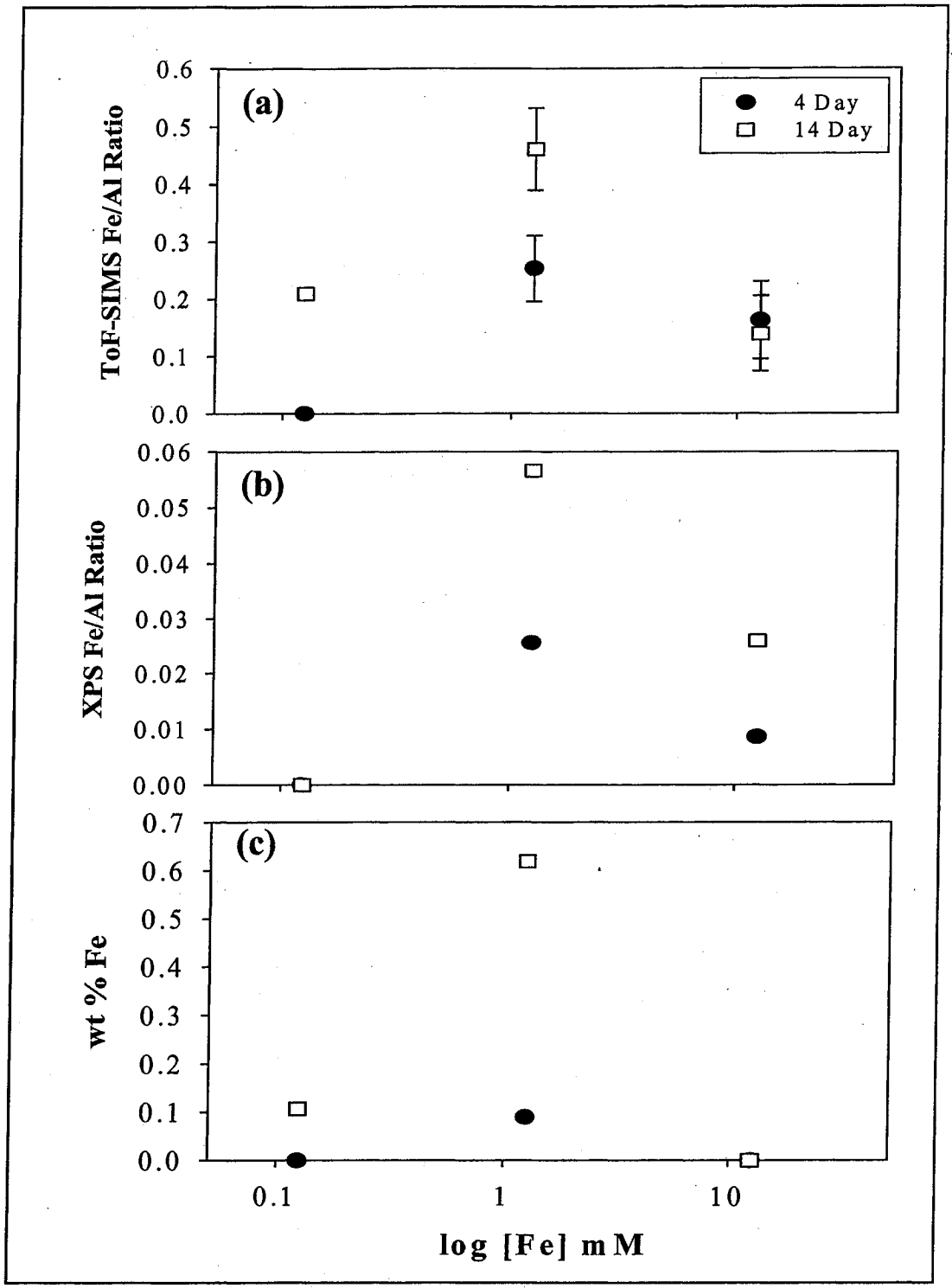

Figure 22. (a) ToF-SIMS Fe/Al ratios, (b) XPS Fe/Al ratios and (c) wt % Fe of planar γ-Al_2O_3 versus initial concentrations of Fe(III). For all plots, the closed circles (•) represent the 4 day reaction time data and the open squares ( ) represent the 14 day data. Error bars represent the standard error of five measurements for ToF-SIMS and duplicate measurements for XPS.

Reproduced with permission of the copyright owner. Further reproduction prohibited without permission.

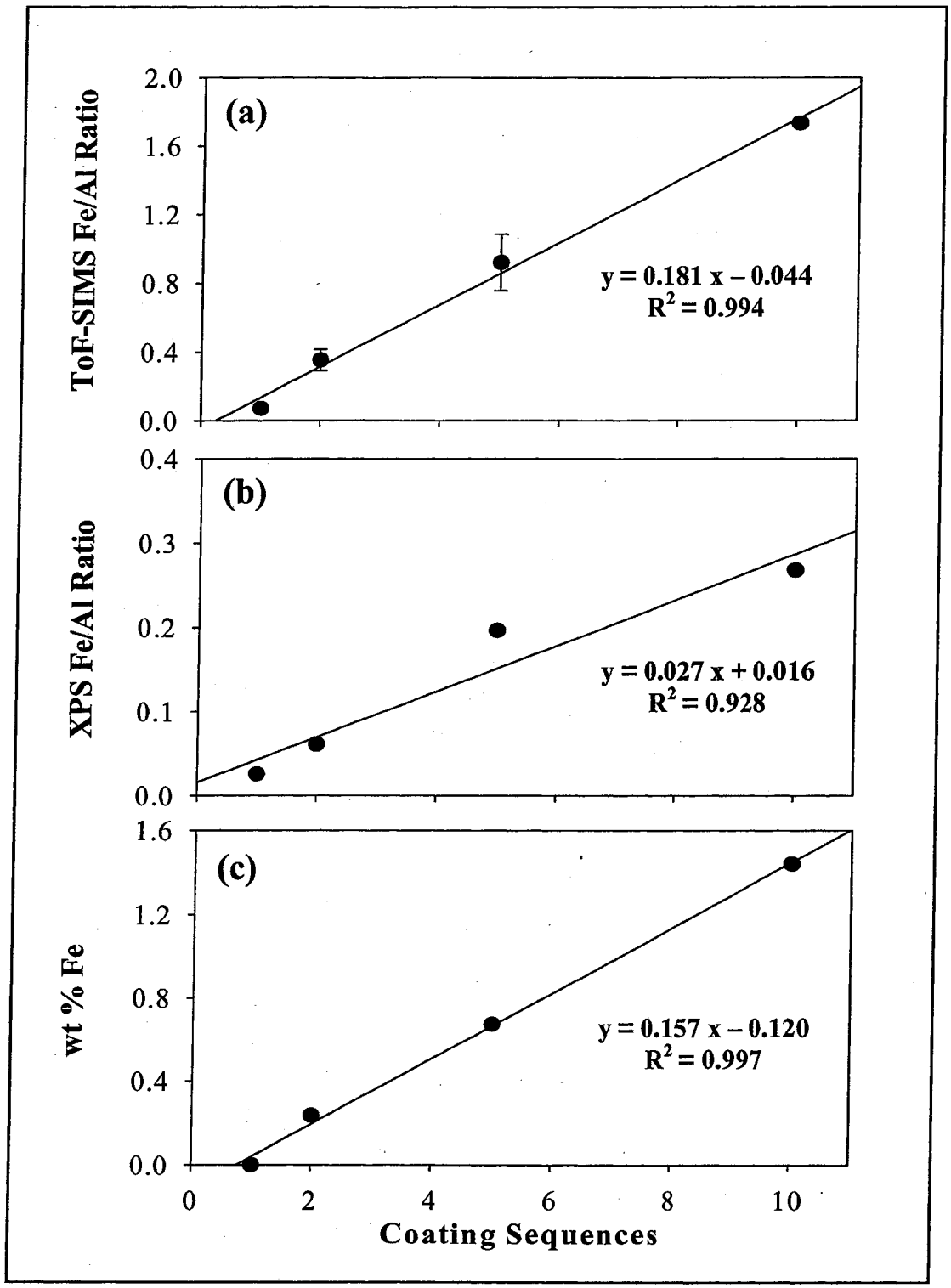

Figure 23. (a) ToF-SIMS Fe/Al ratios, (b) XPS Fe/Al ratios and (c) wt % Fe of planar γ-Al_2O_3 plotted against the number of coatings using 1.25 mM Fe(III) and a 4 day reaction time. Error bars represent the standard error of five measurements for ToF-SIMS and duplicate measurements for XPS.

Reproduced with permission of the copyright owner. Further reproduction prohibited without permission.

Fe(III) Coating Thickness

The thickness of the Fe coating on each of the samples can be estimated from the XPS Fe/Al ratios using a simple attenuation model as outlined in Vitchev et al. (2004). This model assumes that the surface coating is a thin, homogeneous layer. For a sample with a coating of material A with thickness d on a substrate of material S, the exponential attenuation of the XPS signal intensities in the overlayer can be written as:

$$\frac{I_A}{I_S} = \frac{I_A^\infty}{I_S^\infty} \frac{(1-\exp(-d/(\lambda_{A,A}\cos\theta)))}{\exp(-d/(\lambda_{S,A}\cos\theta))} \qquad (5)$$

where I_A^∞ and I_S^∞ are the signal intensities from thick layers of material A and S, and $\lambda_{A,A}$ and $\lambda_{A,S}$ are the effective attenuation lengths in the overlayer of photoelectrons emitted from the overlayer and the substrate, respectively. The emission angle of photoelectrons, θ, is measured towards the surface normal. The effective attenuation length of light metal oxides is usually between 1 and 4 nm (Ratner and Castner, 1997; Vitchev et al., 2004). To determine the thickness of the coating, d, the equation is rearranged to:

$$d = \lambda\cos\theta\ln(1+\frac{(I_A/I_A^\infty)}{(I_S/I_S^\infty)} = \lambda\cos\theta\ln(1+K\frac{I_A}{I_S}) \qquad (6)$$

For the samples used in this study, A and S stand for the Fe $2p_{3/2}$ peak of the Fe coating and Al $2p_{1/2}$ peak of the planar γ-Al_2O_3, respectively, and λ is the effective attenuation length of Al $2p_{1/2}$ electrons in the Fe coating. K is the ratio of the appropriate Fe and Al peaks from thick samples. For these samples, K and λ were chosen to be 1.5 nm and 3.0 nm. These values are similar to other experimental values calculated for light metal oxides (Chastain, 1992; Ratner and Castner, 1997). Using this model, the calculated thickness of the Fe coatings ranged from 0.075 nm to 0.225 nm for samples prepared

Reproduced with permission of the copyright owner. Further reproduction prohibited without permission.

with varying initial [Fe(III)] and reaction times (Table 11) and from 0.243 to 0.934 for sample prepared by sequentially coating the planar surface (Table 12).

Fe(III) Distribution

The model above assumes a uniform surface coating. However, this may not be the case with the Fe coatings formed on the planar γ-Al_2O_3 surfaces. ToF-SIMS was used to create elemental maps of the distribution of Fe on the planar surfaces as a function of the chosen experimental conditions (Figs. 24-26). At the low Fe(III) concentration (0.125 mM), the coatings formed after 4 days are less uniform (% standard deviation = 19.54) and have lower Fe/Al ratios than the 14-day samples (% standard deviation = 4.88) (Table 11, Figs. 24a and 25a). A similar distribution of Fe is seen on samples coated with 1.25 mM Fe(III) regardless of reaction time (Figs. 24b and 25b). The standard deviations of the Fe/Al ratios for these samples are 22.81 % for the 4-day reaction period and 20.72 % for the 14-day reaction period. At the highest Fe(III) concentration, 12.5 mM, the elemental maps show patchy regions of high levels of Fe on both the 4 and 14-day samples (% standard deviation = 41.79 and 41.70, respectively) (Figs. 24c and 25c). This may be a result of precipitation of Fe particles in solution which were subsequently absorbed to the γ-Al_2O_3 surface. The elemental maps of the sequentially coated planar aluminas indicate a relatively homogeneous coverage of the surface for all samples with the coverage becoming more uniform as the number of coating sequences is increased (% standard deviation = 1.764, 12.31 and 0.06 for 2, 5 and 10 coating sequences, respectively) (Fig. 26).

Reproduced with permission of the copyright owner. Further reproduction prohibited without permission.

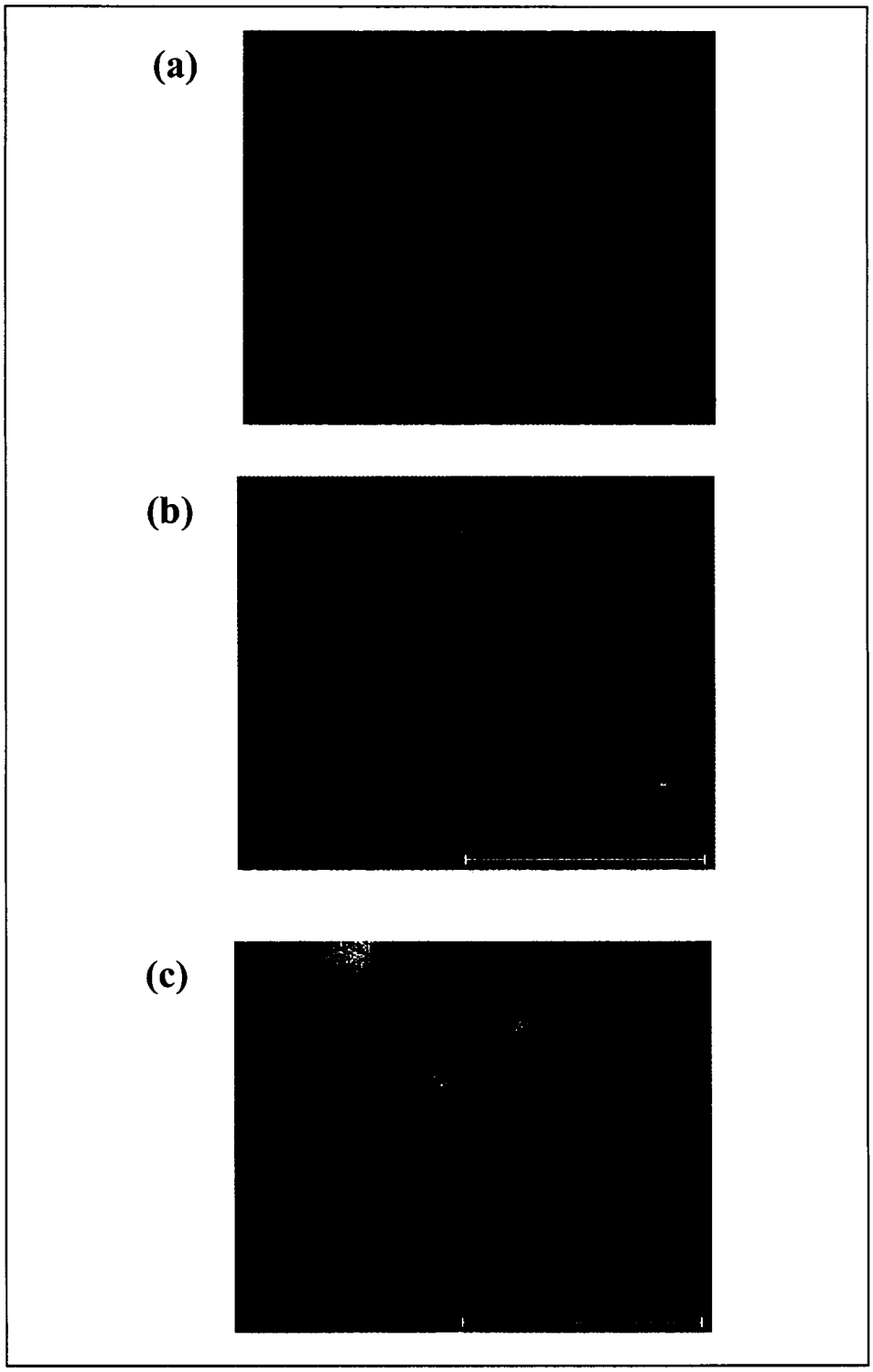

Figure 24. ToF-SIMS elemental maps of the distribution of Fe on planar γ-Al_2O_3 coated with (a) 0.125 mM, (b) 1.25 mM and (c) 12.5 mM Fe(III) using a 4 day reaction period. In all images, the scale bar represents 100 μm.

Reproduced with permission of the copyright owner. Further reproduction prohibited without permission.

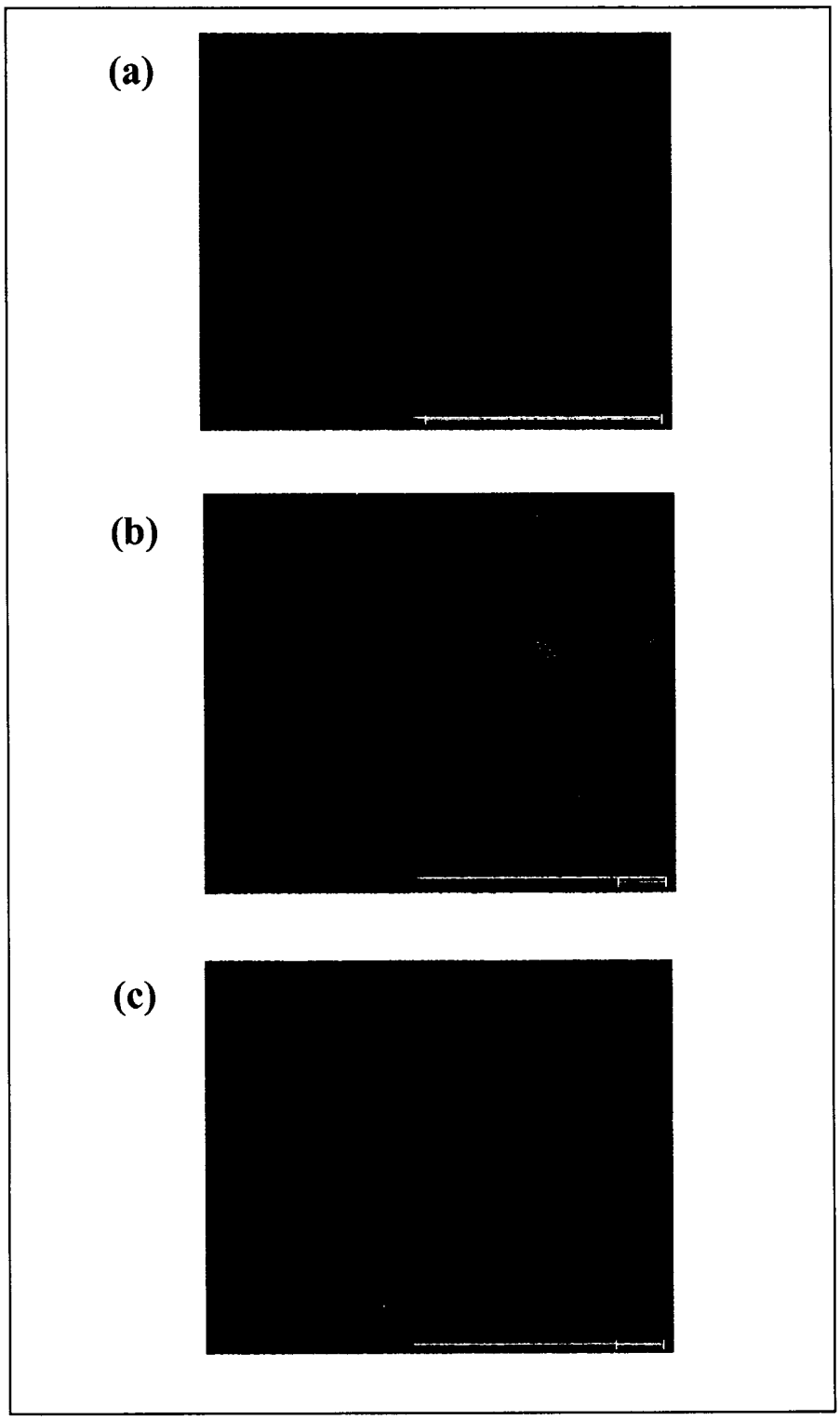

Figure 25. ToF-SIMS elemental maps of the distribution of Fe on planar γ-Al_2O_3 coated with (a) 0.125 mM, (b) 1.25 mM and (c) 12.5 mM Fe(III) using a 14 day reaction period. In all images, the scale bar represents 100 μm.

Reproduced with permission of the copyright owner. Further reproduction prohibited without permission.

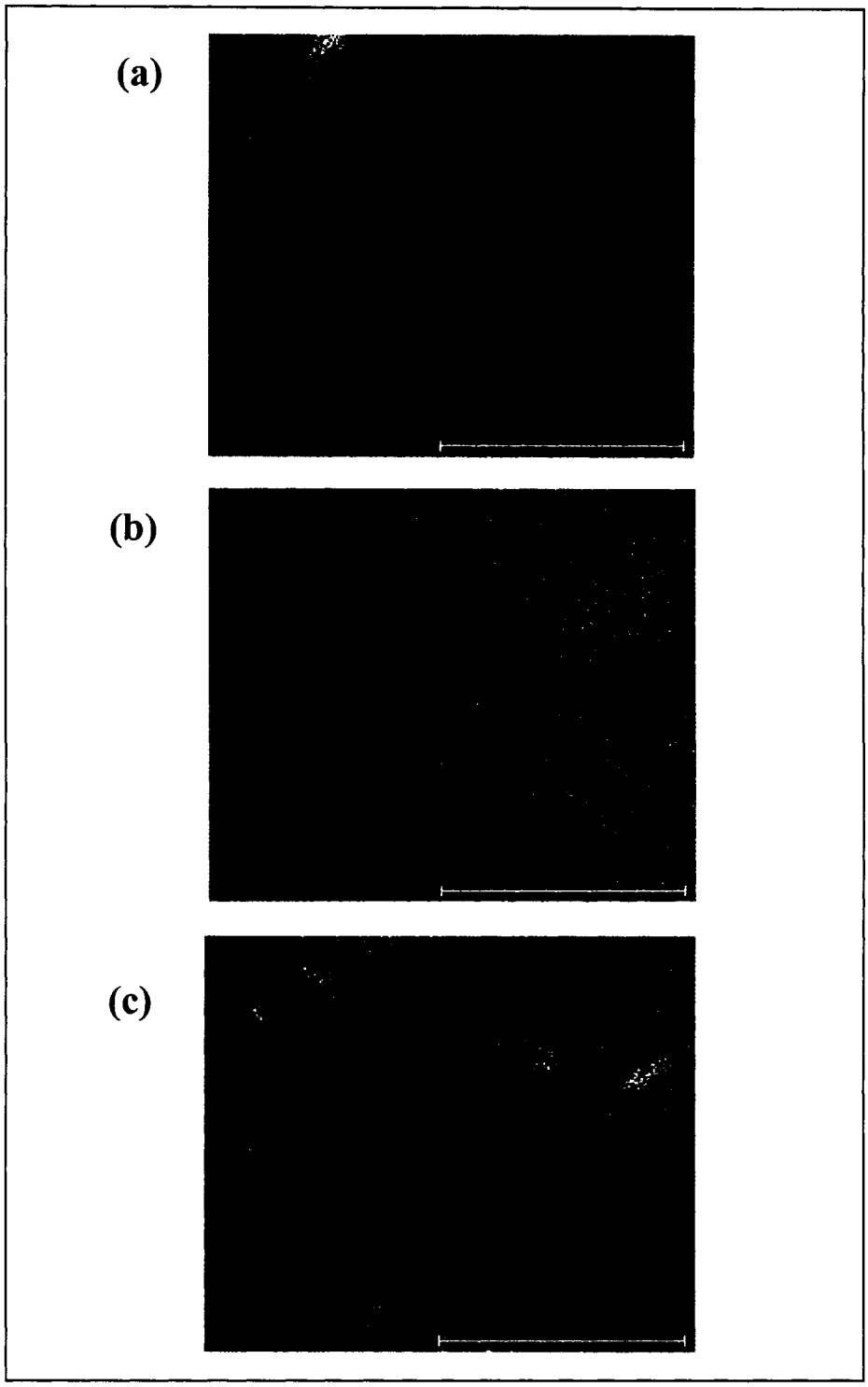

Figure 26. ToF-SIMS elemental maps of the distribution of Fe on planar γ-Al_2O_3 sequentially coated with (a) 2, (b) 5 and (c) 10 coatings of 1.25 mM Fe(III) using a 4 day reaction period. In all images, the scale bar represents 100 μm.

Reproduced with permission of the copyright owner. Further reproduction prohibited without permission.

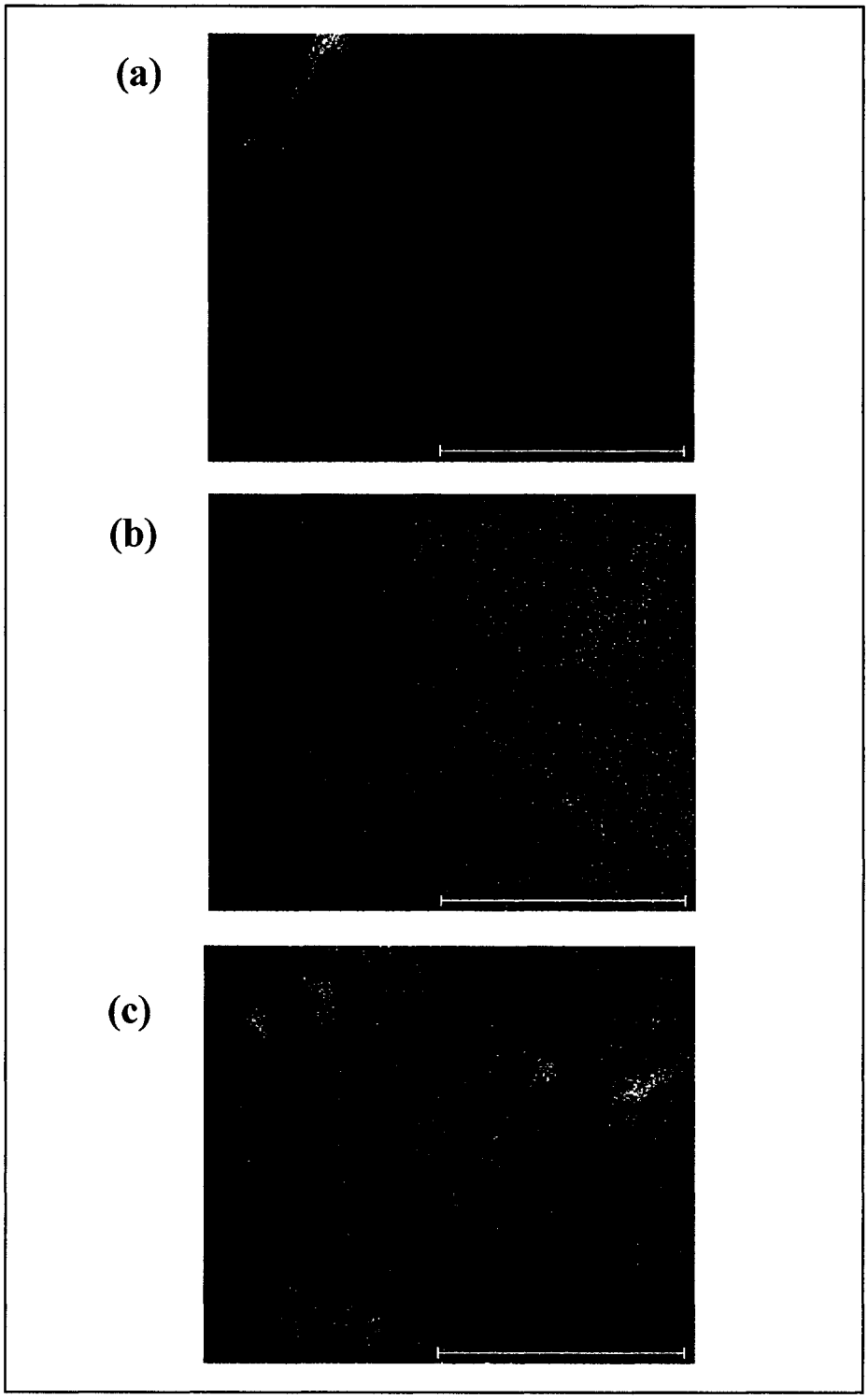

Figure 26. ToF-SIMS elemental maps of the distribution of Fe on planar γ-Al_2O_3 sequentially coated with (a) 2, (b) 5 and (c) 10 coatings of 1.25 mM Fe(III) using a 4 day reaction period. In all images, the scale bar represents 100 μm.

Reproduced with permission of the copyright owner. Further reproduction prohibited without permission.

Surface Morphology

SEM was used to visually inspect the coated planar surfaces in an attempt to identify the crystalline form of the Fe(III) coating. The photomicrographs for the 4 day samples prepared with three initial Fe(III) coatings are shown in figure 27. The planar coated with 0.125 mM Fe(III) exhibits needle-shaped crystals distributed throughout the surface (Fig. 27a). These structures have been seen on the unreacted planar γ-Al_2O_3 (Fig. 6a, Chapter 1) and are also similar to other goethite coatings and Al-substituted acicular goethite crystals (Scheidegger et al., 1993; Schwertmann and Cornell, 2000). The morphology changes to a mixture of cubic and needle shaped crystals for the 4 day sample coated with 1.25 mM Fe(III) (Fig. 27b). These cubic features have also been seen on unreacted planar aluminas (Fig. 5, Chapter 1). A major shift in the crystallography of the surface phase is seen in the SEM image of the sample coated with 12.5 mM Fe(III). This crystalline form is more similar to a mono-disperse platy hematite (Schwertmann and Cornell, 2000). Note the increase in crystal size with increasing Fe(III) concentration.

The crystallinity of the surface coatings for the 14 day samples were different from the 4-day samples prepared with similar Fe(III) concentrations. In contrast to the 4-day sample coated with 0.125 mM Fe(III) where needle shaped crystals were observed, the 14-day sample has an evenly distributed layer of what appears to be pseudocubic hematite (Fig. 28a) (Sugimoto and Sakata, 1992). The coatings produced using an initial Fe(III) concentration of 1.25 mM and a 14-day reaction period are a mixture of cubic and spindle shaped crystals and amorphous materials (Fig. 28b). The spindle shaped crystals may be indicative of the formation of an Al-substituted goethite phase. The coating

Reproduced with permission of the copyright owner. Further reproduction prohibited without permission.

resulting from 12.5 mM Fe(III) and 14 days looks very similar to the corresponding 4-day sample (Fig. 28c). Large crystals similar in appearance to hematite plates are seen. The SEM images of the sequentially coated planar aluminas show an increasingly complex surface from 2 to 10 coatings (Fig. 29). The alumina surface with 2 coatings has very distinct crystalline needles interdispersed between rectangular γ-Al_2O_3 features (Fig. 29a). As with the previous samples, it is difficult to distinguish between the Fe and Al composition of these needles as they are found in both the planar aluminas and pure and Al-substituted goethites. Increasing the number of coatings from 2 to 5 results in less well-defined features along with amorphous looking blobs (Fig. 29b). The rectangular alumina features appear fuzzy, and the entire surface is covered with very small, cylindrical crystals that are ~200 nm in length. The 10-coating sample shows an increase in crystal size, and the surface again has a fuzzy appearance to it (Fig. 29c). The dusty look of the surfaces in the latter two samples may indicate an accumulation of Fe(III) on the alumina and/or iron oxide surfaces.

XRD Phase Identification

X-ray diffraction can be used to obtain fingerprint spectra for the purpose of identifying the crystalline phase of mineral and oxide materials. XRD diffraction patterns were obtained for the Fe(III) coated planars to identify the form of Fe present on the planar surfaces as a function of Fe(III) concentration, reaction time and number of coating sequences. The large peak at 44.2° 2θ is due to the Al metal substrate of the planar oxides. For all samples, there were nine peaks that were seen in the diffraction patterns for both the unreacted and Fe(III) coated planar γ-Al_2O_3 (Figs. 30-32). No new

Reproduced with permission of the copyright owner. Further reproduction prohibited without permission.

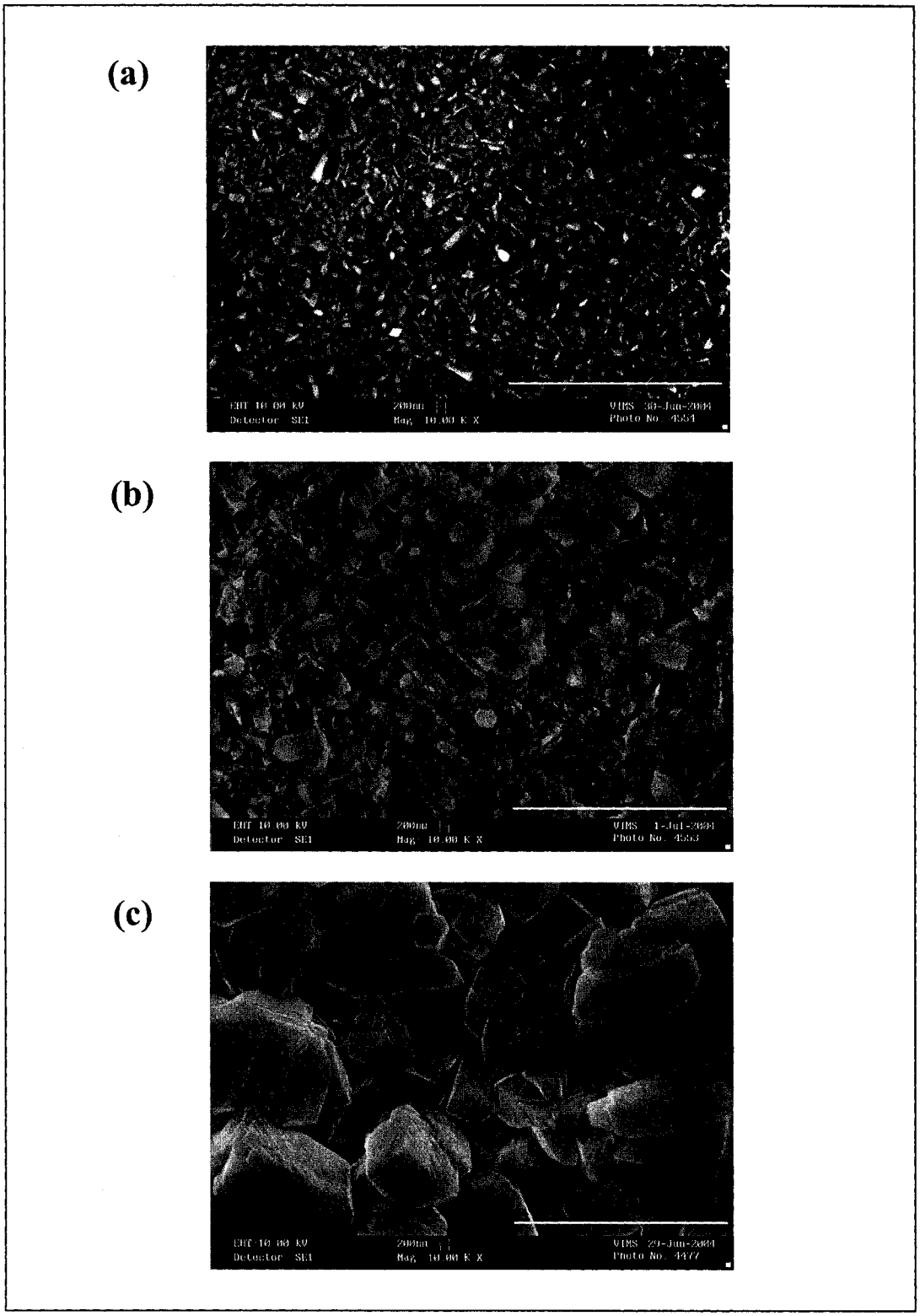

Figure 27. SEM photomicrographs of Fe coatings formed on planar γ-Al_2O_3 using (a) 0.125 mM, (b) 1.25 mM and (c) 12.5 mM $Fe(NO_3)_3$ and a 4-day reaction period. The scale bars represent 2 μm.

Reproduced with permission of the copyright owner. Further reproduction prohibited without permission.

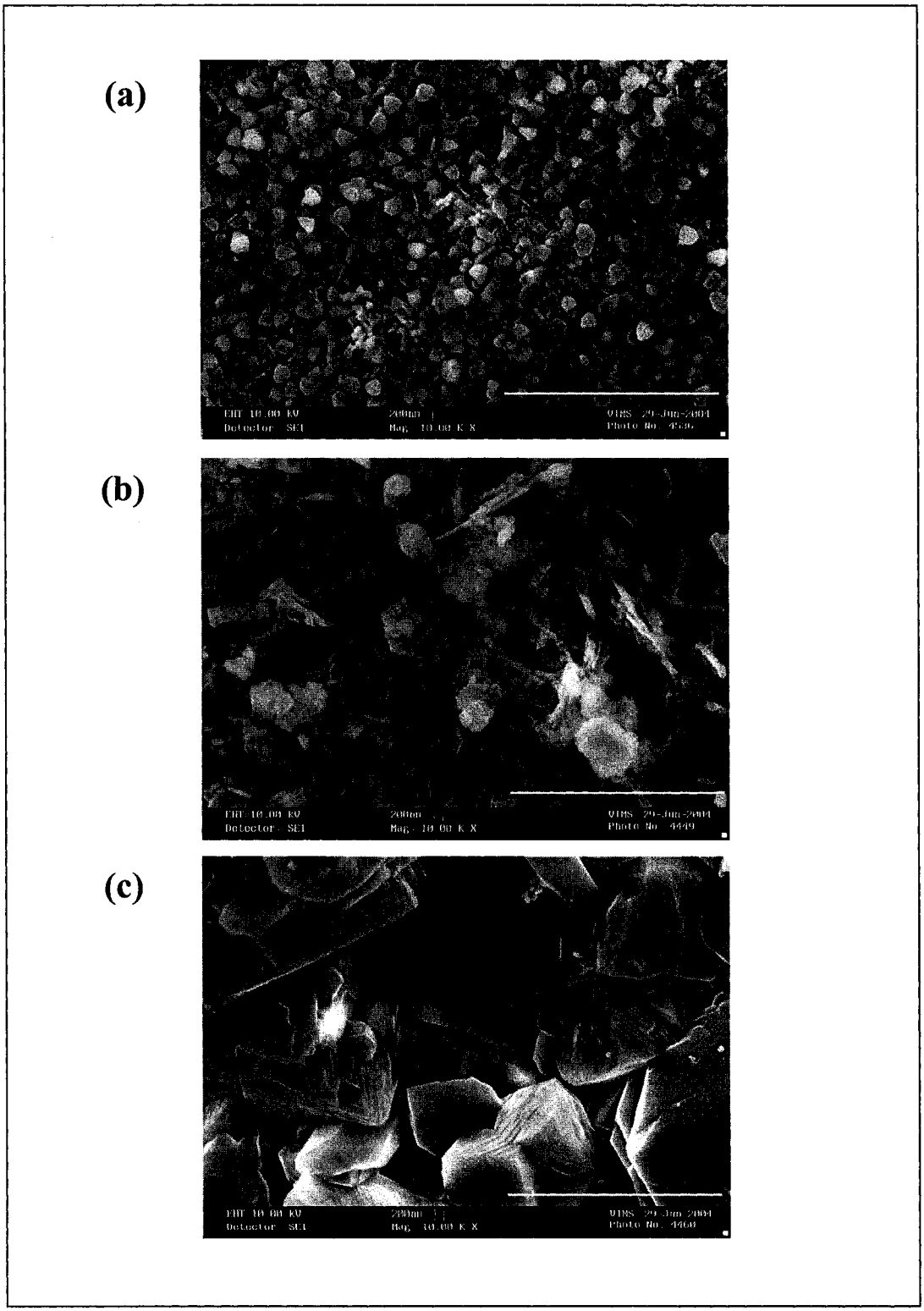

Figure 28. SEM photomicrographs of Fe coatings formed on planar γ-Al_2O_3 using (a) 0.125 mM, (b) 1.25 mM and (c) 12.5 mM $Fe(NO_3)_3$ and a 14-day reaction period. The scale bars represent 2 μm.

Reproduced with permission of the copyright owner. Further reproduction prohibited without permission.

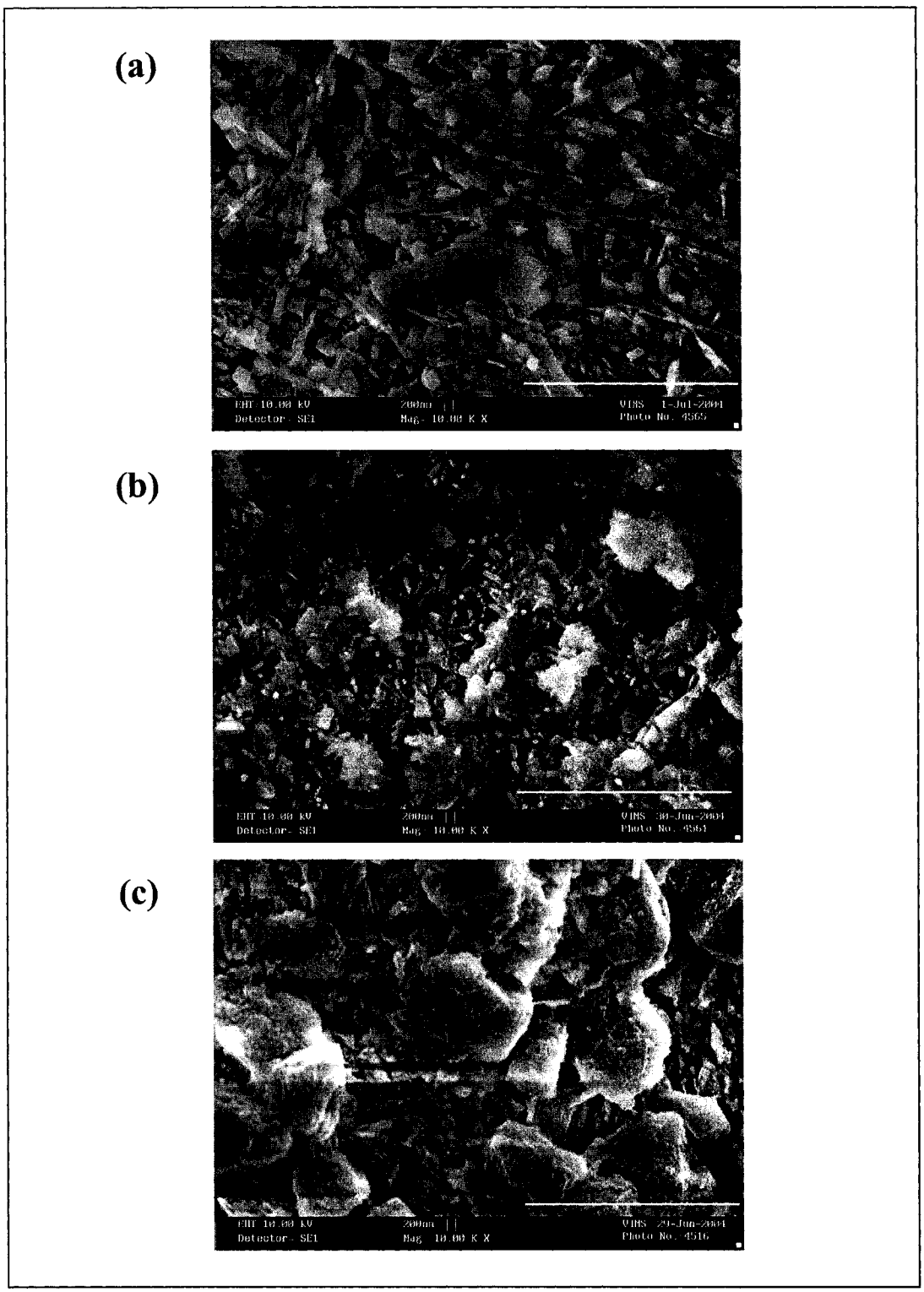

Figure 29. SEM photomicrographs of sequentially coated planar γ-Al_2O_3 with (a) 2, (b) 5 and (c) 10 coatings using 1.25 mM $Fe(NO_3)_3$ and a 4-day reaction period. The scale bars represent 2 μm.

Reproduced with permission of the copyright owner. Further reproduction prohibited without permission.

Peaks were seen in the diffractograms for the Fe(III) coated planars. While the peaks at 27 and 52.6 °2θ do not increase in intensity with increasing initial Fe(III) concentration (Figs. 30, 31), a systematic increase can be seen with an increase in the number of coatings (Fig. 32). The peaks at 16, 18, 20, 38, 40 and 99 °2θ generally decrease in intensity which could indicate a possible masking of the surface by the Fe coating or the reaction of Al into a new phase. However, the decreases in intensities of these peaks do not seem to be directly correlated to the Fe(III) concentrations used in the coating procedures or the number of coating sequences. It is likely that the content of Fe on the planar surface is too low to be identified by this method.

Surface Area and Porosity

The specific surface area (SSA) of the unreacted planar γ-Al_2O_3 was reported in Chapter 1 as 11.5 $m^2 g^{-1}$. The ranges of surface areas for Fe phases possibly present on the coated planars are listed in Table 13 (Schwertmann and Cornell, 2000). Goethites prepared from Fe(III) salts under similar experimental conditions generally have a surface area of approximately 13 to 30 $m^2 g^{-1}$. The surface areas of hematites prepared through methods similar to those used in this study range from 30 to 50 $m^2 g^{-1}$. Ferrihydrite, a highly amorphous Fe phase, may also be present in the coatings. Its surface area ranges from 200 to 320 $m^2 g^{-1}$. Lepidocrocite, with a surface area of 70 to 80

Reproduced with permission of the copyright owner. Further reproduction prohibited without permission.

Reproduced with permission of the copyright owner. Further reproduction prohibited without permission.

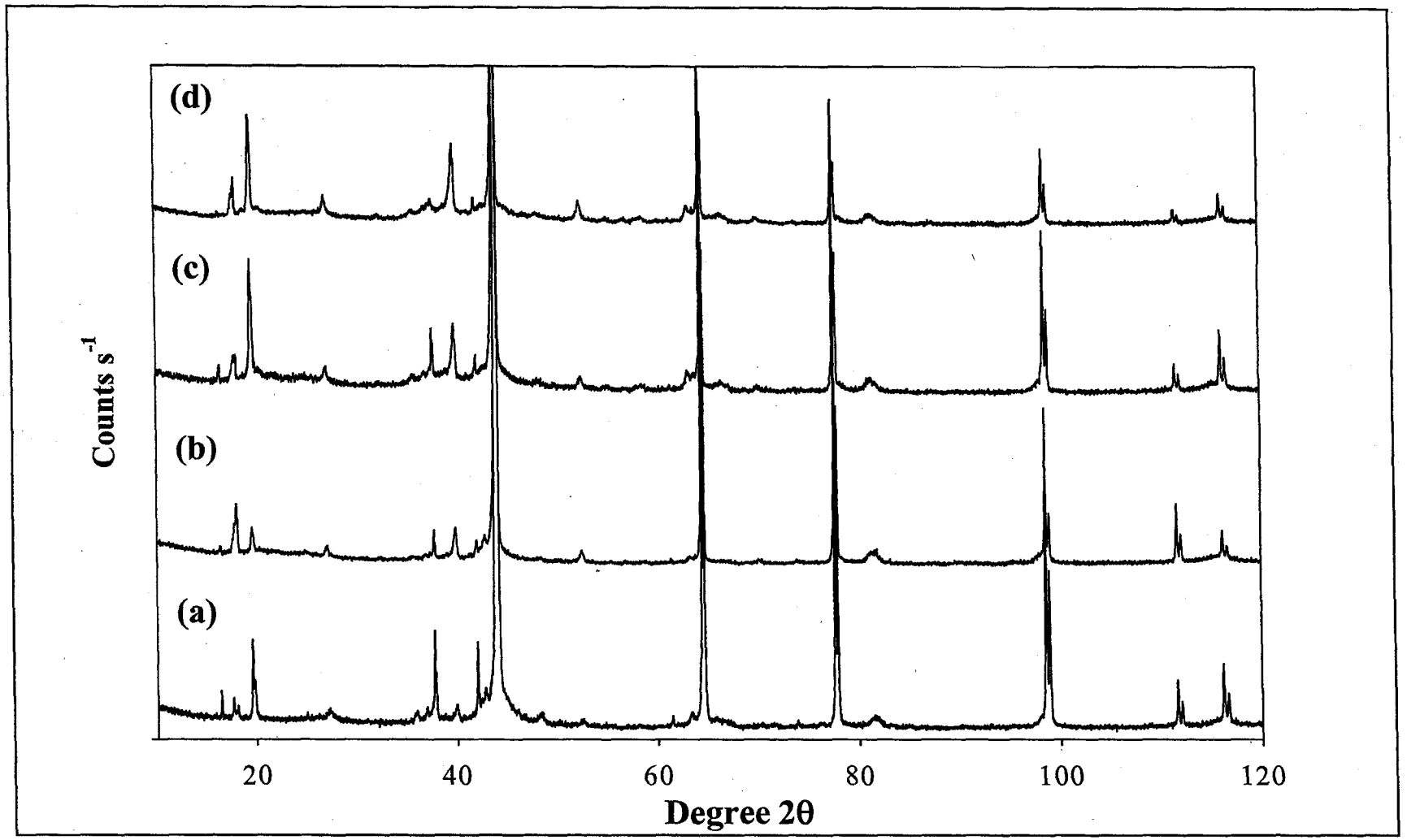

Figure 30. X-ray diffraction patterns of (a) unreacted planar γ-Al_2O_3 and Fe coated planar γ-Al_2O_3 using initial Fe(III) concentrations of (b) 0.125 mM, (c) 1.25 mM and (d) 12.5 mM and a 4 day reaction period. To enhance the visibility of the lower intensity peaks, the patterns are scaled such that the principle Al metal substrate peaks (44.2 °2θ) are truncated.

Reproduced with permission of the copyright owner. Further reproduction prohibited without permission.

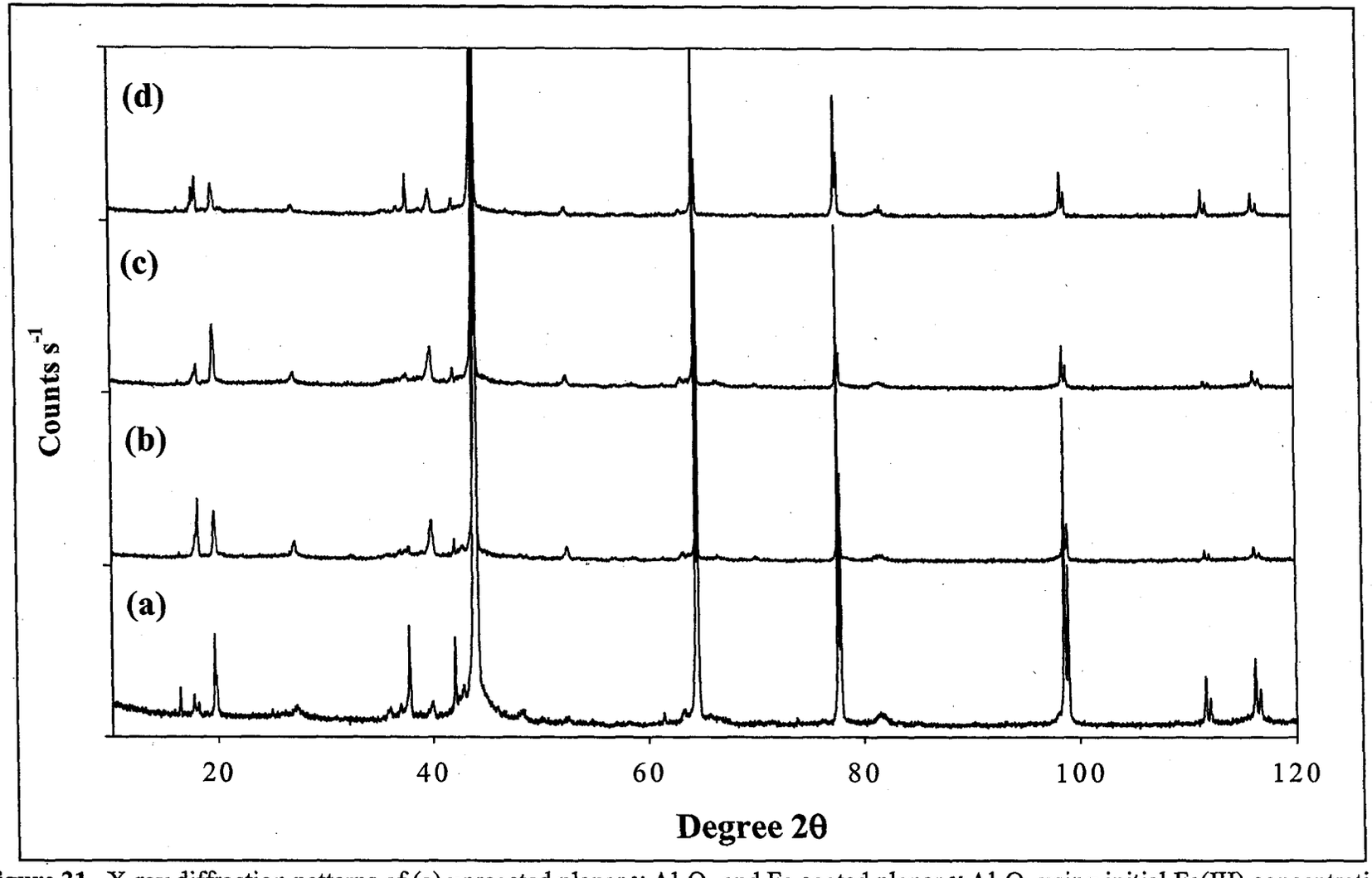

Figure 31. X-ray diffraction patterns of (a) unreacted planar γ-Al_2O_3 and Fe coated planar γ-Al_2O_3 using initial Fe(III) concentrations of (b) 0.125 mM, (c) 1.25 mM and (d) 12.5 mM and a 14 day reaction period. Peak heights are truncated as in Fig. 30.

Reproduced with permission of the copyright owner. Further reproduction prohibited without permission.

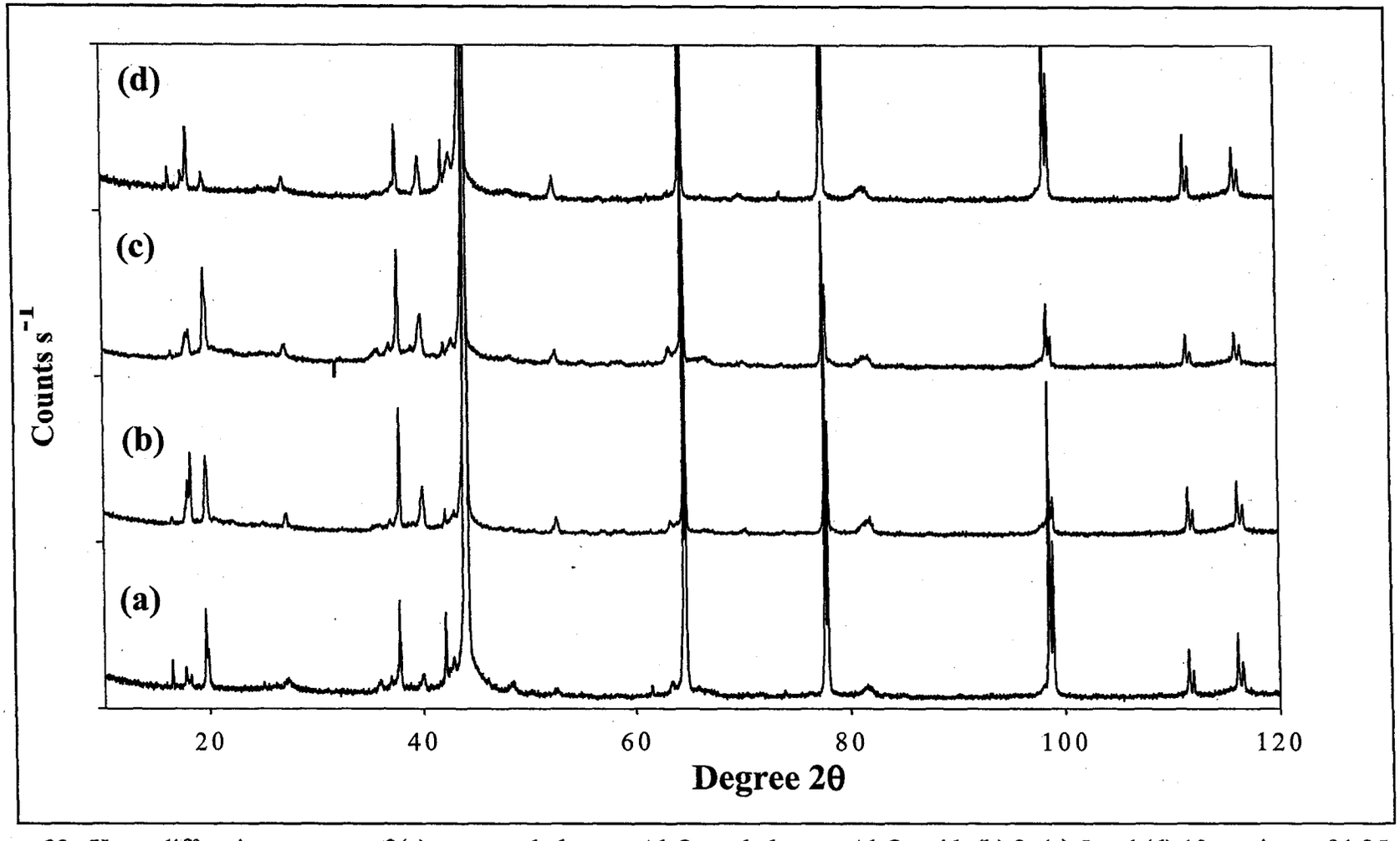

Figure 32. X-ray diffraction patterns of (a) unreacted planar γ-Al_2O_3 and planar γ-Al_2O_3 with (b) 2, (c) 5 and (d) 10 coatings of 1.25 mM Fe(III) and a 4 day reaction period. Peak heights are truncated as in Fig. 30

$m^2 g^{-1}$, may also be present. Given the surface areas of these Fe phases compared to the surface are of the unreacted planar γ-Al_2O_3, it is expected that the surface area of the coated planars would be increased relative to the uncoated planars. However, the BET surface area measurements of the Fe coated planars were never higher than the uncoated planars.

Table 13. Specific surface area ranges for common Fe oxides

Oxide	Formula	SSA ($m^2 g^{-1}$)
Ferrihydrite	$Fe_5HO_8 \bullet 4H_2O$	200 - 320
Goethite	α-FeOOH	13 - 30
Hematite	α-Fe_2O_3	30 - 50
Lepidocrocite	γ-FeOOH	70 - 80

All of the coated samples show the typical BET behavior with increasing P_{Rel} (i.e. a region of slow uptake at low P_{Rel} followed by a region of rapid N_2 adsorption at higher P_{Rel}) (Figs. 33-41). Additionally, all of the adsorption isotherms are generally similar to a Type II isotherm characteristic of non-porous solids.

There are small deviations in the shapes of the isotherms for the different coatings, particularly at low P_{Rel} values. For the coating created with 0.125 mM Fe(III) and a 4-day reaction period, the isotherm has a slightly concave curvature at $P_{Rel} < 0.20$ (Fig. 33a). In contrast, this region on the 1.25 mM, 4-day sample is relatively flat (Fig. 34a). The shape of the isotherm for the 12.5 mM 4-day sample does not have the curvature inflection that occurs in the other two samples at $P_{Rel} \sim 0.50$. Rather, the entire isotherm for this sample is concave in curvature (Fig. 35a). For the coatings created

Reproduced with permission of the copyright owner. Further reproduction prohibited without permission.

using a 14-day reaction period, the isotherms for the coatings produced with 0.125 and 1.25 mM Fe(III) are similar, showing a relatively flat region at $P_{Rel} < 0.50$ followed by a rapid increase in adsorption (Figs. 36a and 37a). The 14-day, 12.5 mM coating has a very pronounced concave curvature at $P_{Rel} < 0.20$ (Fig. 38a). There is a clear transition from a flat isotherm shape to a concave curvature in the isotherm at $P_{Rel} < 0.20$ for the sequentially coated planars moving from 2 to 10 coatings (Figs. 39a, 40a and 41a).

The linear region of the BET adsorption isotherms were used to calculate the specific surface area and c parameters for the Fe(III) coated planar γ-Al_2O_3. Although the entire region from 0.05 to 0.30 often tends to be linear, dramatic shifts in the values of the calculated parameters can result from using different sets of points to define the linear region. For most samples, the linear region chosen ranged from $P_{Rel} = 0.05$ to 0.20. The C values are all positive and within typical values for oxide minerals. In contrast to what was expected, the coated planars all had specific surface areas lower than the uncoated planar γ-Al_2O_3 (Table 14). For the 4-day coatings, the highest surface area was $10.5 \pm m^2 g^{-1}$ for the 1.25 mM sample, followed by 7.2 ± 0.03 $m^2 g^{-1}$ for the 0.125 mM sample. The coating created with the highest Fe(III) concentration had the lowest SSA of this set at 3.6 ± 0.09 $m^2 g^{-1}$. The reverse trend was seen for the 14-day coatings. The highest SSA was measured on the coating prepared with 12.5 mM Fe(III) (9.2 ± 0.10 $m^2 g^{-1}$). The surface areas of the 1.25 mM and 0.125 mM coatings were 3.0 ± 0.03 and 3.5 ± 0.04 $m^2 g^{-1}$, respectively (Table 14). The sequentially coated planars showed an increase in SSA with increasing number of coatings. However, the SSA of the 10 coating sample was only 4.7 ± 0.08 $m^2 g^{-1}$. The surface areas of the samples with 2 and 5 coatings were 0.90 ± 0.01 and 1.9 ± 0.05 $m^2 g^{-1}$, respectively (Table 15). For all samples, the t-plots

Reproduced with permission of the copyright owner. Further reproduction prohibited without permission.

increased linearly with increasing P_{Rel} and the y-intercepts were equal to zero, indicating that the surfaces of all samples were non-porous in nature as operationally defined by N_2 absorption.

Table 14. Specific surface areas of coated† planar γ-Al_2O_3 prepared with varying initial Fe(III) concentrations and reaction times

Reaction Time	[Fe(III)] (mM)	SSA (m^2 g^{-1})	C
4 Days	0.125	7.2 ± 0.03	77.2
	1.25	10.5 ± 0.06	87.4
	12.5	3.6 ± 0.09	15.8
14 Days	0.125	3.5 ± 0.04	140.6
	1.25	3.0 ± 0.03	52.7
	12.5	9.2 ± 0.10	195.3

Table 15. Specific surface areas of planar γ-Al_2O_3 sequentially coated with 1.25 mM Fe(III) and a 4 day reaction period

Coating Sequences	SSA (m^2 g^{-1})	C
2	0.9 ± 0.01	31.7
5	1.9 ± 0.05	9.2
10	4.7 ± 0.08	509.8

Reproduced with permission of the copyright owner. Further reproduction prohibited without permission.

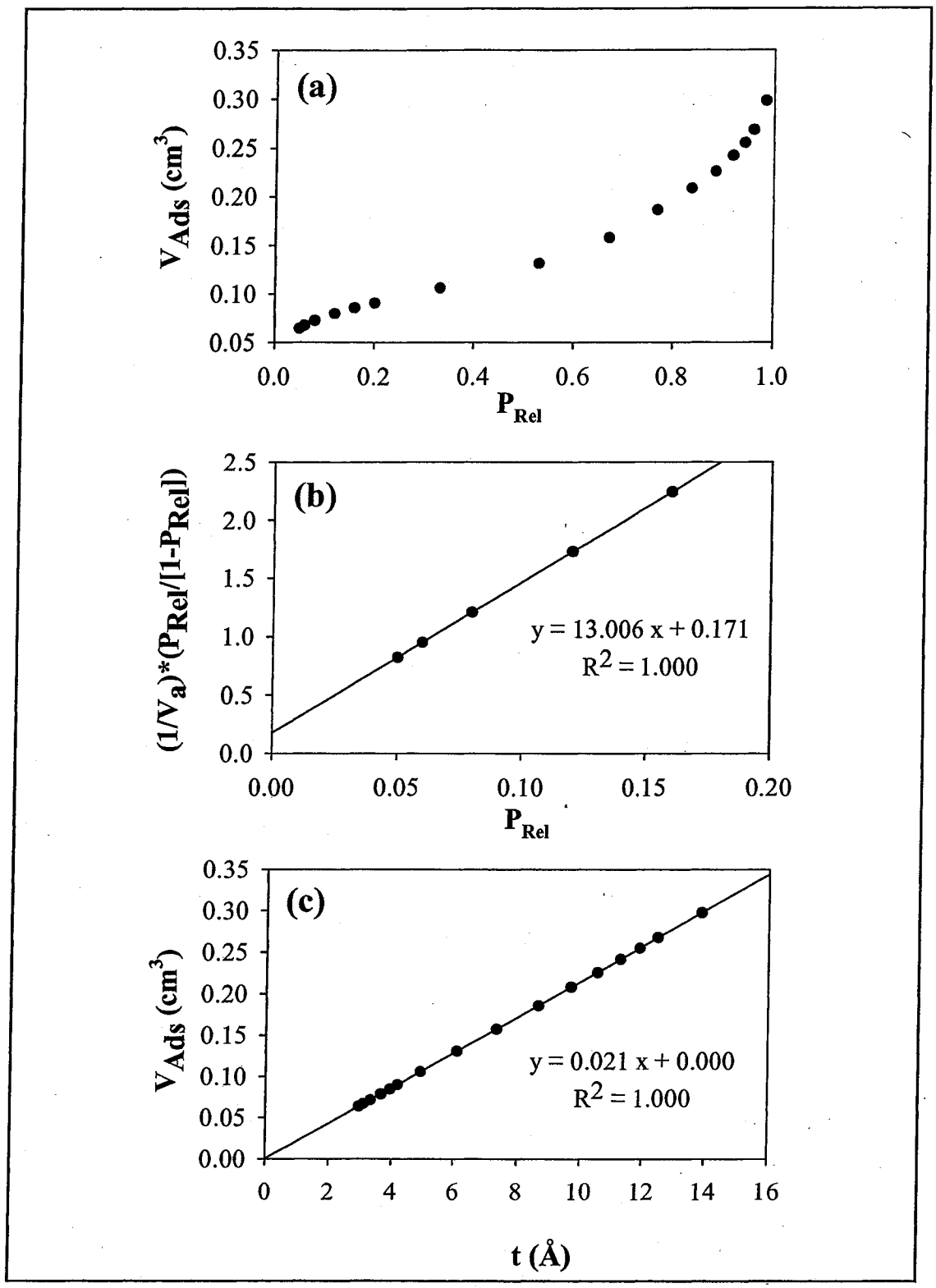

Figure 33. (a) Adsorption isotherm, (b) linear region of the BET equation and (c) t-plot for N_2 adsorption on planar γ-Al_2O_3 coated with 0.125 mM Fe(III) using a 4 day reaction period.

Reproduced with permission of the copyright owner. Further reproduction prohibited without permission.

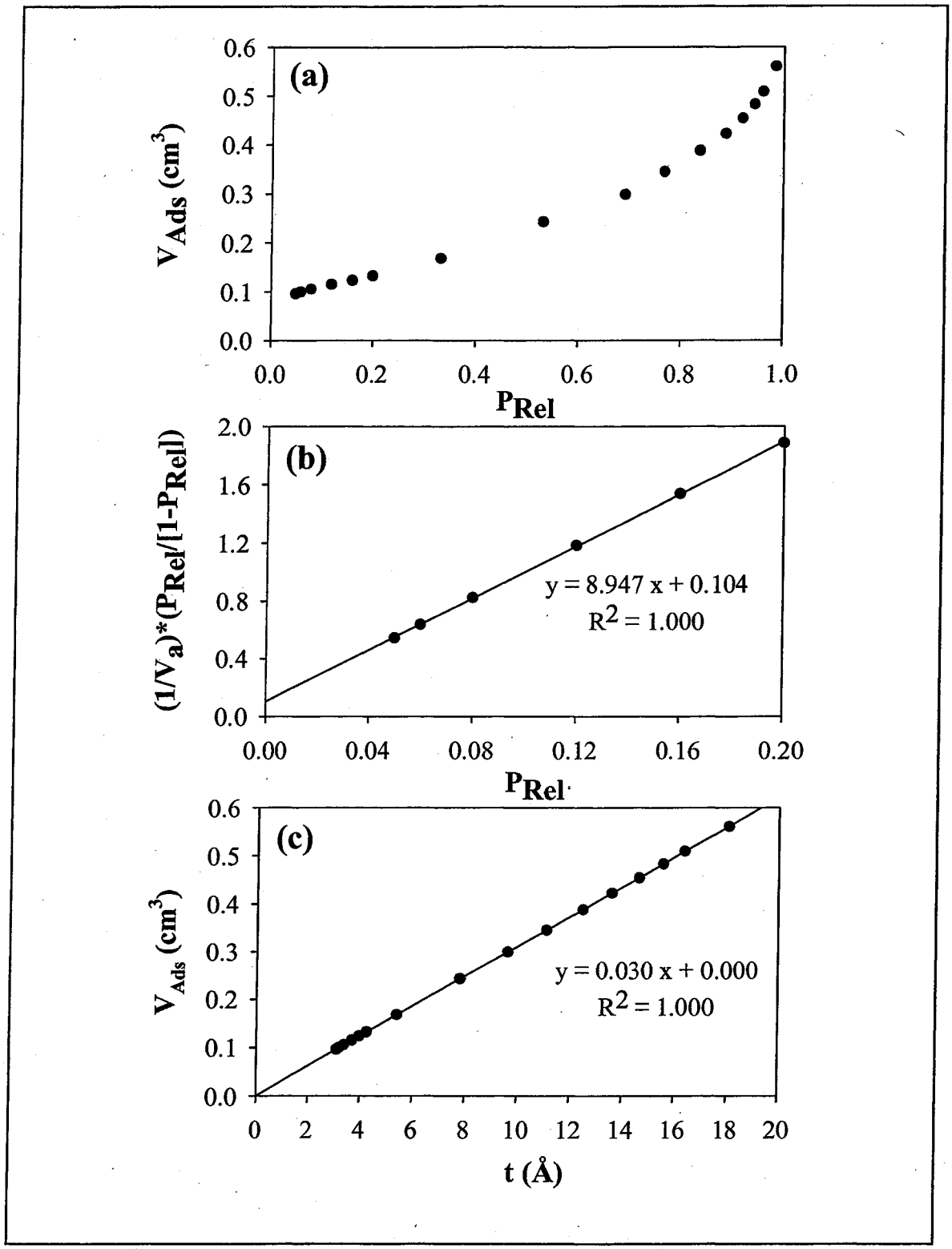

Figure 34. (a) Adsorption isotherm, (b) linear region of the BET equation and (c) t-plot for N_2 adsorption on planar γ-Al_2O_3 coated with 1.25 mM Fe(III) using a 4 day reaction period.

Reproduced with permission of the copyright owner. Further reproduction prohibited without permission.

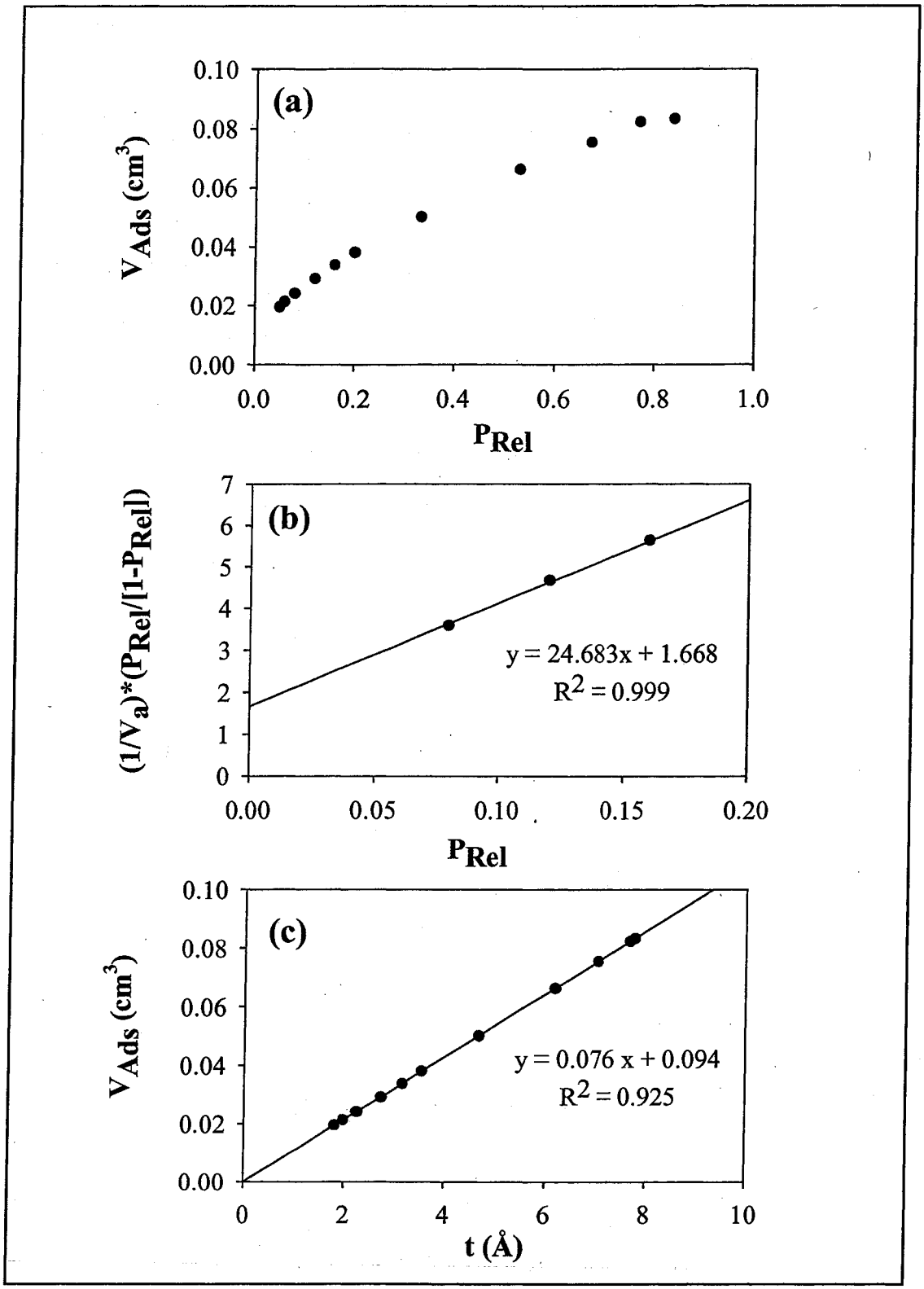

Figure 35. (a) Adsorption isotherm, (b) linear region of the BET equation and (c) t-plot for N_2 adsorption on planar γ-Al_2O_3 coated with 12.5 mM Fe(III) using a 4 day reaction period.

Reproduced with permission of the copyright owner. Further reproduction prohibited without permission.

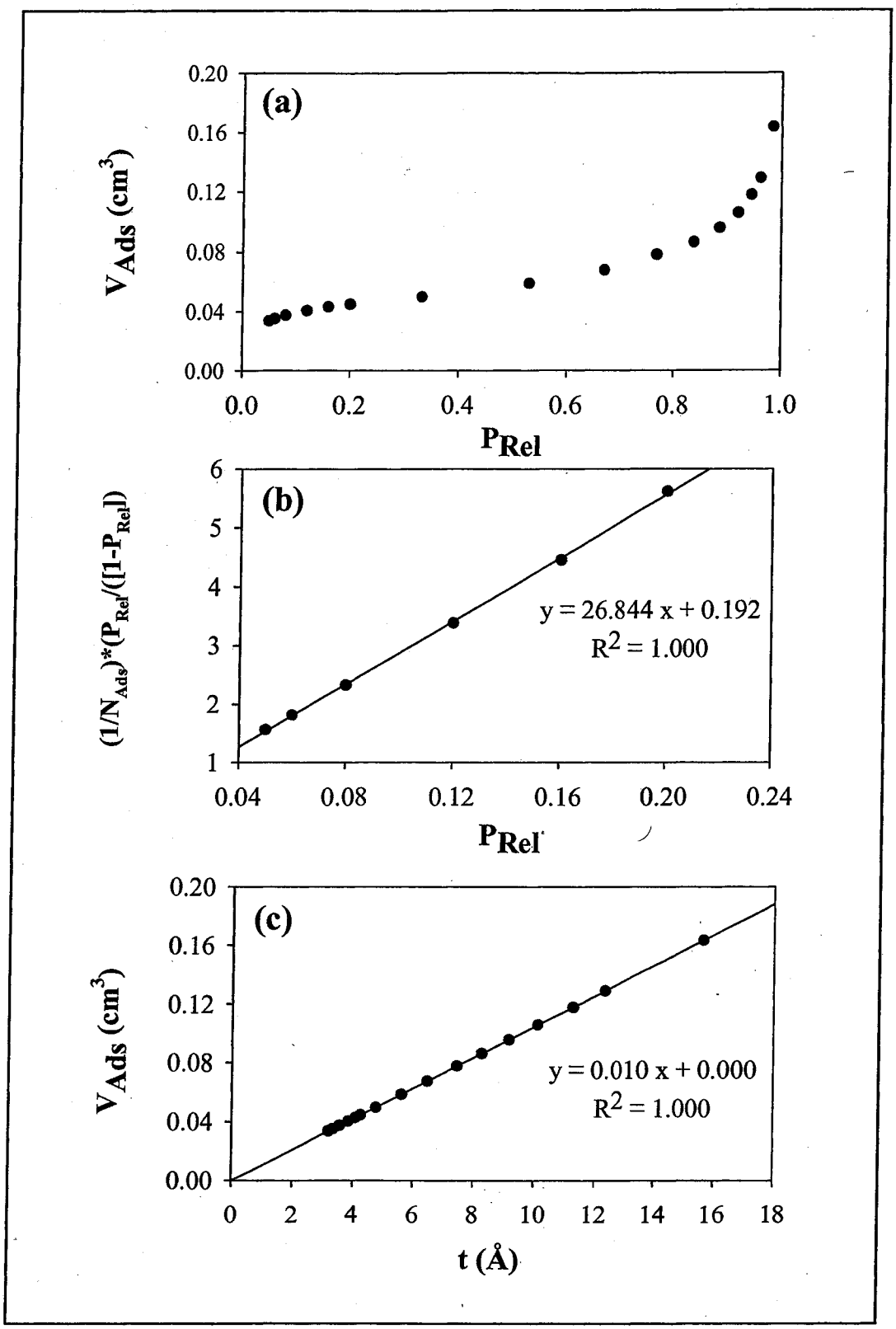

Figure 36. (a) Adsorption isotherm, (b) linear region of the BET equation and (c) t-plot for N_2 adsorption on planar γ-Al_2O_3 coated with 0.125 mM Fe(III) using a 14 day reaction period.

Reproduced with permission of the copyright owner. Further reproduction prohibited without permission.

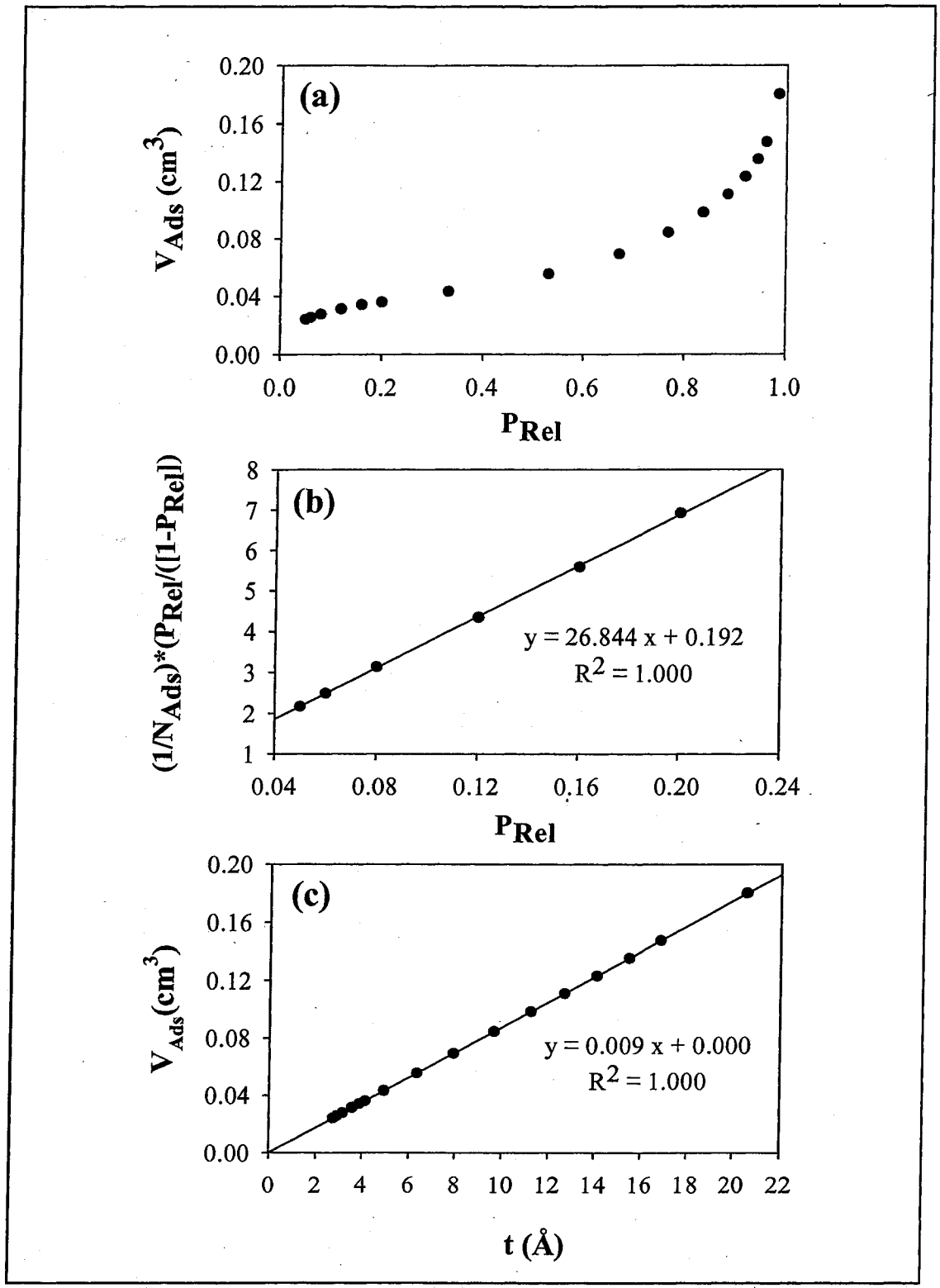

Figure 37. (a) Adsorption isotherm, (b) linear region of the BET equation and (c) t-plot for N_2 adsorption on planar γ-Al_2O_3 coated with 1.25 mM Fe(III) using a 14 day reaction period.

Reproduced with permission of the copyright owner. Further reproduction prohibited without permission.

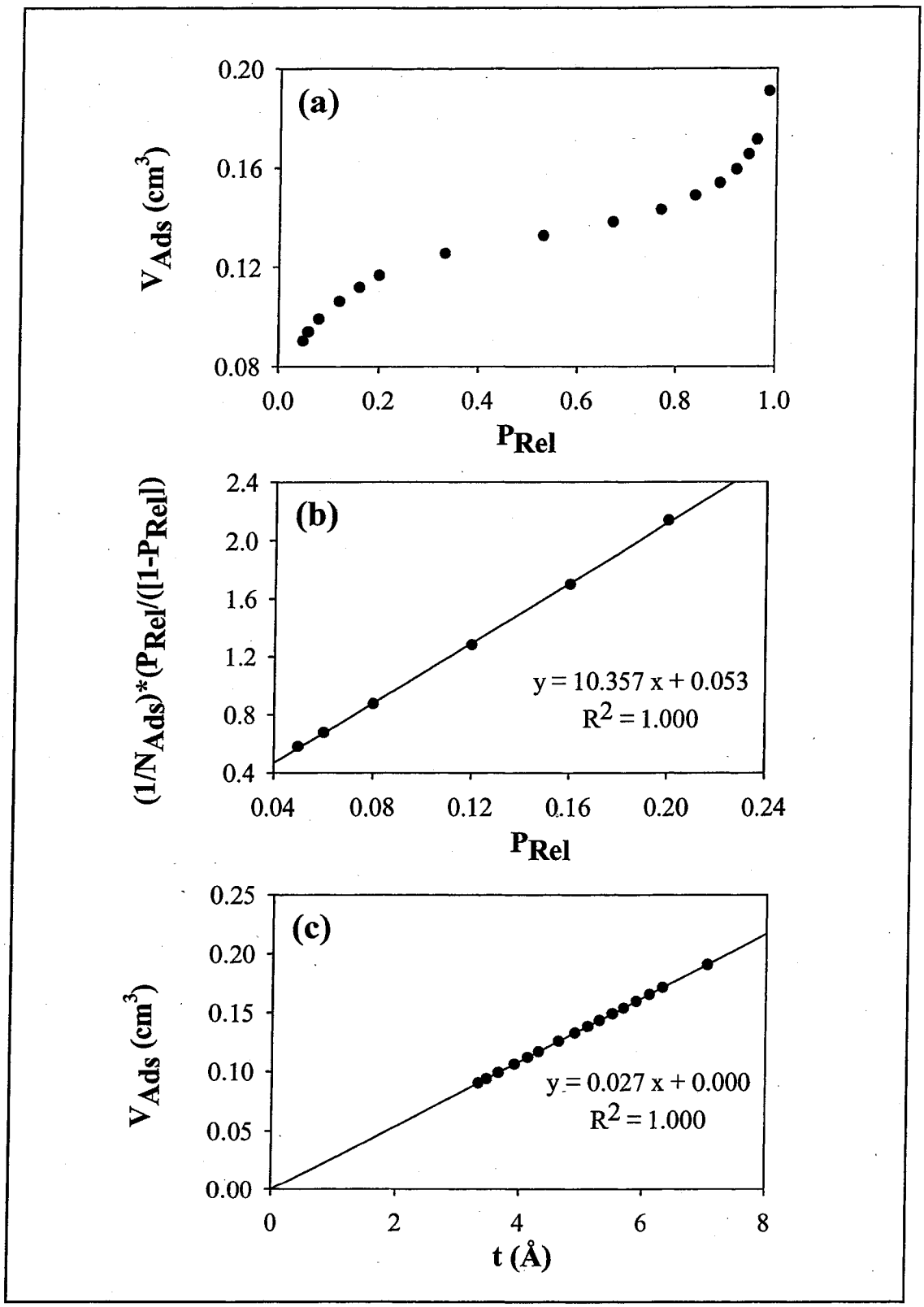

Figure 38. (a) Adsorption isotherm, (b) linear region of the BET equation and (c) t-plot for N_2 adsorption on planar γ-Al_2O_3 coated with 12.5mM Fe(III) using a 14 day reaction period.

Reproduced with permission of the copyright owner. Further reproduction prohibited without permission.

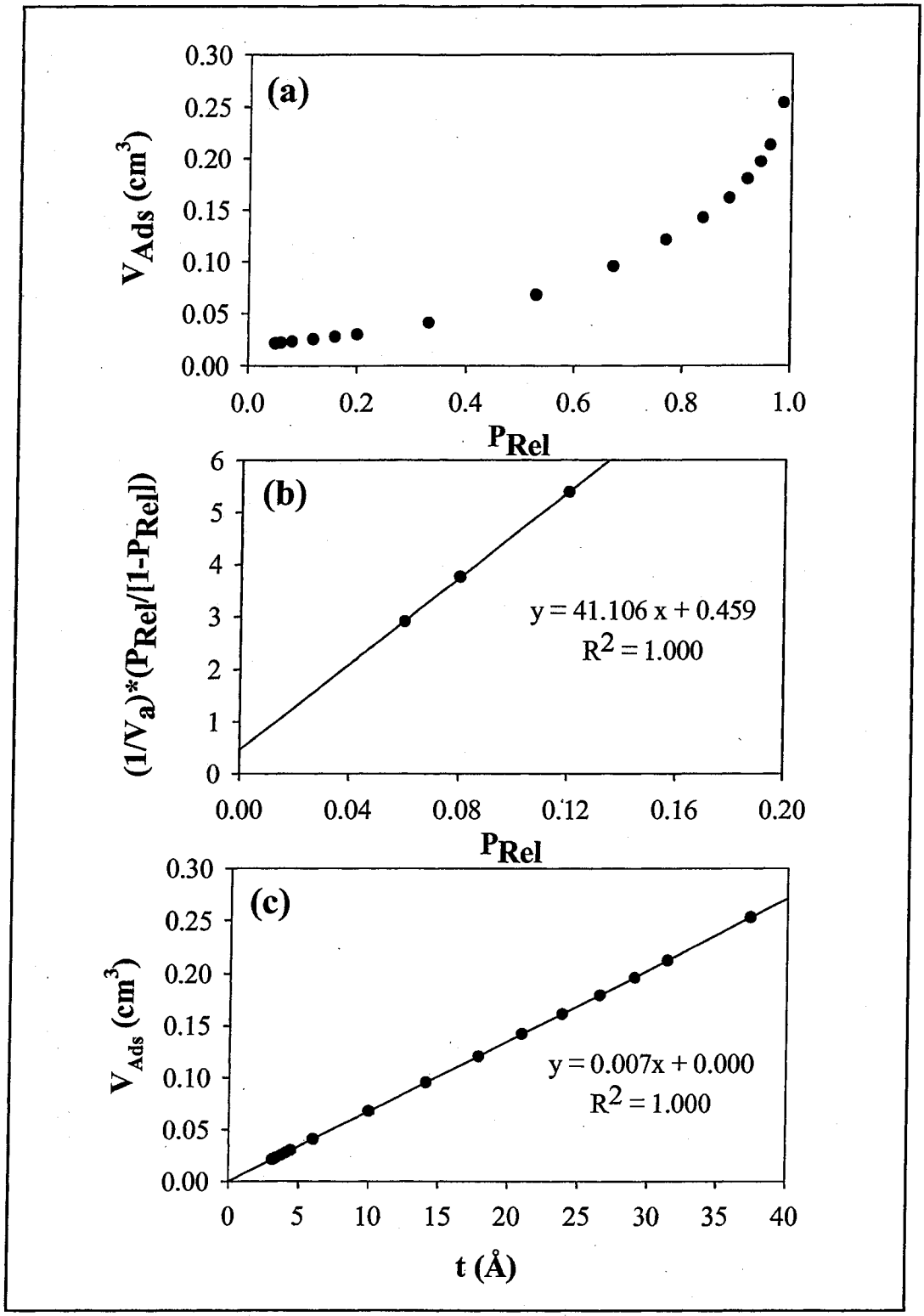

Figure 39. (a) Adsorption isotherm, (b) linear region of the BET equation and (c) t-plot for N_2 adsorption on planar γ-Al_2O_3 with 2 coatings of 1.25 mM Fe(III).

Reproduced with permission of the copyright owner. Further reproduction prohibited without permission.

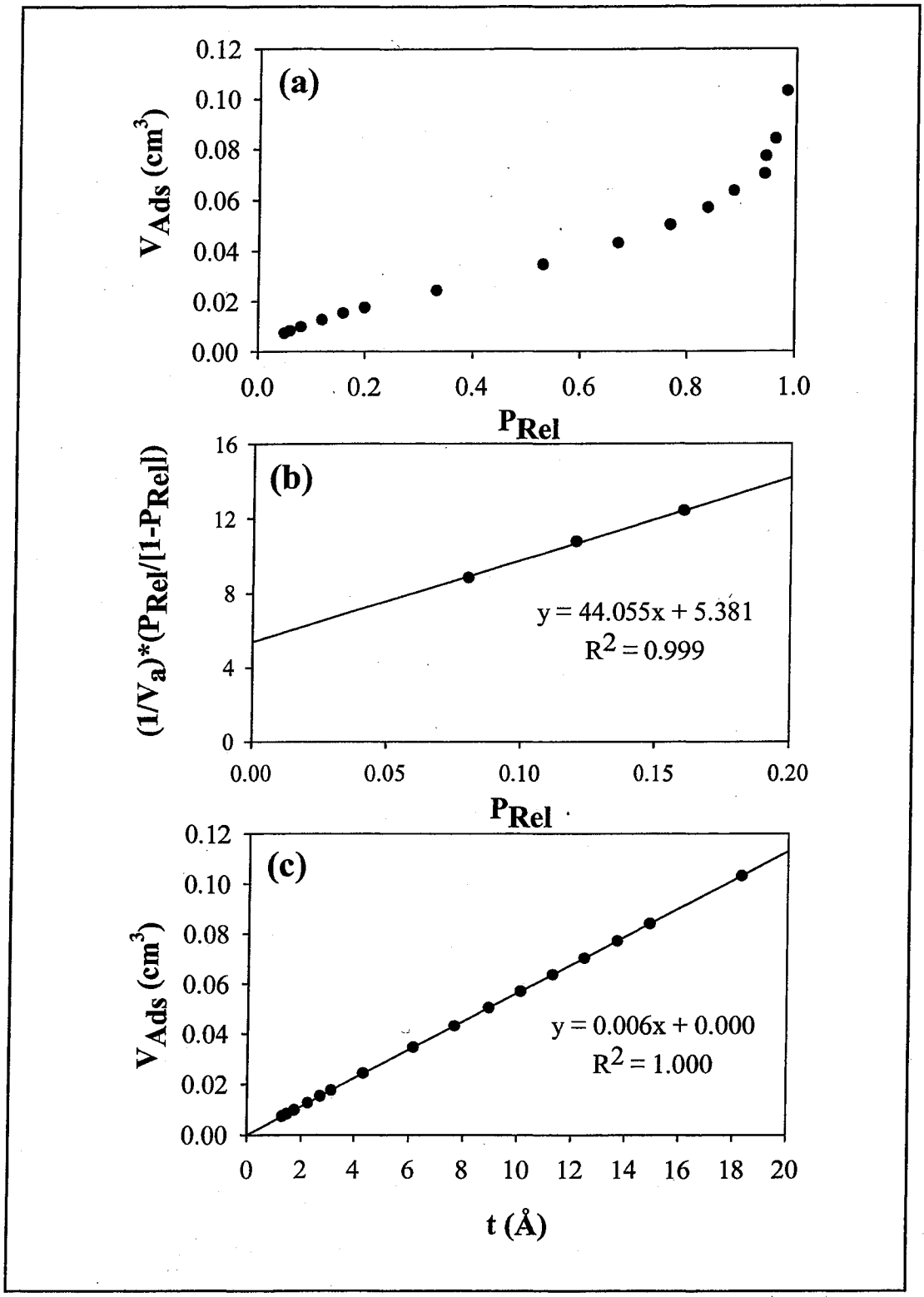

Figure 40. (a) Adsorption isotherm, (b) linear region of the BET equation and (c) t-plot for N_2 adsorption on planar γ-Al_2O_3 with 5 coatings of 1.25 mM Fe(III).

Reproduced with permission of the copyright owner. Further reproduction prohibited without permission.

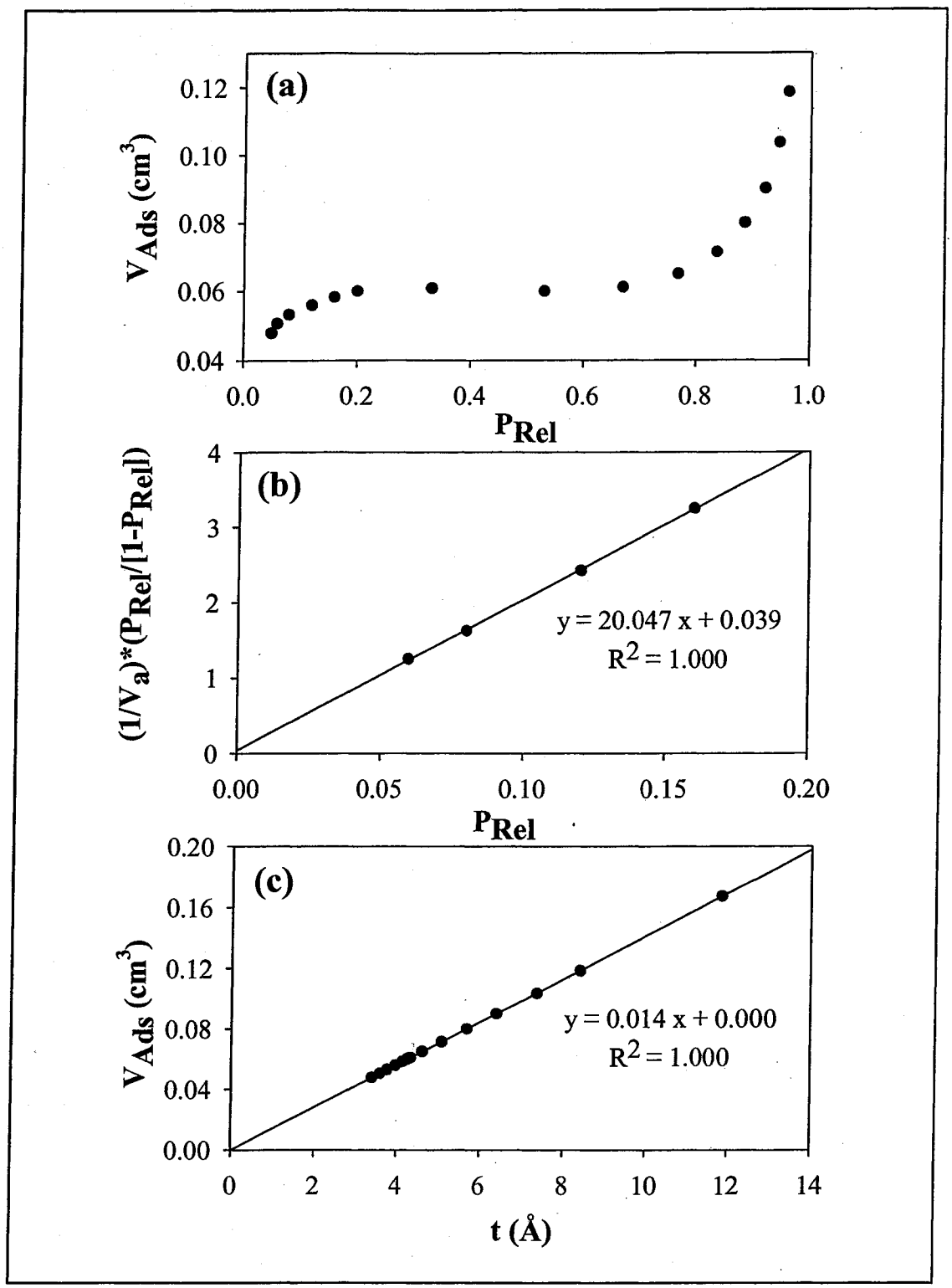

Figure 41. (a) Adsorption isotherm, (b) linear region of the BET equation and (c) t-plot for N_2 adsorption on planar γ-Al_2O_3 with 10 coatings of 1.25 mM Fe(III).

Reproduced with permission of the copyright owner. Further reproduction prohibited without permission.

Discussion

Changes in the initial concentrations of Fe(III), reaction time and the number of coating sequences had profound effects on the concentration, distribution and morphology of the coatings formed on the planar γ-Al_2O_3 surfaces. Changes in the initial concentration of Fe(III) had significant effects on the amount of Fe(III) deposited, as well as the distribution and morphology of the coatings. Increasing the reaction time from 4 to 14 days mainly affected the total amount of Fe(III) present. Using initial Fe(III) concentrations of 0.125mM and 1.25mM produced coatings with relatively uniform distributions for both the 4 and 14 day samples (Figs. 24a, b and 25a, b), but the total amount of Fe(III) present was much lower for the samples using an Fe(III) concentration of 0.125 mM (Table 11). Increasing the Fe(III) concentration to 12.5 mM produced a major shift in the distribution and morphology of the surface phase (Figs. 24c and 25c). Localized areas of high concentrations of Fe(III) were seen on the ToF-SIMS maps. However, examination these coatings with SEM at lower magnifications revealed a uniform morphology across the planar surface, indicating the lack of localized regions of Fe(III) deposition. Large crystals were seen covering the planar γ-Al_2O_3 surface. As the crystalline size of the coating increases, the vertical relief of the surface will also increase. It is possible that due to the inherent surface sensitivity of ToF-SIMS that what appear to be localized area of deposition are instead areas of the coating that are simply much higher than the surrounding surface.

Because of the relatively high % Fe obtained in the coatings using an initial concentration of 1.25 mM Fe(III), this condition was chosen for use in the sequential coating procedure. While a 14-day reaction period increased the % Fe, it was thought

Reproduced with permission of the copyright owner. Further reproduction prohibited without permission.

that using a 4-day reaction for multiple coatings would produce sufficiently concentrated coatings. Indeed, there was a strong relationship between increasing the number of coating sequences from 2 to 10 and the corresponding increases in the %Fe present in the coatings (Fig. 23). The overall distribution of Fe(III) in the coatings remained uniform throughout the sequential procedure (Fig. 26), and the major change noticed in the surface morphology was an increase in crystalline size and the dusty appearance of the surface at 5 and 10 coatings (Fig. 29).

Although attempts at quantifying the amount and distributions of Fe(III) present in the prepared coatings were successful, characterization of the Fe phase present in the coatings proved to be difficult. Visual inspection of the coated planar surfaces often suggested the dominance of a particular Fe phase (e.g. hematite on the 4 and 14 day 12.5 mM samples), but the presence of this phase could not be identified via XRD. For all samples, no peaks corresponding to characteristic peaks of pure Fe phases possibly present in our coatings could be identified (Figs. 30-32). This, along with the fact that the alumina phase may be soluble under these experimental conditions, may suggest the presence of a mixed Fe/Al phase.

Further evidence for the formation of a mixed oxide phase can be found in the BET surface area data. All of the Fe(III) coated samples were found to be non-porous as determined by the shape of their N_2 BET adsorption isotherms and t-plots (Figs. 33-38), but the measured specific surface areas were much lower than anticipated (Tables 14 and 15). Scheidegger et al. (1993) found that the SSA of goethite coated sands could be successfully predicted by the theoretical sum of the surface areas of the pure sands and the corresponding SSA normalized to the weight fractions of goethite present. This

Reproduced with permission of the copyright owner. Further reproduction prohibited without permission.

indicated that binding to the surface did not occupy a significant portion of the surface of the goethite crystal.

After coating the planar γ-Al_2O_3 with Fe(III), the available surface area of the resultant coating has decreased. A possible explanation for the decreased SSAs for the Fe(III) coated planar γ-Al_2O_3 in this study is the incorporation of the Fe(III) atoms into the Al-oxide coating. If binding of the Fe(III) particles to the γ-Al_2O_3 surface were strictly a surface phenomenon, the SSA of the resultant material should be able to be predicted either as described above assuming the attachment of the coating phase to the surface through topitaxical growth. However, if binding of the Fe(III) particles includes some sort of incorporation or filling mechanism with the alumina phase, a significant portion of both the Fe(III) and γ-Al_2O_3 particles may become unavailable to SSA measurements. An alternative hypothesis is that the SSA of the coated phase is lower than that of the alumina. However, this is less likely as Fe oxide phases most always have high surface areas.

The SEM images of the sequentially coated planar γ-Al_2O_3 may also point to the presence of a mixed phase coating. After 5 and 10 coating sequences, the surface takes on a fuzzy appearance. This dusty look is not present in the 2 coating sample. A possible explanation for this is that at lower numbers of coatings, Fe(III) particles are either being incorporated into the γ-Al_2O_3 phase or are filling in gaps between the γ-Al_2O_3 crystallites. As the number of coatings increases, the gaps become filled or the incorporation of Fe(III) into the γ-Al_2O_3 surface ceases, and deposition of Fe(III) on the surface ensues.

Other researchers have observed similar behavior when examining heavy metal sorption to aged iron oxides (Sørensen et al., 2000). This behavior also corresponds to

Reproduced with permission of the copyright owner. Further reproduction prohibited without permission.

the observed increase in SSA measured as a function of the number of coatings for these samples. Extensive incorporation or filling of the γ-Al_2O_3 could cause a depression of the SSA as discussed above. The lowest SSA for the sequentially coated planars was measured for the 2 coating sample where the dusty appearance was not observed. As the extent of incorporation decreases and particles begin to deposit on the surface, the SSA should increase. This increase is seen in the surface areas of the 5 and 10 coating samples.

Implications for Reactivity

In addition to the well-established effects of solution chemistry, researchers have found that the sorption capacity of an oxide is a function of crystallinity, particle size and surface area, as well as elemental composition (Colombo and Violante, 1996; Jackson, 1998; Violante et al., 2003). Some studies have shown SSA to be a controlling factor in metal sorption in natural systems (Horowitz and Elirck, 1987), and others have found that the composition of the solid phase, specifically the content of metal oxides governs trace metal adsorption (Dong et al., 2000; Knapp et al., 2002). However, natural coatings are generally not pure phases, but commonly incorporate varying amounts of Fe and Al (Taylor and Schwertmann, 1978; Nohan, 1986; Coston et al., 1995).

Mixed Fe-Al oxides are generally not simple mixtures of different amounts of Fe and Al oxides, but oxides with different mineralogy, chemical composition and surface properties, and therefore reactive properties towards cations and anions than their pure phase counterparts (Colombo and Violante, 1996; Violante et al., 2003). Thus, the varying crystallinities, surface areas and concentrations of Fe(III) in the surface coatings

Reproduced with permission of the copyright owner. Further reproduction prohibited without permission.

produced on the planar γ-Al_2O_3 in this study could very well have significantly different reactive properties based on their method of preparation. Future studies examining metal ion sorption to the various coatings will help elucidate these differences.

In mixed Fe-Al oxides, the interaction of various components can alter the metal sorption properties of the coatings (Davis and Leckie, 1978; Ballistrieri and Muray, 1982; Tipping and Cooke, 1982; Honeyman and Santshci, 1988). For example, studies have examined the affinity sequences for the sorption of heavy metals by Fe and Al oxides (Pickering, 1979; Forbes et al., 1976; McKenzie, 1980; Kinniburgh and Jackson, 1981; Violante et al., 2003). Affinity sequences were found to change for mixed Fe-Al oxides relative to the pure phase oxides with increasing amounts of Fe, although adsorption was not linearly correlated with Fe content (Violante et al., 2003). However, because Fe and Al are often highly correlated to each other and extraction methods usually remove both phases, distinction between the effects on sorption of the two phases is difficult (Daskalaskis and O'Connor, 1995; Fuller et al., 1996; Knapp et al., 2002).

Planar oxides offer an advantage in this area. As shown here, mixed Fe-Al oxides of varying morphologies and Fe/Al content can be made by coating planar γ-Al_2O_3. These mixed oxide coatings can be used in metal sorption studies to understand the reactivities of these coatings relative to one another, as well as relative to pure phase Fe and Al oxides. Planar oxides can also be used to elucidate the effects of chemical vs physical mixing of Fe and Al oxides on the resultant metal ion sorption reactivity. This has not been accomplished previously, as once pure phase Fe and Al oxides were combined, it was difficult, if not impossible, to physically separate to the materials as well as distinguish between the effects on sorption due to Fe or Al as described above.

Reproduced with permission of the copyright owner. Further reproduction prohibited without permission.

Because planar oxides and the mixed Fe-Al oxides are formed on a support, they can be easily separated from pure phase powders and the effects on sorption can be characterized separately.

In addition to implications for the uptake of metals, the differences in the mixed Fe-Al oxide coatings produced through our methods also have biological implications. Fe plays an essential role in many metabolic pathways for microorganisms. The microbial dissolution of Fe(III) oxides allows for the mineralization of organic matter in oxygen deficient environments, and the production of Fe(III) chelating agents called siderophores allows for the use of Fe by microorganisms in oxic environments (Lovley, 1991; Dubbin and Ander, 2003). The addition of Al into the system can have a profound effect on the ability of these microorganisms to effectively utilize Fe(III). It has been observed that the reductive dissolution of Fe(III) oxides is inhibited by Al substitution (Bousserrhine et al., 1998; Dominik et al. 2002). This inhibition is hypothesized to result from a non-congruent dissolution of Al and Fe, with more Fe being dissolved, and the formation of non-reducible Al coatings on either the mineral or bacterial surface.

These findings imply that the microbial reduction and dissolution rates of the mixed Fe-Al oxide coatings would vary depending on their elemental composition and morphology. In coatings with lower Fe/Al ratios, it is expected that microbial dissolution would be inhibited, whereas coatings with higher Fe/Al ratios may be more readily dissolved. Additionally, the morphology of the coating may have an effect on the biological reduction of Fe from these materials. The samples analyzed in this study were thought to consist of a mixed Fe-Al oxide phase rather than a coating of an Fe oxide on top of the γ-Al_2O_3 phase, indicating that dissolution of the planar γ-Al_2O_3 coating

Reproduced with permission of the copyright owner. Further reproduction prohibited without permission.

occurred. Each coating method may have produced oxide phases with different amounts and crystallinities of Fe and Al exposed at the surface, thus affecting the rate of dissolution of the oxides due to bacterial reduction. Future studies will examine Pb(II) sorption to these mixed planar Fe/Al oxides to determine the effects of different morphologies and Fe/Al ratios on Pb(II) sorption behavior relative to the analogous pure phase Fe and Al oxides.

Reproduced with permission of the copyright owner. Further reproduction prohibited without permission.

CHAPTER 6

Emplacement of Planar γ-Al_2O_3 in Natural Sediments

Introduction

It is well known that the fate and transport of heavy metals in aquatic systems is largely coupled to reactions that occur at the sediment-water interface. These reactions are highly dependent on the nature and abundance of reactive mineral phases. Coatings of Fe, Mn and Al along with organic matter are thought to dominate metal ion surface complexation in oxic sediments (Hem, 1977, Warren and Zimmerman, 1994, Bertsch and Seaman, 1999, Dong et al., 2001). In anoxic sediments, the partitioning of metals is strongly influenced by the presence of sulfide phases (Simpson et al., 2004).

Much of the knowledge regarding metal sorption behavior has been derived from experiments on pure phase model compounds. These studies have provided a large base of knowledge describing the boundary conditions of sorbate/mineral surface interactions and have been successful in identifying surface functional groups involved in complexation reactions (Bertsch and Seaman, 1999). However, reactions in the natural environment are rarely at equilibrium, but rather are in a state of continuous change because of the dynamic processes occurring (Sposito, 1984; Sparks, 1995). The heterogeneous nature of sediments as well as the complexity of the natural environment has made it difficult to extend these laboratory-based results to interpret observations made at the field scale. Additionally, differences in field sampling locations and the

Reproduced with permission of the copyright owner. Further reproduction prohibited without permission.

composition of the particulate matter can result in differences in distribution coefficients from field data making a broad scale application of laboratory data even more complicatec (Müller and Sigg, 1990).

Recently, metal ion sorption processes have been studied in the laboratory through the use of planar oxides (Conrad et al., 2002). Planar oxides consist of thin oxide coatings approximately 20 nm in thickness prepared on an underlying metal substrate. They can be prepared through high-pressure, high-temperature steam oxidation of a metal foil or through discrete particle attachment. Because these oxides are formed on a support, they are more similar to natural reactive phases which are often present as coatings on mineral surfaces. Also, because of their morphology, planar oxides can be used not only in laboratory studies, but can be emplaced directly into natural sediments where they can react in situ. The planars can then be retrieved and the surface complexes formed on them under natural conditions can be characterized and compared to surface complexes formed on identical materials under controlled laboratory conditions. Thus, the use of planar oxides is a step forward in the challenge of bridging the gap between laboratory and field studies.

The metal/oxide system chosen for this study is Pb(II)/γ-Al_2O_3 which has been studied extensively by both spectroscopic and wet-chemical techniques (Hohl and Stumm, 1976; Davis and Leckie, 1978; Chisholm-Brause et al., 1990, Bargar et al., 1996; Bargar et al., 1997). Previous work in our laboratory has compared Pb(II) uptake on planar γ-Al_2O_3 to that on bulk γ-Al_2O_3 under controlled conditions (Conrad et al., 2002, this dissertation, Ch. 3). The results of these studies have shown that Pb(II) uptake on the planar oxides was quantitatively similar to that seen on the bulk materials and that the

Reproduced with permission of the copyright owner. Further reproduction prohibited without permission.

structure of the surface complexes formed are comparable, thus connecting the planar system to the large body of knowledge describing Pb(II) uptake onto the bulk materials.

The work presented here builds on these results by emplacing the planar γ-Al_2O_3 into mesocosm systems containing natural sediments and waters. The objective of this study was to test the ability to use planar oxides as a tool to investigate metal ion sorption/desorption processes in natural sediments, thereby linking laboratory and field studies. Planar oxides with varying initial Pb(II) loadings were emplaced into natural sediments. Changes in Pb(II) concentrations on the planar γ-Al_2O_3 surface were characterized to understand Pb(II) complexation behavior as a function of emplacement time and redox characteristics of the sediments. Associations with Fe and S were also measured, and their effect on Pb(II) concentrations will be assessed.

Methods

Sediments used for this study were collected from Baltimore Harbor, Maryland in July, 2003. Baltimore Harbor is located in the northwest branch of the Patapsco river, a northern tributary of the Chesapeake Bay. Along with the Elizabeth and Anacostia rivers, Baltimore Harbor is one of the most polluted waterways in the Chesapeake Bay system. Sediments here have a long history of contamination by organics and metals, with high levels of PAHs, PCBs, and heavy metals such as Cu, Cr, Hg, Pb and Zn all being present in the sediments. The sediments used in this study consisted of 2 to 5 % OC, 150 ± 20 mg Kg^{-1} Pb, and were composed of mostly clay and silt sized particles (% sand < 20%) (Baker, personal communication).

Reproduced with permission of the copyright owner. Further reproduction prohibited without permission.

A 5-gallon bucket of surface and subsurface sediments were homogenized and placed into two 25-gallon Nalgene containers resulting in mud beds approximately 12 cm in depth. Unfiltered water from the York River was pumped through the tanks at a rate of 3 L/hr (temperature=28°C, pH=7.45 ± 0.05, salinity=18.0 psu). Sediments were allowed to equilibrate for two weeks prior to the experiment. During this time, a visible oxic layer that was approximately 2-3 mm thick formed on the surface sediments in both tanks.

The initial conditions of the experiment consisted of three sets of planar γ-Al_2O_3 prepared according to the methods in chapter 3. One set of planars was unreacted with Pb(II), with the remaining two sets loaded with 0.27 μmol Pb/m^2 (Low [Pb(II)]) and 2.2 μmol Pb/m^2 (High [Pb(II)]) (Table 16, see chapter 3 for details on Pb(II) sorption procedure). Inspection of the Pb(II) loaded planars using ToF-SIMS elemental maps (data not shown) showed a uniform distribution of Pb(II). The three conditions represented the following scenarios: particles with a clean γ-Al_2O_3 surface, particles with low contaminant loads and particles with high contaminant loads being deposited in the sediments. At lower sorption densities, metal surface complexes are often bound to surface sites with very high affinities making the metal more strongly attached to the surface. At higher sorption densities, these high affinity sites may be unavailable, causing metals to bind less strongly to the sediment surface. Previous XAS analysis of the Pb(II) loaded planar γ-Al_2O_3 used for this study showed that at both coverages, Pb(II) was predominantly sorbed as mondentate complexes, with smaller amounts of bidentate complexes present. Variations in the local structure of these complexes were observed as

Reproduced with permission of the copyright owner. Further reproduction prohibited without permission.

well as differences in the relative proportions of these complexes at the two coverages used (see Chapter 4, Table 9).

The planars were approximately 6 cm in length by 1.5 cm in width with a notch cut into the bottom edge to indicate the orientation of the sample (Fig. 42). Each set of planar γ-Al_2O_3 was emplaced in the sediments with approximately 2 cm of the planar being visible above the sediment surface. The oxic anoxic boundary occurred at 2-3 mm depth in the sediments. The remaining 4 cm of the planar was in anoxic sediments. Each set of planars was allowed to react for 1, 4, 7 or 14 days and was run in duplicate in each of two tanks. Each treatment had an area that was exposed to oxic sediments, anoxic sediments and a boundary layer where the redox conditions of the sediments fluctuate. A flowchart of the experimental setup is shown in Fig. 43. After removal from the sediments, the planars were rinsed copiously with DDI (18 mΩ) H_2O and air-dried.

Table 16. ToF-SIMS Pb/Al ratios of planar γ-Al_2O_3 with three Pb(II) loadings prior to emplacement

Sample	Estimated Pb(II) Loading (μmol Pb/m^2 γ-Al_2O_3)	ToF-SIMS Pb/Al
Unreacted	0.0	0.0005 ± 0.0005
Low [Pb]	0.3	0.0080 ± 0.0030
High [Pb]	2.2	0.0120 ± 0.0070

Reproduced with permission of the copyright owner. Further reproduction prohibited without permission.

Surface Analysis

Changes in Pb(II) concentrations, as well as the presence of other complexing agents (e.g., Fe and S), on the planar surfaces under each condition were analyzed using a TFS-2100 TRIFT II Time of Flight Secondary Ion Mass Spectrometer. Samples were analyzed by rastering a 22 KeV Au^+ ion gun over an 80 μm x80 μm area. Data were normalized to Al intensities to minimize instrumental variation. The specific peaks analyzed are listed in Table 17, and raw peak intensities can be found in Appendix 5.

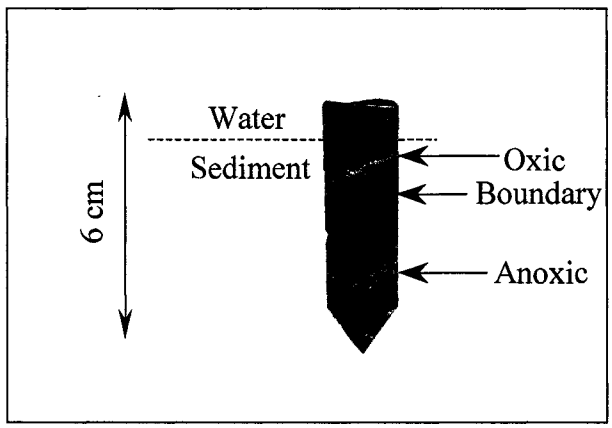

Figure 42. Photograph of a planar γ-Al_2O_3 after emplacement in natural sediments for 7 days. A notch was cut into the bottom of the planar oxide to indicate the orientation of emplacement. Note also that there is a distinguishable region of discoloration on the planar surface corresponding to the boundary layer between oxic and anoxic sediments.

Table 17. Analytical peaks used for ToF-SIMS analysis of emplaced planar γ-Al_2O_3

Element	ToF-SIMS Peak (Mass)
Al	27
Fe	56
Pb	208
S	32

Reproduced with permission of the copyright owner. Further reproduction prohibited without permission.

Reproduced with permission of the copyright owner. Further reproduction prohibited without permission.

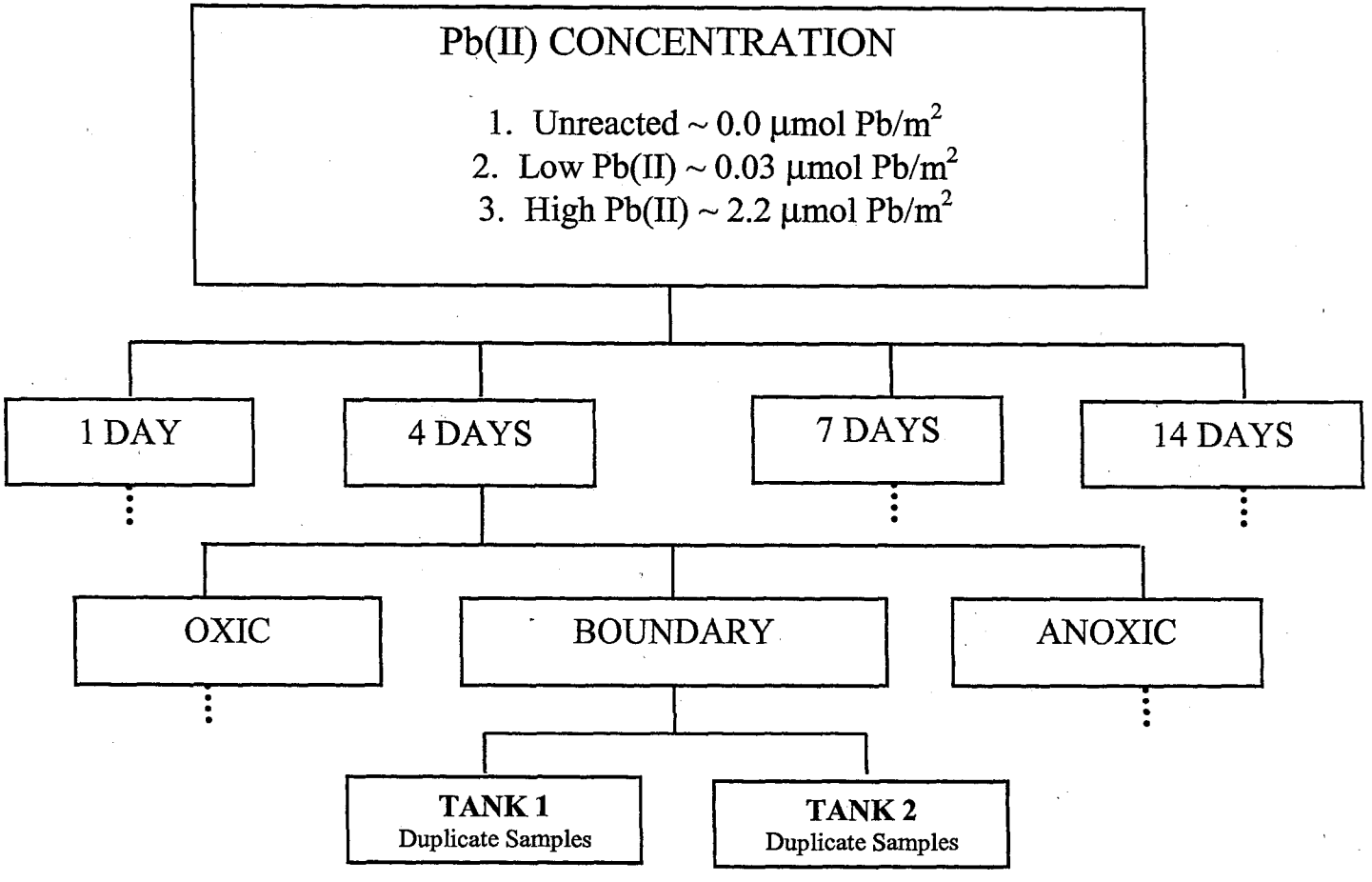

Figure 43. Flowchart depicting the experimental setup for emplacement of the planar γ-Al_2O_3. Three initial Pb(II) concentrations were used. For each of these Pb(II) loadings, the planars were emplaced for 1, 4, 7 and 14 days in oxic, boundary and anoxic sediments. All samples were run in duplicate, and replicate conditions were run in a second tank for a total n = 4 for each experimental condition.

Time of Flight Secondary Ion Mass Spectrometry (ToF-SIMS) analyzes only the first monolayers of a sample and provides detection limits on light element oxides better than 1 mg Kg^{-1} of the surface (Benninghoven, 1994). Also, due to the ability to know the exact location of measurement on the sample with ToF-SIMS, a vertical measurement of the gradient of change from the oxic portion of the sample to the anoxic portion was obtained on each set of samples.

To assess the potential for corrosion of the surface due to biofouling and oxidation, the planar oxides were examined prior to emplacement with a LEO 435VP Zeiss (LEO) / Cambridge scanning electron microscope with a beam current of 12 pA and a beam energy of 10 KV (Fig. 44a, b and c). After removal from the sediments, the planars were re-inspected for signs of corrosion. Both before and after emplacement, three to five fields were inspected on each sample. While a few anomalous areas were observed, the images shown here are representative of the overall appearance of the sample. Most irregularities were due to the precipitation of NaCl crystals on the planar surface.

Statistical Analysis

The influence of initial Pb(II) loadings, emplacement time and redox conditions were assessed in SAS using a nested random model. Prior to analysis, the Pb(II) concentrations were normalized to Al and these data were log transformed to satisfy the condition of equal variance for the statistical analyses. Once significant effects were identified, subsets of the data were examined using ANOVA to ascertain specific interactions of the significant variables. Correlations between Pb/Al and Fe/Al and S/Al

Reproduced with permission of the copyright owner. Further reproduction prohibited without permission.

were determined by regression analysis in Minitab. For each regression (n = 4), data were separated by Pb(II) loading, redox condition and time for each set of experimental conditions (e.g., low Pb(II) loading, oxic sediments, 7 days). All statistical analyses were run at $\alpha = 0.05$.

Results

Changes in Pb(II) Concentrations

Significant effects were seen for initial Pb(II) loading ($p = 0.001$) and emplacement time ($p = 0.010$) at an $\alpha = 0.05$. These two parameters accounted for 40.6 % of the variance in the data (Table 18). No significant effects due to redox conditions were observed. To further examine the effects due to initial Pb(II) loadings, the data were separated into subsets of unreacted, low Pb(II) loaded, and high Pb(II) loaded samples (Fig. 44 a, b and c, respectively). Lead loadings and emplacement times for each loading were compared using a one-way ANOVA. The Pb/Al ratios of the unreacted samples were found to be significantly lower than the low and high Pb(II) loaded samples ($p = 0.002$ and 0.001, respectively). No significant difference was found between the low

Table 18. Results from the nested random model describing the variation of Pb/Al ratios on emplaced planar γ-Al_2O_3

Variance Source	Sum of Squares	Degrees of Freedom	P Value	Percent of Total Variance	Error Term
Initial [Pb(II)]	12.39	2	0.001	26.97	Redox
Redox	1.45	6	0.834	0.00	Time
Time (days)	14.13	27	0.010	13.59	Error
Error	29.53	108	N/A	59.44	N/A

Reproduced with permission of the copyright owner. Further reproduction prohibited without permission.

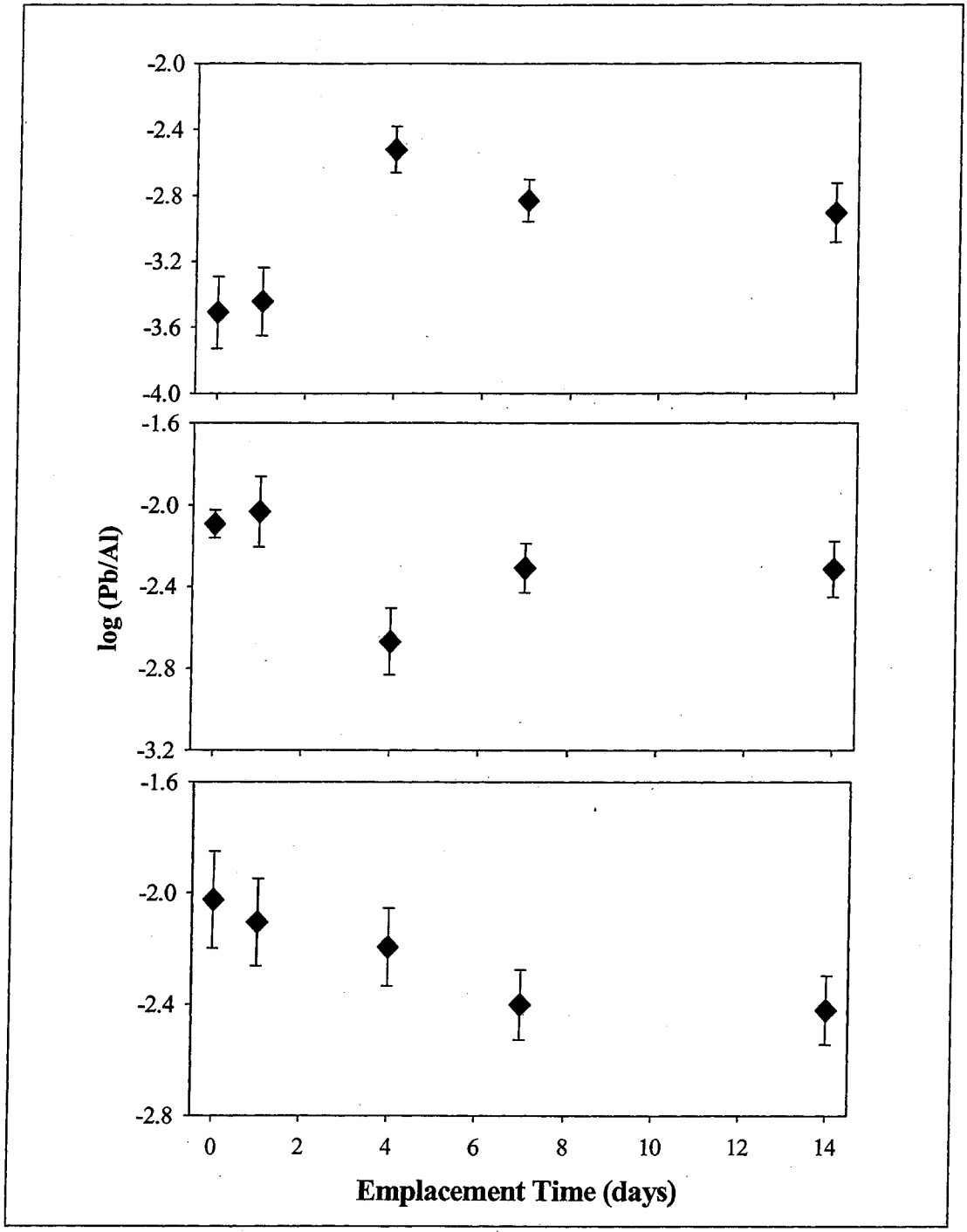

Figure 44. Pb/Al ratios of (a) unreacted, (b) low Pb(II) loaded and (c) high Pb(II) loaded planar γ-Al_2O_3 emplaced for 1, 4, 7 and 14 days. Error bars indicate the positive standard deviation of replicate measurements (n = 4).

Reproduced with permission of the copyright owner. Further reproduction prohibited without permission.

and high Pb(II) loaded samples. The effects of emplacement time were also examined within each of these subsets. A significant effect of emplacement time was found for the unreacted and low Pb(II) loaded planars ($p = 0.002$ and 0.045, respectively). In both cases, the one day sample was different from the 4 day sample, but not significantly different from any other samples. No effect of emplacement time was determined for the high Pb(II) loaded samples.

Pb(II) sorption kinetics onto the unreacted planar γ-Al_2O_3 were examined as a function of reaction time (Fig. 45). These data can be modeled using a single site saturation ligand binding model with the following equation:

$$C_{surf} = a(1 - e^{-bt}) \qquad (7)$$

where C_{surf} is the concentration of Pb on the planar γ-Al_2O_3 surface, a is the ratio of uptake of Pb(II) to desorption of Pb(II) multiplied by the concentration of Pb(II) in the sediments, b is the rate of elimination of Pb(II) from the surface and t is time in units of days. In this model, initial sorption of Pb(II) occurs rapidly and is then followed by a slower increase in surface Pb(II) concentrations.

Pb(II) Association with Fe and S

Correlations with the environmentally important complexants Fe and S were determined using regression analysis in Minitab to try to identify chemical factors controlling Pb(II) concentrations on the emplaced planar γ-Al_2O_3. The results of these correlations are shown in table 19. Significant relationships ($\alpha = 0.05$) are indicated in bold type. The highest number of significant correlations was seen on the low Pb(II) loaded planars. Pb was significantly correlated with Fe in the oxic sediments on the 1

Reproduced with permission of the copyright owner. Further reproduction prohibited without permission.

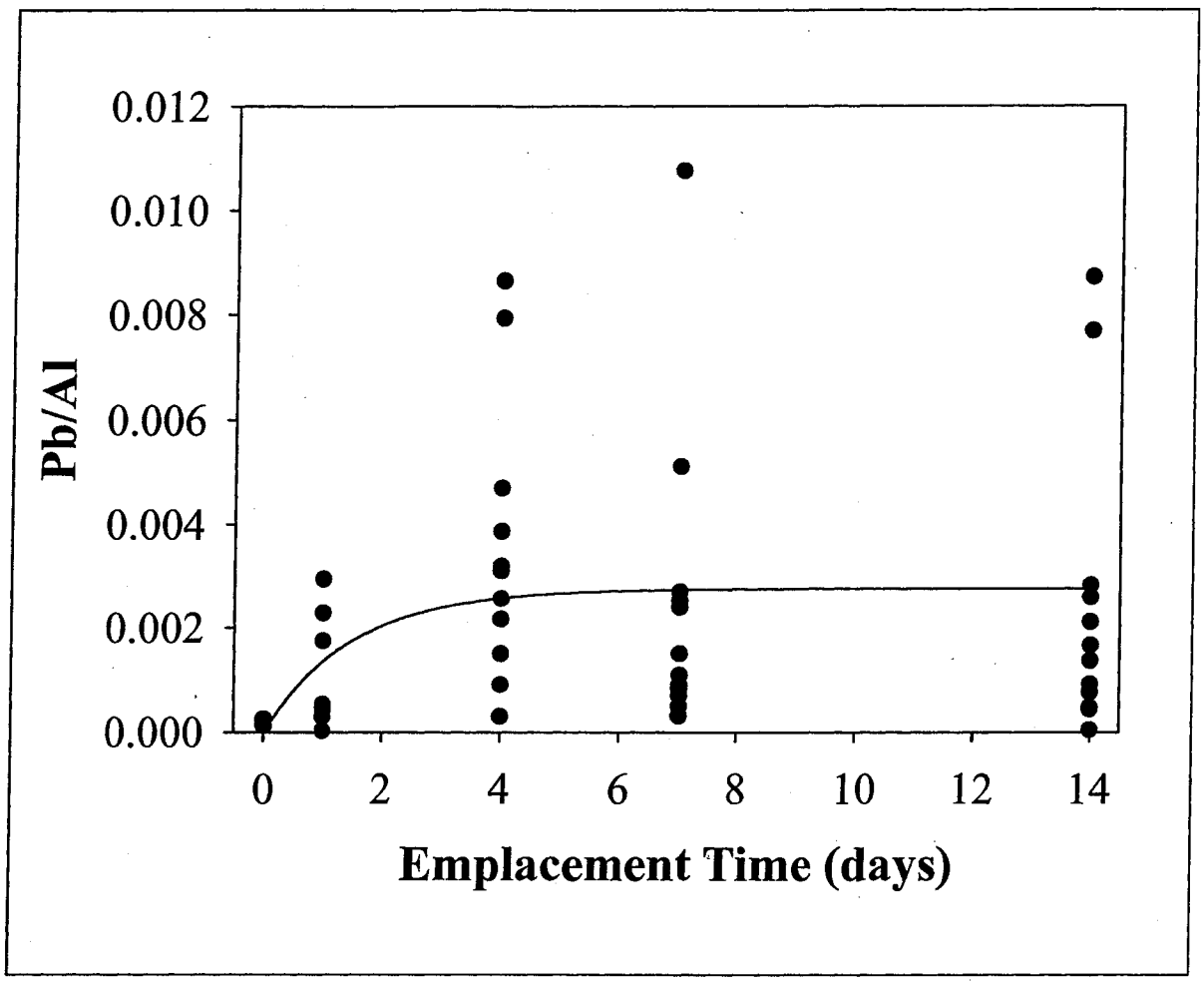

Figure 45. Sorption kinetics of Pb(II) on unreacted planar γ-Al_2O_3 as a function of emplacement time. Data were modeled using an exponential growth to max model and show the typical two stage time-dependent behavior observed for metal sorption to pure phase components.

Reproduced with permission of the copyright owner. Further reproduction prohibited without permission.

and 7 day samples (R^2 = 0.84 and 0.93, respectively), in the boundary sediments on the 1 and 4 day samples (R^2 = 0.86 and 1.0, respectively), and in the anoxic sediments on the 1 and 7 day samples (R^2 = 0.90 and 0.95, respectively). Sulfur was significantly correlated to Pb in the oxic samples at 14 days, in the boundary samples at 7 days and in the anoxic samples at 1 day (R^2 = 0.88, 0.81 and 0.90, respectively). The unreacted planars had the next highest number of significant correlations with Fe and S. Three significant correlations were observed with Fe, on the oxic samples at 1 day (R^2 = 1.0) and 7 days (R^2 = 0.85), and on the anoxic samples at 4 days (R^2 = 0.81). Only two correlations were seen between Pb and S. Significant relationships were observed on the boundary samples at 4 days and on the anoxic samples at 14 days (R^2 = 0.98 and 1.0, respectively). The fewest number of significant relationships between Pb and Fe and S was found on the high Pb(II) loaded planar γ-Al_2O_3 samples. Two significant correlations with Fe were seen, one in the oxic samples at 7 days (R^2 = 0.98) and one in the boundary samples at 4 days (R^2 = 0.99). One significant correlation with S was found for the anoxic samples at 14 days (R^2 = 0.87).

Reproduced with permission of the copyright owner. Further reproduction prohibited without permission.

Table 19. Pb(II) correlations† with Fe and S on emplaced planar γ-Al_2O_3

Time (days)	Redox	Unreacted		Low Pb(II)		High Pb(II)	
		Fe	S	Fe	S	Fe	S
1	Oxic	**1.00**	0.39	**0.84**	0.05	0.02	0.80
	Boundary	0.59	0.01	**0.86**	0.30	0.17	0.19
	Anoxic	0.09	0.16	**0.90**	**0.90**	0.63	0.56
4	Oxic	0.22	0.03	0.03	0.65	0.73	0.54
	Boundary	0.02	**0.98**	**1.00**	0.31	**0.99**	0.71
	Anoxic	**0.81**	0.07	0.77	0.78	0.59	0.55
7	Oxic	**0.85**	0.00	**0.93**	0.65	**0.98**	0.06
	Boundary	0.13	0.22	0.79	**0.81**	0.61	0.59
	Anoxic	0.38	0.00	**0.95**	0.19	0.41	0.07
14	Oxic	0.46	0.78	0.48	**0.88**	0.13	0.80
	Boundary	0.21	0.02	0.26	0.14	0.22	0.24
	Anoxic	0.41	**1.00**	0.63	0.10	0.08	**0.87**

†Bold numbers indicate significant correlations at $\alpha = 0.05$.

Changes in Planar γ-Al_2O_3 Surface Morphology

Pre-Emplacement

Prior to emplacement, the crystalline, needle-like oxide structures were seen on the unreacted planar γ-Al_2O_3 surface (Fig. 46a). In contrast, the planars that had been loaded with low and high Pb(II) concentrations contained dense patches of globular oxide islands (Fig. 46 b and c).

Unreacted Planar γ-Al_2O_3

SEM investigation of the emplaced unreacted planar surfaces showed little variation in the overall morphology with time. In all three redox zones, oxic (Fig. 47), anoxic (Fig. 48) and boundary (Fig. 49), the same trend was observed. After 1 day of

Reproduced with permission of the copyright owner. Further reproduction prohibited without permission.

emplacement, the planar surface was relatively unchanged. After 4 days of emplacement, the shape of the oxide islands had become slightly more amorphous. However, after 7 days of emplacement, the islands returned to the more crystalline form and increased in density up to 14 days.

Low Pb(II) Loading

The surfaces of emplaced planar γ-Al_2O_3 with low Pb(II) loadings were quite different after emplacement from their original appearance prior to emplacement. After 1 day in oxic sediments, the amorphous oxide islands on the planar surface had disappeared, leaving a smooth exterior (Fig. 50). The planars remained this way through 4 days of emplacement. Very faint pit marks are visible on the 1 and 4 day samples. After 7 days, cracks and bubbles in the surface coating were seen. These features subsided after 14 days, and the surface was generally smooth with small, amorphous oxide islands present. A similar trend was seen on the surfaces exposed to the boundary zone sediments (Fig. 51). The surface appeared smooth and free of oxide islands for the first 4 days, and faint pit marks could also be seen on these samples. An amorphous phase was seen on the surface after 7 days, and was confirmed by EDS to be enriched in Fe. This phase grew more dense with time as seen by the photomicrograph of the 14 day sample. The planars emplaced in anoxic sediments were characterized by smooth surfaces with minor pitting alternating with large, amorphous oxide islands (Fig. 52). The samples emplaced for 1 and 7 days were relatively smooth with some minor pitting. The samples emplaced for 4 and 14 days exhibited large patches of sizable amorphous islands.

Reproduced with permission of the copyright owner. Further reproduction prohibited without permission.

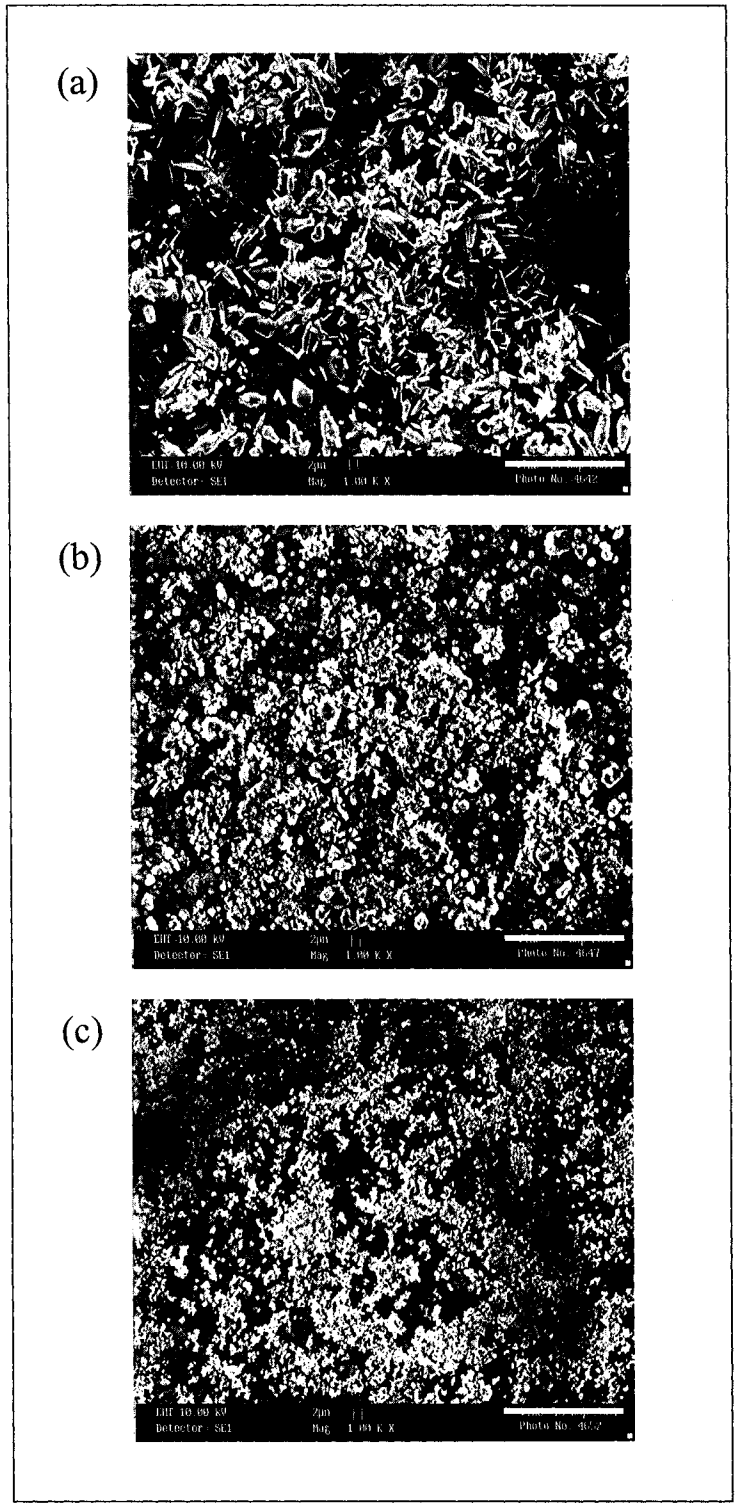

Figure 46. Photomicrographs (1000 X) of planar γ-Al_2O_3 with no Pb(II) (a), low Pb(II) (b), and high Pb(II) (c) loadings prior to emplacement. Crystalline, needle-like oxide islands are present on the unreacted planars, while more rounded, amorphous islands are seen on the Pb(II) loaded samples. Scale bars in the lower right-hand corner are 10 μm.

Reproduced with permission of the copyright owner. Further reproduction prohibited without permission.

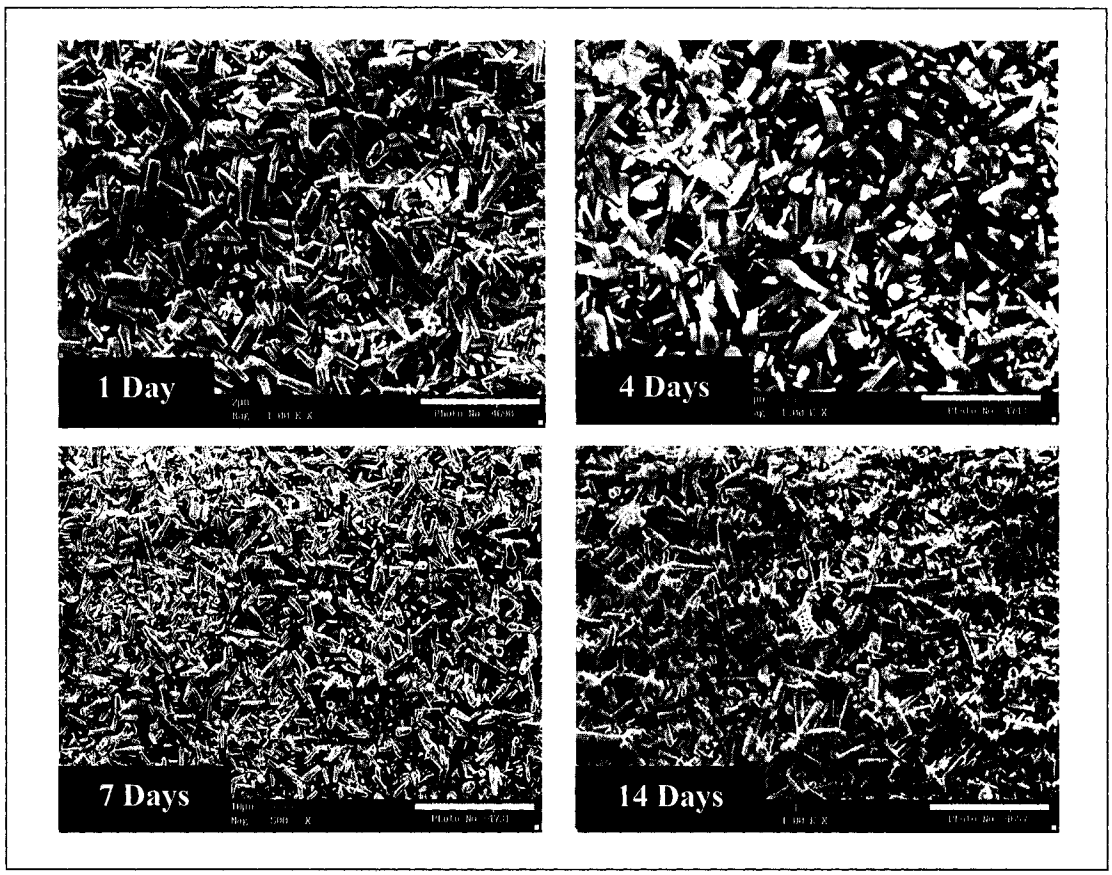

Figure 47. Photomicrographs (1000 X) of unreacted planar γ-Al_2O_3 after 1, 4, 7 and 14 days of emplacement in oxic sediments. The oxide islands become slightly less well-defined after 4 days of emplacement, but overall retain their crystalline form and become more densely packed with time. Scale bars in the lower right-hand corner are 10 μm.

Reproduced with permission of the copyright owner. Further reproduction prohibited without permission.

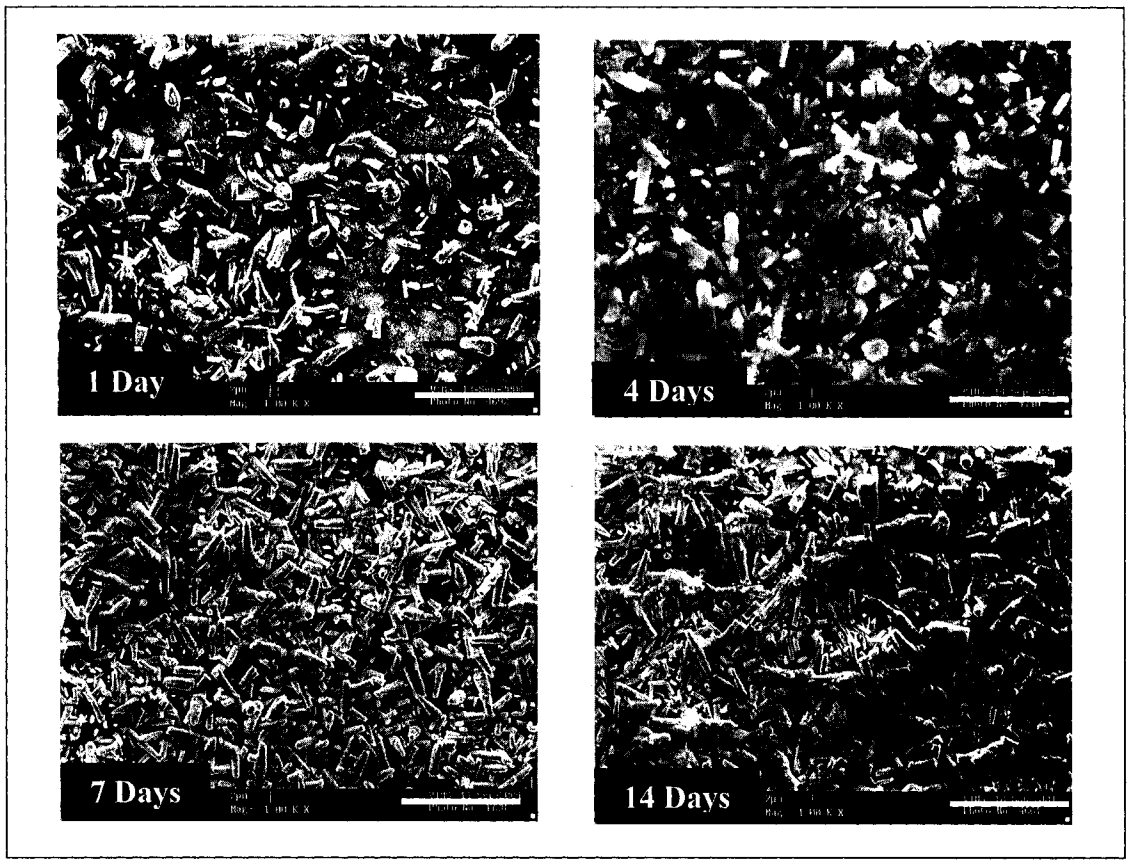

Figure 48. Photomicrographs (1000 X) of unreacted planar γ-Al_2O_3 after 1, 4, 7 and 14 days of emplacement in boundary sediments. After 4 days, the oxide islands look slightly less well-defined, but become more distinct again after 7 days. The distribution of the oxide islands becomes denser with time. Scale bars in the lower right-hand corner are 10 μm.

Reproduced with permission of the copyright owner. Further reproduction prohibited without permission.

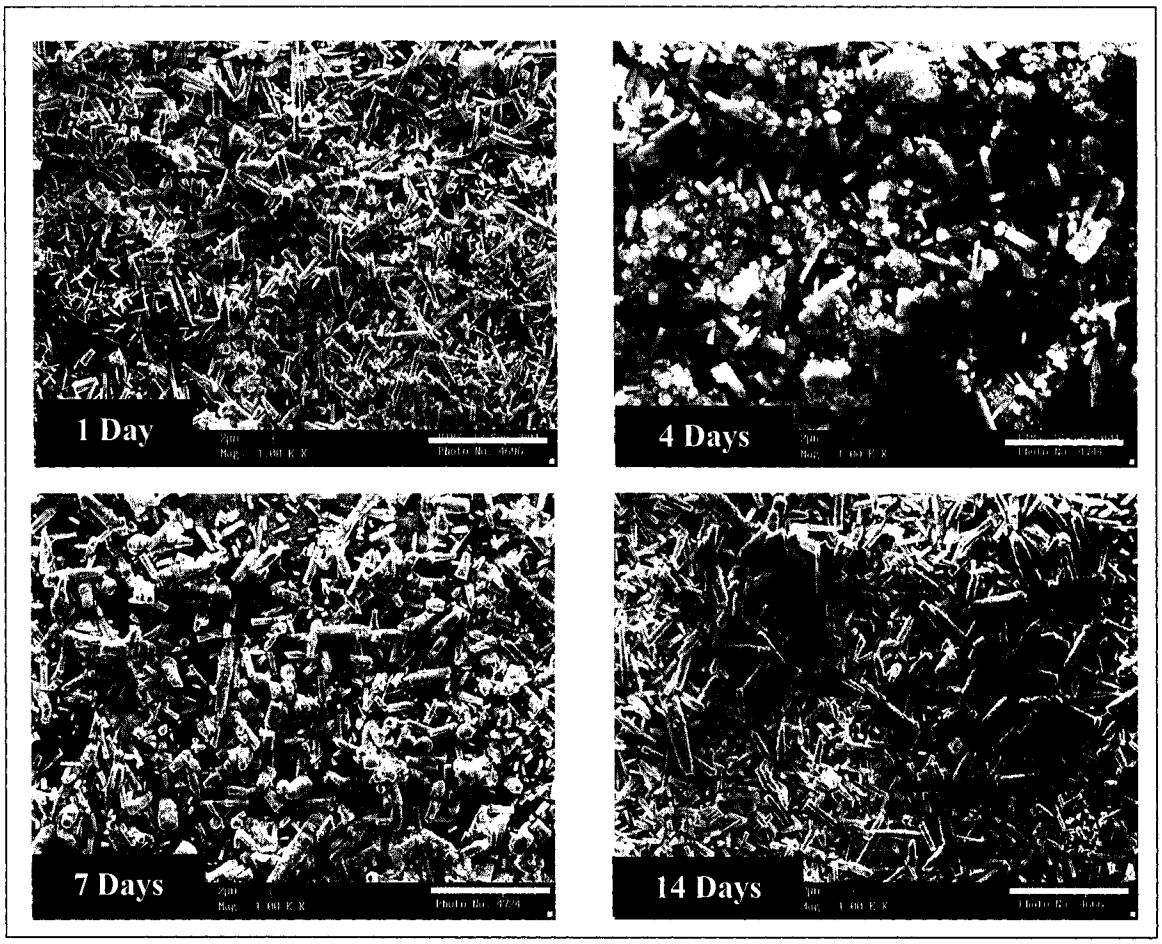

Figure 49. Photomicrographs (1000 X) of unreacted planar γ-Al_2O_3 after 1, 4, 7 and 14 days of emplacement in anoxic sediments. As with the planars emplaced in oxic and boundary sediments, the oxide islands look less distinct after 4 days but revert back to the a more defined form after 7 days of emplacement. The coverage of these islands increases with emplacement time. Scale bars in the lower right-hand corner are 10 μm.

Reproduced with permission of the copyright owner. Further reproduction prohibited without permission.

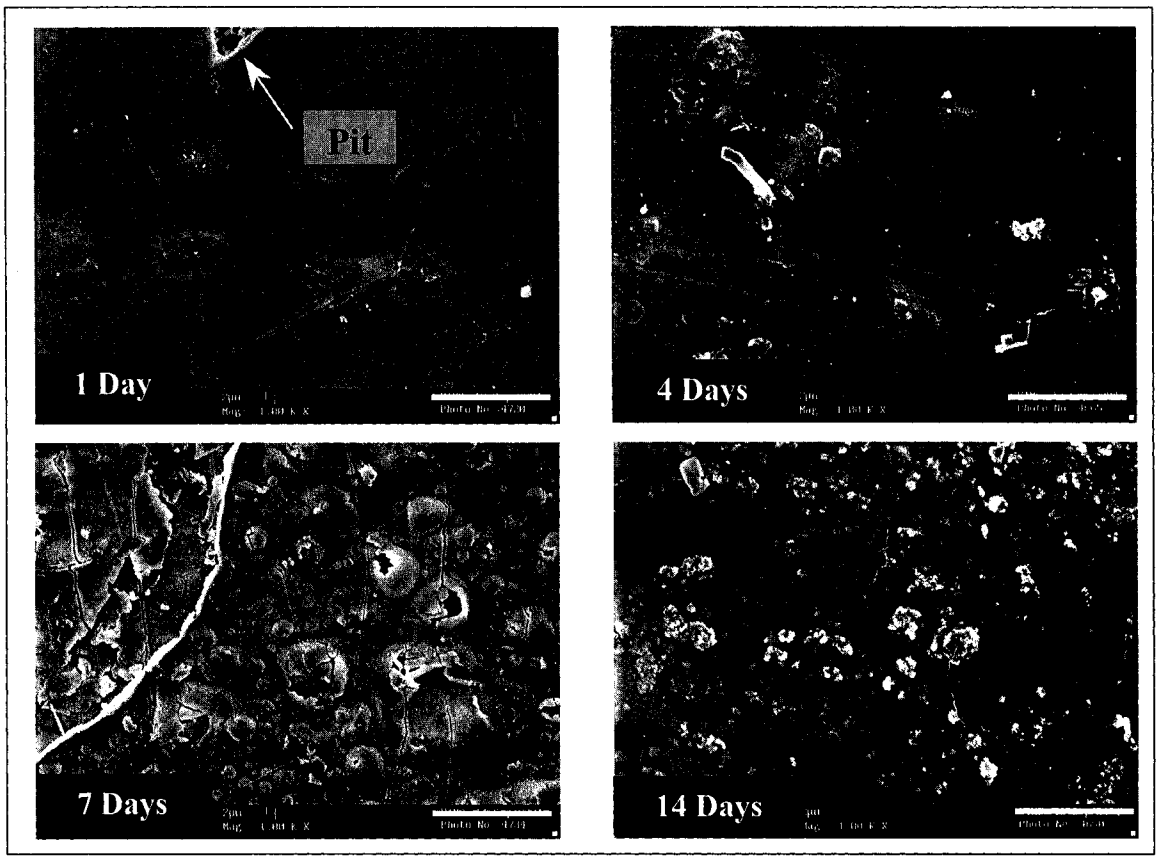

Figure 50. Photomicrographs (1000 X) of planar γ-Al_2O_3 with low Pb(II) loading after 1, 4, 7 and 14 days of emplacement in oxic sediments. The planar surface appears smooth after 1 and 4 days of emplacement. After 7 days, cracks and bubbles in the surface coating can be seen. After 14 days, the surface is generally smooth with small, globular oxide islands present. Scale bars in the lower right-hand corner are 10 μm.

Reproduced with permission of the copyright owner. Further reproduction prohibited without permission.

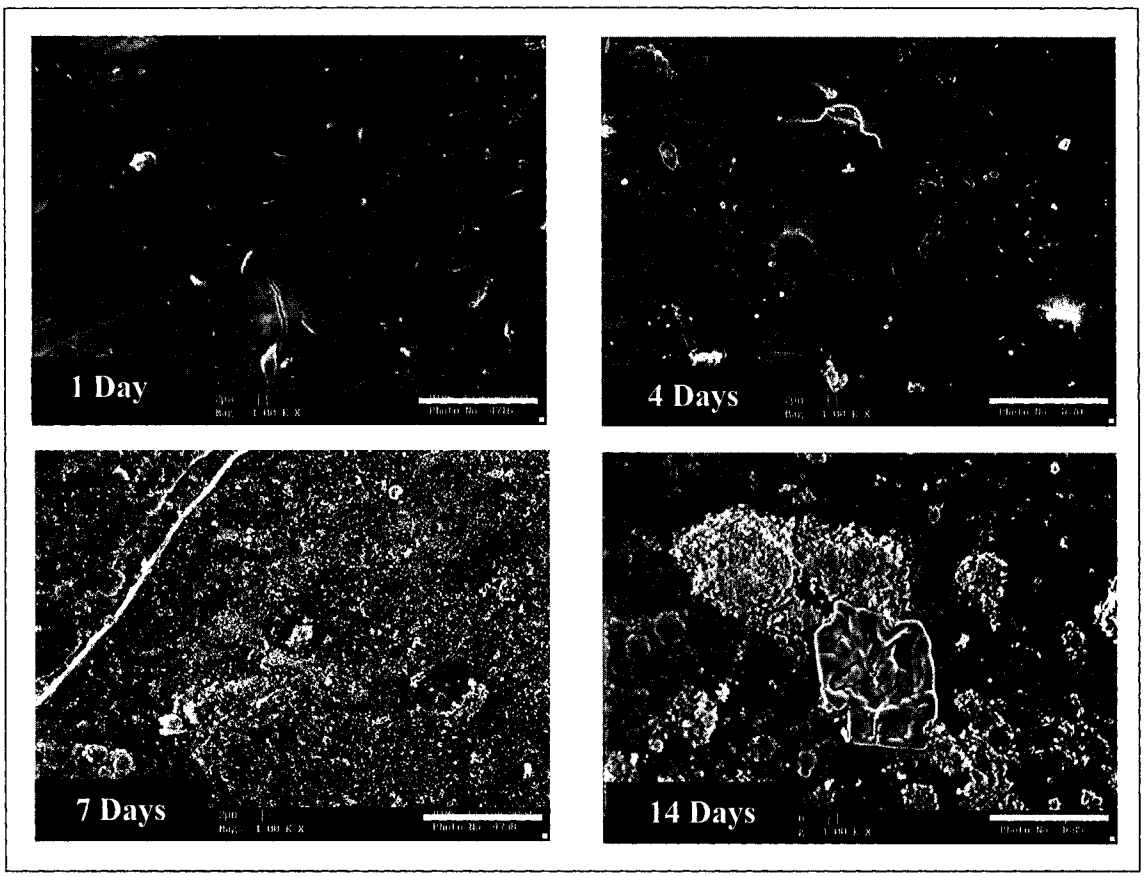

Figure 51. Photomicrographs (1000 X) of planar γ-Al_2O_3 with low Pb(II) loading after 1, 4, 7 and 14 days of emplacement in boundary sediments. After 1 and 4 days of emplacement, the surface appears smooth. Scale bars in the lower right-hand corner are 10 μm. Very faint pit markings can be seen on these two surfaces. After 7 days of emplacement, small, globular islands are visible. EDS confirmed these to be rich in Fe. After 14 days of emplacement, the number of islands has decreased. The rectangular shaped feature in the 14-day photomicrograph is an $AlCl_3$(s).

Reproduced with permission of the copyright owner. Further reproduction prohibited without permission.

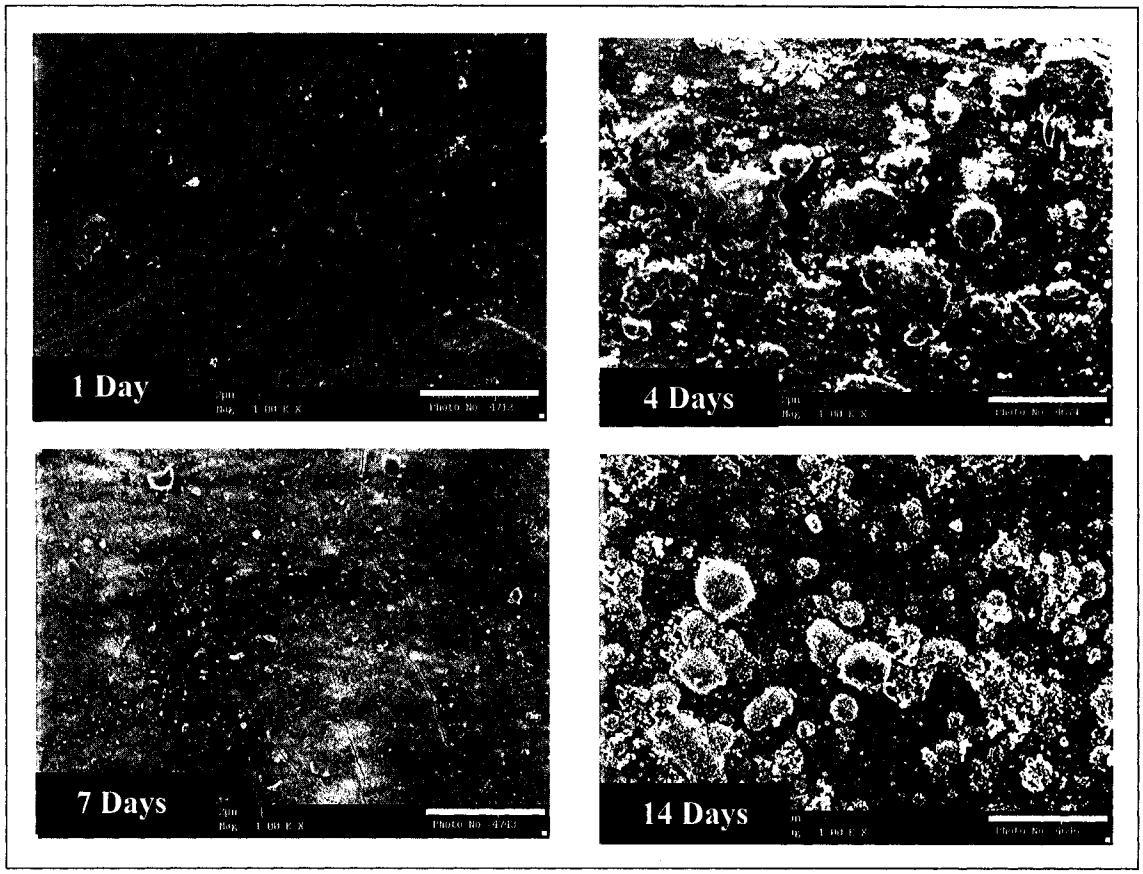

Figure 52. Photomicrographs (1000 X) of planar γ-Al_2O_3 with low Pb(II) loading after 1, 4, 7 and 14 days of emplacement in anoxic sediments. After 1 day of emplacement, the surface appears smooth and no oxide islands are present. Scale bars in the lower right-hand corner are 10 μm. Faint pit marks are present. After 4 days of emplacement, large globular islands can be seen. These islands disappear after 7 days, leaving a slightly rough surface with some minor pitting. The islands reappear after 14 days of emplacement.

Reproduced with permission of the copyright owner. Further reproduction prohibited without permission.

Reproduced with permission of the copyright owner. Further reproduction prohibited without permission.

High Pb(II) Loading

The morphologies of the emplaced planars with high Pb(II) loadings were similar to the low Pb(II) loading samples. The surfaces exposed to oxic sediments after 1 day showed extensive pitting on an otherwise smooth surface (Fig. 53). After 4 days, clusters of 3-dimensional amorphous oxide islands had formed. These islands flattened after 7 days, and were gone after 14 days. Pits were seen on the 14 day samples. In the boundary zone, an Fe rich phase was seen after 1 day of emplacement (Fig. 54). This phase grew more patchy after 4 days of emplacement, and was virtually gone after 7 days. The Fe rich phase returned after 14 days of emplacement. Maximum Fe concentrations measured in this phase were ~10% by weight. In the anoxic zone, the planar surfaces were fairly smooth with clusters of small pits after 1 day (Fig. 55). From 4 to 7 days of emplacement, amorphous oxide islands formed and grew in density. After 14 days, the islands were gone, and a pitted surface was seen again.

Discussion

The main objective of this work was to test the ability to use planar oxides as tools to characterize metal ion sorption processes in natural sediments and waters. To be successful, two basic requirements need to be met. First, the planar materials must be able to withstand emplacement for relatively long periods of time without undergoing significant corrosion (i.e. dissolution of the γ-Al_2O_3 surface phase) and/or biofouling, and second, the metal complexes that form on the planar surfaces must be able to be characterized. Results from this study show that these two conditions can be met with these materials. While in some cases the surfaces of the planar γ-Al_2O_3 underwent

Reproduced with permission of the copyright owner. Further reproduction prohibited without permission.

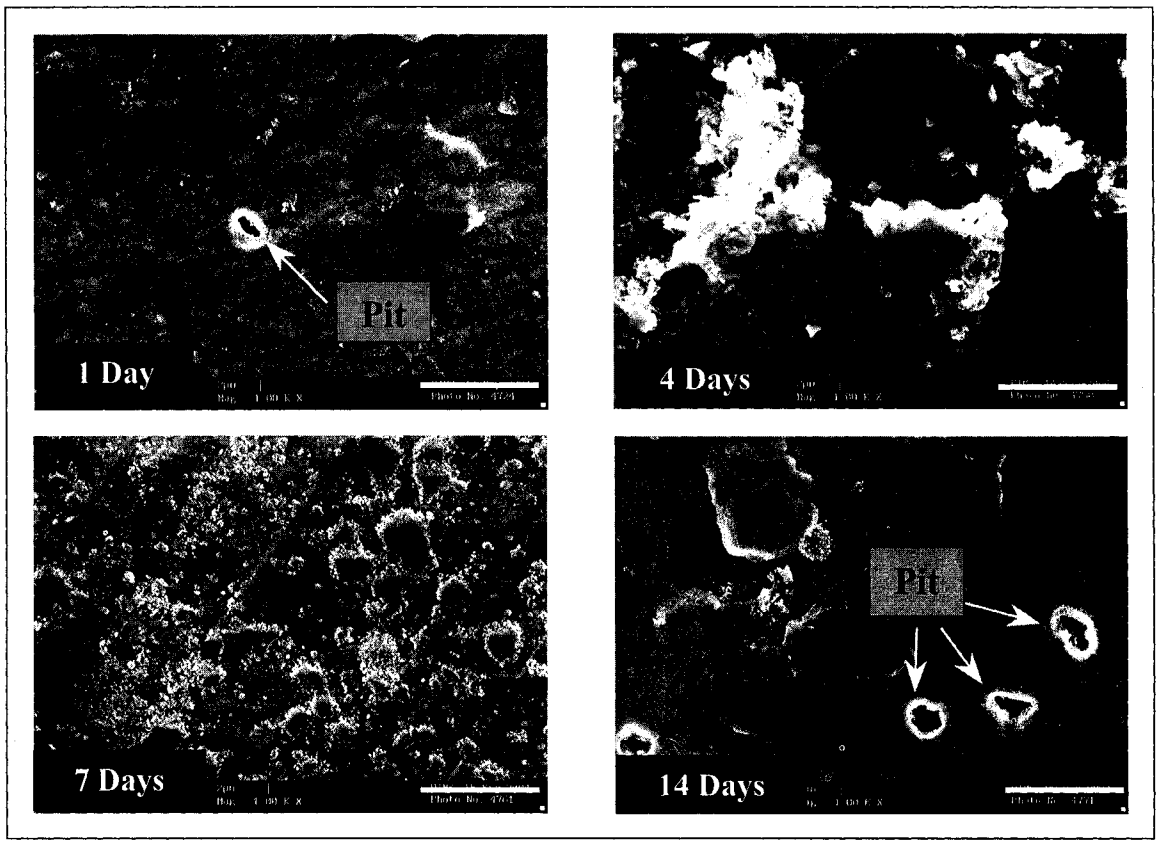

Figure 53. Photomicrographs (1000 X) of planar γ-Al_2O_3 with high Pb(II) loading after 1, 4, 7 and 14 days of emplacement in oxic sediments. Scale bars in the lower right-hand corner are 10 μm. Small pits are visible in the alumina coating after 1 day of emplacement. Also, the globular islands present prior to emplacement are gone. After 4 days, large clusters of oxide islands are seen. These islands become smaller and more evenly dispersed after 7 days of emplacement. By the 14^{th} day of emplacement, the islands have disappeared and small clusters of pits are visible in the coating.

Reproduced with permission of the copyright owner. Further reproduction prohibited without permission.

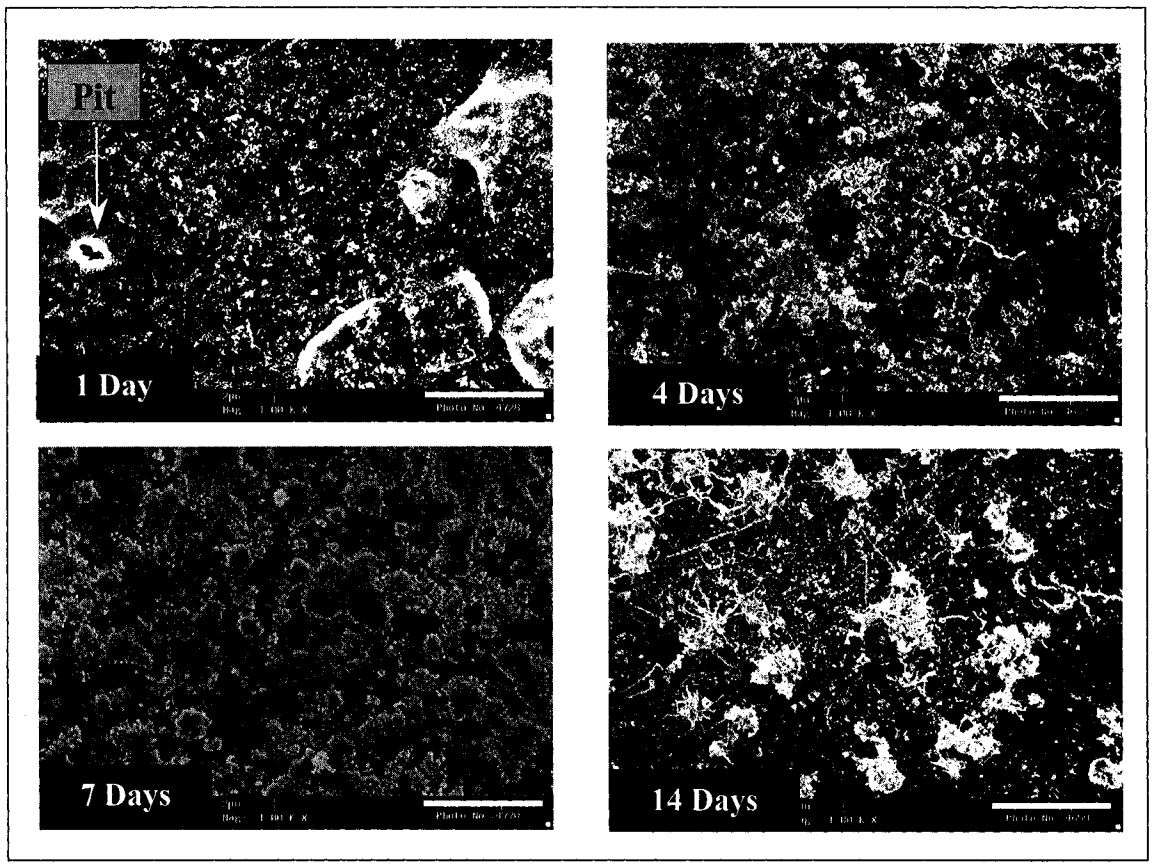

Figure 54. Photomicrographs (1000 X) of planar γ-Al_2O_3 with high Pb(II) loading after 1, 4, 7 and 14 days of emplacement in boundary sediments. Scale bars in the lower right-hand corner are 10 μm. Some minor pitting was observed after 1 day of emplacement, but not seen after. The oxide islands are significantly diminished after 1 day as compared to the pre-emplacement surface. After 4 days, a new phase begins to form. EDS confirmed this phase to be enriched in Fe (up to 10% by wt). The phase disappears after 7 days and is replaced by globular-shaped oxide islands. After 14 days, the Fe rich phase is prevalent again.

Reproduced with permission of the copyright owner. Further reproduction prohibited without permission.

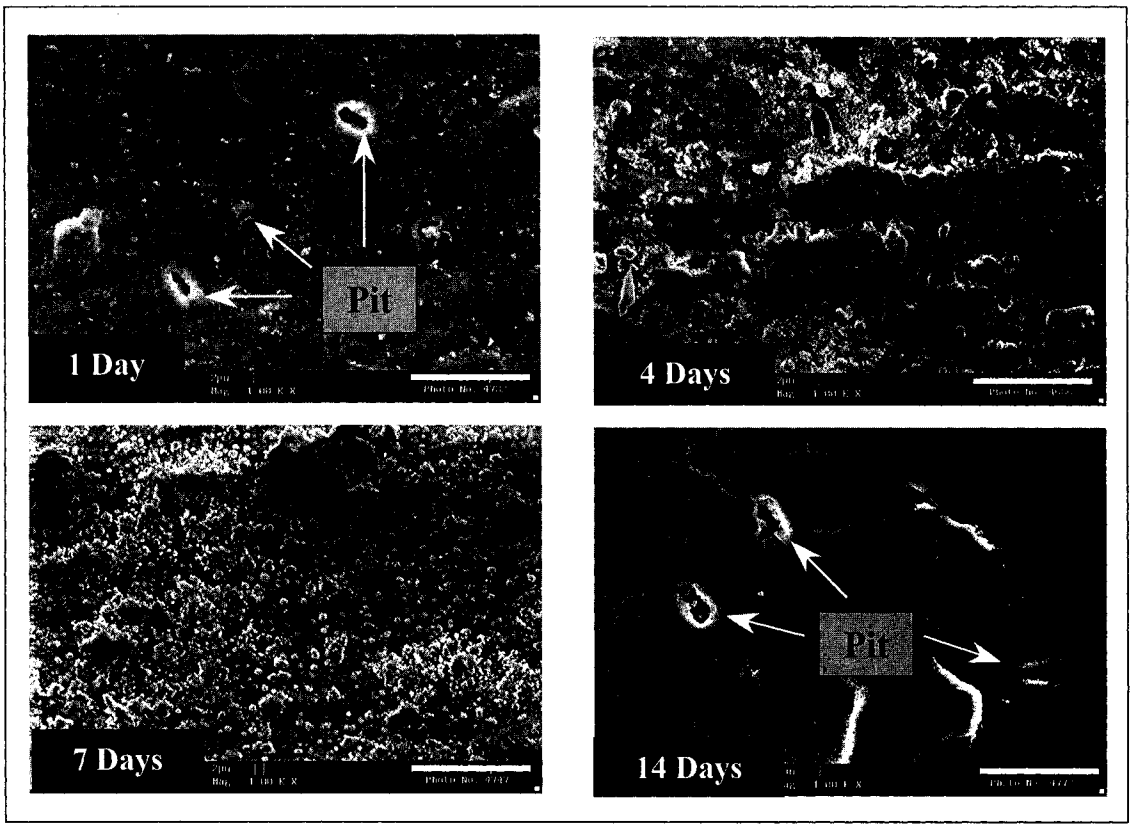

Figure 55. Photomicrographs (1000 X) of planar γ-Al_2O_3 with high Pb(II) loading after 1, 4, 7 and 14 days of emplacement in anoxic sediments. Scale bars in the lower right-hand corner are 10 μm. Clusters of pits were seen on the surface after 1 day of emplacement. Only very small oxide islands can be seen. After 4 days, the islands are larger in size and no pitting is seen. After 7 days, small, evenly distributed islands are seen. These islands disappear after 14 days and clusters of pits in the oxide coating are again present.

Reproduced with permission of the copyright owner. Further reproduction prohibited without permission.

significant morphological changes, there seemed to be little to no corrosion of the substrate itself, although it was not possible to discern whether or not any dissolution and precipitation had occurred. Additionally, in all cases, Pb(II) was detected on the surfaces of the emplaced planars and was able to be quantified by our methods. These results indicate that the technique of emplacing planar oxides into sediments to understand metal sorption behavior in natural systems is promising.

While the two broad objectives have been met, more specific information can be obtained from our results regarding physical, chemical and biological controls on the sorption and/or desorption of Pb(II) from the planar surfaces under these conditions. Specifically, chemical and physical controls may be suggested by the results from the ANOVA anlayses which indicated significant effects of initial Pb(II) loadings and emplacement time, as well as from the different correlations of Pb/Al with Fe/Al and S/Al. Additionally, the changing appearances of the planar surfaces may suggest some effects of microbial interactions with the surfaces.

The Pb/Al ratios for the emplaced unreacted planars were found to be significantly lower than the ratios for the emplaced low and high Pb(II) loaded planars. Within the unreacted samples, the Pb/Al ratios for the samples emplaced for 1 day were significantly lower than the samples emplaced for 4, 7 and 14 days. This behavior is similar to that observed in controlled laboratory experiments where sorption is generally complete after 96 hours (Hayes and Leckie, 1986; Strawn et al. 1998; Strawn and Sparks, 2000). After the initial period of rapid uptake, sorption becomes much slower and may include diffusion, precipitation, and/or sorption reactions on sites that have a higher activation energy than the fast sorption sites (Strawn and Sparks, 2000).

Reproduced with permission of the copyright owner. Further reproduction prohibited without permission.

For the low Pb(II) loaded planars, the 1 day sample was higher than the other samples within this subset. This is opposite of what was seen on the unreacted planars where the 1 day sample was significantly lower than the others. Thus, it seems that planar surfaces with Pb(II) present on the surface prior to emplacement may undergo different sorption/desorption mechanisms during the first day of emplacement relative to a planar surface without Pb(II). The 4, 7 and 14 day samples showed no significant differences in the Pb/Al ratios. This again may indicate that either a balance of processes is present, or that a different sorption mechanism is controlling the surface Pb(II) concentrations.

There was no significant relationship between the Pb/Al ratios on the high Pb(II) loaded planars with time. Earlier spectroscopic analyses of these samples showed that Pb(II) was bound to the planar γ-Al_2O_3 as inner-sphere monodentate and bidentate complexes. These types of surface complexes are generally thought to be stable and unlikely to be releases from the surface except in cases of large changes in the solution chemistry of the system (e.g., a change in pH). No such changes were present in the experimental system used here, so the lack of change in the surface concentrations of Pb(II) with time on these samples is consistent with the type of surface complexes present on the planar surface.

Effects due to emplacement time can also be seen in the surface morphologies of the low Pb(II) loaded planars. The surfaces of these samples seem to undergo a cycling process on the scale of 7-14 days (Figs. 50-52). A complete cycling of the surface can be defined as the time required for oxide islands (and/or another surface phase) to appear on a smooth surface, and subsequently disappear, returning the surface to its initial smooth

Reproduced with permission of the copyright owner. Further reproduction prohibited without permission.

morphology. These morphological changes coupled with the significant variations of the Pb/Al ratios with emplacement time on the low Pb(II) loaded planars may suggest that physical processes occurring on different time scales play important roles in the sorption behavior of Pb(II) on these surfaces.

The number and identity of correlations between Pb/Al with Fe/Al and S/Al vary with time of emplacement and initial Pb(II) loading, supporting the statistical findings that there are significant effects from these two parameters. On all planar samples, correlations between Pb and Fe were only seen between 0 and 7 days (Table 19). However, with the exception of the unreacted planar γ-Al_2O_3, correlations with S were only seen at the longer emplacement times (7-14 days). These results are consistent with the observation that the sulfide complexes form relatively slowly in sediments and are usually the result of precipitation reactions (Simpson et al., 2004) while iron complexes form rapidly through sorption reactions.

The planar γ-Al_2O_3 with low Pb(II) loadings have the highest number of significant correlations with Fe and S (Table 19), indicating an increased interaction of these samples with the surrounding environment relative to the other two Pb(II) loadings. This may be due to an increased positive charge on the planar γ-Al_2O_3 with increasing Pb(II) loadings. The unreacted planars likely did not accumulate high enough metals concentrations to measure significant interactions. At the highest Pb(II) loading, these interactions seem to be inhibited and may be due to the toxicity of Pb(II) at higher concentrations. However, because these sediments were collected from a relatively contaminated region, the microorganisms present may be acclimated to higher levels of

Reproduced with permission of the copyright owner. Further reproduction prohibited without permission.

metals, and another process may be the cause of the low number of correlations for these samples.

Evidence for biological interaction with the planar surfaces can be seen by the appearance of pits and pit markings on the planar γ-Al_2O_3 after emplacement. Clusters of small pits, approximately 2 μm x 1 μm, were seen exclusively on planar γ-Al_2O_3 with Pb(II) loaded prior to emplacement (for example, Fig. 53). A similar pattern of pitting on iron oxide coatings has also been observed in the presence of the bacteria *S. putrefaciens* (Grantham et al., 1997), thus the pitting observed on the planar γ-Al_2O_3 surfaces may be an indicator of biological activity. The occurrence of these pits was more prevalent on the high Pb(II) loaded planars as compared to the planars with low Pb(II) loadings and was seen in all three redox zones. While the samples were not stained after removal from the sediments, no cells were visually observed on the surfaces. Future studies should incorporate the use of a staining technique to confirm the presence or absence of microorganisms.

It is well known that microorganisms can profoundly effect metal speciation and mobilization, as well as control the dissolution and precipitation of mineral surfaces. There are many mechanisms by which these processes can occur. Mobilization of metals can be achieved by protonation, chelation, and chemical transformation. Heterotrophic metabolism can also lead to the leaching of metals and metal oxides as a result of the efflux or organic acids, such as oxalic acid, which can act as a leaching agent for metals that form stable oxalate complexes, including Al and Fe (Sansone, 1986; Strasser et al., 1994, Gadd, 2004). Immobilization can be achieved by precipitation or crystallization of insoluble organic or inorganic compounds or by sorption, uptake and intracellular

Reproduced with permission of the copyright owner. Further reproduction prohibited without permission.

sequestration (Gadd, 2004). While Al and Pb are often considered to be toxic to microorganisms, studies have increasingly shown that the presence of heavy metals has a strong influence on the community structure of microorganisms (Frostergård et al., 1996; Sandaa et al., 1999; Kelly et al., 1999; Kozdroj and van Elsas, 2001; Suhadolc et al., 2004). The bacteria in these communities have been shown to be able to develop tolerances against heavy metals (Olson and Thornton, 1982; Arnebrant et al., 1987; Kelly et al., 1999), and in some cases have shown affinities for trace metals that approach those for Fe(III), an essential component of many metabolic pathways (Hernlem et al., 1996; Dubbin and Ander, 2003). The sediments used in this study were collected from the Baltimore Harbor which has been designated a toxic hot spot by the EPA. While the microbial communities were not characterized for the purpose of this study, it is possible that the microorganisms living in these sediments may have developed similar tolerances.

In the study by Grantham et al. (1997), the occurrence of pits was limited to aerobic conditions on Fe oxide coatings. In their study, no localized pitting was observed under anaerobic conditions, and no pits were found on Al oxide coatings although the bacteria could not be detached for inspection of the underlying substrate. Grantham et al. (1997) proposed that the mechanism for pit formation was due to the presence of local anoxia beneath the individual cells attached to the oxide coating, permitting iron reduction to occur. Although no microorganisms were observed on the planar surface upon removal from the sediments, it is reasonable to assume that interaction between the γ-Al_2O_3 surface and microorganisms present in the sediments could have occurred.

While Grantham et al. (1997) did not observe localized pitting on Al oxide coatings, the presence of different microbial communities in the natural sediments used in

Reproduced with permission of the copyright owner. Further reproduction prohibited without permission.

this study may explain why pitting is observed on our materials under all redox conditions. However, since Al is not a redox active metal, it is unlikely that the redox mechanisms proposed by Grantham et al. (1997) is responsible for the formation of pits on our materials. The efflux of organic acids from microorganisms present on the surface is a more likely mechanism for our samples.

Similar pits have also been observed on planar γ-Al_2O_3 films due to saturation by hydrogen, a by-product of the production reaction (Hart and Maurin, 1965). However, since no such pits were observed prior to emplacement, their formation was more likely due to processes occurring in the sediments. Also, if pitting were due to physical corrosion or dissolution of the oxide surface, it would likely be seen on all of the planars, whereas the pits were only observed on planars with some initial Pb(II) loading. From this experiment, it is not possible to fully determine whether the formation of pits on the planar surface is due to corrosional processes or interaction with microbial communities. Further investigation is required to elucidate the physical and/or biological causes of pits in the γ-Al_2O_3 coating.

Results from this work have shown that planar γ-Al_2O_3 can be emplaced into natural sediments and successfully used to characterize quantitative changes in the surface concentration of Pb(II) present. It was determined that emplacement time and initial Pb(II) concentration had an effect on the Pb/Al content of the samples. Sorption of Pb(II) to the unreacted planar γ-Al_2O_3 could be accurately described using models obtained from laboratory based studies. These models suggest a two phase sorption process whereby Pb(II) sorbs rapidly to high affinity surface sites followed by a slower reaction mechanism possibly due to diffusion of Pb(II) into the material. Changes in the

Reproduced with permission of the copyright owner. Further reproduction prohibited without permission.

Pb/Al ratios of the low Pb(II) loaded planars with time is likely due to a combination of sorption and desorption reactions. Other phases such as Fe and organic matter are known to be more reactive with Pb than Al, and the desorption of Pb(II) from the γ-Al_2O_3 surface may be due to the repartitioning of Pb to these phases. The Pb/Al ratios on the high Pb(II) loaded planars did not change significantly as a function of time. This is consistent with other studies that have suggested that inner-sphere complexes are not likely to desorb from mineral surfaces except in cases of extreme changes in solution chemistry. No significant effect due to redox conditions was determined. This is not surprising as neither Pb nor Al are redox active metals, and indicates that these materials may be used in a variety of environments. However, the absence of a significant difference in the concentration of Pb(II) on the surface due to redox does not mean that the surface complexes formed in the different zones are the same. Further work investigating the structure of the surface complexes formed under these conditions will aid in discerning the physical, chemical and biological processes controlling Pb(II) concentrations on emplaced γ-Al_2O_3 surfaces.

Reproduced with permission of the copyright owner. Further reproduction prohibited without permission.

CHAPTER 7

Conclusions

The fate and transport of trace metals in natural systems is a complex process involving physical, chemical and biological phenomenon. Reactions with sediment and particle surfaces play a large role in the distribution and reactivity of metal contaminants in aquatic systems. While these processes are well-understood for simplified components under laboratory conditions, connecting this knowledge to processes occurring at the larger field scale has proved to be extremely difficult. The purpose of this dissertation was to investigate the possibility of a novel approach to understanding the variety of processes that affect metal uptake at both the laboratory and field scales while investigating Pb(II) sorption behavior under increasingly complex conditions.

The focus of this research was to develop planar oxides as tools that could be used to investigate metal ion sorption behavior under a variety of conditions. This was achieved through investigation of Pb(II) uptake on planar γ-Al_2O_3 under controlled laboratory conditions. This work was then expanded upon by increasing the scale of complexity for both the planar surface, through the creation of planar mixed Fe-Al oxide coatings, and the reaction environment through direct emplacement into natural sediments. The objectives of this study were to illustrate the range of environments over which planar oxides could be a useful tool to understanding natural processes and also to

Reproduced with permission of the copyright owner. Further reproduction prohibited without permission.

gain a better understanding of how the various physical, chemical and biological forcings affect metal ion uptake in natural systems.

The specific hypotheses of this research were as follows:

1. Pb(II) sorption behavior to the planar γ-Al_2O_3 surface is similar to the sorption behavior to bulk γ-Al_2O_3 at both a macroscopic and microscopic level.
2. Well characterized, reproducible Fe(III) coatings of varying physical and chemical properties can be created using planar γ-Al_2O_3 as a substrate.
3. Planar oxides can be used to investigate Pb(II) sorption/desorption processes on the planar γ-Al_2O_3 surface in natural sediments and waters in both oxic and anoxic environments.

Hypothesis 1

This hypothesis was supported through investigation of the composition and chemical reactivity of the planar γ-Al_2O_3 relative to the bulk γ-Al_2O_3 through spectroscopic and wet-chemical techniques. Results from this work showed that while the morphological form of the planar γ-Al_2O_3 was distinctly different from bulk phase γ-Al_2O_3, their overall chemical composition and physical characteristics were similar as seen by the XRD patterns and measures of porosity. Small deviations in these measurements, specifically variations in the occurrences and intensities of the XRD peaks, is likely due to differences in the orientation of the planar γ-Al_2O_3 as compared to the bulk phase.

Investigation of Pb(II) sorption to the planar and bulk γ-Al_2O_3 phases expanded on these results by comparing the chemical reactivities of the two materials. Through ToF/SIMS and XPS studies, the relative quantitative uptake of Pb(II) was shown to be similar for bulk and planar γ-Al_2O_3 over a range of Pb(II) loadings, although it was found that absolute Pb(II) uptake was higher on the bulk alumina surface. XANES and EXAFS

Reproduced with permission of the copyright owner. Further reproduction prohibited without permission.

results showed that Pb(II) sorption complexes formed on planar γ-Al_2O_3 were similar to those formed on the pure phase analog oxides in both the Pb-O geometry and the Pb-Al coordination environment. Multinuclear Pb species were found to be present on all sorption samples. Additionally, the results obtained in this work were comparable to previous studies of Pb(II) sorption to bulk γ-Al_2O_3 oxide surfaces under similar experimental conditions.

XANES results indicated that Pb(II) is present in a mixture of binding environments ranging from distorted trigonal pyramidal to distorted pentagonal pyramidal on both the planar and bulk oxides. Fourier transforms of the EXAFS spectra of the sorption samples indicated that two distinct sorption complexes formed on the alumina surfaces, a corner-sharing monodentate complex and an edge-sharing bidentate complex, as well as small, flat polynuclear Pb(II) complexes. However, the presence of these polynuclear complexes did not coincide with the detection of oligomeric species by ToF-SIMS, suggesting that the ToF-SIMS data may have been due to instrumental artifact. Variations in sorption complexes formed on the planar vs. bulk γ-Al_2O_3 were seen in changes in the local structure of the Pb-Al complexes at low vs. high coverages and the relative distribution of Pb(II) bound as mono vs. bidentate complexes as coverage increased. Thus, the overall chemical reactivity of the planar γ-Al_2O_3 surface is comparable to the bulk phase analog. However, differences in the structure of the Pb(II) complexes at low coverages suggests variations in the number or identities of high affinity surface sites on the planar vs. bulk γ-Al_2O_3. Changes in the relative proportions of mono- vs. bidentate complexes with increasing coverage is likely due to constraints on the available binding environment due to the morphologies of the surfaces.

Reproduced with permission of the copyright owner. Further reproduction prohibited without permission.

Hypothesis 2

The effects of varying initial Fe(III) concentration, reaction time and number or coating procedures was determined for Fe(III) coatings formed on planar γ-Al_2O_3. Changes in the reaction conditions produced mixed Fe-Al oxide coatings of varying elemental composition, surface area and crystallinity, and therefore are likely to have distinctly different reactivities from one another. While the exact identification of the Fe phase present on the surface was not possible, the homogeneity and concentration of the resultant coatings could be controlled quite closely, supporting the hypothesis. This suggests that using these techniques, reproducible coatings can be made on planar γ-Al_2O_3 surfaces. Future studies designed to investigate the coordination environment of Fe(III), such as EXAFS, would be useful in helping to determine the crystalline form of the coating. Once the coatings are fully characterized, differences in chemical and biological reactivity due to differences in the chemical and physical form of the coatings can be investigated leading to a better understanding of how these variations affect reactivities of particles in natural systems.

Hypothesis 3

The results from this study support the third hypothesis and have shown that emplacement of supported oxide surfaces may be a valuable tool for investigating and understanding metal ion sorption processes in natural sediments. Not surprisingly, several physical, chemical and biological factors seemed to combine to control the overall sorption/desorption behavior of Pb on the planar γ-Al_2O_3 surfaces. Pb/Al ratios, as well as interaction between the emplaced planars and the surrounding sediments,

Reproduced with permission of the copyright owner. Further reproduction prohibited without permission.

varied as a function of time and initial Pb(II) loading as evidenced by the changes in the surface morphologies, Pb(II) surface concentrations and changes in correlations with Fe and S present in the surrounding sediments.

Lead uptake on the emplaced unreacted planar γ-Al_2O_3 exhibited a two-stage sorption behavior characterized by an initially fast uptake followed by a slower sorption reaction. The low Pb(II) loaded planars initially showed sorption of Pb(II) onto the surface. However, after 1 day of emplacement, the Pb/Al ratios decreased and then remained the same throughout the emplacement. There was no significant effect of emplacement time on the Pb/Al ratios of the high Pb(II) loaded planars.

Changes in correlations between Pb, Fe and S were also seen as a function of emplacement time. Significant relationships between Pb and Fe were seen exclusively on samples emplaced for 7 days or less. With one exception, correlations between S and Pb were seen for emplacement times greater than 7 days. This is consistent with other studies that have shown that Fe complexes form relatively quickly and that S complexes are often formed through precipitation reactions and develop over longer periods of time.

Biological controls may be suggested by the presence of clusters of pits found on the planar surfaces after emplacement. These pits were only seen on planar surfaces loaded with Pb(II) prior to emplacement, exemplifying the interconnection between biological and chemical controls. However, these pits may also be due to the corrosion of the planar surface. From these experiments, we are not able to distinguish between a physical and biological mechanism of pit formation. The results from this experiment do clearly illustrate the need for an interdisciplinary approach to fully understand metal contaminant interactions with sediment surfaces. Planar oxides provide a unique

Reproduced with permission of the copyright owner. Further reproduction prohibited without permission.

opportunity for this interdisciplinary technique by allowing for the investigation of a wide range of important physical, chemical and biological processes at both the laboratory and field scale.

The use of planar oxides as proxy surface phases in laboratory and field investigations of metal ion sorption appears promising. Through spectroscopic and wet-chemical techniques, a connection between the reactivities of the often used pure phase γ-Al_2O_3 and the planar γ-Al_2O_3 was able to be made. The relative quantitative uptake of Pb(II) on the planar γ-Al_2O_3 was found to be similar to that on the bulk oxides. Also, the Pb(II) sorption complexes formed on each material were found to have the same Pb-O coordination environment and Pb-Al sorption geometries. Variations in the local structure and relative proportions of these complexes likely reflect differences in the morphologies and number and identities of reactive surface sites on the planar vs. bulk γ-Al_2O_3. These results allow for future work to build upon the already extensive body of knowledge obtained from work done on the bulk phase oxides.

It was also shown that planar oxides can be used to systematically increase the complexity of the experimental system by altering the oxide surface. Mixed oxide coatings are ubiquitous in nature, and the interactions of different chemical phases within these coatings makes predicting the overall reactivity difficult. Mixed planar Fe-Al oxides afford opportunities not available through the use of traditional bulk phase materials. The methods used in this work produced mixed planar Fe/Al coatings of varying chemical and physical characteristics. Subsequent studies of Pb(II) sorption to these mixed oxides can be used to assess the reactivity of mixed phase oxides relative to

Reproduced with permission of the copyright owner. Further reproduction prohibited without permission.

their pure phase counterparts. Specifically, the two oxide phases can be combined both chemically and physically and the interaction due to each phase can be quantified.

Perhaps one of the largest challenges facing environmental scientists is the ability to translate laboratory based knowledge to natural systems. Bridging this gap would have far reaching implications for better remediation strategies and cost management of clean up efforts. Planar oxides may be a step in the direction of linking the lab to the field. The results from this dissertation provide a small outline as to the many ways in which planar oxides may be useful tools in understanding sorption behavior. While much work still remains in fully understanding how different processes affect metal uptake in natural systems, it is clear that an interdisciplinary approach is needed to better connect laboratory studies to processes occurring in more complex, large scale systems.

Reproduced with permission of the copyright owner. Further reproduction prohibited without permission.

APPENDIX 1

Summary of Spectroscopic Techniques

Many spectroscopic techniques have been used with success in characterizing metal ion complexes formed on oxide surfaces (Kim, et al., 1973; Chisholm-Brause et al., 1990; Bargar et al., 1996; Scheidigger et al., 1996; Scheidigger et al., 1997; Bargar et al., 1998; Trainor et al., 2000). While having their limitations, each of these spectroscopic methods provides a unique insight into the interaction of an adsorbing metal with a solid surface (Table 20). It is the combination of these techniques that provides a powerful analytical tool for understanding metal ion complexation at the molecular level. The information contained in this section will outline some of the fundamental principles of the techniques used in this study, as well as their applications to geochemical studies.

Table 20. Summary of surface analytical techniques used in this study.

Analytical Technique	Typical Applications	Signal Detected	Detection Limits	Depth Resolutions	Lateral Resolution
XPS/ ESCA	Surface analysis of organic and inorganic molecules	Photoelectrons	0.01 – 1 at%	1 – 10 nm	10 μm – 2 mm
TOF SIMS	Surface microanalysis of polymers, plastics and organics	Secondary ions, atoms, molecules	<1 ppm, $1x10^8$ at/cm^2	1 monolayer	0.10 μm
XAS	In situ bulk analysis of solid materials	Fluoresced or transmitted photoelectrons	>10% wt transmission, <10% wt in fluorescence	Determined by experimental setup	100 nm - mm

Reproduced with permission of the copyright owner. Further reproduction prohibited without permission.

X-ray Photoelectron Spectroscopy (XPS)

X-ray Photoelectron Spectroscopy (XPS) is one of the most widely used surface analytic techniques and has been used successfully for many years to investigate metal sorption complexes on oxide surfaces because of the inherent surface sensitivity of the technique (Tewari and Lee, 1974; Schenk et al., 1983, Hochella, Jr., 1988). The analysis depth for this technique ranges between a few to over 100 Å depending on the surface analyzed and the instrument conditions.

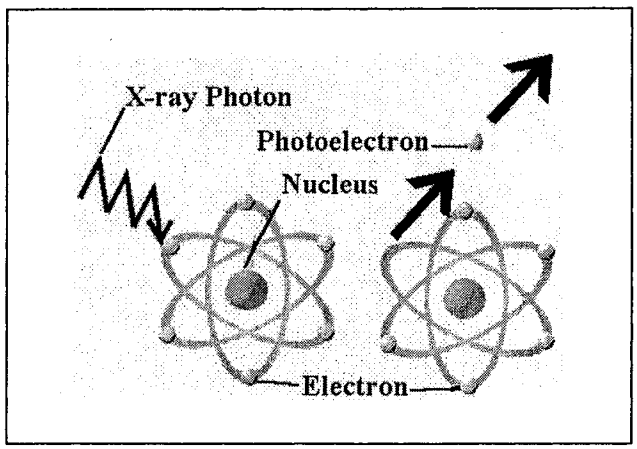

Figure 56. Schematic illustration of the physical interaction between the x-ray beam and the sample resulting in the ejection of photoelectrons.

In XPS studies, a surface is bombarded with x-rays which cause photoelectrons to be ejected from their parent atom if the photon energy exceeds that of their bound state, or their 'binding energy' (Fig. 56). Photoelectrons that have not lost energy on the way out of the sample have characteristic energies that are equal to the energy of the photon minus the electron binding energy. This statement is expressed in the following equation

$$E_K = h\upsilon - E_B \quad (8)$$

Where E_K is the kinetic energy of a photoelectron, $h\upsilon$ is the energy of the incident photons and E_B is the energy by which the photoelectron had been bound to its parent

Reproduced with permission of the copyright owner. Further reproduction prohibited without permission.

atom. It has also been shown that the exact position of photoelectron peaks can be indicative of the chemical and/or structural environment of the analyte, as well as the formal oxidation state (Hochella, Jr., 1988; Ratner and Castner, 1997). Therefore, XPS can provide compositional information, oxidation states, and binding energies of atoms located at or near the surface. The major drawback to using XPS in sorption studies is the fact that the measurements are made under high vacuum, which may alter surface species vulnerable to these conditions, as might be the case for a hydrated surface complex.

Time of Flight Secondary Ion Mass Spectroscopy (ToF-SIMS)

ToF-SIMS complements XPS measurements, but offers ultimate surface sensitivity, viewing only the first monolayers. ToF-SIMS operates by bombarding a surface with a high energy beam (normally between 15 and 22 KeV) beam of ions or neutrals. The particle energy is transferred to the atoms of the solid through a 'collision cascade' (Vickerman and Swift, 1997) (Fig. 57). Some of these collisions return to the surface and result in the emission of atoms and atom clusters which may become ionized as they leave the surface. These particles are termed secondary ions. Because of the energy needed for these secondary ions to escape from the surface, over 95% of the detected ions originate from the top two layers of the solid (Vickerman and Swift, 1997).

Reproduced with permission of the copyright owner. Further reproduction prohibited without permission.

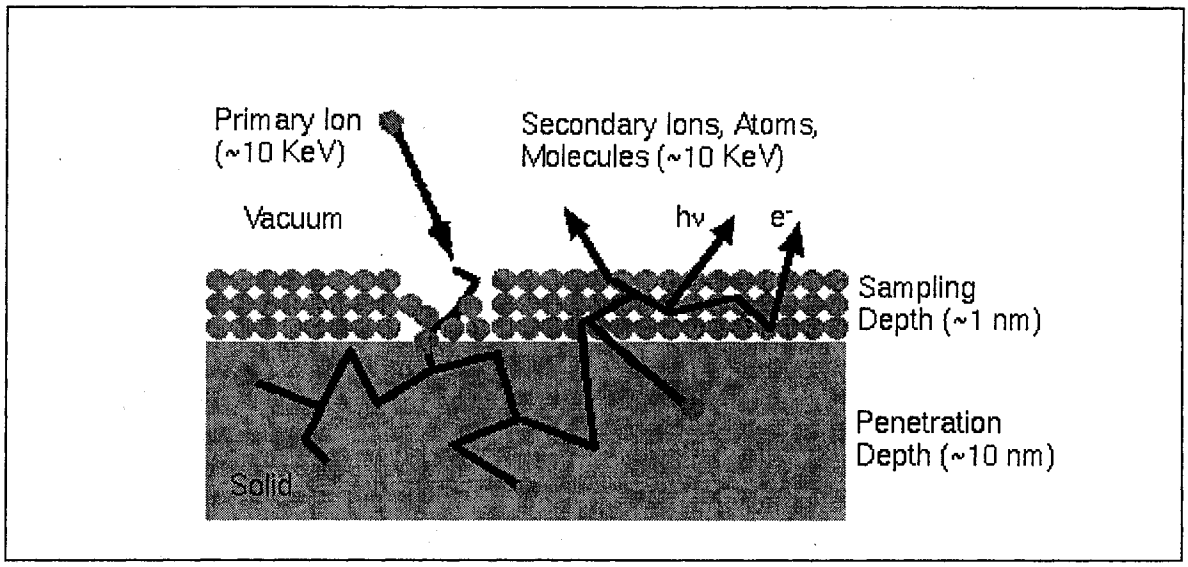

Figure 57. Collision cascade diagram depicting the interaction of the primary ion beam with a solid sample in SIMS analysis. In this model, the primary ion passes energy to secondary ions creating a "collision cascade" within the sample. This cascade causes ions, atoms and molecules to be ejected from the surface. The sampling depth is limited to the first few monlayers due to the energy needed to escape the surface.

Particle yield is related to the crystallinity and topography of the bombarded materials, as well as the electronic state of the surface (yields vary by orders of magnitude across the periodic table) and the chemical state of the surface (e.g., a pure metal compared to its oxide). ToF-SIMS has been shown to provide detection limits for metals on light element oxides better than 1 ppm of the surface (Benninghoven, 1994; Douglas and Chen, 1998). Peaks in the ToF-SIMS spectra may be able to be used as a measure of surface coverage based on their relative intensities. Additionally, ToF-SIMS can be used to qualitatively map the surface distribution of elements of interest.

Reproduced with permission of the copyright owner. Further reproduction prohibited without permission.

X-ray Absorption Spectroscopy (XAS)

XAS is an element specific technique that can be used to probe of the local atomic environment of a sorbed species. It employs the principles of the adsorption of electromagnetic radiation by matter to study the discrete energy levels of electrons in atoms, molécules and condensed matter (Glenn and Dodd, 1968). The use of XAS as a molecular-level structural probe came about with advances in theory and the availability of intense sources of continuous x-ray radiation referred to as synchrotron radiation (Sayres et al., 1970; Sayers et al., 1971; Winick and Doniach, 1980). XAS spectra are especially sensitive to the formal oxidation state, coordination chemistry, and the distances, coordination number and species of the atoms immediately surrounding the selected element (Chisholm-Brause et al., 1990; Bargar et al., 1997; Trainor et al., 2000; Newville, 2004). As such, XAS can be used to directly probe sorbed metal ions. An advantage of XAS is that direct in situ measurements can be made on oxide surfaces in the presence of water. However, because the total metal content is probed, XAS lacks the resolution to distinguish between chemically inequivalent sites of the same element (Evans, 1990). Thus, XAS is most powerful when used in combination with other techniques that can provide such information.

An X-ray absorption spectra can be divided into three distinct regions, the pre-edge, the X-ray Absorption Near Edge Structure (XANES) region and the Extended X-ray Absorption Fine Structure (EXAFS) region (Fig. 58). The pre-edge region occurs approximately 2-10 eV below the main absorption edge. Features in this region are due to electronic transitions from a core level to the lowest energy, unoccupied or partially occupied level. The energy and intensity of pre-edge features provide information on the

Reproduced with permission of the copyright owner. Further reproduction prohibited without permission.

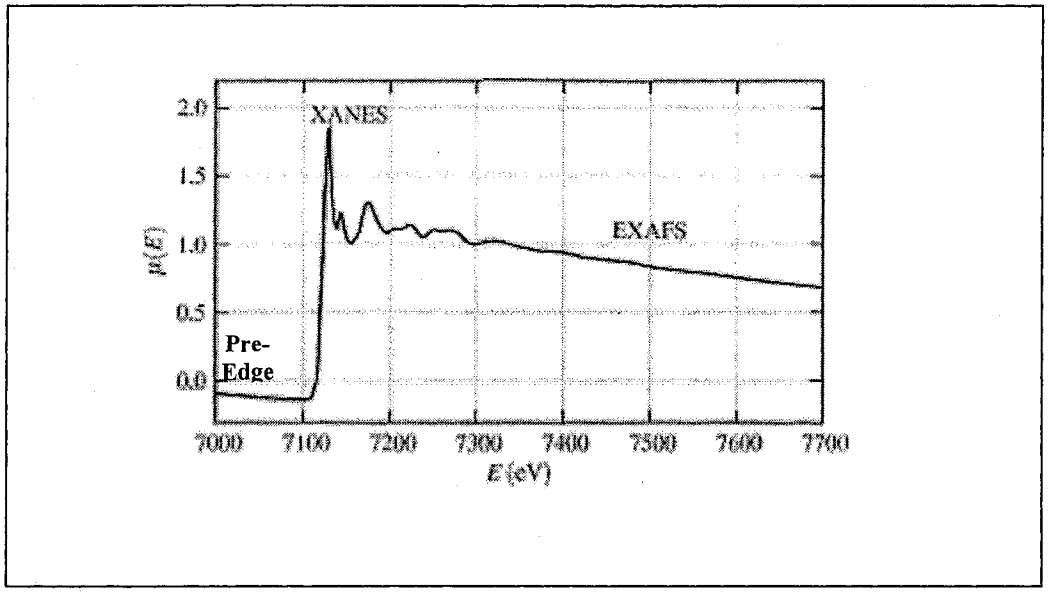

Figure 58. XAS μ(E) spectrum measured for FeO with the pre-edge, XANES and EXAFS regions labeled.

adsorber's oxidation state, the site geometry of the adsorber, and adsorber-ligand bonding (Brown et al., 1988). The XANES region extends from a few eV above the pre-edge to about 50 eV above the absorption edge. Transitions in the XANES are particularly sensitive to the geometrical arrangement of first and more distant neighbors around the central atom. Thus, XANES features can be used to obtain information on site geometry and bond angles. The third and final region, the EXAFS region, extends from about 50 eV above the edge to as much as 1000 eV above the edge. This region is characterized by weak oscillations of low frequency which arise from interference effects in the wavefunction of the excited electron. After absorption of a photon, the wavefunction propogates away from the atomic core, and is partially backscattered by the surrounding atoms (Fig. 59). These paths can be either single or multiple scattering paths depending on the number of atoms involved (Fig. 60). Interference between the outgoing and

Reproduced with permission of the copyright owner. Further reproduction prohibited without permission.

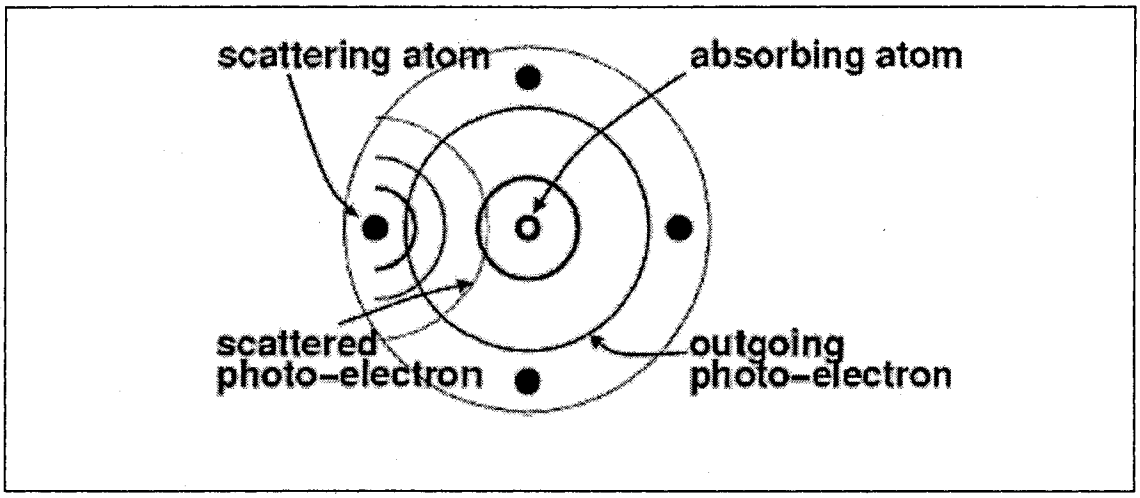

Figure 59. Schematic showing the wavefunction of a photoelectron leaving the central absorbing atom, interacting with a neighboring atom, and being backscattered. The phase of the backscattered wavefunction has been shifted from its original phase due to its interaction with the scattering atom. It is the interferences between the outgoing and backscattered wavefunctions that give rise to EXAFS. (From Newville, 2004)

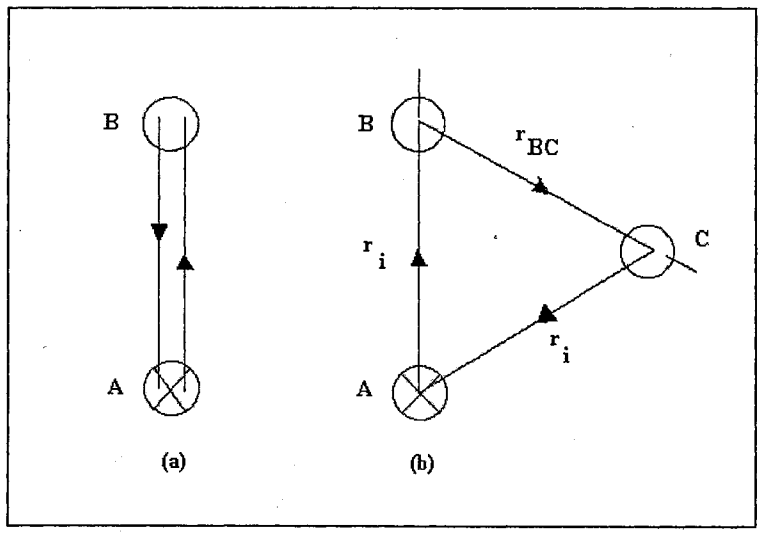

Figure 60. Schematic illustrating an (a) single-scattering path for the photoelectron and (b) a double-scattering path. The absorbing atom is designated by a circle with an x in the middle (from Stern, 1998).

Reproduced with permission of the copyright owner. Further reproduction prohibited without permission.

backscattered wave produces the extended oscillations observed in the EXAFS region (Flavell, W. in Vickerman). Thus, EXAFS can be analyzed to provide information about the distance from the absorber to near neighbors and about the number and type of backscatterers. Further information on data reduction and analysis can be found in Appendix C.

Reproduced with permission of the copyright owner. Further reproduction prohibited without permission.

APPENDIX 2

Specific Surface Area Measurements

Volume of N_2 (g) adsorbed at 173 K as a function of relative pressure, measured using a Micromeritics Gemini 2365 Surface Area and Pore Size Analyzer. Pressure was increased from 0.05% to 0.98% of saturation pressure (P_{rel}) and the volume adsorbed was measured (N_{ads}). To calculate the BET surface area, the isotherm was inspected to find a suitable linear region between relative pressures of 0.05 and 0.20. Once this region was designated, the following transform was performed on each point

$$B_1 = \frac{P_{rel_1}}{(1.0 - P_{rel_1}) \times N_{ads_1}} \tag{9}$$

where B_1 is in units of g/cm^3 STP. A least-squares fit was performed on the (P_{rel}, B) pairs. From this fit, the slope, y-intercept and correlation coefficient were calculated. These parameters were then used to calculate the BET Surface Area (m^2/g) and the BET C value using the following equations:

$$SA_{BET} = \frac{CSA \times (6.023 \times 10^{23})}{(22414\ cm^3\ STP) \times (10^{18}\ \frac{nm^2}{m^2}) \times (S + Y_{INT})} \tag{10}$$

$$C = \frac{S + Y_{INT}}{Y_{INT}} \tag{11}$$

where CSA is the molecular cross-sectional area of the analysis gas (N_2 = 3.55 nm^2) and S and Y_{INT} are the slope and y-intercept of the least-squares line, respectively.

Reproduced with permission of the copyright owner. Further reproduction prohibited without permission.

MODEL COMPOUNDS

γ-Al_2O_3 (Degussa Aluminum Oxide C)

P_{rel}	N_{ads} (mmol/g)	B_1 (g/cm^3)	Slope
0.050	0.931	0.056	0.991
0.060	0.958	0.066	
0.080	1.006	0.086	
0.120	1.084	0.126	**Y-Intercept**
0.160	1.153	0.165	0.007
0.200	1.218	0.206	
0.332	1.427	0.348	
0.530	1.772	0.637	**SSA (m^2/g)**
0.670	2.092	0.968	95.624
0.768	2.416	1.368	
0.837	2.768	1.851	
0.885	3.128	2.465	**C**
0.919	3.611	3.146	142.514
0.943	4.141	4.002	
0.960	4.719	5.072	
0.984	6.474	9.440	

Goethite

P_{rel}	N_{ads} (mmol/g)	B_1 (g/cm^3)	Slope
0.050	1.175	0.045	0.820
0.060	1.199	0.053	
0.080	1.246	0.070	
0.120	1.331	0.102	**Y-Intercept**
0.160	1.410	0.135	0.004
0.200	1.484	0.169	
0.332	1.720	0.289	
0.530	2.015	0.560	**SSA (m^2/g)**
0.670	2.240	0.904	115.713
0.768	2.477	1.335	
0.837	2.743	1.868	
0.885	3.052	2.527	**C**
0.919	3.428	3.314	206.100
0.943	3.885	4.267	
0.960	4.424	5.411	
0.984	6.188	9.876	

Reproduced with permission of the copyright owner. Further reproduction prohibited without permission.

Hematite

P_{rel}	N_{ads} (mmol/g)	B_1 (g/cm^3)	Slope
0.050	0.004	12.358	
0.060	0.005	13.586	114.190
0.080	0.005	16.014	
0.120	0.007	20.475	**Y-Intercept**
0.160	0.008	24.420	
0.200	0.009	27.999	6.799
0.332	0.012	40.992	
0.530	0.017	67.391	**SSA (m^2/g)**
0.670	0.020	100.184	
0.768	0.023	143.330	0.788
0.837	0.026	198.670	
0.885	0.029	270.460	**C**
0.919	0.032	359.637	
0.943	0.035	475.056	17.796
0.960	0.039	619.344	
0.984	0.051	1200.625	

Unreacted Planar γ-Al_2O_3

P_{rel}	N_{ads} (mmol/g)	B_1 (g/cm^3)	Slope
0.050	0.109	0.480	
0.060	0.113	0.563	8.217
0.080	0.119	0.730	
0.120	0.129	1.058	**Y-Intercept**
0.160	0.137	1.386	
0.200	0.146	1.714	0.071
0.332	0.171	2.902	
0.530	0.220	5.137	**SSA (m^2/g)**
0.670	0.280	7.249	
0.768	0.352	9.404	11.510
0.837	0.411	12.466	
0.886	0.462	16.693	**C**
0.920	0.511	22.304	
0.944	0.558	29.849	116.080
0.961	0.605	39.799	
0.985	0.712	85.801	

Reproduced with permission of the copyright owner. Further reproduction prohibited without permission.

Fe Coated Planar γ-Al_2O_3

VARYING Fe(III) CONCENTRATION AND REACTION TIME

0.125 mM $Fe(NO_3)_3$, 4 day reaction

P_{rel}	N_{ads} (mmol/g)	B_1 (g/cm^3)	Slope
0.050	0.064	0.822	
0.060	0.067	0.951	13.006
0.080	0.072	1.210	
0.120	0.079	1.729	**Y-Intercept**
0.160	0.085	2.244	
0.200	0.090	2.779	0.171
0.332	0.106	4.704	
0.530	0.131	8.622	**SSA (m^2/g)**
0.670	0.158	12.897	
0.768	0.186	17.817	7.240
0.837	0.208	24.640	
0.886	0.226	34.253	**C**
0.920	0.242	47.431	
0.944	0.255	65.708	77.192
0.961	0.268	91.490	
0.985	0.298	214.836	

1.25 Mm $Fe(NO_3)_3$, 4 day reaction

P_{rel}	N_{ads} (mmol/g)	B_1 (g/cm^3)	Slope
0.050	0.097	0.544	
0.060	0.100	0.637	8.947
0.080	0.106	0.823	
0.120	0.115	1.183	**Y-Intercept**
0.160	0.124	1.538	
0.200	0.133	1.886	0.104
0.333	0.168	2.965	
0.532	0.243	4.676	**SSA (m^2/g)**
0.691	0.299	4.457	
0.768	0.345	9.591	10.541
0.837	0.388	13.220	
0.886	0.423	18.330	**C**
0.919	0.454	24.965	
0.943	0.484	34.216	87.441
0.960	0.509	47.126	
0.984	0.561	109.622	

Reproduced with permission of the copyright owner. Further reproduction prohibited without permission.

12.5 mM $Fe(NO_3)_3$, 4 day reaction

P_{rel}	N_{ads} (mmol/g)	B_1 (g/cm^3)	Slope
0.050	0.020	2.693	
0.060	0.021	2.988	24.683
0.080	0.024	3.600	
0.120	0.029	4.680	**Y-Intercept**
0.160	0.034	5.643	
0.200	0.038	6.579	1.668
0.332	0.050	9.907	
0.531	0.066	17.035	**SSA (m^2/g)**
0.670	0.075	26.907	
0.768	0.082	40.237	3.620
0.837	0.083	61.684	
0.886			**C**
0.920			
0.944			15.794
0.961			
0.985			

0.125 mM $Fe(NO_3)_3$, 14 day reaction

P_{rel}	N_{ads} (mmol/g)	B_1 (g/cm^3)	Slope
0.050	0.034	1.561	
0.060	0.035	1.813	26.844
0.080	0.037	2.326	
0.120	0.040	3.384	**Y-Intercept**
0.160	0.043	4.453	
0.200	0.045	5.615	0.192
0.332	0.050	9.991	
0.531	0.059	19.278	**SSA (m^2/g)**
0.670	0.068	30.093	
0.769	0.078	42.712	3.528
0.838	0.086	59.957	
0.886	0.096	81.568	**C**
0.920	0.106	108.569	
0.944	0.118	143.010	140.594
0.961	0.129	192.070	
0.985	0.163	388.502	

Reproduced with permission of the copyright owner. Further reproduction prohibited without permission.

1.25 mM $Fe(NO_3)_3$, 14 day reaction

P_{rel}	N_{ads} (mmol/g)	B_1 (g/cm^3)	Slope
0.050	0.024	2.173	
0.060	0.026	2.500	31.365
0.080	0.028	3.138	
0.120	0.031	4.350	**Y-Intercept**
0.160	0.034	5.592	
0.200	0.036	6.927	0.607
0.332	0.043	11.520	
0.530	0.056	20.314	**SSA (m^2/g)**
0.670	0.069	29.225	
0.768	0.085	39.169	2.984
0.837	0.098	52.175	
0.886	0.111	69.747	**C**
0.920	0.123	93.238	
0.944	0.135	124.444	52.664
0.961	0.148	165.630	
0.985	0.180	357.493	

12.5 mM $Fe(NO_3)_3$, 14 day reaction

P_{rel}	N_{ads} (mmol/g)	B_1 (g/cm^3)	Slope
0.050	0.090	0.581	
0.060	0.094	0.677	10.358
0.080	0.099	0.875	
0.120	0.106	1.282	**Y-Intercept**
0.160	0.112	1.700	
0.200	0.117	2.138	0.053
0.332	0.126	3.953	
0.530	0.133	8.509	**SSA (m^2/g)**
0.670	0.138	14.691	
0.469	0.143	23.175	9.163
0.838	0.149	34.597	
0.886	0.154	50.621	**C**
0.920	0.160	72.247	
0.944	0.166	102.199	195.334
0.961	0.171	143.713	
0.985	0.191	339.283	

Reproduced with permission of the copyright owner. Further reproduction prohibited without permission.

SEQUENTIAL COATINGS: 1.25 mM $Fe(NO_3)_3$, 4 day reaction

2 Coatings

P_{rel}	N_{ads} (mmol/g)	B_1 (g/cm^3)	Slope
0.050	0.006	8.902	
0.060	0.006	10.114	108.340
0.080	0.007	12.282	
0.120	0.008	16.351	**Y-Intercept**
0.160	0.009	20.749	
0.200	0.010	25.361	3.528
0.332	0.011	43.350	
0.530	0.014	80.389	**SSA (m^2/g)**
0.671	0.017	116.652	
0.769	0.021	158.298	0.853
0.838	0.025	202.509	
0.886	0.031	255.074	**C**
0.920	0.037	311.147	
0.944	0.044	386.239	31.705
0.961	0.052	468.915	
0.985	0.077	822.641	

5 Coatings

P_{rel}	N_{ads} (mmol/g)	B_1 (g/cm^3)	Slope
0.050	0.007	7.175	
0.060	0.008	7.690	44.055
0.080	0.010	8.837	
0.120	0.013	10.773	**Y-Intercept**
0.160	0.015	12.434	
0.200	0.018	14.166	5.381
0.332	0.024	20.386	
0.530	0.035	32.531	**SSA (m^2/g)**
0.670	0.043	46.997	
0.768	0.050	65.664	1.930
0.837	0.057	90.111	
0.886	0.064	121.773	**C**
0.920	0.070	163.270	
0.944	0.077	217.803	9.188
0.961	0.084	290.290	
0.985	0.103	623.155	

Reproduced with permission of the copyright owner. Further reproduction prohibited without permission.

10 Coatings

P_{rel}	N_{ads} (mmol/g)	B_1 (g/cm^3)	Slope
0.050	0.048	1.095	20.047
0.060	0.051	1.256	
0.080	0.053	1.630	
0.120	0.056	2.430	**Y-Intercept**
0.160	0.058	2.253	0.039
0.200	0.060	4.151	
0.332	0.061	8.155	
0.530	0.060	18.767	**SSA (m^2/g)**
0.670	0.061	33.102	4.749
0.768	0.065	50.772	
0.837	0.072	71.695	
0.886	0.080	96.536	**C**
0.920	0.090	126.980	509.807
0.944	0.104	162.228	
0.961	0.119	204.822	
0.985	0.167	372.288	

Reproduced with permission of the copyright owner. Further reproduction prohibited without permission.

APPENDIX 3

EXAFS Data Analysis

I. Background

In the EXAFS region, we are interested in the oscillations well above the adsorption edge. The different frequencies apparent in the oscillations in this region correspond to different near-neighbor coordination shells which can be described and modeled according to the EXAFS equation:

$$\chi(k) = \sum_j \frac{N_j f_j e^{-2k^2\sigma_j^2}}{kR_j^2} \sin[2kR_j + \delta_j(k)] \qquad (12)$$

where $f(k)$ and $\delta(k)$ are scattering properties of the atoms neighboring the excited atom, N is the number of neighboring atoms, R is the distance to the neighboring atom, and σ^2 is the disorder in the neighbor distance. Thus, the EXAFS equation allows us to determine N, R, and σ^2 knowing the scattering amplitude $f(k)$ and phase-shift $\delta(k)$. EXAFS is also sensitive to the atomic species of the neighboring atom as the scattering factors depend on the Z of the neighboring atom.

The general steps for EXAFS data analysis are shown in figure 61. After data collection, the raw data is reduced. This involved converting the measured intensities to $\mu(E)$ while possibly correcting for systematic measurement errors such as self-adsorption effects and detector dead time. A suitable background is subtracted from the pre-edge function of $\mu(E)$ to remove any instrumental background and adsorption from other

Reproduced with permission of the copyright owner. Further reproduction prohibited without permission.

edges. The maximum energy of the first derivative of $\mu(E)$, E_o, is identified. Normalize $\mu(E)$ to go from 0 to 1. This adjusts the spectrum so that it represents the adsorption of 1 x-ray (normalized spectra are most useful for XANES analysis). A smooth, post-edge background is then removed and the EXAFS region is isolated and its energy is converted from eV to $Å^{-1}$ ($\chi(k)$). This function should not remove the EXAFS itself but needs only to remove the very low frequency components of the oscillations. The transformed EXAFS range is then fourier transformed into R-space.

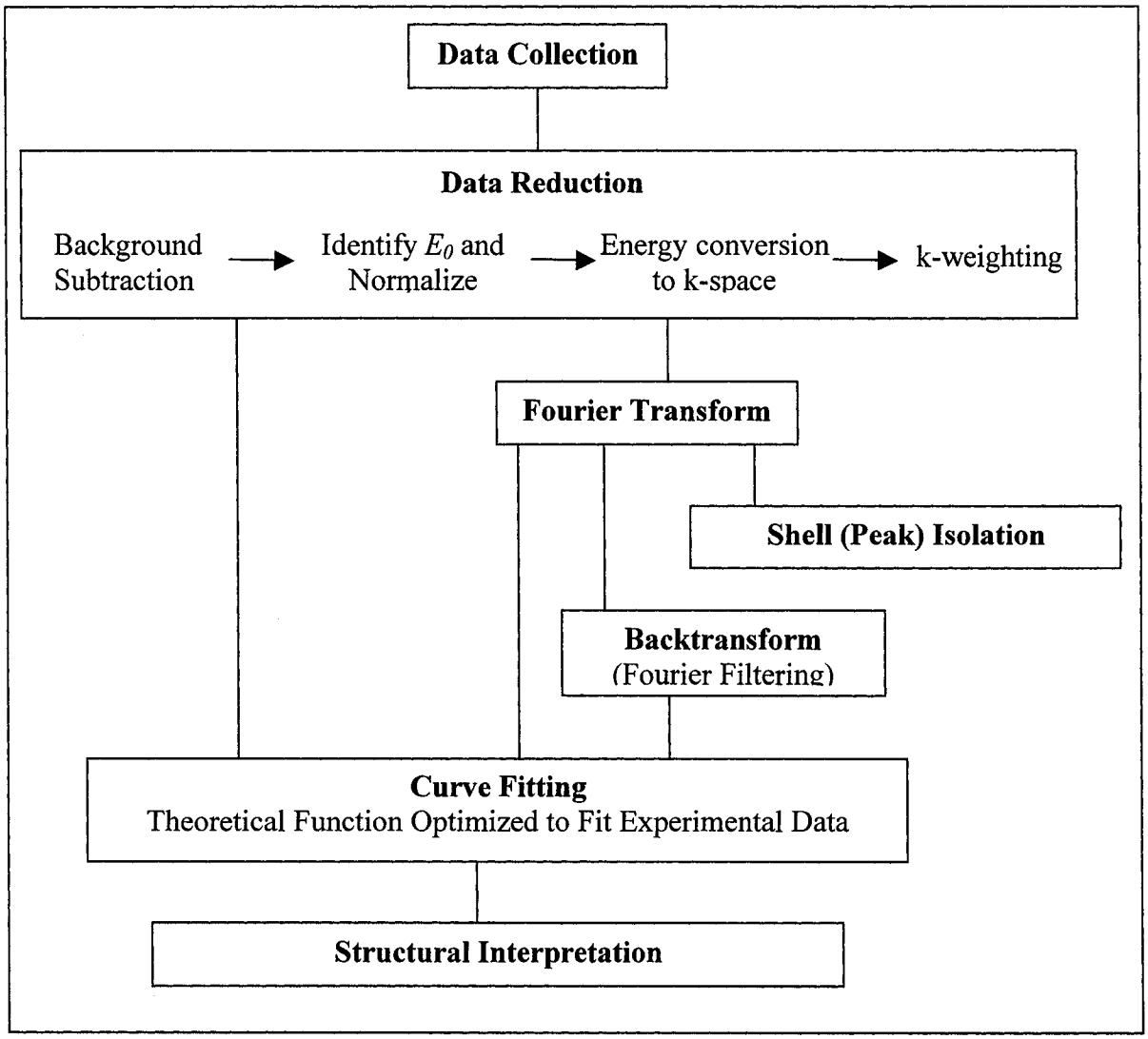

Figure 61. EXAFS analysis steps beginning with data collection, reduction of raw data, conversion of data to k- and R-space and analysis (adapted from Fendorf, 1999).

Reproduced with permission of the copyright owner. Further reproduction prohibited without permission.

II. Data Collection

XAS data was collected at the National Synchrotron Light Source at Brookhaven National Laboratory on EXXON beamline X-10C. This beamline is designed specifically for x-ray absorption spectroscopy and consists of horizontal and vertical tantalum slits, a double crystal monochromator, bent-cylindrical focusing mirror, photon shutter and a small experimental hutch. A VMS based microvax computer system is used for data acquisition and beamline control.

The UHV double crystal monochromator is configured in a non-dispersive geometry with the energy resolution being determined by a convolution of source parameters, entrance slits and crystal cut (Sansone et al., 2004). The first crystal is water-cooled, and the heat is extracted from the crystal sides to minimize thermal gradient at the crystal surface. The first crystal position determines the beam height while the second crystal is positioned to intercept the x-ray beam from the first. A 60 cm long rhodium coated bent cylindrical mirror with a measured surface roughness less than 5Å RMS is used for horizontal and vertical focusing. The mirror is also used as a harmonic rejection filter. Thus, it is not necessary to detune the monochromator. This methodology permits the use of an A/C feedback system which dynamically compensates for thermal effects of the first monochromator crystal and minimizes x-ray modulation from beam position fluctuations. During experiments, the crystal positions are fixed and the beam height changes. The vertical position of the mirror, beamline and experimental table are adjusted to compensate for the beam height changes.

Reproduced with permission of the copyright owner. Further reproduction prohibited without permission.

For our experiments, a 30 element solid-state detector was used to detect fluoresced electrons at an angle of 45 degrees to the sample. Pb(II)/bulk γ-Al_2O_3 sorption data is the average of a minimum of 4 scans. Pb(II)/planar γ-Al_2O_3 sorption data is the average of a minimum of 20 scans. The scan parameters are shown in table 21.

Table 21. Scan parameters used to collect Pb XAFS data on beamlins X-10C

Region	Start	Increment	Total Points	End	Dwell Time
1	12855 eV	13 eV	14	13024 eV	1s
2	13024.5 eV	0.5 eV	122	13085 eV	1s
3	2.8 K	0.07 K	46	6.0 K	5s
4	6.0 K	0.07 K	129	14.9 K	10s

III. Data Analysis

The XAS analysis programs IFEFFIT (Newville, 2001) and SixPACK (Webb, 2002) were used to perform data reduction and analysis. For all Pb(II) sorption samples in this study it was found that the same set of parameters could be used for data reduction and conversion to *k*- and *R*-space. These parameters are listed in table 22.

Table 22. Parameters used in background subtraction of the pre- and post-edge regions, and conversion to *k*- and *R*-space for EXAFS data analysis.

Pre-Edge (eV)	Post-Edge (eV)	Spline (k)	E_0	Rbkg	K-weight	FT Window	Low Clamp	High Clamp
Linear -200.0 to – 50.0	Quadratic 150.0 to 852.07	1.0 to 12.0	13052	1.75	3	Kaiser-Bessel	None	None

Reproduced with permission of the copyright owner. Further reproduction prohibited without permission.

E_0 was set to the maximum energy of the secondary peak in the first derivative spectrum. This avoids interference of the white-line region of the spectrum with the spline-fitting routine.

IV. EXAFS Modeling

The feff 7 input parameters were based on a model of PbO_4 sorbed to hematite with the Fe atoms replaced with Al atoms. This model depicts Pb in a distorted trigonal pyramid geometry as an edge-sharing bidentate complex with an Al octahedral (fig. 61).

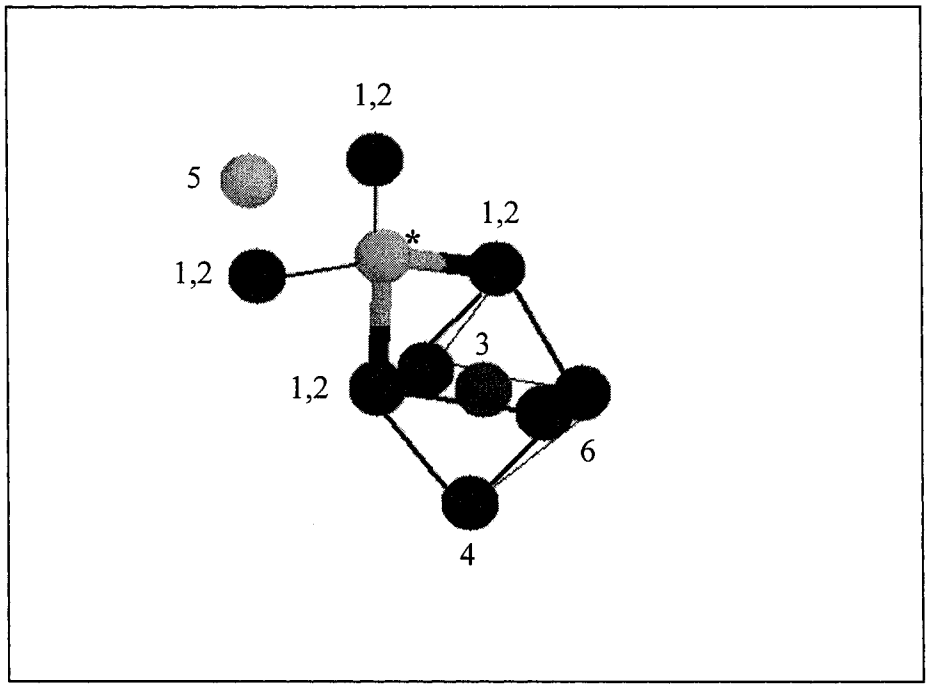

Figure 62. Edge-sharing bidentate PbO_4 complex sorbed to Al octahedral. The numbers correspond to the calculated feff 7 scattering paths from the central Pb atom, marked with an *.

Reproduced with permission of the copyright owner. Further reproduction prohibited without permission.

The feff 7 model input is as follows:

```
*Bidentate PbO4 on Alumina; Pb-Al = 3.22 Å
*Pb has 4 oxygen atoms (2@2.28, 2@2.40) at corners of sq pyramid
*Pb has edge-shared Pb neighbor @ 3.80 Å
*Al is octahedral with Al-O = 2.12, 1.945 Å
*
*
TITLE Bidentate Pb on AlOx
HOLE 4 1.0
CONTROL 1 1 1 1
PRINT 1 0 0 3

*EXCHANGE 3 0.0

*SCF 4
NLEGS 2
RMAX 6.0

*FOLP 0 1.0
*FOLP 1 1.0
*FOLP 2 1.0

POTENTIALS
        0       82
        1       8
        2       13
        3       82

ATOMS
*Pb central atom:
        0.0000          0.0000          1.7210 0

*Oxygen atoms:
        0.0000          -1.4960         0.0000          1       Obr(1)
        0.0000          1.4960          0.0000          1       Obr(2)
        1.8380          -1.4540         2.1630          1       O(1)
        1.8380          1.4540          2.1630          1       O(2)

        1.9450          0.0000          -1.4960         1       Oax(1)
       -2.1160          0.0000          -1.4960         1       Oax(2)
        0.0000          -1.3750         -2.8710         1       Oeq(1)
        0.0000          1.3750          -2.8710         1       Oeq(2)
```

Reproduced with permission of the copyright owner. Further reproduction prohibited without permission.

```
*Al atom at 3.22 A:
      0.0000      0.0000     -1.4960     2     Al

*Pb atom at 3.80 A:
      3.6690      0.0000      2.5900     3     Pb

*H atoms for O(br), O(U1), O(U2)
*     0.0000      0.0000      2.4770     5     H(br1)
*     0.0000      0.0000     -2.4770     5     H(br2)
*     0.0000     -5.0840      1.4770     5     H1[O(U1)]
*     0.0000     -4.0840      2.4770     5     H2[O(U1)]
*     0.0000     -5.0840     -1.4770     5     H1[O(U2)]
*     0.0000     -4.0840     -2.4770     5     H2[O(U2)]
```

The first 7 paths from the feff 7 output file were chosen for use in modeling the Fourier-transformed EXAFS data. They are shown below.

Bidentate PbO_4 on AlOx
X7 7.00

Abs z=82 Rmt=1.371 Rnm=1.741 LIII Shell
Pot 1 z=8 Rmt=0.949 Rnm=1.210
Pot 2 z=13 Rmt=1.081 Rnm=1.413
Pot 3 z=82 Rmt=1.461 Rnm=1.884
Gam_ch=5.481E+00 H-L exch
Mu=-2.014E+00 kf=1.782E+00 Vint=-1.411E+00 Rs_int=2.035

file	sig2	amp ratio	deg	nlegs	r effective
feff0001.dat	0.00000	100.00	2.000	2	2.2803
feff0002.dat	0.00000	88.232	2.000	2	2.3849
feff0003.dat	0.00000	19.182	1.000	2	3.2170
feff0004.dat	0.00000	11.175	1.000	2	3.7593
feff0005.dat	0.00000	16.824	1.000	2	3.7997
feff0006.dat	0.00000	10.327	1.000	2	3.8505
feff0007.dat	0.00000	9.687	2.000	2	4.7934

Paths 1 and 2 (feff0001.dat and feff0002.dat, respectively) represent the oxygen atoms bound to the Pb(II) atom at two distances (due to distortion of the complex caused by a

Reproduced with permission of the copyright owner. Further reproduction prohibited without permission.

pair of free electrons on the Pb atom) (Fig. 2). Path 3 is the scattering path between the Al and Pb atom. Path 4 is the scattering path between the equatorial oxygens of the Al octahedral lattice and Pb, and path 6 is the scattering path between the axial oxygens of the Al octahedral and Pb. Path 5 is the scattering path between a second Pb atom and the primary Pb absorber atom, and path 7 is the scattering path between the primary Pb absorber and oxygen sorbed to the secondary Pb atom. An eighth scattering path was added to the feff model to account for a third oxygen distance in the Pb tetrahedral.

Reproduced with permission of the copyright owner. Further reproduction prohibited without permission.

APPENDIX 4

ToF-SIMS and XPS Analysis of Fe Coated Planar γ-Al_2O_3

Integrated Areas of ToF-SIMS Analytical peaks

VARYING FE(III) CONCENTRATION

4 Day Reaction

Fe(III) Concentration mM	**Total Counts**	**Al(27)**	**Fe (55-57)**	**Fe/Al**
0.125	3293275	1602369	125815	0.0785
0.125	3031201	1340204	138973	0.1037
1.25	3170121	994818	292279	0.2938
1.25	2661317	931138	197632	0.2122
12.5	4482740	1213679	139083	0.1146
12.5	2661317	937402	197591	0.2108

14 Day Reaction

Fe(III) Concentration mM	**Total Counts**	**Al(27)**	**Fe (55-57)**	**Fe/Al**
0.125	1396805	425110	85724	0.2017
0.125	1295864	360136	77828	0.2161
1.25	2617251	687789	351999	0.5118
1.25	2210269	828303	340497	0.4111
12.5	3387495	1043019	193975	0.1860
12.5	2851624	1080080	99826	0.0924

Reproduced with permission of the copyright owner. Further reproduction prohibited without permission.

SEQUENTIAL COATINGS

1.25 mM Fe(III), 4 Day

Coatings	Total Counts	Al(27)	Fe (55-57)	Fe/Al
1	810668	532682	38133	0.0716
1	1095520	744637	52295	0.0702
2	1394899	800817	247519	0.3091
2	1173719	550625	218689	0.3972
5	1307107	501590	520269	1.0372
5	1791947	964224	777001	0.8058
10	1865783	384568	666506	1.7331
10	1671720	314796	546051	1.7346

XPS Spectra Analysis

Sensitivity Factors:

Al 2p = 0.19, Fe 2p = 2.96

VARYING FE(III) CONCENTRATION

0.125 mM Fe(III), 4 Day Reaction

Peak	Center BE	Area	Atom %
Al 2p	73.9	2877.67	18.02
C 1s	284.5	3918.33	24.54
Fe 2p	710.7	38.71	0.24
O 1s	531.3	9130.3	57.19

*BE = Binding Energy (eV)

1.25 mM Fe(III), 4 Day Reaction

Peak	Center BE	Area	Atom %
Al 2p	73.9	2253.84	16.39
C 1s	284.5	3761.4	27.35
Fe 2p	709.7	58.24	0.42
O 1s	531.6	7679.64	55.84

Reproduced with permission of the copyright owner. Further reproduction prohibited without permission.

12.5 mM Fe(III), 4 Day Reaction

Peak	Center BE	Area	Atom %
Al 2p	73.8	2347.86	16.26
C 1s	284.5	4711.18	32.63
Fe 2p	710.9	19.63	0.14
O 1s	531.1	7358.89	50.97

0.125 mM, 14 Day

Peak	Center BE	Area	Atom %
Al 2p	73.7	3825.26	15.51
C 1s	284.5	12747.90	33.70
Fe 2p	ND	ND	ND
O 1s	531.22	46156.90	50.79

1.25 mM, 14 Day

Peak	Center BE	Area	Atom %
Al 2p	73.7	3741.21	15.56
C 1s	284.5	12300.90	33.36
Fe 2p	710.7	3241.94	0.88
O 1s	531.1	44468.30	50.20

12.5 mM, 14 Day

Peak	Center BE	Area	Atom %
Al 2p	73.9	2344.06	11.29
C 1s	284.5	14010.70	44.00
Fe 2p	710.9	934.91	0.29
O 1s	531.5	33974.20	44.42

Reproduced with permission of the copyright owner. Further reproduction prohibited without permission.

SEQUENTIAL COATINGS

2 Coatings

Peak	Center BE	Area	Atom %
Al 2p	73.7	4479.62	15.95
C 1s	284.5	11784.00	27.35
Fe 2p	710.4	4200.07	0.98
O 1s	531.1	57662.70	55.72

5 Coatings

Peak	Center BE	Area	Atom %
Al 2p	73.8	3303.60	12.97
C 1s	284.5	13219.90	33.83
Fe 2p	710.6	9955.02	2.55
O 1s	530.9	47544.70	50.65

10 Coatings

Peak	Center BE	Area	Atom %
Al 2p	73.8	2731.41	10.91
C 1s	284.5	14148.10	36.85
Fe 2p	711.0	11214.30	2.92
O 1s	530.5	45484.49	49.32

Reproduced with permission of the copyright owner. Further reproduction prohibited without permission.

APPENDIX 5

ToF-SIMS Peak Analysis of Emplaced Planar γ-Al_2O_3

Integrated Areas of ToF-SIMS Analytical peaks

PRE-EMPLACEMENT

Sample ID	Replicate	Cts +ve	Cts -ve	Na(23)	Al(27)	S(32)	Fe(56)	Pb(208)
Unreacted	1	230300	1002916	3056	129461	10823	785	32
	2	1547165	2085936	13434	916031	20820	9048	108
	3	2498512	2574089	59791	1321371	28529	10510	313
	4	2949463	2209973	331318	876809	13856	19133	1125
Low Pb(II)	1	479902	2201773	6203	330133	50117	847	2564
	2	2299283	3115672	65836	1549611	79287	3783	19246
	3	1998181	2994121	37406	1387976	74402	3182	10428
	4	742684	817790	8010	633255	7152	260	3705
High Pb(II)	1	710853	2293425	104791	420994	41858	1266	4060
	2	2198616	2959050	298175	1339257	66483	4927	4056
	3	2354254	2935189	221612	1438943	75113	6243	21010
	4	2839273	3138289	281051	1639385	79399	8500	30389

UNREACTED

1 Day Emplacement

Sample ID	Cts +ve	Cts -ve	Na(23)	Al(27)	S(32)	Fe(56)	Pb(208)
UN1T1R1_OX	345613	572215	183124	46704	5914	5932	22
BOUND	149157	736158	31511	24168	7381	2611	42
ANOX	184919	818785	68543	54893	8006	657	16
UN1T1R2_OX	2409843	2199074	409826	882796	23288	22527	335
BOUND	1964187	3320736	416975	591246	27214	33032	310
ANOX	2149559	2994389	415610	734964	24876	36962	289
UN1T2R1_OX	144659	178984	36479	33035	1529	1738	14
BOUND	20838	191329	594	8847	2030	585	0
ANOX	168817	175806	1707	112935	1338	3167	3
UN1T2R2_OX	1653564	1877171	279336	113348	14802	110161	332
BOUND	3429705	2585834	947383	178731	22388	174164	407
ANOX	614852	601740	320011	29616	6821	3065	9

Reproduced with permission of the copyright owner. Further reproduction prohibited without permission.

4 Day Emplacement

Sample ID	Cts +ve	Cts -ve	Na(23)	Al(27)	S(32)	Fe(56)	Pb(208)
UN4T1R1_OX	130487	275978	15515	8565	1533	1470	74
BOUND	187922	175601	60018	29159	1350	13111	26
ANOX	196011	295324	26747	16269	2989	9612	35
UN4T1R2_OX	2057235	3041020	634068	341371	17255	25123	508
BOUND	2461606	3223104	131039	187597	27754	177609	1486
ANOX	1916438	3176467	214760	286049	23952	49254	732
UN4T2R1_OX	66131	819754	2162	7688	6061	426	36
BOUND	192306	344505	42436	13693	3548	4008	277
ANOX	172853	596964	15688	10673	5012	1247	33
UN4T2R2_OX	1530479	1939786	169052	239880	20715	46124	923
BOUND	2114335	2163802	137322	905414	25388	14708	259
ANOX	2397233	2277815	293256	358035	28633	30539	1137

7 Day Emplacement

Sample ID	Cts +ve	Cts -ve	Na(23)	Al(27)	S(32)	Fe(56)	Pb(208)
UN7T1R1_OX	2057235	2286133	634068	341371	19112	25123	508
BOUND	2857943	2518969	715728	614114	24365	124231	501
ANOX	2410553	2876336	385249	653423	22419	141466	444
UN7T1R2_OX	642913	761459	206697	50428	6606	8532	257
BOUND	1238376	1681043	588552	86421	20001	150555	76
ANOX	912744	734987	376577	143911	5777	24507	43
UN7T2R1_OX	2139622	1662809	175092	271516	14403	21605	732
BOUND	3831198	2568611	918962	401269	20133	100801	962
ANOX	2967511	2222503	408165	454035	19475	36627	1143
UN7T2R2_OX	121163	318472	79001	10400	1668	739	5
BOUND	748785	1481376	285272	44371	9608	12110	477
ANOX	2967511	2222503	408165	454035	19475	36627	1143

14 Day Emplacement

Sample ID	Cts +ve	Cts -ve	Na(23)	Al(27)	S(32)	Fe(56)	Pb(208)
UN14T1R1_OX	2531105	2343284	772975	294793	17567	166459	762
BOUND	2167637	2499076	216446	895206	23830	35459	383
ANOX	2971437	2771196	606516	620362	22075	158448	556
UN14T1R2_OX	393674	1447307	15945	20563	10292	11498	158
BOUND	27712	129671	984	2479	117	223	7
ANOX	391370	2378600	18311	20424	23627	5917	178
UN14T2R1_OX	2376424	1902996	424436	265242	19169	39426	360
BOUND	3115902	1983416	468655	527472	22332	67771	394
ANOX	2756072	2626886	378063	888993	27936	41184	405
UN14T2R2_OX	671769	1242891	166626	42819	11370	6271	90
BOUND	395486	1014298	39277	145421	9211	3748	6
ANOX	548285	1360710	110442	57606	10742	2742	95

Reproduced with permission of the copyright owner. Further reproduction prohibited without permission.

LOW Pb

1 Day Emplacement

Sample ID	Cts +ve	Cts -ve	Na(23)	Al(27)	S(32)	Fe(56)	Pb(208)
051T1R1_OX	9612	219606	2130	2252	2299	73	14
BOUND	122164	226785	48837	22552	2718	1072	96
ANOX	176662	574802	120238	10185	5184	1561	970
051T1R2_OX	3628532	1905180	1247333	834862	21505	70001	18639
BOUND	3733147	1923779	940337	886179	18879	146312	15929
ANOX	3335053	3279390	867161	910550	40515	35036	7692
051T2R1_OX	76107	103880	32376	12926	997	449	9
BOUND	110833	232911	48227	14306	2376	2517	464
ANOX	97769	444340	69195	6205	2093	237	218
051T2R2_OX	3868221	1989270	1761019	778562	21385	19523	5124
BOUND	2503126	1718750	835662	773221	14875	12470	1351
ANOX	1708233	3453173	465394	559667	20301	21606	2853

4 Day Emplacement

Sample ID	Cts +ve	Cts -ve	Na(23)	Al(27)	S(32)	Fe(56)	Pb(208)
054T1R1_OX	156662	513021	56266	25548	5178	1154	33
BOUND	174289	345963	54527	15730	3976	19271	439
ANOX	172566	531019	15448	49680	6004	2691	148
054T1R2_OX	2235780	2524696	131020	419803	33984	12637	1916
BOUND	2017814	2582953	378871	548614	24807	23180	584
ANOX	2011046	2154689	220562	925714	19231	13399	243
054T2R1_OX	428436	357298	47595	56571	3266	5459	163
BOUND	149137	627252	61396	26428	6635	693	46
ANOX	405076	502049	129431	120755	5383	3148	31
054T2R2_OX	3442470	2576061	1280292	688332	31065	38416	4104
BOUND	3297779	3490560	103896	388790	46859	74164	1445
ANOX	3718010	3811388	425781	772253	43665	23534	1710

7 Day Emplacement

Sample ID	Cts +ve	Cts -ve	Na(23)	Al(27)	S(32)	Fe(56)	Pb(208)
057T1R1_OX	3367231	1877664	926343	610840	20944	62161	2332
BOUND	3230749	2003630	705416	1216179	25639	18948	2539
ANOX	4578757	2144785	1068898	958175	21532	180256	30084
057T1R2_OX	624376	2270555	336166	30714	10509	6273	912
BOUND	323138	1578510	63055	69389	17444	5641	279
ANOX	626888	1035267	240202	179660	10484	6147	233
057T2R1_OX	3562042	2130003	1159807	713070	25810	76001	4407
BOUND	2886774	2722333	649473	1228378	36746	151385	2947
ANOX	3710878	2497196	1274712	1150734	30653	83757	5233
057T2R2_OX	1049694	1780886	526723	93804	19717	6307	357
BOUND	10640	2408766	4755	1462	22348	501	9
ANOX	353787	1916641	107030	108164	23649	2423	329

Reproduced with permission of the copyright owner. Further reproduction prohibited without permission.

14 Day Emplacement

Sample ID	Cts +ve	Cts -ve	Na(23)	Al(27)	S(32)	Fe(56)	Pb(208)
0514T1R1_OX	3766475	1869390	1164566	652717	20661	84247	4122
BOUND	3911803	2150587	819770	753818	26996	393645	6550
ANOX	4399753	2367137	1074305	1057558	31491	403155	16966
0514T1R2_OX	137590	795096	20877	7229	7101	4942	115
BOUND	1470550	1353830	160318	53584	4645	17293	1098
ANOX	213170	1054916	31625	39826	9201	2145	79
0514T2R1_OX	3168270	2551705	1114255	529676	29458	30385	1946
BOUND	4478296	2877637	1477167	913664	34809	146854	659
ANOX	3372589	1909522	890649	1019336	25175	35797	1048
0514T2R2_OX	900958	1488146	314785	100427	18913	48604	328
BOUND	289064	1125050	12270	158585	14621	6901	448
ANOX	496654	1796899	109351	197077	29645	7052	2062

HIGH Pb

1 Day Emplacement

Sample ID	Cts +ve	Cts -ve	Na(23)	Al(27)	S(32)	Fe(56)	Pb(208)
61T1R1_OX	119169	159063	49250	19972	1625	913	117
BOUND	101526	551284	35454	6822	3562	4792	486
ANOX	207681	27010	70623	54484	2727	1610	306
61T1R2_OX	2820247	15487	969359	548668	163	95326	14267
BOUND	2506343	1720028	595881	225764	15889	396667	8051
ANOX	2085640	1801421	643649	718249	19572	8333	1603
61T2R1_OX	275322	338914	86898	87010	3285	2838	176
BOUND	127440	630154	23922	15879	6257	23419	499
ANOX	331582	693891	80304	112084	8938	4052	651
61T2R2_OX	3359954	2223729	1198873	900702	21648	20718	1599
BOUND	2718432	2832821	1013371	512734	23923	7605	1855
ANOX	2643133	2540452	482489	744258	25565	29402	3346

4 Day Emplacement

Sample ID	Cts +ve	Cts -ve	Na(23)	Al(27)	S(32)	Fe(56)	Pb(208)
64T1R1_OX	107237	238808	4412	5777	4220	1047	96
BOUND	329586	299206	166367	18467	2726	18337	95
ANOX	276504	227566	96826	27960	1926	12837	112
64T1R2_OX	2670332	2561353	867514	326638	28825	154162	9203
BOUND	3569308	2643380	931952	324788	28658	545669	22632
ANOX	2915551	3463432	447957	982931	36788	66401	6004
64T2R1_OX	2899611	1813517	1220868	456425	16256	24331	1492
BOUND	4696605	2890099	1350224	773241	29502	219686	5590
ANOX	4201962	3812430	893761	745600	48265	27600	3338
64T2R2_OX	3616747	2348737	975825	1092164	26321	38126	4382
BOUND	3696993	2316817	1500489	915955	22819	101815	1582
ANOX	2901949	2558944	840957	1089091	32657	35080	1599

Reproduced with permission of the copyright owner. Further reproduction prohibited without permission.

7 Day Emplacement

Sample ID	Cts +ve	Cts -ve	Na(23)	Al(27)	S(32)	Fe(56)	Pb(208)
67T1R1_OX	2915188	2144409	891771	642842	27520	36177	1367
BOUND	3057289	2966749	611578	1146136	40706	32344	2537
ANOX	3455311	2773437	634587	1427980	45337	40288	3526
67T1R2_OX	246462	1505594	48619	42563	17056	5147	229
BOUND	970230	2124369	282720	269433	33116	25829	492
ANOX	581355	971974	79006	188746	123737	8050	788
67T2R1_OX	4082373	2764282	1590697	595224	35055	207174	15928
BOUND	5607671	3802890	1902468	688999	31989	318079	14616
ANOX	4825646	3554310	1699814	1488345	51447	48486	5104
67T2R2_OX	237900	1357790	75069	53299	15460	4292	162
BOUND	684734	854353	86951	305998	10576	17088	248
ANOX	789528	3596643	184233	271150	55788	9325	1726

14 Day Emplacement

Sample ID	Cts +ve	Cts -ve	Na(23)	Al(27)	S(32)	Fe(56)	Pb(208)
614T1R1_OX	2034252	1878884	323950	728747	23282	17983	374
BOUND	3079741	2409858	643033	631870	27495	28060	1606
ANOX	3422739	2150536	648000	857225	27720	23205	2571
614T1R2_OX	536368	689204	174928	114233	6377	10795	377
BOUND	583772	713780	203507	188052	7666	4877	1447
ANOX	1037456	1409474	605433	151275	14301	10965	1819
614T2R1_OX	3691286	2759370	1182419	1269795	42359	20771	1974
BOUND	5229981	2577020	1732690	981862	27598	429462	10387
ANOX	3359333	2206585	635429	1370935	27117	23682	6096
614T2R2_OX	448904	641797	121632	59351	7410	8961	349
BOUND	1203806	632073	471266	218183	8128	24879	299
ANOX	707236	960152	116628	233567	13713	14585	2845

Reproduced with permission of the copyright owner. Further reproduction prohibited without permission.

LITERATURE CITED

Anderson, P. R. and Benjamin, M. M. (1990) Modeling of adsorption in aluminum-iron binary oxide suspensions. *Environmental Science and Technology* **24**, 1586-1592.

Arnebrant, K., Bååth, E. and Nordgren, A. (1987) Copper tolerance of microfungi isolated from polluted and unpolluted forest soil. *Mycologia* **79**, 890-895.

Aston, S. R. (1978) Estuarine Chemistry. *In:* Chemical Oceanography, vol. 7, 2nd ed. (J. P. Riley and R. Chester, eds.) Academic Press, New York, pp. 362-440.

Baes, C. F. I. And Mesmer, R. E. (1976) *The Hydrolysis of Cations*. John Wiley and Sons.

Balistrieri, L. S. and Murray, J. W. (1982) The adsorption of Cu, Pb, Zn and Cd on goethite from seawater. *Geochimica Cosmochimica Acta* **46**, 1253-1265.

Bargar, J. R., Towle, S. N., Brown, Jr., G. E. and Parks, G. A. (1996) Outer-sphere Pb(II) sorbed at specific surface sites on single crystal α-alumina. *Geochimica Cosmochimica Acta* **60**, 3541-3547.

Bargar, J. R., Brown, Jr., G. E. and Parks, G. A. (1997) Surface complexation of Pb(II) at oxide-water interfaces: I. XAFS and bond-valence determination of mononuclear and polynuclear Pb(II) sorption products on aluminum oxides. *Geochimica Cosmochimica Acta* **61**, 2617-2637.

Bargar, J. R., Brown, Jr., G. E. and Parks, G. A. (1997) Surface complexation of Pb(II) at oxide-water interfaces: II. XAFS and bond-valence determination of mononuclear Pb(II) sorption products and surface functional groups on iron oxides. *Geochimica Cosmochimica Acta* **61**, 2639-2652.

Bargar, J. R., Brown, Jr., G. E. and Parks, G. A. (1998) Surface complexation of Pb(II) at oxide-water interfaces: III. XAFS determination of Pb(II) and Pb(II)-chloro adsorption complexes on goethite and alumina. *Geochimica Cosmochimica Acta* **62**, 193-207.

Bargar, J. R., Persson, P. and Brown, Jr., G. E. (1999) Outer-sphere adsorption of Pb(II)EDTA on goethite. *Geochimica Cosmochimica Acta* **63**, 2957-2969.

Bassett, R. I. And Melchior, D. C. (1990) Chemical modeling of aqueous systems. *In:* Chemical Modeling of Aqueous Systems II (D. L. Melchior and R. I. Bassett, eds.), American Chemical Symposium Series No. 416, American Chemical Society, pp. 1-14.

Baumgarten, E. and Kirchhausen-Düsing, U. (1997) Sorption of metal ions on alumina. *Journal of Colloid and Interface Science* **194,** 1-9. Article No. CS975085.

Baumgarten, E. and Dick, P. (1999) Infrared spectroscopic characterization of the alumina surface: 1. Infrared spectra of $Cr(CO)_6$ adsorbed at different surface sites on γ-alumina. *Journal of Colloid and Interface Science* **209**, 16-19.

Reproduced with permission of the copyright owner. Further reproduction prohibited without permission.

Benfer, S., Hofmann, P. and Knözinger, E. (1997) IR spectroscopic monitoring of new chemistry on the surface of nanometer-sized metal oxide particles. *Journal of Molecular Structure* **410-411**, 115-118.

Benjamin, M. M. and Leckie, J. O. (1981) Multiple-site adsorption of Cd, Cu, Zn and Pb on amorphous iron oxyhydroxide. *Journal of Colloid and Interface Science* **79**, 209-221.

Benninghoven, A. (1994) Chemical Analysis of Inorganic and Organic Surfaces and Thin Films by Static Time-of-Flight Secondary Ion Mass Spectrometry (TOF-SIMS). Angew. Chem. International, Editors, England.

Bertsch, P. M. and Seaman, J. C. (1999) Characterization of complex mineral assemblages: implications for contaminant transport and environmental remediation. *Proceedings of the National Academy of Science* **96**, 3350-3357.

Bourg, A. C. M. (1983) Role of freshwater/sweater mixing on trace metal adsorption phenomena. *In:* Trace Metal in Seawater (C. S. Wong, E. Boyle, K. W. Bruland, J. D. Burton and E. D. Goldberg, eds.) Planum Press, New York, pp. 195-208.

Bousserrhine, N., Gasser. U., Jeanroy, E., and Berthelin, J. (1998) Effect of aluminum substitution of ferri-reducing bacterial activity and dissolution of goethites. *Earth and Planetary Sciences* **326**, 617-624.

Brown, Jr., G. E., Calas, G., Waychunas, G. A. and Petiau, J. (1988) X-ray absorption spectroscopy: applications in mineralogy and geochemistry. *In:* Spectroscopic Methods in Mineralogy and Geology (F. C. Hawthorne, ed.), Mineralogical Society of America, vol. 18, pp. 431-512.

Brown, Jr., G. E., Foster, A. L. and Ostergren, J. O. (1999) Mineral surfaces and bioavailability of heavy metals: a molecular scale perspective. *Proceedings of the National Academy of Science* **96**, 3388-3395.

Chastain, J. (Ed.) (1992) Handbook of X-ray Photoelectron Spectroscopy. Perkin Elmer Corporation, Eden Prairie, Minnesota.

Cheah, S.-F., Brown, Jr., G. E. and Parks, G. A. (1998) XAFS spectroscopy study of Cu(II) sorption on amorphous SiO_2 and γ-Al_2O_3: effect of substrate and time on sorption complexes. *Journal of Colloid and Interface Science* **208**, 110-128.

Chisholm-Brause, C. J., Hayes, K. F., Roe, A. L., Brown, Jr., G. E., Parks, G. A., and Leckie, J. O. (1990) Spectroscopic investigation of Pb(II) complexes at the γ-Al_2O_3 / water interface. *Geochimica Cosmochimica Acta* **54**, 1897-1909.

Chisholm-Brause, C. J., Berg, J. M., Matznen, R. A., and Morris, D. E. (2000) Uranium(VI) sorption complexes on montmorillonite as a function of solution chemistry. *Journal of Colloid and Interface Science* **232**, 1-12. DOI:10.100h/jcis.2000.7227

Cocke, D. L., Johnson, E. D. and Merrill, R. P. (1984) Planar models for alumina-based catalysts. *Catalysis Reviews in Science and Engineering* **26**, 163-231.

Colombo, C. and Violante, A. (1996) Effect of time and temperature on the chemical composition and crystallization of mixed iron and aluminum species. *Clays and Clay Minerals* **1**, 113-120.

Conrad, C. F., Chisholm-Brause, C. J., and Kelley, M. J. (2002) Pb(II) sorption onto γ-Al_2O_3 surfaces at the oxide-water interface: a novel approach using planar oxides. *Journal of Colloid and Interface Science* **248**, 275-282. DOI:10.1006/jcis.2002.8242

Reproduced with permission of the copyright owner. Further reproduction prohibited without permission.

Cornell, R. M. and Schwertmann, U. (1996) The Iron Oxides: Structure, Properties, Reactions, Occurrences and Uses. VCH, Weinheim, Germany.

Coston, J. A., Fuller, C. C., and Davis, J. A. (1995) Pb^{2+} and Zn^{2+} adsorption by a natural aluminum- and iron-bearing surface coatings on an aquifer sand. *Geochimica Cosmochimica Acta* **59,** 3535-3547.

Daskalaskis, , K. D. and O'Conner, T. P. (1995) Normalization and elemental sediment contamination in the coastal United States. *Environmental Science and Technology* **29**, 470-477.

Davies-Colley, R. J., Nelson, P. O and Williamson, K. J. (1984) Copper and cadmium uptake by estuarine sedimentary phases. *Environmental Science and Technology* **18**, 491-499.

Davis, J. A. and Hem, J. D. (1989) The surface chemistry of aluminum oxides and hydroxides. *In:* Mineral-Water Interface Geochemistry (M. F. Hochella and A. F. White, eds.) Mineralogical Society of America, pp. 177-260.

Davis, J. A. and Leckie, J. O. (1978) Surface ionization and complexation at the oxide/water interface: II. surface properties of amorphous iron oxyhydroxide and adsorption of metal ions. *Journal of Colloid and Interface Science* **67,** 90-107.

Davis, J. A. and Kent, D. B. (1990) Surface complexation modeling in aqueous geochemistry. *In:* Mineral-Water Interface Geochemistry (M. F. Hochella and A. F. White, eds.), pp. 177-260. Mineralogical Society of America.

Davis, J. A., Coston, J. A., Kent, D. B. and Fuller, C. C. (1998) Applications of the surface complexation concept to complex mineral assemblages. *Environmental Science and Technology* **32**, 2820-2828.

Digne, M. Sautet, P. Raybaud, P. Euzen, P. and Toulhoat, H. (2004) Use of DFT to achieve a rational understanding of acid-basic properties of γ-alumina surfaces. *Journal of Catalysis* **226**, 54-68.

Ding, M., De Jong, B. H. W. S., Roosendaal, S. J., and Vredenberg, A. (2000) XPS studies on the electronic structure of bonding between solid and solutes: adsorption of arsenate, chromate, phosphate, Pb^{2+}, and Zn^{2+} ions on amorphous black ferric oxyhydroxide. *Geochimica Cosmochimica Acta* **64,** 1209-1219.

Dominik, P., Pohl, H. N., Bousserrhine, N., Berthelin, J. and Kaupenjohann, M. (2002) Limitations to the reductive dissolution of Al-substituted goethites by *Clostridium butyricum*. *Soil Biology and Biochemistry* **34**, 1147-1155.

Dong, D., Li, Y. and Hua, H. (2001) Investigation of Fe, Mn oxides and organic material in surface coatings and Pb, Cd adsorption to surface coatings developed in different natural waters. *Microchemical Journal* **70**, 25-33.

Dubbin, W. E. and Ander, E. L. (2003) Influence of microbial hydroxamate siderophores on Pb(II) desorption from α-FeOOH. *Applied Geochemistry* **18**, 1751-1756.

Dzombak, D. A. and Morrel, F. M. (1987) Development of a data base for modeling adsorption of inorganics on iron and aluminum oxides. *Environmental Progress* **6**, 133-137.

Dzombak, D. A. and Morrel, F. M. (1990) Surface Complexation Modeling: Hydrous Ferric Oxide. John Wiley & Sons, New York.

Edwards, M., Benjamin, M. and Ferguson, J. (1989) New approaches to treatment of metal-bearing wastes. *43rd Perdue Industrial Waste Conference Proceedings*, Lewis Publishers, Inc., Michigan, pp. 389-396.

Reproduced with permission of the copyright owner. Further reproduction prohibited without permission.

Elbaz-Poulichet, F., Hollinger, P., Huang, W. W. and Martin, J.-M. (1984) Lead cycling in estuaries, illustrated by Gironde estuary, France. *Nature* **308**, 409-414.

Elzinga, E. J., Peak, D. and Sparks, D. L. (2003) Spectroscopic studies of Pb(II)-sulfate interactions at the goethite-water interface. *Geochimica Cosmochimica Acta* **65**, 2219-2230.

Evans, J. (1990) Applications of EXAFS to the study of metal catalysts. *In*: Applications of Synchrotron Radiation (C. R. A. Catlow and G. N. Greaves, eds.) Chapman and Hall, New York, pp. 201-220.

Farley, K. J., Dzombak, D. A. and Morel, F. M. M. (1985) A surface precipitation model for the sorption of cations on metal oxides. *Journal of Colloid and Interface Science* **106**, 226-242.

Fendorf, S. (1999) Fundamental aspects and applications of x-ray absorption spectroscopy in clay and soil science. *In:* Synchrotron X-ray Methods in Clay Science (D. G. Schulze, J. W. Stucki and P. M. Bertsch, eds.), The Clay Minerals Society, pp.19-67.

Fitzpatrick, E. A. (1980) Soils: Their Formation, Classification and Distribution. Longman, London.

Flavell, W. (2000) Surface structure determination by interference techniques. *In:* Surface Analysis: The Principle Techniques (J. C. Vickerman, ed.), John Wiley and Sons, New York, pp. 313-392.

Forbes, E. A., Posner, A. M. and Quirk, J. F. (1976) The specific adsorption of divalent Cd, Co, Cu, Pb, and Zn on goethite. *Journal of Soil Science* **27**, 154-166.

Frostergård, A., Tunlid, A., and Bååth, E. (1996) Changes in microbial community structure during long-term incubation in two soils experimentally contaminated with metals. *Soil Biology and Biochemistry* **28**, 55-63.

Fuller, C. C., Davis, J. A., Coston, J. A. and Dixon, E. (1996) Characterization of metal adsorption heterogeneity in a sand and gravel aquifer, Cape Cod, Massachusettes. *Journal of Contaminant Hydrology* **22**, 165-187.

Gadd, G. M. (2004) Microbial influence on metal mobility and application for bioremediation. *Geoderma* **122**, 109-119.

Glenn, G. L. and Dodd, C. G. (1968) Use of molecular orbital theory to interpret x-ray K-absorption spectral data. *Journal of Applied Physics* **39**, 5372-5377.

Goldberg, S. and Glaubig, R. A. (1988) Boron and silicon adsorption on an aluminum oxide. *Soil Science Society of America Journal* **52**, 87-91.

Grantham, M. C., Dove, P. M. and DiChristina, T. J. (1997) Microbially catalyzed dissolution of iron and aluminum oxyhydroxide mineral surface coatings. *Geochimica Cosmochimica Acta* **61**, 4467-4477.

Greenwood, N. N. and Earnshaw, A. (1985) Chemistry of the Elements. Permagon Press.

Gregg, S. J. and Sing, K. S. W. (1982) Adsorption, surface area and porosity. Academic Press, Inc.

Harju, M., Levänen, E. and Mäntylä, T. (2004) Surface characterization of plasma sprayed oxide materials: estimation of surface acidity using mass titration. *Journal of Colloid and Interface Science* **276**, 346-353.

Hart, R. K. and Maurin, J. K. (1965) Morphology and structure of oxides grown on aluminum in superheated steam. *Corrosion* **21**, 222-234.

Reproduced with permission of the copyright owner. Further reproduction prohibited without permission.

Hart, R. K. and Maurin, J. K. (1970) The nucleation and growth of oxide islands on aluminum. *Surface Science* **20**, 285-303.

Harvey, D. T. and Linton, R. W. (1984) X-ray photoelectron spectroscopy (XPS) of adsorbed zinc on amorphous hydrous ferric oxide. *Colloids and Surfaces* **11**, 81-96.

Hayes, K. F. and Leckie, J. O. (1986) Mechanism of lead ion adsorption at the goethite-water interface. *In:* Geochemical Processes at Mineral Surfaces, vol. 323, American Chemical Society, Washington D.C., pp. 115-141.

Heimstra, T. and Van Riemsdijk (1999) Surface structural ion adsorption modeling of competitive binding oxyanions by metal (hydr)oxides. *Journal of Colloid and Interface Science* **210**, 182-193.

Hem, J. D. (1976) Geochemical controls on lead concentrations in stream water and sediments. *Geochimica Cosmochimica Acta* **40**, 599-609.

Hem, J. D. (1977) Reactions of metal ions at surfaces of hydrous iron oxides. *Geochemica Cosmochimica Acta* **41**, 527-538.

Hendershot, W. H. and Lavkulich, L. M. (1983) Effect of sesquioxide coatings on surface charge of standard mineral and soil samples. *Soil Science Society of America Journal* **47**, 1252-1260.

Hernlem, B. J., Vane, L. M. and Sayles, G. D. (1996) Stability constants for complexes of the siderophore desferrioxamine B with selected heavy metal cations. *Inorganic Chimica Acta* **244**, 179-184.

Hiemenz, P. C. and Rajagopalan, R. (1997) Principles of Colloid and Surface Chemistry, 3rd ed. Marcel Dekker, Inc.

Hochella, Jr., M. F. (1990) Atomic structure, microtopography, composition, and reactivity of mineral surfaces. *In:* Mineral-Water Interface Geochemistry, vol. 23. (M. F. Hochella, Jr. and A. F. White, eds.) Mineralogical Society of America, 87-132.

Hochella, Jr., M. F. (1988) Auger electron and x-ray photoelectron spectroscopies. *In:* Spectroscopic Methods in Mineralogy and Geology (F. C. Hawthorne, ed.), Mineralogical Society of America, vol. 18, pp.573-638.

Hohl, H. and Stumm, W. (1976) Interaction of Pb^{2+} with hydrous γ-Al_2O_3. *Journal of Colloid and Interface Science* **55**, 281-288.

Honeyman, B. D. (1984) Cation and adion adsorption at the oxide-solution interface in systems containing binary mixtures of adsorbents: an investigation of the concept of adsorption additivity. Ph. D., Stanford University.

Honeyman, B. D. and Santshci, P. H. (1988) Metal in aquatic systems. *Environmental Science and Technology* **22**, 862-871.

Hong, S. and Olin, Å (1974) The crystal structure of $[Pb_4(OH)_4](ClO_4)_4x2H_2O$. *Acta Chemica Scandinavia* **A28**, 233-238.

Horowitz, A. J. and Elrick, K. A. (1987) The relationship of stream sediment surface area and composition to trace element chemistry. *Applied Geochemistry* **2**, 437-451.

Huang, C.-P. and Stumm, W. (1972) The specific surface area of γ-Al_2O_3. *Surface Science* **32**, 287-296.

Huheey, J. E., Keiter, E. A. and Keiter, R. L. (1993) Inorganic Chemistry: The Principles of Structure and Reactivity. Harper Collins.

Reproduced with permission of the copyright owner. Further reproduction prohibited without permission.

James, R. O. and Healy, T. W. (1972) Adsorption of hydrolysable metal ions at the oxide-water interface. I. Co(II) adsorption on SiO_2 and TiO_2 as model systems. *Journal of Colloid and Interface Science* **40**, 42-52.

Katz, L. E. and Hayes, K. F. (1995) Surface complexation modeling: (II) strategy for modeling polymer and precipitation reactions at high surface coverages. *Journal of Colloid and Interface Science* **170**, 491-501.

Kelly, J. J., Haggblom, M. and Tate, III, R. L. (1999) Changes in soil microbial communities over time resulting from one time application of zinc: a laboratory microcosm study. *Soil Biology and Biochemistry* **31**, 1455-1465.

Kim, K. S., O'Leary, T. J. and Winograd, N. (1973) X-ray photoelectron spectra of lead oxides. *Analytical Chemistry* **45**, 2214-2218.

Kinniburgh, D. G. and Jackson, M. L. (1981) Cation adsorption by hydrous metal oxides and clays. *In:* Adsorption of Inorganics at Solid-Liquid Interfaces (M. A. Anderson and A. J. Rubin, eds.) Ann Arbor Science, pp. 91-160.

Knapp, E. P., Herman, J. S., Mills, A. L. and Hornberger, G. M. (2002) Changes in the sorption capacity of Coastal Plain sediments due to redox alteration of mineral surfaces. *Applied Geochemistry* **17**, 387-398.

Knözinger, H. and Ratnasamy, P. (1978) Catalytic aluminas: surface models and characterizations of surface sites. *Catalytic Reviews in Science and Engineering* **17**, 31-70.

Koppelman, M. H. and Dillard, J. G. (1978) An x-ray photoelectron spectroscopic (XPS) study of cobalt adsorbed on the clay mineral chlorite. *Journal of Colloid and Interface Science* **66**, 345-351.

Kozdroj, J. and van Elsas, J. D. (2001) Structural diversity of microorganisms in chemically perturbed soil assessed by molecular and cytochemical approaches. *Journal of Microbiological Methods* **43**, 197-212.

Lai, C. H., Lo, S. L. and Chiang, H. L. (2000) Adsorption/desorption properties of copper ions on the surface of iron-coated sand using BET and EDAX analyses. *Chemosphere* **41**, 1249-1255.

Langmuir, D. (1997) Aqueous Environmental Geochemistry. Prentice Hall, New Jersey.

Leppard, G. G. and Droppo, I. G. (2003) The need and means to characterize sediment structure and behavior prior to the selection and implementation of remediation plans. *Hydrobiologia* **494**, 313-317.

Lippens, B. C. and DeBoer, J. H. (1965) Study of phase transformations during calcinations of aluminum hydroxides by selected area electron diffraction. *Acta Crystallography* **17**, 1312-1321.

Lovley, D. R. (1991) Dissimilatory Fe(III) and Mn(IV) reduction. *Microbiolgical Reviews* **55**, 259-287.

Manceau, A., Charlet, L., Boisset, M. C., Didier, B. and Spadini, L. (1992) Sorption and speciation of heavy metals on hydrous Fe and Mn oxides: from microscopic to macroscopic. *Applied Clay Science* **7**, 201-223.

McKenzie, R. M. (1980) The adsorption of lead and other heavy metals on oxides of manganese and iron. *Australian Journal of Soil Research* **21**, 61-73.

Reproduced with permission of the copyright owner. Further reproduction prohibited without permission.

Meng, X. and Letterman, R. D. (1993) Effect of component oxide interaction on the adsorption properties of mixed oxides. *Environmental Science and Technology* **27**, 970-975.

Moore, D. M. and Renolds, Jr., R. C. (1997) X-Ray Diffraction and the Identification and Analysis of Clay Minerals, 2nd ed. Oxford University Press, New York.

Morin, G., Ostergren, J. D., Juillot, F. Ildefonse, P., Calas, G. and Brown, Jr., G. E. (1999) XAFS determination of the chemical form of lead in smelter-contaminated soils and mine tailings: importance of adsorption processes. *American Mineralogist* **84**, 420-434.

Müller, B. and Sigg, L. (1990) Interaction of trace metals with natural particle surfaces: comparison between adsorption experiments and field measurements. *Aquatic Science* **52**, 1015-1621.

Nahon, D. B. (1996) Evolution of crusts in tropical landscapes. *In:* Rates of Chemical Weathering in Rocks and Minerals (S. M. Coleman and D. P. Dethier, eds.), Academic Press, pp. 169-192.

Newville, M. (2001) IFEFFIT: interactive EXAFS analysis and FEFF fitting. *Journal of Synchrotron Radiation* **8**, 322-324.

Newville, M. (2004) Fundamentals of EXAFS. http://cars9.uchicago.edu/xafs/xas_fun/

Norman, D. and King, D. A. (1990) Looking at solid surfaces with synchrotron radiation. *In:* Applications of Synchrotron Radiation (C. R. A. Catlow and G. N. Greaves, eds.) Chapman and Hall, New York, pp. 221-240.

Oakley, S. M., Nelson, P. O. and Williamson, K. J. (1981) Model of trace-metal partitioning in marine sediments. *Environmental Science and Technology* **15**, 474-480.

O'Day, P. A., Rehr, J. J., Zabinsky, S. I., and Brown, Jr., G. E. (1994) Extended x-ray absorption fine structure (EXAFS) analysis of disorder and multiple-scattering in complex crystalline solids. *Journal of the American Chemical Society* **116**, 2938-2948.

Olin, Å and Söderquist, R. (1972) The crystal structure of β-$[Pb_6O(OH)_6](ClO_4)_4xH_2O$. *Acta Chemica Scandinavia* **26**, 3505-3514.

Olson, B. H. and Thornton, I. (1982) The resistance patterns to metals of bacterial populations in contaminated land. *Journal of Soil Science* **33**, 271-277.

Ostergren, J. D., Brown, Jr., G. E., Parks, G. A. and Tingle, T. N. (1999) Quantitative speciation of lead in selected mine tailings from Leadville, CO. *Environmental Science and Technology* **33**, 1627-1636.

Ostergren, J. D., Trainor, T. P., Bargar, J. R., Brown, Jr., G. E. and Parks, G. A. (2000) Inorganic ligand effects of Pb(II) sorption to goethite (α-FeOOH): I. Carbonate. *Journal of Colloid and Interface Science* **225**, 466-482.

Palmqvist, U., Ahlberg, E., Lövgren, L. and Sjöberg, S. (1999) Competitive metal ion adsorption in goethite systems using in situ voltametric methods and potentiometry. *Journal of Colloid and Interface Science* **218**, 388-396.

Peri, J. B. and Hannan, R. B. (1960) Surface hydroxyl groups on γ-alumina. *Spectrochimica Acta* **64**, 1526-1530.

Pickering, W. F. (1979) Copper retention by soil/sediment components. *In*: Copper in the Environment. I. Ecological Cycling, (J. O. Nriagu, ed.) John Wiley, New York, pp. 217-253.

Reproduced with permission of the copyright owner. Further reproduction prohibited without permission.

Rao, K. J. and Wong, J. (1984) A XANES investigation of the bonding of divalent lead in soils. *Journal of Chemistry and Physics* **81**,4832-4843.

Ratner, B. and Castner, D. (1997) Electron spectroscopy for chemical analysis. *In:* Surface Analysis: The Principle Techniques (J. C. Vickerman, ed.), John Wiley and Sons, New York, pp.43-98.

Robert, M. and Terce, M. (1989) Effect of gels and coatings on clay mineral chemical properties. *In:* Inorganic Contaminants in the Vadose Zone (B. Bar-Yosef, N. J. Barrow and J. Goldshmid, eds.), Springer, Berlin, pp. 57-71.

Robertson, A. P. and Leckie, J. O. (1997) Cation binding predictions of surface complexation models: effects of pH, ionic strength, cation loading, surface complex, and model fit. *Journal of Colloid and Interface Science* **188**, 444-472.

Roe, A. L., Hayes, K. F., Chisholm-Brause, C. J., Brown, Jr., G. E., Parks, G. A., Hodgson, K. O. and Leckie, J. O. (1991) In situ x-ray adsorption study of lead ion surface complexes at the goethite-water interface. *Langmuir* **7**, 367-373.

Rubin, A. J. (1976) Aqueous-Environmental Chemistry of Metals. Ann Arbor Science.

Sakurai, K., Teshima, A. and Kyuma, K. (1990) Changes in zero point of charge (ZPC), specific surface area (SSA), and cation exchange capacity (CEC) of kaolinite and montmorillonite, and strongly weathered soils caused by Fe and Al coatings. *Soil Science and Plant Nutrition* **36**, 73-81.

Sandaa, R. A., Torsvik, V., Enger, O., Daae, F. L., Castberg, T. and Hahn, D. (1999) Analysis of bacterial communities in heavy-metal contaminated soils at different levels of resolution. *FEMS Microbiology Ecology* **30**, 237-251.

Sansone, F. J. (1986) Depth distribution of short-chain organic acid turnover in Cape Lookout Bight sediments. *Geochimica Cosmochimica Acta* **50**, 99-105.

Sansone, M., Via, G., George, G., Meitzner, G. and Hewitt, R. (2004) Exxon beamline X10C as NSLS, Brookhaven National Laboratory. Ch. 171, 656-658.

Sayers, D. E., Lytle, F. W. and Stern, E. A. (1970) Point scattering theory of x-ray K absorption fine structure. *Advances in X-ray Analysis* **13**, 248-271.

Sayers, D. E., Stern, E. A. and Lytle, F. W. (1971) New technique for investigating noncrystalline structures: Fourier analysis of the extended x-ray absorption fine structure. *Physical Review Letters* **27**, 1204-1207.

Scheidigger, A. M., Lamble, G. M. and Sparks, D. L. (1996) Investigation of Ni sorption on pyrophyllite: an XAFS study. *Environmental Science and Technology* **30**, 548-554.

Scheidigger, A. M., Lamble, G. M. and Sparks, D. L. (1997) Spectroscopic evidence for the formation of mixed-cation hydroxide phases upon metal sorption on clays and aluminum oxides. *Journal of Colloid and Interface Science* **186**, 118-128. Article No. CS964624.

Schmitt, J., Gu, B., Shorer, M., Flemming, H.-C. and McCarthy, J. J. (1996) The role of natural organic matter as a coating on iron oxide and quartz. *Archives of Hydrobiology Special Issues in Advanced Linmology* **47**, 315-322.

Schneck, C. V., Dillard, J. G. and Murray, J. W. (1983) Surface analysis and the adsorption of Co(II) on goethite. *Journal of Colloid and Interface Science* **95**, 398-409.

Schwertmann, U. and Cornell, R. M. (2000) Iron Oxides in the Laboratory: Preparation and Characterization. Wiley-VCH, New York.

Reproduced with permission of the copyright owner. Further reproduction prohibited without permission.

Scokart, P. O. and Rouxhet, P. G. (1982) Comparison of the acid base properties of various oxides and chemically treated oxides. *Journal of Colloid and Interface Science* **86**, 96-104.

Simpson, S. L., Angel, B. M. and Jolley, D. F. (2004) Metal equilibration in laboratory-contaminated (spiked) sediments used for the development of whole-sediment toxicity tests. *Chemosphere* **54**, 597-609.

Sørensen, M. A., Stackpoole, M. M., Frenkel, A. I., Bordia, R. K., Korshin, G. V. and Christensen, T. H. (2000) Aging of iron (hydr)oxides by heat treatment and effects on heavy metal binding. *Environmental Science and Technology* **34**, 3991-4000.

Sparks, D. L. (1995) Environmental Soil Chemistry. Academic Press, Sand Diego, CA.

Spiro, T. G., Templeton, D. H. and Zalkin, A. (1969) Critical Stability Constants Volume 4: Inorganic Complexants. Okenum Press.

Sposito, G. (1984) The Surface Chemistry of Soils. Oxford University Press, New York.

Sposito, G. (1996) The Environmental Chemistry of Aluminum, 2nd ed., CRC Press, London.

Sposito, G., Skipper, N. T., Sutton, R., Park, S. and Soper, K. (1999) Surface geochemistry of the clay minerals. *Proceedings of the National Academy of Science* **96**, 3358-3364.

Stefanov, P., Stoychev, D., Aleksandrova, A., Nocolova, D., Atanasova, G. and Marinova, Ts. (2004) Compositional and structural characterization of alumina coatings deposited electrochemically on stainless steel. *Applied Surface Science* **235**, 80-85.

Stern, E. A. (1998) Theory of EXAFS. *In:* X-Ray Absorption: Principles, Applications, Techniques of EXAFS, SEXAFS, and XANES. (D. C. Koningsberger and R. Prins, eds.) John Wiley and Sons, New York, pp.3-51.

Stipp, S. L. S., Hansen, M., Kristensen, R., Hochella, Jr., M. F., Bennedsen, L., Dideriksen, K., Balic-Zunic, T., Leonard, D. and Mathieu, H.-J. (2002) Behavior of Fe-oxides relevant to contaminant uptake in the environment. *Chemical Geology* **190**, 321-337.

Strasser, H., Burgstaller, W. and Schinner, F. (1994) High yield production of oxalic acid for metal leaching purposed by *Aspergillus niger*. *FEMS Microbiological Letters* **119**, 365-370.

Strawn, D. G., Scheidegger, A. M. and Sparks, D. L. (1998) Kinetics and mechanisms of Pb(II) sorption and desorption at the aluminum oxide-water interface. *Environmental Science and Technology* **32**, 2596-2601.

Strawn, D. G. and Sparks, D. L. (1999) The use of XAFS to distinguish between inner- and outer-sphere lead adsorption complexes on montmorillonite. *Journal of Colloid and Interface Science* **216**, 257-269.

Strawn, D. G. and Sparks, D. L. (2000) Effects of soil organic matter on the kinetics and mechanisms of Pb(II) sorption and desorption in soil. *Soil Science Society of America Journal* **64**, 144-156.

Stumm, W. (1992) Chemistry of the Solid-Water Interface: Processes at the Minera-Water and Particle-Water Interface in Natural Systems. John Wiley and Sons, New York.

Reproduced with permission of the copyright owner. Further reproduction prohibited without permission.

Stumm, W. and Morgan, J. J. (1996) Aquatic Chemistry: Chemical Equilibria and Rates in Natural Waters. John Wiley and Sons, New York.

Sugimoto, T. and Sakata, K. (1992) Preparation of monodispersed pseudocubic α-Fe_2O_3 particles from condensed ferric hydroxide gel. *Journal of Colloid and Interface Science* **152**, 587-590.

Suhadolc, M., Schroll, R., Gattinger, A., Schloter, M., Munch, J. C. and Lestan, D. (2004) Effects of modified Pb-, Zn-, and Cd- availability on the microbial communities and on the degradation of isoproturon in a heavy metal contaminated soil. *Soil Biology and Biochemistry* **36**, 1943-1954.

Szecsody, J. E., Zachara, J. M. and Bruckhart, P. L. (1994) Adsorption-dissolution reactions affecting the distribution and stability of Co(II)-EDTA in an iron oxide-coated sand. *Enviornmental Science and Technology* **28**, 1706-1716.

Taylor, R. M. and Schwertmann, U. (1978) The influence of aluminum on iron oxides. Part I. The influence of Al on Fe oxide formation from the Fe(II) system. *Clays and Clay Minerals* **26**, 373-383.

Tessier, A. (1992) Sorption of trace elements on natural particles in oxic environments. *In:* Environmental Particles. Lewis Publishers, pp. 425-453.

Tewari, P. H. and Lee, W. (1975) Adsorption of Co(II) at the oxide-water interface. *Journal of Colloid and Interface Science* **52,** 77-88.

Thompson, H., Brown, Jr., G. E. and Parks, G. A. (1997) XAFS spectroscopic study of uranyl coordination in solids and aqueous solutions. *American Mineralogist* **82**, 483-496.

Tingle, T. N., Borch, R. S., Hochella, Jr., M. F., Becker, C. H. and Walker, W. J. (1993) Characterization of lead on mineral surfaces in soils contaminated by mining and smelting. *Applied Surface Science* **72**, 301-306.

Tipping, E. and Cooke, D. (1982) The effects of adsorbed humic substances on the surface charge of goethite in freshwaters. *Geochimica Cosmochimica Acta* **60**, 75-80.

Tipping, E., Griffith, J. R. and Hilton, J. (1983) The effect of adsorbed humic substances on the uptake of copper(II) by goethite. *Croatica Chemica Acta* **56**, 613-621.

Towle, S. N., Bargar, J. R., Brown, Jr., G. E. and Parks, G. A. (1997) Surface precipitation of Co(II) (aq) on Al_2O_3. *Journal of Colloid and Interface Science* **187,** 62-82.

Trainor, T. P., Brown, Jr., G. E. and Parks, G. A. (2000) Adsorption and precipitation of aqueous Zn(II) on alumina powders. *Journal of Colloid and Interface Science* **231**, 359-372.

Trivedi, P., Dyer, J. A. and Sparks, D. L. (2003) Lead sorption onto ferrihydrite. 1. A macroscopic and spectroscopic assessment. *Environmental Science and Technology* **37**, 908-914.

Turner, A. and Millward, G. E. (2002) Suspended particles: their role in estuarine biogeochemical cycles. *Estuarine, Coastal and Shelf Science* **55**, 857-883.

Tyliszczak, Y. H. Y. and Hitchcock, P. (1990) Pb L_3 EXAFS and near-edge studies of lead metal and lead oxides. *Journal of the Physical Chemistry of Solids* **51**, 445-451.

Reproduced with permission of the copyright owner. Further reproduction prohibited without permission.

Van Veen, J. A. R. (1988) A method for the quantitative determination of the basic hydroxyl groups on an alumina surface. *Journal of Colloid and Surface Science* **121**, 214-219.

Vickerman, J. C. and Swift, A. (1997) Secondary ion mass spectrometry—the surface mass spectrometry. *In:* Surface Analysis: The Principle Techniques (J. C. Vickerman, ed.), John Wiley and Sons, New York, pp.135-214.

Violante, A., Ricciardella, M. and Pigna, M. (2003) Adsorption of heavy metals on mixed Fe-Al oxides in the absence and presence of organic ligands. *Water, Air and Soil Pollution* **145**, 289-306.

Vitchev, R. G., Pireaux, J. J., Conrad, T., Bender, H., Wolstenholme, J. and Defranoux, Chr. (2004) X-ray photoelectron spectroscopy characterization of high-k dielectric Al_2O_3 and HfO_2 layers deposited on SiO_2/Si surface. *Applied Surface Science* **235**, 21-25.

Warren, L. A. and Zimmerman, A. P. (1994) The importance of surface area in metal sorption by oxides and organic matter in a heterogeneous natural sediment. *Applied Geochemistry* **9**, 245-254.

Webb, P. A. and Orr, C. (1997) Analytical Methods in Fine Particle Technology. Micromeritics Instrument Corporation.

Webb, S. M. (2002) Sam's Interface for XAS package (SixPACK). http://www-ssrl.slac.stanford.edu/~swebb/sixpack.htm

Wen, X., Du, Q. and Tang, H. (1998) Surface complexation model for the heavy metal adsorption on natural sediments. *Environmental Science and Technology* **32**, 870-875.

Westall, J. and Hohl, H. (1980) A comparison of electrostatic models for the oxide/solution interface. *Advances in Colloid and Interface Science* **12**, 265-294.

Winick, H. and Doniach, S. (1980) Synchrotron Radiation Research, Plenum Press, New York.

Yong, R. N. and MacDonald, E. M. (1998) Influence of pH, metal concentrations, and soil component removal on retention of Pb and Cu by an illitic soil. *In:* Adsorption of Metals by Geomedia: Variables, Mechanisms, and Model Applications (E. A. Jenne, ed.), Academic Press, San Diego, pp. 229-253.

Yu, Y. H., Tyliszczak, T. and Hitchcock, P. (1990) Pb L_3 EXAFS and near-edge studies of lead metal and lead oxides. *Journal of the Physical Chemistry of Solids* **51**, 445-451.

Zachara, J. M., Resch, C. T. and Smith, S. C. (1994) Influence of humic substances on Co^{2+} sorption by a subsurface mineral separate and its mineralogic components. *Geochimica Cosmochimica Acta* **58**, 553-566.

Zhuang, J. and Yu, G.-R. (2002) Effects of surface coatings on electrochemical properties and contaminant sorption of clay minerals. *Chemosphere* **49**, 619-628.

Reproduced with permission of the copyright owner. Further reproduction prohibited without permission.

VITA

CHRISTINE FORSYTHE CONRAD

Born in Poquoson, Virginia, 17, May, 1976. Graduated from Poquoson High School in 1994. Earned a B. S. in Chemistry and Marine Science from Coastal Carolina University in 1998. Entered doctoral program at the College of William & Mary, School of Marine Science, in 1998.

Reproduced with permission of the copyright owner. Further reproduction prohibited without permission.